NASA SP-5053

CONFERENCE ON SELECTED TECHNOLOGY for the PETROLEUM INDUSTRY

LEWIS RESEARCH CENTER

CLEVELAND, OHIO

DECEMBER 8-9, 1965

NATIONAL AERONAUTICS AND SPACE ADMINISTRATION

NASA SP-5053

CONFERENCE ON SELECTED TECHNOLOGY for the PETROLEUM INDUSTRY

Lewis Research Center
Cleveland, Ohio
December 8-9, 1965

Scientific and Technical Information Division 1966
NATIONAL AERONAUTICS AND SPACE ADMINISTRATION
Washington, D.C.

For sale by the Superintendent of Documents, U.S. Government Printing Office
Washington, D.C. 20402 Price $1.25

FOREWORD

Our nation's space program is both an illustration of the dynamic and growing scientific and technical activity of the country and a prime mover in it. The space program attacks, in an organized way, problems at the frontiers of knowledge and know-how in science and engineering. This attack uses and creates new information and new technology.

With the premise that most of the new technology derived from the space program is applicable to other activities, topics of interest and potential value to the petroleum industry were selected for this conference. The choice of content was determined through a series of meetings between the NASA Lewis Research Center staff and petroleum industry specialists.

ABE SILVERSTEIN
Director
Lewis Research Center

Page intentionally left blank

CONTENTS

Introduction

WALTER T. OLSON
Lewis Research Center

THIS CONFERENCE ON SELECTED TECHNOLOGY for the petroleum industry is intended to acquaint an audience from that industry with some of the technology that underlies the Nation's space effort. The conference is undergirded with the belief that any comprehensive technical effort—be it in petroleum, in space, or in other fields—can contribute advances to others. It has been prepared as a unique experiment in technical communication, an attempt to select and to describe technical topics from one area of activity, aerospace, that might have value in another area of activity, the petroleum industry.

An introduction to the conference requires discussion both of the setting and the background for it. Because the technical topics are presented by the staff of the Lewis Research Center and relate to the work of the Center, Lewis and its work is described briefly. Then, a short discussion of how we arrived at this conference and the material in it follows.

The reader is assumed to have a general familiarity with the national space program as managed by the National Aeronautics and Space Administration: its scientific studies of space phenomena; its manned explorations; its applications programs such as meteorology, geodesy, and communications; and the extensive research and development both to support present activities and to make future undertakings possible.

Major tasks of the Lewis Research Center are research and advanced technology in propulsion and power for flight.

One of 10 major centers of NASA, the Lewis Center is currently the second largest with a staff of approximately 4800 people, more than 1800 of whom are professional engineers and scientists.

Physically, the Center occupies 350 acres with an auxiliary location of 6000 acres at Plum Brook, near Sandusky, Ohio. Lewis comprises extensive laboratories in many buildings for almost every kind of physical, chemical, electrical, and metallurgical research. In addition, unusual tools for propulsion and power technology include such items as space simulation chambers, high-speed wind tunnels of various sizes, engine test facilities that simulate altitude operation, test stands for rockets and components, and radiation sources, including a cyclotron and a 60 000-kilowatt reactor.

The Lewis Center came into being in 1941 as an outgrowth of the powerplants group at the National Advisory Committee for Aeronautics (NACA) Langley Aeronautical Laboratory (now NASA's Langley Research Center). Langley was established in 1917 as the first research laboratory for studying flight in the Nation. During World War II, the Lewis Center made major contributions to reciprocating engine cooling and high octane fuels. The period immediately following saw the development to a high degree of the air-breathing turbojet and ramjet engines. Development of these engines relied heavily on basic results from compressor, fuels, combustion, and turbine research here. Almost every major U. S. engine-powered jet aircraft today has been put through its paces here to have some item or other of Lewis research incorporated into it. Incidentally, an advisory committee to NACA comprising key technical leaders from the petroleum and aircraft engine industries helped both to guide and to evaluate our fuels research programs for reciprocating and turbojet engines. Early work on liquid-fueled rockets, mostly high-energy propellant rockets, paralleled the air-breathing engine program and expanded rapidly in 1957.

Today, the program of the Center is oriented to advancing the technology of chemical, nuclear, and electric rockets and of space electric power for a wide spectrum of power levels. It includes the background research and technology in metallurgy, basic chemistry, plasma physics, fuels, fluid flow, heat transfer, electronics, control dynamics, nucleonics and other topics pertinent to these engines and to new and unusual propulsion and power generation systems.

Lewis also has responsibility for development of the operational Atlas-Centaur launch vehicle and the improved Atlas-Agena launch vehicle. Centaur, a 37 000-pound upper stage on Atlas, is propelled with two 15 000-pound-thrust engines. This vehicle is based on the hydrogen-oxygen technology that was pioneered at Lewis within the last decade; the technology of flying liquid hydrogen is vital to many of our future missions, notably Apollo, while Centaur itself is a vehicle that is planned to soft-land instruments on the moon. The Atlas-Agena launch vehicle has been used for a variety of important space science missions, including Nimbus, OGO, the history-making Ranger photographs of the moon, and the Mariner flights to Venus and to Mars.

For the present fiscal year, Lewis expects to account for over $350 million of NASA's budget. About one-forth will be used for salaries, operations, and general support of in-house projects including construction. The other approximately three-fourths represents contracted research and development work. Most of it is in support of a few large projects: Centaur, Agena, the M–1 hydrogen-oxygen engine; but it also supports a wide variety of projects in universities and industry.

In presenting this Conference on New Technology from Lewis, we are contributing to a major NASA effort, namely, to ensure maximum value from national space activities. Under the Space Act of 1958, it is a part of NASA's broad responsibility to disseminate aerospace-related technology as widely as practicable and appropriate.

At its present level of about $5 billion per year, the space program is a large part of the $16 billion that the Federal Government is spending annually for research and development. Federal research and development expenditures represent about three-fourths of the national total. It is important that the Nation use the results of all these expenditures as effectively as possible.

A problem of first importance is that of usefully disseminating the technical information being generated in our country, especially when this information is so profuse, so fragmented, and so isolated from many users by company, by industry, by geography, and by many subtle but nonetheless powerful factors, including even psychological ones. For example, there is the "it wasn't invented here" syndrome. And so NASA has addressed itself to this problem by experimenting with a variety of ways of better communicating its results and findings.

This Conference is one such experiment. Other experiments and their results are described in the section entitled "Technology Utilization." In another sense, this Conference is a partial report by NASA of its stewardship of men and money.

The idea of describing selected technology to a particular industry followed logically after a presentation of certain aerospace-related technology to several hundred industrialists from Northeastern Ohio in June 1964 (NASA Special Publication SP–5015). That conference was held to acquaint industry with several technical areas in such a way that the type and extent of accomplishments in them and the prospects and limitations for their future growth would be evident. The conference was apparently a successful communication mechanism. It elicited requests for more technical information and for a repetition, which was held for a similar audience from a larger geographical area in October 1964.

The petroleum industry was chosen for this first attempt at a conference structured for a particular industry for several reasons. It is a large industry. It is vital to our Nation's well-being. It is technically oriented and technically advanced. And it is equipped with good scientific and engineering information handling systems. In other words, the petroleum industry looked like a good receiver for our transmitter.

The meeting contents are derived from the work of the Lewis Center: combustion, heat transfer, fluid mechanics, physics of solids, cryogenics, materials, and rotating machinery. The contents are only a small part of the work at Lewis, however, and the Lewis work is only 10 percent, or less, of the NASA budget; therefore the conference represents only a very small sampling of aerospace-related technology.

Choice of the particular contents was guided by a series of meetings between Lewis staff members and petroleum industry specialists intended to identify aerospace subject matter of interest and potential value to the petroleum industry. The meetings consisted of both prepared technical briefings and subsequent evaluation sessions. We thank the Esso Research and Engineering Company, the Standard Oil Company of Ohio, and the American Petroleum Institute for their assistance in this process. The American Petroleum Institute was also most helpful in selecting the audience.

Actually, the composition of the conference includes most of the topics identified as of interest but not all of them. Some of the topics included are in addition to the findings of the meetings; we don't discount serendipity!

Finally, no attempt was made to put aerospace-related technology into the frame of reference of particular technical problems in the petroleum industry; such an attempt would seem presumptuous. Although the material is presented as it was derived for aerospace requirements, nevertheless, its broad applicability should be evident.

Further examination of whatever appears important is invited.

Page intentionally left blank

I Combustion

RICHARD S. BROKAW, FRANK E. BELLES, BRUCE J. CLARK, AND FRANK J. ZELEZNIK
Lewis Research Center

IN HIS RESTLESS URGE TO BE ON THE MOVE, man has harnessed the combustion process to propel him on his way. Today, autos and trucks powered by internal combustion clog our highways, and combustion-fired jet transports hurry us from coast to coast and across the seas. Mighty rockets launch unmanned vehicles to explore the moon and nearby planets, while even more advanced systems for manned missions are being tested. Five F–1 engines, each generating 1 500 000 pounds of thrust from the combustion of kerosene-type fuel and liquid oxygen at almost 3 tons per second will launch our Apollo astronauts toward the moon. And larger engine types are under development; for example, a 3 000 000-pound-thrust solid-propellant engine was successfully fired recently.

Combustion as it relates to propulsion is obviously of great importance to NASA and is especially of interest at the Lewis Research Center, where most of NASA's basic propulsion research is conducted. Here, too, is managed the development of major propulsion systems by NASA contractors. These combustion systems are varied and complex, and many different processes may be taking place simultaneously.

In trying to understand such systems, we will idealize them by considering only one process at a time. Furthermore, since the Lewis Center is interested in propulsive devices, we will use rocket and ramjet engines as a framework for our discussion.

Perhaps the simplest idealization of the engine would be to regard it as a chemical reactor (fig. I–1). Here a fuel—in this case methane, but it could be as mundane as kerosene—reacts with an oxidant—shown here as oxygen, but it could be air, or as exotic as fluorine. This reactor differs from those used in the chemical-process industries in two important ways: (1) It is adiabatic rather than isothermal; (2) thrust is wanted, not chemicals. Therefore, the reaction products are exhausted through a nozzle to convert the random thermal energy of the high-temperature gases into directed kinetic energy, or thrust.

The optimum behavior of such a device can be estimated by assuming that the fuel and oxidant mix perfectly and react instantaneously to give an equilibrium mixture of reaction products. In this example, they are not merely carbon dioxide and water; the high temperature also produces molecules such as carbon monoxide, hydrogen, and oxygen, radicals like hydroxyl, and the atoms of hydrogen and oxygen. Thus, the first topic to be discussed is the chemical thermodynamics of high-temperature gas mixtures, or how to calculate the composition, properties, and ideal behavior of such mixtures.

Of course, this picture is oversimplified. In practice, such a combustion chamber must be

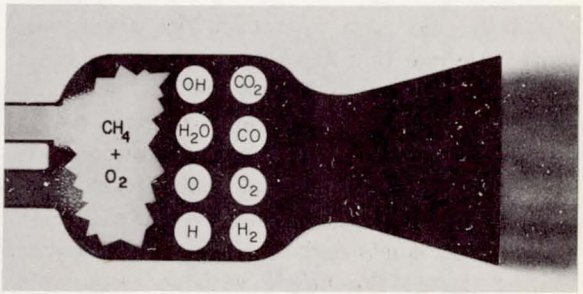

FIGURE I–1.—Chemical thermodynamics.

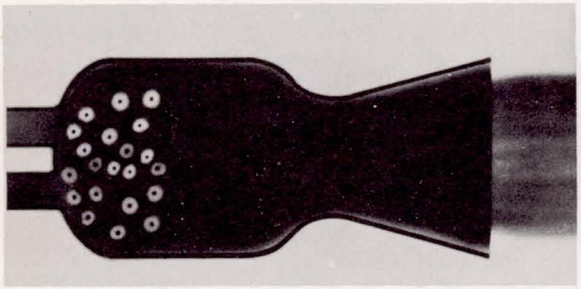

FIGURE I–2.—Transport properties.

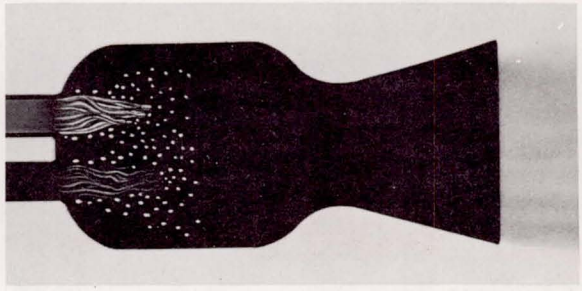

FIGURE I–3.—Atomization and vaporization.

cooled. Hence, a second topic is the transport properties of gases—thermal conductivity and viscosity (fig. I–2). These properties must be known not only to calculate cooling requirements, but also to estimate the rates at which liquid fuel or oxidant drops vaporize in the hot combustion environment.

The assumption that the fuel and oxidant mix and react instantaneously was an idealization. In fact, one or both of the propellants must first be broken up from a liquid stream into ligaments and droplets and then vaporized, which introduces a third topic, atomization and vaporization (fig. I–3).

Vaporization in an operating rocket occurs in a sea of flame, so that there is no problem in igniting the reactants. However, this is not necessarily so in other kinds of engines. Figure I–4 shows schematically an air-breathing ramjet engine, where fuel is injected into a hot high-velocity airstream. (The air inlet system is not shown.) No flames or ignition sources are provided. Thus, another topic involves the processes leading to the spontaneous ignition of such fuel-air mixtures.

Finally, consider the rocket-like device once more. Assume that the reactants have come to chemical equilibrium. What happens when this gas is expelled through the nozzle? There are two extremes. First, if chemical reaction rates are very slow, the chemical composition of the gas remains unchanged as it flows out the nozzle. Figure I–5 depicts carbon monoxide and oxygen flowing out of the nozzle without recombining in the upper half of the jet. At the other extreme, if rates are fast enough, carbon monoxide and oxygen will combine to form carbon dioxide, as shown in the lower part of the figure. In this case, additional chemical energy is converted into thrust. To estimate accurately the nature of the exhaust requires high-temperature reaction rates—chemical kinetics. The use of shock tubes to obtain such information will be discussed.

CHEMICAL THERMODYNAMICS

To simulate a chemical rocket thermodynamically, assume first of all that the fuel and the oxidant react at a constant pressure and energy and then the hot combustion gases expand adiabatically through the nozzle to convert thermal energy into the directed velocity of the gas (fig. I–1). Since the calculations for any thermodynamic process are similar, the combustion process can illustrate the complexity of the calculations. Thermodynamically, the situation can be illustrated with combustion as it occurs on a kitchen range when a mixture of air and natural gas, largely methane, is ignited to produce a high-temperature flame containing the reaction products (fig. I–6). In a simplified calculation, it would be assumed that only carbon dioxide and water are possible reaction products. However, because of the high temperature, a considerable amount of dissociation takes place, and under these conditions there are potentially many different reaction products, for example, carbon monoxide; various low-molecular-weight hydrocarbons, such as acetylene and ethylene; and

FIGURE I-4.—Ignition.

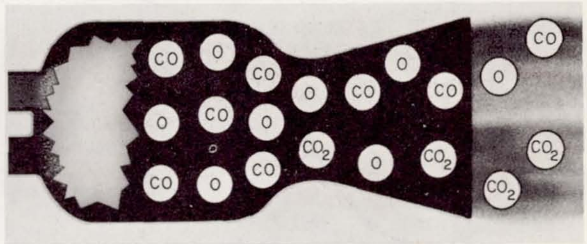

FIGURE I-5.—Chemical reaction rates.

fragmentary species, such as the free radicals OH, CH, and CH_2. When combustion is poor, some soot could also form.

In any particular problem, only a few of these species are present in significant amounts. However, it is not known *a priori* which of these species will be the important ones for any given problem. All the species must be considered in the calculation and then the calculation will reveal which are the significant ones. The system of equations that describes this particular process contains equations for conservation of mass for each of the four elements—in this case, carbon, hydrogen, oxygen, and nitrogen. It also contains an equation for conservation of energy. In addition, another equation specifies the pressure at which combustion takes place, and finally, for this particular example, there are an additional 16 equilibrium constant equations for a grand total of 22 similtaneous equations to solve. These simultaneous equations are not linear equations and cannot be solved analytically but require an iterative solution on a computer.

Any chemical system other than methane and air requires both different equations and a different number of equations to be solved. A new computer program is required for each chemical system encountered. What would certainly be preferable is to have a program capable of handling all chemical systems, that is, a program that can select the appropriate equations and then solve them. Such a computer program has been prepared at the Lewis Research Center.

An important feature of this general program for chemical equilibrium computations is its flexibility, that is, it can perform thermodynamic computations for a system containing up to 15 different chemical elements, and it can accommodate as many as 90 different reaction products. For such a chemical system, the program can perform any one of several calculations. For example, it can calculate flame temperatures, it can obtain equilibrium properties for assigned temperatures and pressures, it can perform rocket performance calculations, and it can perform gaseous detonation calculations. Of prime importance is the ease with which a problem can be specified for the computer. Input information requires only a chemical formula and a state. For example, methane would be indicated simply as CH_4 and whether it was injected as a gas or as a liquid. In certain cases, as for example, combustion calculation, the heat of formation of the reactants would also be specified to define the problem completely. In addition, the answers that are printed out by the computer

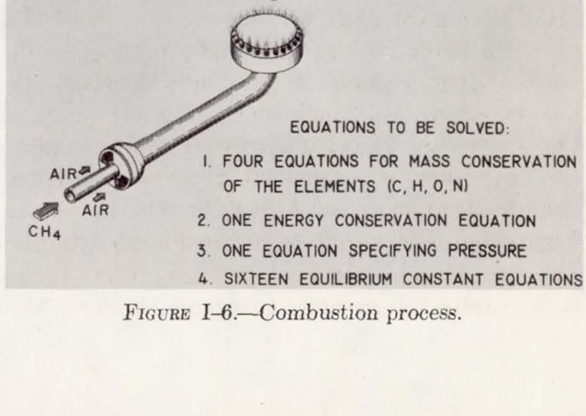

FIGURE I-6.—Combustion process.

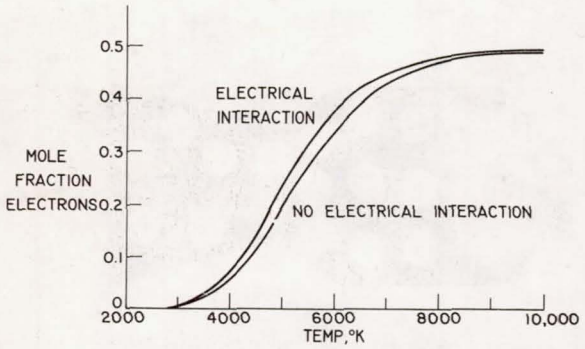

FIGURE I–7.—Mole fraction of electrons in cesium plasma.

program are in an understandable form and can be readily used.

Although the program itself is extremely general and can handle almost any type of chemical equilibrium computations problem, it can do so only for those systems for which thermodynamic data exist. At Lewis, data have been compiled for over 270 species formed from the first 18 elements of the periodic chart, that is, elements such as hydrogen, boron, carbon, nitrogen, up to and including aluminum, silicon, phosphorus, sulfur, chlorine, and argon. For use with the computer program, the data are on a reel of magnetic tape and are automatically selected by the program. However, a substantial portion of these data is also available in tabular form in an NASA Special Publication, SP–3001 by McBride, et al. (see bibliography), which contains the data for approximately 210 chemical species formed from the same chemical elements.

The program adapts to several computers. It has been sent to more than 70 universities and industrial laboratories both in this country and in foreign countries. The program is in use on IBM equipment at Lewis; however, some of the organizations that have received this program do not use IBM equipment. Instead, they use the Control Data computers or the Univac computers, and to our knowledge this program has been used successfully on all three types of computer.

Currently, there is strong interest in partly ionized gases. In that case, the thermodynamic calculation requires that the effects of long-range electrostatic interactions be accounted for. The necessary changes have been incorporated into the computer program; the effect of these electrical interactions between electrons and ions can be illustrated by considering a cesium plasma. Figure I–7 shows the mole fraction of electrons in a cesium plasma at 1 atmosphere pressure. The lower curve is obtained by neglecting all electrical interactions, and the upper curve is obtained by considering the effect of the electrical interactions. The electrical interactions increase the amount of ionization that occurs by only about 10 percent in the mole fraction; however, the electrical conductivity is proportional to the number density of electrons. The electrical interactions increase the number density of the electrons by approximately 30 percent at about 4500° K (fig. I–8), and this is certainly not an effect to be neglected.

This computer program is very versatile and can perform thermodynamic calculations for a wide variety of situations, including the consideration of plasma problems. It is potentially applicable to many problems of practical interest.

TRANSPORT PROPERTIES

Transport properties, such as heat conductivity, viscosity, and diffusivity of high-temperature reacting gases are needed both to calculate heat transfer pertinent to cooling the chamber and in connection with the vaporization of propellants (fig. I–2). The kinetic theory of gases promises to provide a way of computing these

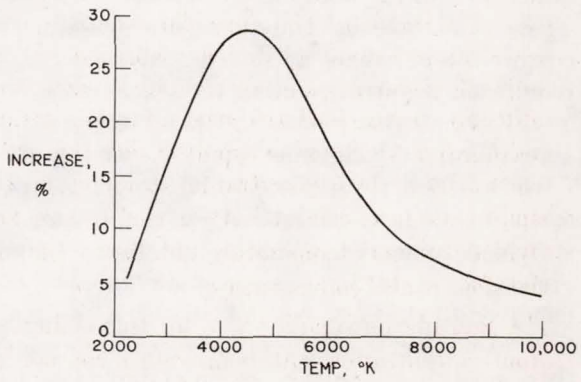

FIGURE I–8.—Increase in electron concentration produced by electrical interactions in cesium plasma for pressure of 1 atmosphere.

properties, and experiments have been conducted at Lewis to try to verify aspects of that theory that are in doubt or uncertain.

Consider first the heat conduction in a chemically reacting gas. If a gas that dissociates into two atoms or two monomeric molecules is confined between two walls with one at a higher temperature than the other, a temperature gradient is established between the walls, and heat is conducted because the molecules collide with one another and transfer kinetic energy in the usual fashion, as depicted in figure I–9. In addition, however, near the hotter plate there is a higher partial pressure of the atoms, and near the cold plate, the molecules predominate. Thus there is a concentration gradient established as well, and atoms diffuse from the hot region into the cool region where they recombine. When they recombine, they give up the heat of dissociation and consequently transfer heat. Contrariwise, the molecules diffuse in the opposite direction, so that there is no net flow of mass.

For the dissociation of a simple dimer A_2, it is not difficult at all to write the heat conductivity due to the chemical reaction:

$$\lambda_e=\lambda_f+\frac{\Delta H}{2}D'\frac{\dfrac{dC_A}{dr}}{\dfrac{dT}{dr}}$$

The total heat conductivity λ_e is the sum of two terms. The first is a frozen heat conductivity λ_f, which would be present as a result of collisions even in the absence of reactions. The second part is a result of the chemical reaction. The heat flux associated with the diffusion of the atoms or monomer can be calculated; each atom diffusing carries half the heat of the reaction, and the flux of atoms is simply a diffusion coefficient times the concentration gradient of the atom. The heat conductivity is simply this flux divided by the temperature gradient; the dimensions cancel conveniently.

A limiting maximum value for this change of atom concentration with temperature can be calculated with the assumption that the chemical reaction rate, in other words, the reversible dissociation, occurs so rapidly that, at every point

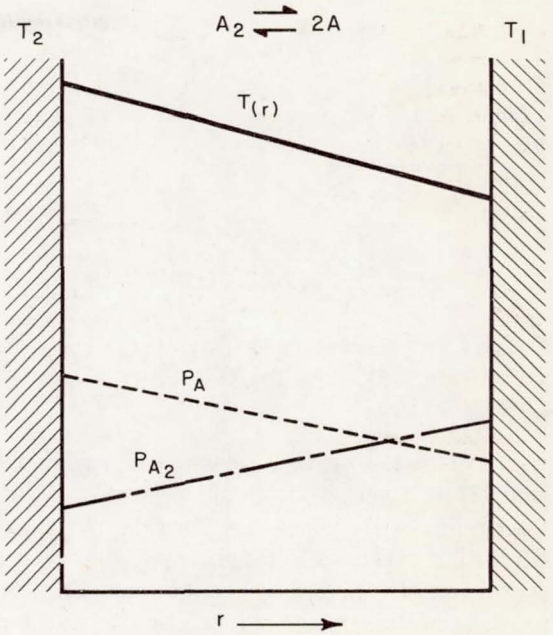

FIGURE I–9.—Heat conduction in a dissociating gas.

in the gas, chemical equilibrium exists. The result is

$$\lambda_e=\lambda_f+\frac{DP}{RT}\frac{\Delta H^2}{RT^2}\frac{X_A X_{A_2}}{(1+X_{A_2})^2}$$

Note that the chemical reaction term depends on the diffusive properties of the gas, very strongly on the heat of reaction (the square of the heat of reaction), and also on the mole or volume fractions of the atom and molecule, or monomer and dimer. The equation predicts that, at low temperature, the atom concentration will be very small and the reaction will not contribute to the heat transfer. When the temperature is high enough, the molecules will all be dissociated, and again the reaction will not affect the heat conductivity. A maximum should exist at some intermediate temperature.

Data for the dissociation of nitrogen tetroxide illustrate the result. Nitrogen tetroxide is convenient to study because it dissociates very rapidly and reversibly around room temperature to give two nitrogen dioxide molecules. In figure I–10, the lower dashed curve shows the conduc-

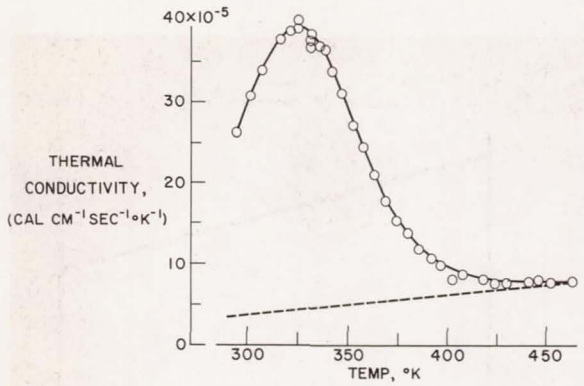

FIGURE I–10.—Thermal conductivity of nitrogen tetroxide —nitrogen dioxide system at pressure of 1 atmosphere.

tivity predicted in the absence of chemical reaction. It is about what would be expected for a heavy gas such as carbon dioxide. The solid curve has been calculated from the relation shown in the preceding equations. The data points represent measured values. At low temperature, when the gas is predominantly nitrogen tetroxide, the heat conductivity is low; it rises through a maximum and then declines again as the dissociation goes toward completion. The effect is not small. As a matter fact, the heat conductivity is 8 to 10 times what it would be in the absence of reaction. Indeed, at the maximum, the heat conductivity is more like that of a light gas, such as hydrogen or helium.

For nitrogen tetroxide, there is excellent agreement between theory and experiment. These computed properties also do an excellent job of correlating heat transfer from this same reacting mixture in a more practical sort of configuration; for example, a turbulent pipe flow, or heat transfer to a cylinder in a cross flow.

Also, of course, most practical cases involve much more complex gas mixtures. Hence, the theory has been worked out for mixtures involving any number of chemical reactions. The equation involves exactly the same terms, namely, diffusivities, heats of reaction, and compositions expressed in mole fractions. The ideas are exactly the same, but there are so many terms that a computer becomes useful. Indeed, this theory has been used to calculate the properties for a system of practical interest, namely, hydrogen-oxygen combustion products, over a wide range of variables of interest to rocket designers. NASA Special Publication SP–3011 by Svehla (see bibliography) contains both equilibrium thermodynamic properties and transport properties. These properties include heat conductivity and viscosity for the hydrogen-oxygen system consisting of 14 compositions ranging from pure hydrogen to pure oxygen for 45 temperatures at 100° intervals from 600° to 5000° K, and at 13 pressures ranging from 0.001 to 1000 atmospheres.

There are problems remaining; for example, consider the data on the Prandtl number of helium-air mixtures (fig. I–11). (These mixtures involve no chemical reaction.) The Prandtl number, that is, the specific heat times the viscosity divided by the thermal conductivity, is an important property in practical heat-transfer calculations. Figure I–11 shows that the Prandtl number of air is a little over 0.7 and that of helium is about 0.66, and many people have blithely assumed that the Prandtl numbers of the mixtures should lie somewhere between. This is clearly not so. Some of the mixtures have Prandtl numbers as low as 0.4 to 0.5 The solid line has been calculated according to the best theory available, the kind of theory incorporated in the calculations described for the hydrogen-oxygen mixtures. The theory predicts the gross effect rather well. However, appreciable errors between theory and experiment remain: For pure air,

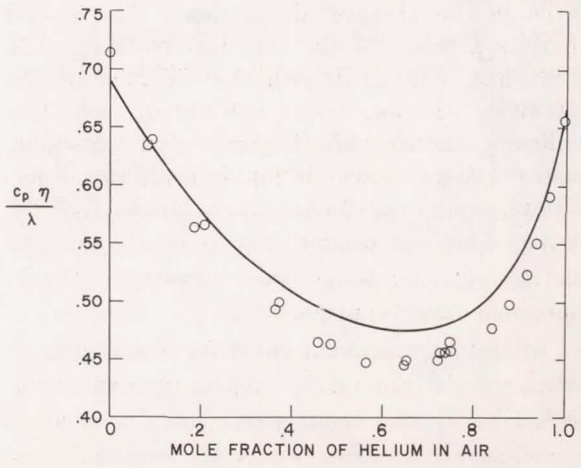

FIGURE I–11.—Prandtl number of helium-air mixtures.

errors of perhaps 4 percent and for the mixtures as much as 8 percent may be noted. Recently, a new theory was proposed that shows promise of explaining these discrepancies, and experiments are in progress at Lewis to test these hypotheses.

ATOMIZATION

For a rocket engine, the fuel and the oxidant often start out as liquids. Liquid is sprayed through an injector that consists of one or more nozzles. Then the spray of this reactant vaporizes rapidly in the hot environment, and the vapor burns as it mixes with the vapor of the other reactant. High-speed motion pictures of hydrogen-oxygen combustion at 20 atmospheres in an 8-inch-long transparent rocket engine show liquid-oxygen jets silhouetted by back lighting as they enter the combustion chamber. The gases are accelerating rapidly as the oxygen vaporizes and burns with hydrogen. Even though oxygen is a cryogenic liquid, the liquid state persists for considerable distance into the combustion zone. Photographs of other combustion systems, for example, hydrocarbon-oxygen and nitrogen tetroxide—hydrazine combustion, are similar except for the color of the radiation. Because it is very difficult to obtain photographs such as these, most of the photographic studies of sprays and drops are taken under cold-flow conditions, that is, in the absence of combustion. Slow-motion pictures of the sprays from different types of injector reveal qualitatively the gross differences in the sprays from the different injectors.

From a single photograph, as for impinging water jets as shown in figure I–12, the drops in a particular area of this spray can be counted and their size measured. Drops of similar sizes can be grouped, as in figure I–13, in this case, for about 5000 drops of the spray. While drops of 100 to 200 microns in diameter appear most frequently, a plot of the mass distribution as added shows that most of the mass is concentrated in drops of about 1000 microns in diameter. These large drops must be vaporized to convert most of the liquid mass to vapor. A machine that counts and sizes these drops and then groups them according to size relieves much of the tedium and difficulty from the task of counting thousands of drops.

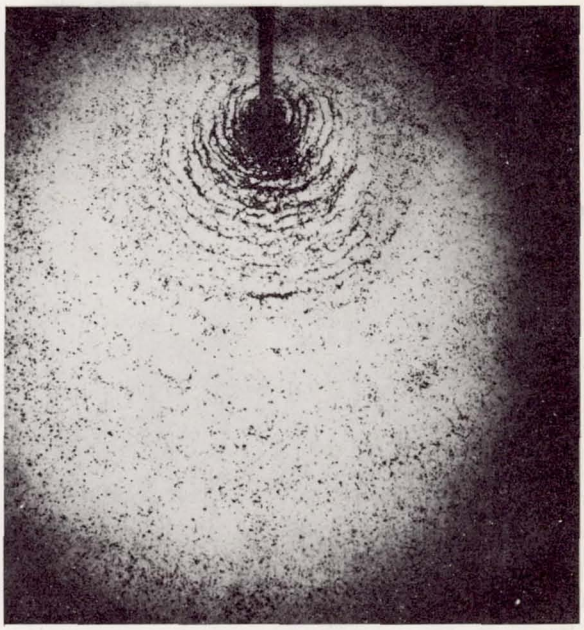

FIGURE I–12.—Spray from impinging water jets.

Also we have developed a computer program, or technique, for getting the best curve fit for the size distributions; and the resulting curves for the data are shown as the solid curve (fig. I–13). One of the difficulties in obtaining size distributions of this kind is to get a representation for the small drops because of the difficulties in photography. Also, a true mass distribution for the large drop sizes is difficult because it requires a long time to get a representative sample of the large drops that appear. For instance, the mass in the largest category measured represents only two drops. The computed curve indicates the distribution of mass that would be expected from a much larger sample of drops.

Drop size data of the sort just illustrated have been measured for various injector types, such as straight jets, concentric tubes, and swirl atomizers, as well as for these impinging jets. The data have been obtained under a variety of

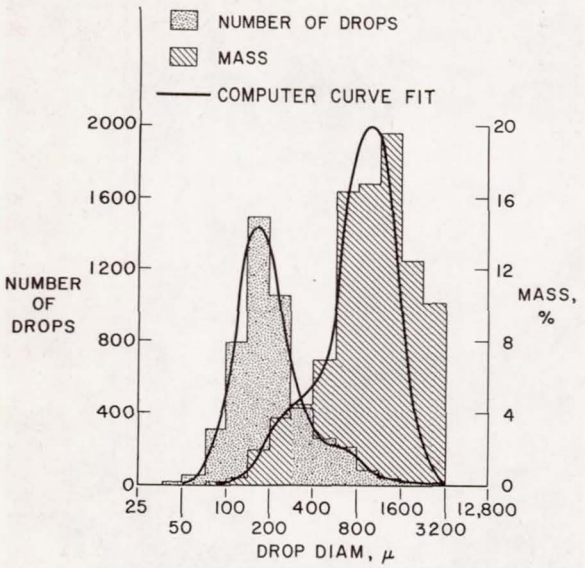

FIGURE I–13.—Drop size distribution for impinging jet spray.

environmental conditions, such as different ambient pressures and gas velocities; for a variety of fluids, such as water, glycerine, ethanol, heptane, or other hydrocarbons; and for a variety of flow conditions, as different injector geometries, different length-to-diameter ratios of the hole, different diameters, and different flow velocities through these holes. The bibliography lists a number of reports on this work. In making tests of this sort, it was found that the most important single criterion for producing small drops is a small orifice diameter.

VAPORIZATION

It is possible to calculate the rate at which drops of known size vaporize if the standard equations for heat, mass flow, and momentum transfer are used. The complexity of the processes involved requires a computer to make such calculations. The results of such a calculation are illustrated in figure I–14 for a single stationary drop of *n*-decane in a steady flow of heated air. The drop is heated rapidly to its wet bulb temperature while its radius is decreasing as vaporization progresses. Experimental points are also shown for both the temperature of the drop and the drop radius. These experimental points were obtained for a decane drop that was suspended on a thermocouple and photographed to obtain its size. The calculations for this case are substantially in agreement with the measured data. As shown in the figure, these calculations include vaporization that occurs while the drop is being heated; this is a part of the calculation that is often omitted in simplified analyses. In the actual case for rocket combustion, and in many other cases, the acceleration of the gases as the drops vaporize and burn must be included; because of the drag on the drops, they will also be accelerated. Results of calculations for the case of heptane drops are shown in figure I–15; this calculated history of a drop may be described as follows: The drop heats rapidly to its wet bulb temperature, in this case 845° R. The heating period of the drop requires about 20 percent of the total distance required to vaporize the drop. Meanwhile, the radius of the drop initially increases slightly by thermal expansion and then decreases rapidly as vaporization progresses. The change in radius occurs simultaneously with the temperature increase. The velocity of the gas in the combustion chamber increases from zero at the injector end to 790 feet per second, for example, near the nozzle as drops vaporize and the vapor burns. Now, because of this gas flow, the drop experiences a drag force, causing it to accelerate until it approaches the gas velocity. The difference in velocity between the surrounding gas and the drop is important in determining the drag and

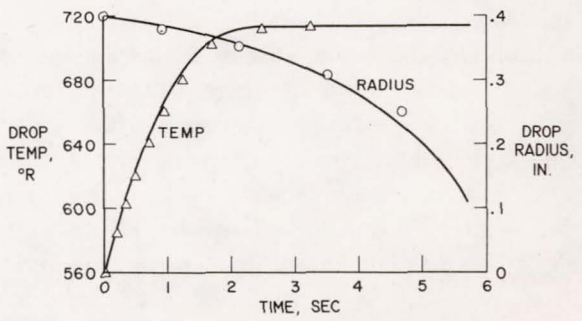

FIGURE I–14.—Calculated and experimental drop histories in *n*-decane. Air temperature, 1070° R; air flow, 90 inches per second.

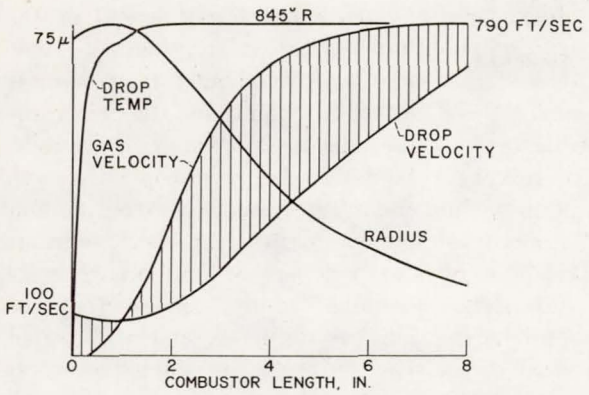

FIGURE I–15.—Calculated vaporization process for uniform heptane drops.

vaporization. The lifetime of a 75-micron drop in a typical case is of the order of 5 milliseconds.

Calculations like these have been carried out for a variety of conditions, that is, for different pressures, injection velocities, drop sizes, and size distributions, and for different liquids as well. As a result, the combustion rate of a spray can be calculated with the assumption that vaporization is the rate-controlling step. The results seem to correlate with rocket performance measurements under many conditions. Of course, the reaction is exceedingly complex, and under many conditions, other processes may control the rate of combustion.

Studies like these on atomization and vaporization may have general applicability to other systems where the same processes are taking place. One example is that of an industrial boiler that uses the combustion of fuel oil as a source of heat. Here, the drop distribution data and the vaporization studies might both be of use in designing an efficient burner.

IGNITION

In systems of the rocket type, atomization and vaporization occur in the presence of active combustion so that a flame is always present to ignite the fuel-oxidant mixture. However, in some systems, this is not so. For example, in the hypersonic ramjet illustrated in figure I–4, fuel is injected into a supersonic heated airstream. (The air is captured by an inlet, not shown in the figure.) No ignition sources are provided, so that ignition must take place simply as a consequence of the high temperature. A somewhat similar situation exists in diesel engine combustion where again the fuel is sprayed into high-temperature air, and ignition occurs spontaneously.

For some cases, quite a lot is known about the chemistry of the processes that lead to such thermal ignition. For example, the reaction between hydrogen and oxygen is fairly well understood, and, incidentally, hydrogen is the fuel that is proposed for use in a hypersonic ramjet.

The stoichiometric relation for the burning of hydrogen is

$$H_2 + \frac{1}{2} O_2 \rightarrow H_2O$$

Thermodynamically, the reaction is

$$H_2 + O_2 \text{ mixture} \rightarrow \text{Equilibrium mixture of } H_2, O_2, H, O, OH, H_2O$$

But the actual chemical reactions for the burning of hydrogen, like many combustion processes, are complicated and include chain-branching reactions as well as recombination reactions. First, there is the chain branching, or ignition phase, in which four reactions dominate the behavior and build up large free-radical concentrations; thus

$$\text{I. } H_2 + O_2 \rightarrow 2\,OH$$
$$\text{II. } OH + H_2 \rightarrow H_2O + H$$
$$\text{III. } H + O_2 \rightarrow OH + O$$
$$\text{IV. } O + H_2 \rightarrow OH + H$$

Reaction I is the "initiation" reaction in which two hydroxyl radicals are produced from hydrogen and oxygen molecules. After a very short initial phase, the next three reactions quickly take over the process and dominate the ignition phase of the combustion. In reaction II, a hydroxyl radical reacts with a hydrogen molecule and is replaced by a different free radical, a hydrogen atom. It is the production of this hydrogen atom that is really the key to the chain-branching character of hydrogen combustion, because this atom then goes into the next step to react with the oxygen molecule to regenerate hydroxyl. An oxygen atom is also formed. The oxygenation, in turn, regenerates a hydrogen

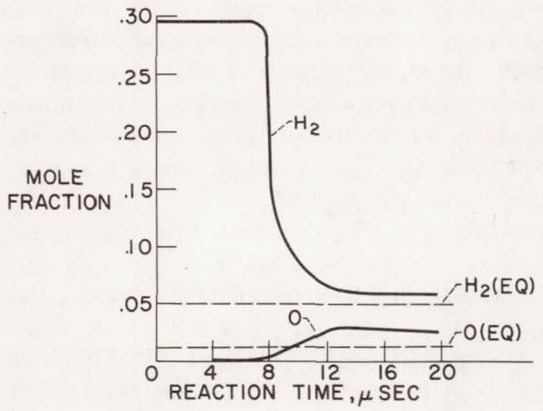

FIGURE I–16.—Characteristics of hydrogen-oxygen ignition reaction for hydrogen burning in air at 1 atmosphere and 1700° K.

atom that can start reaction III over again and, in addition, forms still another hydroxyl radical to start again at step II. Thus, the concentration of free radicals builds up like an avalanche during this early part of the reaction. Another important characteristic of this ignition phase is that these reactions are nearly thermoneutral; there is very little heat either released or absorbed in the course of these reactions.

After the free-radical concentrations build up to fairly high levels, the second phase of the reaction starts. The radicals begin to react with themselves, recombining to produce heat and the final products.

A typical example of the time for the ignition phase is shown in figure I–16 for hydrogen burning in air at 1 atmosphere and at an initial temperature of 1700° K. Assume that this mixture has been heated very suddenly to 1700° K. In other words, only the chemistry is being considered, and no allowance at all is being made for the time required to mix and heat the two gases. These calculated results show what happens as a function of time after the temperature is raised. The calculations were performed on a computing machine to integrate the differential rate equations based on all the reactions involved, that is, both the chain-branching reactions I to IV and the recombination reactions as well. For a while, nothing appears to happen to the hydrogen concentration; then there is an abrupt drop. Simultaneously, the oxygen-atom concentration quickly rises, which constitutes the end of the ignition phase of the reaction. Experiments show that at this same time, at about 8 microseconds under these particular conditions, the free radicals begin to become detectable. For example, hydroxyl can be detected spectroscopically, both in absorption and in emission. Moreover, the first temperature change occurs. In short, various kinds of physical evidence of ignition correlate with these calculated results. After 8 microseconds, ignition has occurred, and the second phase of the reaction begins in which the excess concentrations of free radicals are cleaned up by recombination. This takes a much longer time, because the recombination reactions are much slower than the chain-branching reactions. Figure I–16 indicates the final equilibrium mole fractions of the hydrogen molecule and the oxygen atom that would eventually be obtained.

In figure I–17 the oxygen atom concentration during the ignition phase is plotted logarithmically to show more detail. At very short times and for a very brief period, the initiation of the reactions occurs, and after that the oxygen atom concentration rises in a strictly exponential fashion up to the ignition time of about 8 microseconds. Because the four reactions that dominate the ignition period are thermoneutral, and because up to the end of the ignition period the reactant concentrations are hardly changed at all, it is possible to make an analytic solution

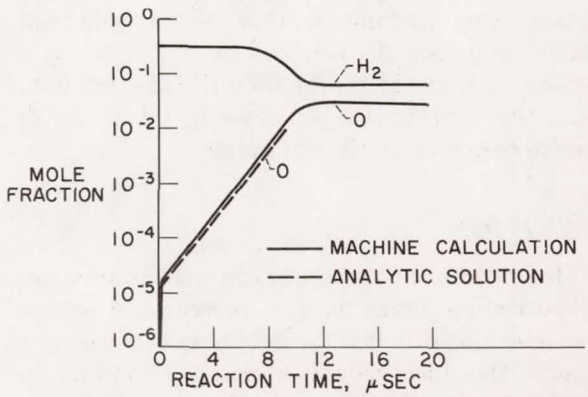

FIGURE I–17.—Semilogarithmic plot of characteristics of hydrogen-oxygen ignition reaction for hydrogen burning in air at 1 atmosphere and 1700° K.

of the differential equations based only on those four reactions. This solution is indicated in figure I–17 by a dashed line. These analytic solutions are very complex algebraic expressions, and the dashed line represents approximations to them developed by R. S. Brokaw. They are excellent approximations to the full machine calculation that is represented by the solid line. Therefore, there is a readily available means of calculating ignition delays for hydrogen-oxygen without going to the complexity of a calculating machine program.

An excellent set of data from the General Electric Research Laboratory, Schenectady, New York, permits comparison of these theoretical estimates with experimental ignition delay times (fig. I–18). The experimental data are represented by circles, and the results of the approximate analytic solution are represented by the solid lines. Agreement is excellent for a 10 000-fold range in hydrogen-oxygen ratio and over a large range of temperature. This good agreement was only possible, though, because of about 60 years of basic research into the mechanism of hydrogen combustion, which produced the detailed information about the elementary steps of the reaction and reliable rate constants for each of those steps.

In order to make such calculations for other systems, for example, the ignition of methane,

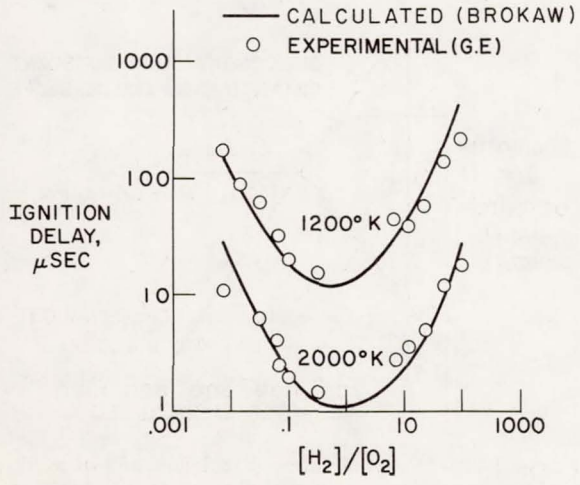

FIGURE I–18.—Hydrogen-oxygen ignition delays. Pressure, approximately 1 atmosphere.

the reaction in question must proceed in this same chain-branching manner, with the first steps being thermoneutral. Also, detailed information about the chemical kinetics must be available. Incidentally, at present, such information exists for only one or two other fuels besides hydrogen. There is room here for a great deal of challenging research.

CHEMICAL REACTION RATES

Consider now the problem of expanding an equilibrium mixture of high-temperature gases out the exhaust nozzle. From the viewpoint of thermodynamics, two extreme limits can be calculated. In one case, the reaction rates may be so very slow that the chemical composition remains the same as that in the combustion chamber, the gases merely cool as they expand, and the thermal energy is converted into directed kinetic energy. At the other extreme, the chemical reaction rates may be very fast, so that, locally, equilibrium exists as the gases proceed out through the nozzle. In this case, some of the chemical energy, bound up in the dissociated free radicals and so forth, can be converted into thrust in the expansion process. Of course, thermodynamics cannot state which one of these extremes will actually exist. To calculate what the true state of affairs will be, information on chemical kinetics and chemical reaction rates is required.

The experimental techniques that can be used to obtain this rate information can be illustrated by describing a set of shock-tube studies on the dissociation and the recombination of carbon dioxide—dissociation into carbon monoxide and oxygen atoms and then the recombination of carbon monoxide and oxygen to reform carbon dioxide. A shock tube is like a temperature switch. By throwing the switch, the chemist heats a gas from room temperature to thousands of degrees. Furthermore, events happen so quickly in the shock tube that there is not time for heat transfer or diffusion to the walls; therefore, wall effects are completely absent.

Figure I–19 is a photograph of a typical shock-tube installation that shows the general

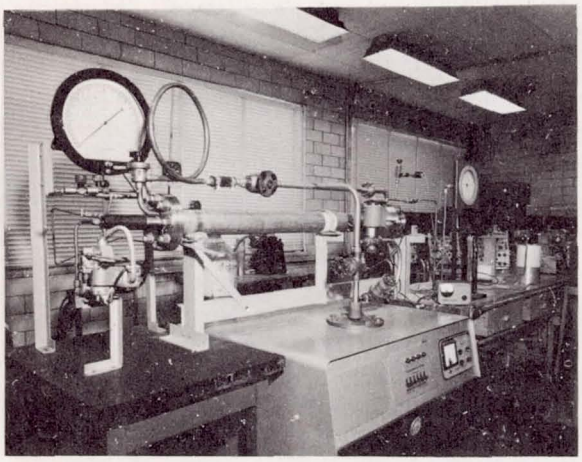

FIGURE I–19.—Shock tube for dissociation studies.

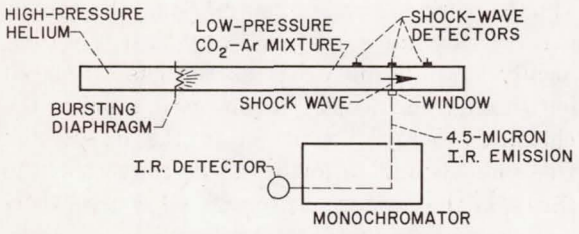

FIGURE I–20.—Dissociation of carbon dioxide behind incident shock waves.

scale of the equipment. It is a pipe about 15 to 20 feet long and typically 2 to 4 inches in diameter. The features of operation are shown as a schematic diagram (fig. I–20). The tube is divided into two chambers by a diaphragm of plastic or metal. In the smaller chamber (the driver section) is a high-pressure gas, usually helium. The gas mixture, which is to be heated by the shock wave (in this case a mixture containing carbon dioxide heavily diluted with argon), is in the other longer chamber (the driven section of the tube) and at a much lower pressure. The only purpose of all the argon is to prevent the temperature from changing appreciably as the reaction proceeds.

When the pressure in the driver is raised high enough to burst the diaphragm, the shock wave is formed and travels toward the right at several times the speed of sound. Thin-film resistance thermometers determine the velocity of the shock wave by detecting its passage at a series of fixed points along the tube. The temperature and pressure behind the shock wave, in other words, the reaction conditions, are calculated from this measured velocity. The other observation is the infrared emission from the hot carbon dioxide behind the shock front; radiation at 4.5 microns is selected with a monochromator and its intensity is measured with a special liquid-nitrogen-cooled detector. The signal from the detector is displayed on an oscilloscope.

Figure I–21 shows typical data; it is reproduced from a photograph of the oscilloscope

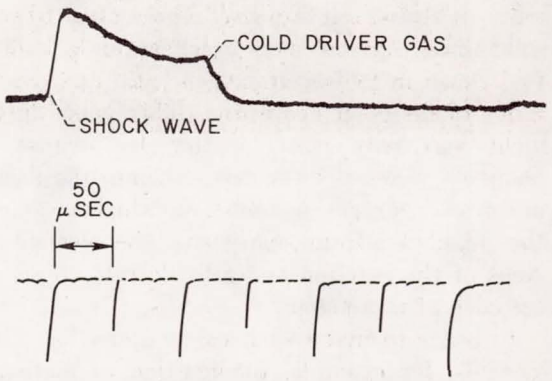

FIGURE I–21.—Infrared emission from dissociating carbon dioxide.

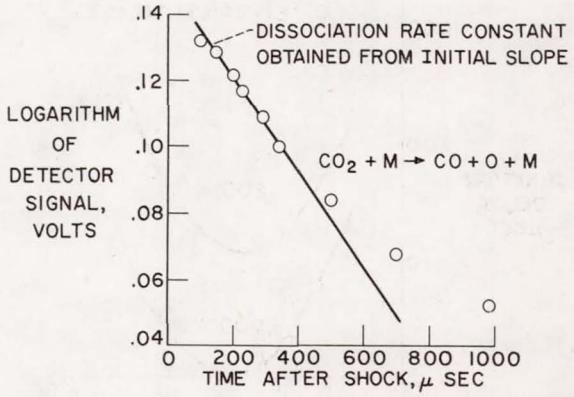

FIGURE I–22.—Decay of infrared emission of carbon dioxide dissociation behind incident shock. Mixture, 0.10 carbon dioxide—0.90 argon; temperature, 3240° K; pressure, 0.4 atmosphere.

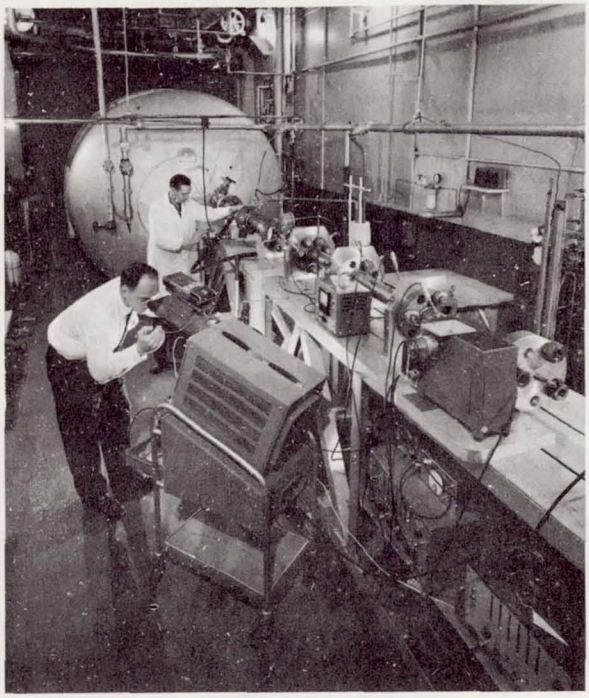

FIGURE I–23.—Shock tube for recombination studies.

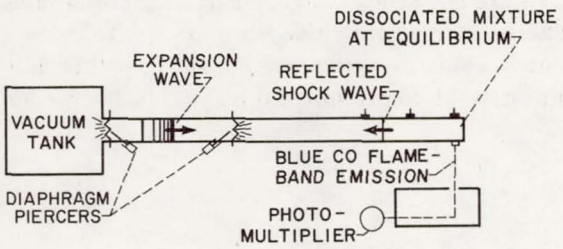

FIGURE I–24.—Recombination of carbon monoxide and oxygen in expansion waves.

screen and shows the signal from the infrared detector. When the shock wave passes the window and the carbon dioxide is heated, the emission intensity increases very quickly to a high value; as the carbon dioxide dissociates, the intensity of the emission dies away toward chemical equilibrium. Then there is a very abrupt drop back to zero emission intensity. The drop corresponds to the time at which the cold helium driver gas passed the window.

To translate this sort of information into reaction rate constants, the logarithm of the detector voltage is plotted against the time after the shock passed the window (fig. I–22). The initial slope of the data is then directly related to the dissociation rate constant for the assumption that the dissociation involves carbon dioxide colliding with a molecule M to produce carbon monoxide, oxygen, and M again. The linear period in figure I–22 provides a reliable slope, and then the data at later times deviate from that straight line as the mixture approaches chemical equilibrium. Dissociation rate constants from data of this kind have been obtained over the temperature range from about 3000° to 5000° K and for various mixtures of carbon dioxide and argon.

A revised apparatus to measure recombination rates is shown in figures I–23 and 24. Both a large vacuum tank and an extra diaphragm have been added to the other end of the driver. Furthermore, the incident shock wave is allowed to reflect from the wall at the end of the tube before measurements are recorded. The reflected shock is used for the recombination studies because there is more time available behind the reflected wave to achieve a known chemical equilibrium of partly dissociated gases. The vacuum tank generates an expansion wave that cools the hot equilibrium sample of gas by adiabatic expansion and thus starts the recombination processes. Proper timing is achieved with the diaghragm piercers, which allow the hot gases in the tube to flow into the large vacuum. The recombination reaction is followed by observation of the so-called carbon monoxide flame-band emission. This emission is the characteristic blue light that is emitted from a mixture of gases whenever carbon monoxide and oxygen atoms are both simultaneously present; it is seen in the mantle of an ordinary gas flame. A monochromator isolates the proper wavelength, and it is detected by the photomultiplier.

A typical oscillogram is shown in figure I–25. The upper trace is a pressure record at the end of the tube; when the reflected wave arrives, the pressure suddenly jumps, levels off for a long

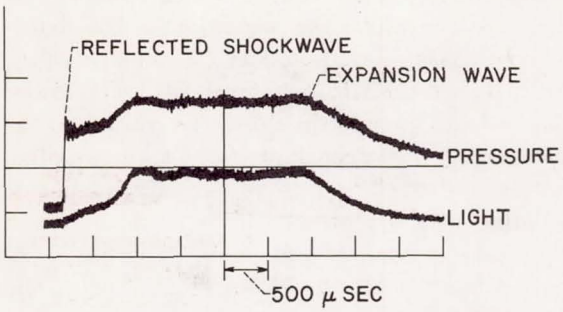

FIGURE I–25.—Carbon monoxide flame-band emission from recombining carbon monoxide and atomic oxygen.

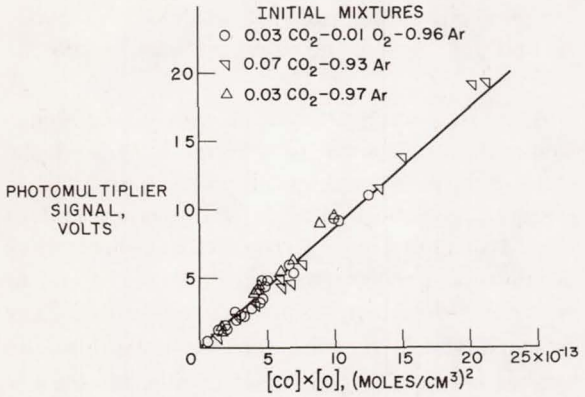

FIGURE I–26.—Flame-band intensity in equilibrium mixtures behind reflected shocks. Temperature, 3000° to 3600° K; pressure, 8 to 22 atmospheres; $CO+O \rightarrow CO_2^* \rightarrow CO_2 + h\nu$.

period of time, and then, when the expansion wave arrives, falls. The lower trace shows the intensity of the flame-band emission. It also rises when the reflected shock arrives and achieves a constant value that is assumed to indicate chemical equilibrium. It drops when the expansion wave arrives, which indicates that the carbon monoxide and oxygen atom are disappearing, that is, recombining. Several years ago, it was discovered that the flame-band emission is directly proportional to the product of carbon monoxide and oxygen atom concentrations. The intensity at the equilibrium condition, that is, the height of the flat part of the trace, is measured and plotted against the calculated product of carbon monoxide and oxygen atom concentrations from the computations program described earlier (fig. I–26). The result provides a satisfactory calibration and indicates what the conditions are prior to the expansion of the equilibrium mixtures. It also establishes the fact that there is a tool for observing the product of carbon monoxide and oxygen concentrations after the expansion starts and that, in this way, the course of the recombination reaction can be followed. Figure I–27 is a typical result for one run. The curve labeled "Shifting equilibrium" was calculated with the equilibrium computations program previously described. For the upper curve, the mole fractions remain fixed, but the concentrations change because the pressure changes. The dashed line represents the experimental data. Analysis of these results provides the recombination rate constants; figure I–28 shows some of the results. The assumed recombination reaction is shown at the top of the figure, that is, it is a three-body reaction in which carbon monoxide and oxygen atom react in the presence of an inert molecule M, whose function is to carry off the energy of recombination. Data points are shown for two different concentrations of carbon dioxide in argon. The experiments were carried out over a temperature range of about 2800° to 3600° K. The two upper solid lines are not at all in agreement with our results. These are recombination rate constants extrapolated from measurements made by other laboratories at low temperatures. This poor com-

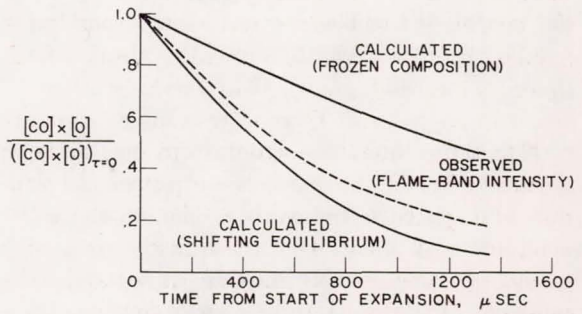

FIGURE I–27.—Recombination of carbon monoxide and atomic oxygen during expansion of equilibrium mixture of carbon dioxide, carbon monoxide, atomic oxygen, molecular oxygen, and argon. Starting conditions: temperature, 3498° K; pressure, 8.66 atmospheres.

parison stresses the importance of measuring these rate constants at the high temperatures of interest; these long extrapolations are risky.

If the recombination actually does occur as indicated, then it is exactly the reverse of the process of dissociation, which has already been studied by an independent technique. If the two processes are the exact reverse of one another, there is a special relation between them: the equilibrium constant. Therefore, since the dissociation rate constants k_d were measured in previous work, and since the equilibrium constant is known from thermodynamic data, the previous measurements can be used to calculate recombination rate constants. These are indicated by the solid line (fig. I–28), and there is quite good agreement with the directly measured recombination rate constant. While it is a general principle to assume that recombination is just the reverse of dissociation, in recent years there has been considerable doubt about its validity in these high-temperature reactions. For carbon dioxide, the experimental evidence is that the principle holds.

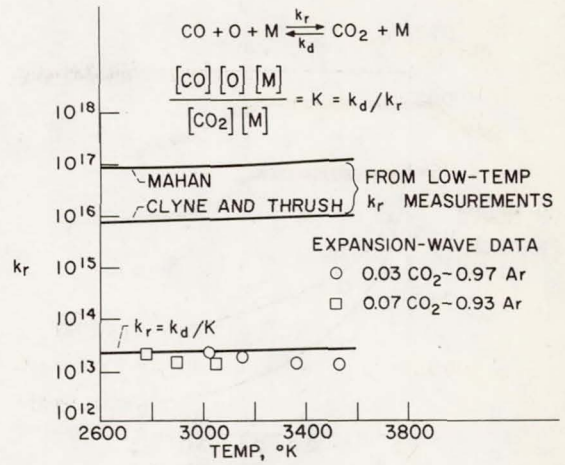

FIGURE I–28.—Recombination rate constants of carbon monoxide and atomic oxygen.

EFFECTS OF REACTION RATE ON NOZZLE FLOWS

When good rate-constant data are available, a much better job of predicting the performance of a rocket engine should be possible compared with the predictions from thermodynamics alone. However, the calculation including chemical kinetics is much more difficult than the purely thermodynamic calculations, since in place of the nonlinear algebraic equations of thermodynamics, one now must contend with the nonlinear differential equations of chemical kinetics. The United Aircraft Corporation under contract to NASA has written a program to do this type of kinetic calculation for a one-dimensional nozzle. It can treat as many as 15 simultaneous reactions, and for each of these reactions, it can consider the effect of temperature on the rate constant. Results of this calculation procedure can be compared with some data for the stoichiometric hydrogen-air system where the combustion gases are flowing through a nozzle (fig. I–29). The temperature of the gases as they pass

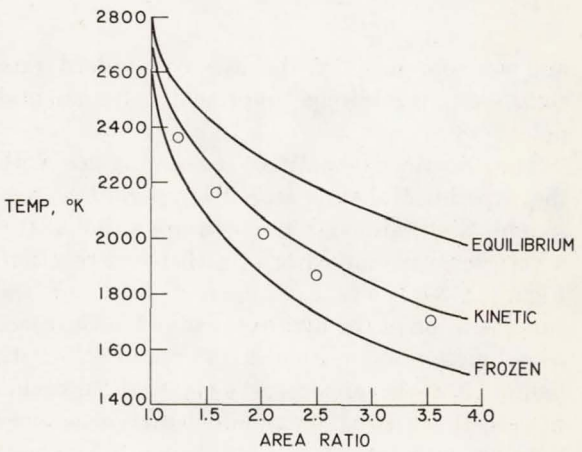

FIGURE I–29.—Effect of chemical kinetics on temperature for stoichiometric hydrogen-air system. Combustion pressure, 3.6 atmospheres.

through the nozzle provides an indication of the overall state of the gas. The upper curve represents the temperature that would exist in the nozzle if chemical equilibrium were attained at each point in the nozzle. The lower curve is also a thermodynamic calculation; however, here it has been assumed that the composition remains fixed at the composition in the combustion chamber. The middle curve, labeled "Kinetic," was calculated with the United Aircraft program

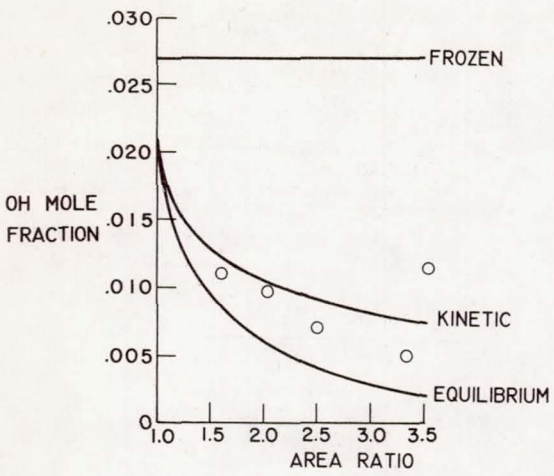

FIGURE I–30.—Effect of chemical kinetics on hydroxyl radical concentration for stoichiometric hydrogen-air system. Combustion pressure, 3.6 atmospheres.

and was obtained by the use of standard rate constants; the circles represent experimental points.

The kinetic calculations seem to agree with the experimentally measured temperatures reasonably well, although temperature is not really a very sensitive indicator of a chemical reaction. Figure I–30 shows experimental data for the concentration of the hydroxyl radical in the gases as a function of position in the nozzle. As with figure I–29, the upper curve, labeled "Frozen," represents a thermodynamic calculation as does the lower curve marked "Equilibrium." The middle curve, which reasonably well approximates the experimental measurements, was obtained from the United Aircraft computer program again using standard rate constants.

Figures I–29 and 30 showed substantial agreement between theoretical calculations and a controlled laboratory experiment. Figure I–31 shows the case of a practical hardware item, the hydrogen-oxygen rocket engine used for the Centaur upper stage. Vacuum specific impulse, the thrust produced per unit mass flow rate of propellant, is plotted as a function of the weight ratio of oxygen to hydrogen. The curves are the result of theoretical calculation; the circles represent experimental points that have been corrected both for combustion inefficiencies and for nozzle inefficiencies such as friction. The discrepancy between kinetic calculation and corrected data is not too serious since there is some uncertainty in making these corrections.

EFFECTS OF REACTION RATE ON HEAT CONDUCTION

A theory for calculating heat conductivities for reacting gases with intermediate reaction rates has also been developed. The heat conductivity depends first on the chemical reaction rates, but in addition it depends on the geometry and the scale of the system. Thus heat conductivity cannot be considered solely as a gas property. Referring to figure I–10, for the thermal conductivity of the nitrogen tetroxide—nitrogen dioxide dissociating system shows that, at atmospheric pressure, the experimental data agree very well with the chemical equilibrium curve. Figure I–32 presents similar data at 296° K, this time as a function of pressure, from about 0.05 atmosphere to atmospheric pressure. The upper dashed curve was calculated by assuming that rates are very fast so that the gas is locally in chemical equilibrium. The lower dashed curve is the other extreme assumption—

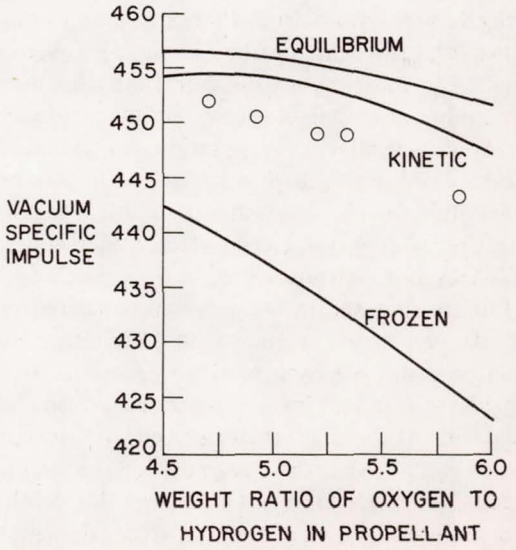

FIGURE I–31.—Centaur rocket engine performance.

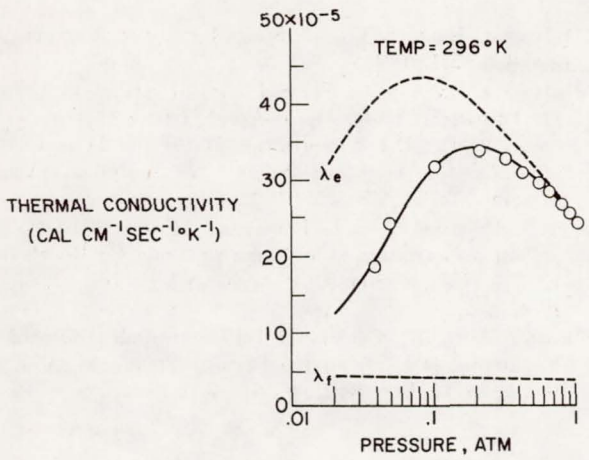

FIGURE I–32.—Effect of chemical reaction rate on thermal conductivity of nitrogen tetroxide—nitrogen dioxide system. Temperature, 296° K.

that the rates are very slow. Note that, at atmospheric pressure, the experimental data are very close to the equilibrium curve, but that they fall away as the pressure decreases. The solid curve has been calculated from the theory we have developed by using experimental rate constants determined by shock-tube techniques and also from acoustical measurements.

CONCLUDING REMARKS

In summary, first, chemical thermodynamics for multicomponent systems have been discussed. The ideal performance of rockets has been emphasized, but the techniques are suitable for obtaining chemical composition and thermodynamics of any complex gas phase reaction equilibrium. Second, the transport properties of gases have been discussed. Although our interest stems from rocket cooling and propellant vaporization, our understanding of heat conductivity and viscosity can be applied to any gases involved in industrial heat-transfer and cooling processes. Third, atomization and vaporization have been discussed, again in terms of preparing propellants for combustion, but the same processes occur in industrial furnaces or even paint spray guns, and the same techniques can be used to obtain droplet histories. Fourth, spontaneous thermal ignition in connection with the hypersonic ramjet engine has been discussed, but spontaneous ignition occurs in diesel engines and perhaps also in knocking gasoline engines. Finally, chemical kinetics in terms of exhaust nozzle losses have been discussed, and it was shown how shock tubes can be used to obtain reaction-rate data. But the shock tube is a versatile tool for clean studies of high-temperature phenomena and may be applicable to cracking, isomerization, and other reactions.

BIBLIOGRAPHY

Chemical Thermodynamics

GORDON, SANFORD; and ZELEZNIK, FRANK J.: A General IBM 704 or 7090 Computer Program for Computation of Chemical Equilibrium Compositions, Rocket Performance, and Chapman-Jouguet Detonations. Supplement I—Assigned Area-Ratio Performance. NASA TN D-1737, 1963.

MCBRIDE, BONNIE J.; HEIMEL, SHELDON; EHLERS, JANET G.; and GORDON, SANFORD: Thermodynamic Properties to 6000° K for 210 Substances Involving the First 18 Elements. NASA SP-3001, 1963.

ZELEZNIK, FRANK J.; and GORDON, SANFORD: A General IBM 704 or 7090 Computer Program for Computation of Chemical Equilibrium Compositions, Rocket Performance, and Chapman-Jouguet Detonations. NASA TN D-1454, 1962.

ZELEZNIK, FRANK J.; and GORDON, SANFORD: Equilibrium Computations for Multicomponent Plasmas. NASA TN D-2806, 1965.

Transport Properties

BAKER, CHARLES E.; and BROKAW, RICHARD S.: Thermal Conductivities of Ordinary and Isotopically Substituted Polar Gases and Their Equimolar Mixtures. J. Chem. Phys., vol. 43, no. 10, Nov. 15, 1965, pp. 3519–3528.

BROKAW, RICHARD S.: Correlation of Turbulent Heat Transfer in a Tube for the Dissociating System $N_2O_4 \rightleftarrows 2NO_2$. NACA RM E57K19a, 1958.

BROKAW, RICHARD S.: Thermal Conductivity of Gas Mixtures in Chemical Equilibrium II. J. Chem. Phys., vol. 32, no. 4, Apr. 1960, pp. 1005–1006.

BROKAW, RICHARD S.: Alignment Charts for Transport Properties, Viscosity, Thermal Conductivity, and Diffusion Coefficients for Nonpolar Gases and Gas Mixtures at Low Density. NASA TR R-81, 1960.

BROKAW, RICHARD S.: Approximate Fomulas for Viscosity and Thermal Conductivity of Gas Mixtures. NASA TN D-2502, 1964.

BROKAW, RICHARD S.; SVEHLA, ROGER A.; and BAKER, CHARLES E.: Transport Properties of Dilute Gas Mixtures. NASA TN D-2580, 1965.

BUTLER, JAMES N.; and BROKAW, RICHARD S. Thermal Conductivity of Gas Mixtures in Chemical Equilibrium. J. Chem. Phys., vol. 26, no. 6, June 1957, pp. 1636–1643.

COFFIN, KENNETH P.; and O'NEAL, CLEVELAND, JR.: Experimental Thermal Conductivities of the $N_2O_4 \rightleftarrows 2NO_2$ System. NACA TN 4209, 1958.

SVEHLA, ROGER A.: Estimated Viscosities and Thermal Conductivities of Gases at High Temperatures. NASA TR R-132, 1962.

SVEHLA, ROGER A.: Thermodynamic and Transport Properties for the Hydrogen-Oxygen System. NASA SP-3011, 1964.

SVEHLA, ROGER A.; and BROKAW, RICHARD S.: Thermodynamic and Transport Properties for the $N_2O_4 \rightleftarrows 2NO_2 \rightleftarrows 2NO+O_2$ System. NASA TN D-3327, 1966.

Sprays

BITTKER, DAVID A.: Effect of Ambient Air Velocity on Atomization of Two Impinging Water Jets. NASA TN D-2087, 1964.

CLARK, BRUCE J.: Breakup of a Liquid Jet in a Transverse Flow of Gas. NASA TN D-2424, 1964.

FOSTER, HAMPTON H.; and HEIDMANN, MARCUS F.: Spatial Characteristics of Water Spray Formed by Two Impinging Jets at Several Jet Velocities in Quiescent Air. NASA TN D-301, 1960.

HEIDMANN, MARCUS F.; PRIEM, RICHARD J.; and HUMPHREY, JACK C.: A Study of Sprays Formed by Two Impinging Jets. NACA TN 3835, 1957.

HEIDMANN, MARCUS F.: Photography and Analysis of Time Variation in Drop Size Distribution of a Liquid Spray. Proceedings of the Fifth International Congress on High Speed Photography, J. S. Courtney-Pratt, ed., Soc. Motion Picture and Television Engineers, 1962, pp. 519-524.

HEIDMANN, MARCUS F.; and FOSTER, HAMPTON H.: Effect of Impingement Angle on Drop-Size Distribution and Spray Pattern of Two Impinging Water Jets. NASA TN D-872, 1961.

INGEBO, ROBERT D.; and FOSTER, HAMPTON H.: Drop-Size Distribution for Crosscurrent Breakup of Liquid Jets in Airstreams. NACA TN 4087, 1957.

INGEBO, ROBERT D.: Drop-Size Distributions for Impinging-Jet Breakup in Airstreams Simulating the Velocity Conditions in Rocket Combustors. NACA TN 4222, 1958.

MORRELL, GERALD; and POVINELLI, FREDERICK P.: Breakup of Various Liquid Jets by Shock Waves and Applications to Resonant Combustion. NASA TN D-2423, 1964.

Vaporization

DEJUHASZ, KALMAN J., ed.: Spray Literature Abstracts. Vol. I, ASME, 1959.

DEJUHASZ, KALMAN J.: Spray Literature Abstracts, Vol. II. Druckerei Winter (Heidleberg), 1964.

INGEBO, ROBERT D.: Vaporization Rates and Drag Coefficients for Isooctane Sprays in Turbulent Air Streams. NACA TN 3265, 1954.

PRIEM, RICHARD J.; and HEIDMANN, MARCUS F.: Propellant Vaporization as a Design Criterion for Rocket-Engine Combustion Chambers. NASA TR R-67, 1960.

WIEBER, PAUL R.: Calculated Temperature Histories of Vaporizing Droplets to the Critical Point. AIAA J., vol. 1, no. 12, Dec. 1963, pp. 2764–2770.

Ignition

BELLES, FRANK E.; and LAUVER, MILTON R.: Effects of Concentration and Vibrational Relaxation on Induction Period of Hydrogen-Oxygen Reaction. NASA TN D-2540, 1964.

BELLES, F. E.; and LAUVER, M. R.: Origin of OH Chemiluminescence During the Induction Period of the H_2-O_2 Reaction Behind Shock Waves. J. Chem. Phys., vol. 40, no. 2, Jan. 15, 1964, pp. 415-422.

BROKAW, RICHARD S.: Analytic Solutions to the Ignition Kinetics of the Hydrogen-Oxygen Reaction. NASA TN D-2542, 1964.

MOMTCHILOFF, I. N.; TABACK, E. D.; and BUSWELL, R. F.: Kinetics in Hydrogen-Air Flow Systems: I. Calculation of Ignition Delays for Hypersonic Ramjets. Ninth Symposium (International) on Combustion, W. G. Berl, ed., Academic Press, 1963, pp. 220–230.

WHITE, DONALD R.; and MOORE, GEORGE E.: Structure of Gaseous Detonation. IV. Induction Zone Studies in H_2-O_2 and CO-O_2 Mixtures. Tenth Symposium (International) on Combustion, Combustion Institute, 1965, pp. 785–795.

Chemical Kinetics

BRABBS, THEODORE A.; BELLES, FRANK E.; and ZLATARICH, STEVEN A.: Shock-Tube Study of Carbon Dioxide Dissociation Rate. J. Chem. Phys., vol. 38, no. 8, Apr. 15, 1963, pp. 1939–1944.

BRABBS, THEODORE A.; and BELLES, FRANK E.: Contact-Surface Tailoring in Real Shock Tubes. NASA TN D-3043, 1965.

CLYNE, M. A. A.; and THRUSH, B. A.: Mechanism of Chemiluminescent Combination Reactions Involving Oxygen Atoms. Roy. Soc. (London) Proc., vol. 269, no. 1338, Sept. 25, 1962, pp. 404-418.

LAUVER, MILTON R.; HALL, JERRY L.; and BELLES, FRANK E.: Shock-Tube Gas Temperature Measurements by Infrared Monochromatic Radiation Pyrometry. NASA TN D-2955, 1965.

MAHAN, BRUCE H.; and SOLO, RICHARD B.: Carbon Monoxide—Oxygen Atom Reaction. J. Chem. Phys., vol. 37, no. 11, Dec. 1, 1962, pp. 2669–2677.

Effects of Reaction Rate on Nozzle Flows

LEZBERG, ERWIN A.; ROSE, CHARLES M.; and FRIEDMAN, ROBERT: Comparisons of Experimental Hydroxyl Radical Profiles with Kinetic Calculations in a Supersonic Nozzle. NASA TN D-2883, 1965.

SARLI, V. J.; BURWELL, W. G.; and ZUPNIK, T. F.: Investigation on Nonequilibrium Flow Effects in High Expansion Ratio Nozzles. Rep. No. C–910096–13, United Aircraft Corp. (NASA CR-54221), Dec. 1964.

ZUPNIK, T. F.; NILSON, E. N.; and SARLI, V. J.: Investigation of Nonequilibrium Flow Effects in High Expansion Ratio Nozzles. Rep. No. C–910096–11, United Aircraft Corp. (NASA CR-54042), Sept. 1964.

Effects of Reaction Rate on Heat Conduction

BROKAW, RICHARD S.: "Thermal Conductivity" and Chemical Kinetics. J. Chem Phys., vol. 35, no. 5, Nov. 1961, pp. 1569–1580.

Page intentionally left blank

II Some Developments in Aerospace Heat Transfer

ROBERT SIEGEL, ROBERT W. GRAHAM, VERNON H. GRAY, JOHN R. HOWELL, AND WILLIAM L. JONES
Lewis Research Center

Some of the many heat-transfer problems encountered in the space vehicles that are seen quite commonly in this age of space exploration are considered in this discussion. For example, the exhaust from a rocket provides an indication of the high-temperature gas that the engineer has to contend with inside the rocket engine. In a manned space capsule, the astronauts must be protected from the fierce heat arising from air compression when the capsule plunges back through the Earth's atmosphere. At the other end of the temperature spectrum are many problems associated with handling the supercold liquid fuels that go into the rocket tanks.

The Lewis heat-transfer work is illustrated herein by discussing some problems that arise in two types of systems: a nuclear rocket engine, and a space electric powerplant. Although these problems have been created by specific needs in designing devices for space use, the information is quite basic and has a general applicability in advancing the heat-transfer field.

NUCLEAR ROCKET ENGINE

Problem Areas

A simplified diagram of a nuclear rocket is given in figure II–1. The system is composed of a propellant storage and pumping system, a nuclear reactor to add heat to the propellant, and a nozzle or thrustor to expand the heated propellant and provide a thrust velocity. Consider the flow chart of the liquid propellant. The propellant starts as cryogenic hydrogen stored in the tank at a temperature of 420° F below zero. It flows from the tank into passages used to cool the rocket nozzle wall and then into the nuclear reactor, where it is heated to 4000° F. The hot gas is then discharged through the nozzle to provide thrust. Because of the tremendous energy contained in the gas and the extremes in temperature in this propulsion system, severe heat-transfer problems are encountered that are far beyond the usual engineering practice. A brief summary of some of these problems is as follows: In the reactor core, there are extreme temperature differences of several thousand degrees between the hot reactor surfaces and the very cold gas. This causes large fluid property variations that affect the convective heat transfer. In the nozzle, the large flow accelerations influence the heat transfer from the hot gas to the wall. Within the nozzle cooling passages, the effect of the sharp channel curvature at the nozzle throat must be known and the fact that the cool-

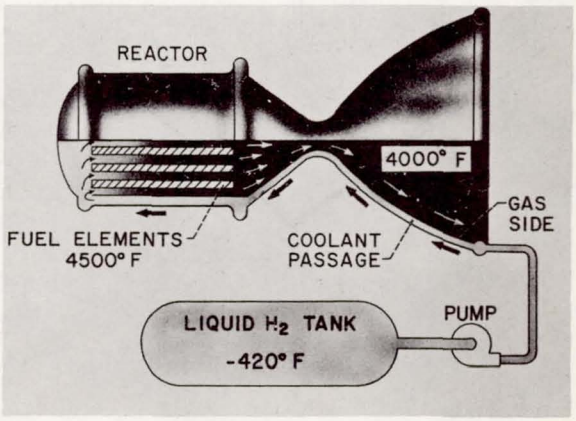

FIGURE II–1.—Nuclear rocket engine.

ant may be near its critical temperature must be accounted for. The interaction of these unknowns between the gaseous heat transfer and the liquid coolant must be understood to assure that the nozzle does not burn up. As illustrated in figure II–2, the heat flow from the hot gas to the nozzle wall is very large. In a square foot area of the throat, the cooling must dispose of as much heat as could be supplied by 100 large house heating plants operating at rated capacity. The study of this propulsion system has resulted in some extensions of heat-transfer knowledge. The information is applicable to other systems that utilize flow accelerations, large temperature differences, severe bends, or near-critical liquids.

Gas-Side Heat Transfer in Rocket Nozzle

Of these major heat-transfer problems, those on the gas side of the nozzle will be considered first. To gain some indication of the magnitude of the problem, the heat transfer from the hot gas to the wall must be estimated. A simple prediction method is to treat the nozzle as if it were a variable diameter pipe as depicted in figure II–3. Correlations for turbulent heat transfer in pipes are well known. They involve a relation between Nusselt and Reynolds numbers.

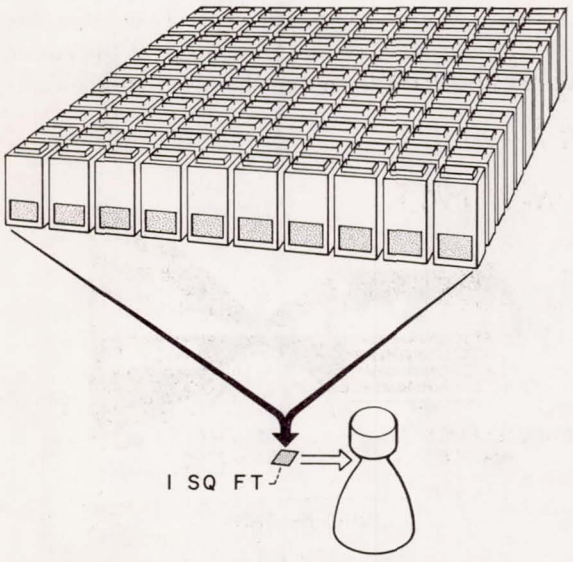

FIGURE II–2.—Heat flux at nozzle throat equivalent to 100 home heating units.

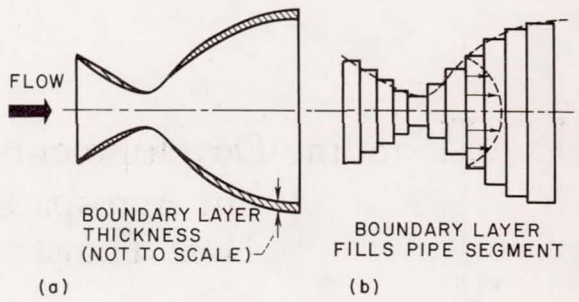

(a) Actual nozzle. (b) Pipe flow approximation.

FIGURE II–3.—Pipe flow approximation for analysis of nozzle heat transfer.

The correlations reveal that the heat-transfer coefficient is primarily a function of the mass flux through the pipe, which is the product of the fluid density times its velocity. By using the pipe flow correlations and inserting the local velocities and densities from the rocket nozzle, the local value of the heat-transfer rate throughout the nozzle can be estimated. The heat flux values that are obtained from this type of calculation are quite discouraging. It looks as though the nuclear nozzle cannot be cooled regeneratively by passing the cold hydrogen through the passages in the nozzle wall. However, any estimate should be compared with experimental results. A good source of experimental information would be nozzle heat-transfer data from high-energy chemical rockets. As shown in figure II–4, by using rocket heat-transfer data, it was found that the pipe flow type of prediction technique over-predicted the heat flux imposed at the nozzle throat by a factor of 2 to 1. This was cause for some hope because it meant that the nuclear rocket might still be cooled regeneratively, but it was going to be a difficult problem.

Because of the discrepancy between the theoretical and experimental results, the method of analysis has to be considered in critical detail. One factor is that the rocket nozzle is rather short to consider it a pipe. Pipe flow heat-transfer correlations are for long pipes, where the boundary layer has enough distance to grow until it completely fills the pipe cross section. Certainly the boundary layer in the rocket nozzle does not fill the passage. In fact, at the nozzle

throat, the boundary layer is so thin it is very difficult to measure with boundary layer probes. A second consideration is that when computing the heat transfer through boundary layers, an important factor is the velocity profile normal to the wall. In a pipe, this velocity profile is a well-established predictable pattern, as shown by the dotted line in figure II–3. In the thin boundary layer of the nozzle the velocity profile might be quite different from that in fully developed pipe flow.

In an effort to improve the theoretical predictions, more sophisticated calculation procedures involving boundary layer theory have been applied to the rocket nozzle problem. These methods involve solving the energy and momentum equations in the boundary layer and require the insertion of such inputs as friction laws, velocity and temperature profiles, and turbulent eddy diffusivities. Interestingly, these approaches also overpredicted the heat-transfer rate to about the same degree as the more simple pipe flow technique. However, some of the inputs to the boundary layer solutions were for the case of nonaccelerating flow. For example, the velocity profiles were for the nonaccelerating case. Intuitively one would guess that the boundary layer in the accelerating flow field would be different from the nonaccelerating case. This has been borne out by measurements of the boundary layer in a nozzle. Figure II–5 portrays a nozzle experimental facility and the associated boundary layer probes used for the investigation. Figure II–6 compares a nonaccelerating velocity profile obtained at a station upstream of the nozzle with a profile measured in the convergent portion of the nozzle where the flow is accelerating. There are two salient features in this comparison: the accelerated profile is flatter in the portion of the boundary layer away from the wall, and the accelerated profile is much steeper near the wall. However, no profile measurements were made immediately adjacent to the wall.

It might be expected that the computed heat-transfer rates would be even higher when a steeper velocity profile is utilized in the energy equation. Yet the measured heat transfer turns out to be lower than that predicted using the

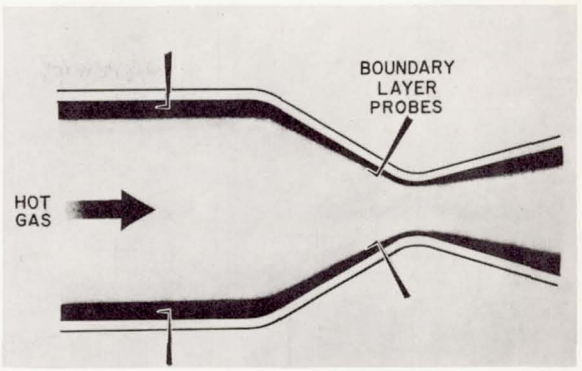

FIGURE II–5.—Experimental nozzle boundary layer facility.

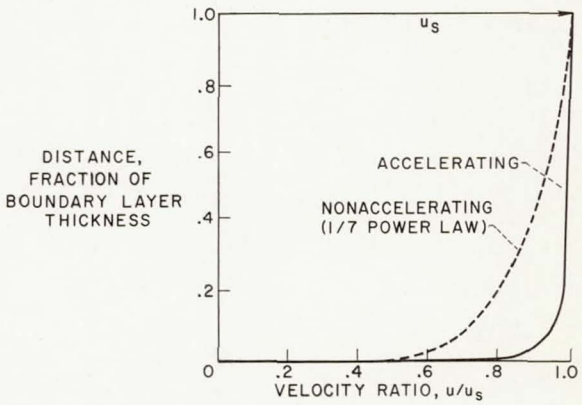

FIGURE II–6.—Comparison of accelerating and nonaccelerating turbulent boundary layers.

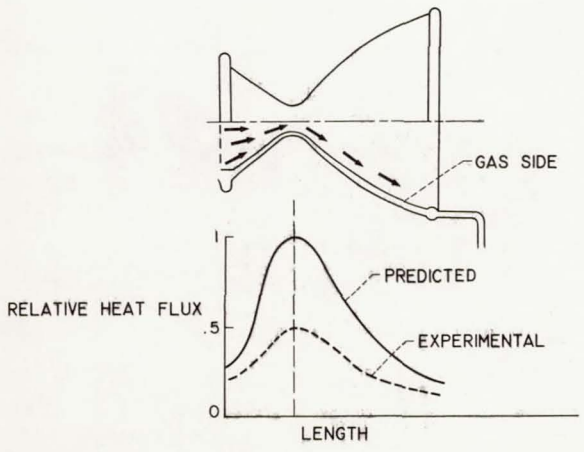

FIGURE II–4.—Comparison of experimental and predicted gas side heat transfer.

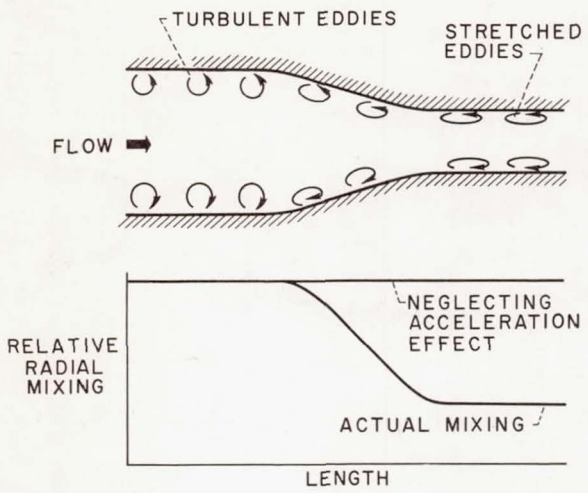

FIGURE II–7.—Effect of flow contraction on radial turbulent mixing.

relatively less steep one-seventh-power pipe flow profile. This means that other factors besides the velocity profile must be considered in the analysis.

Another very important factor must be the detailed behavior of the turbulent mixing in the fluid during the flow acceleration. In figure II–7 are pictured some turbulent eddies near the wall at the entrance of a flow contraction such as in the rocket nozzle. Both analysis and experiment have shown that the large flow acceleration stretches the eddies in the contracting section as illustrated. This tends to keep the turbulence, which transfers heat from the hot gas to the wall, from developing as rapidly in the flow direction as might be expected. In other words, the suddenness of the acceleration prevents the turbulence from keeping pace with the flow velocity. On the graph in figure II–7, the horizontal line represents how large the average turbulence would be relative to the stream velocity, when the turbulence can keep up with the flow acceleration and remain in equilibrium with the local velocity. The lower curve illustrates how the turbulence actually falls below the expected level. This low turbulence may account for the fact that the observed heating of the rocket nozzle by the hot gas is lower than that predicted by the analysis. The observed heating is lower than the predicted because the analysis has not properly accounted for the detailed behavior of the turbulence. The fundamentals of the turbulence is one subject of current research with reference to accelerated flows.

To investigate further all aspects of the effects of acceleration on heat transfer there is a concerted effort in this problem at the Lewis Research Center and at the Jet Propulsion Laboratory. There are several NASA reports available that provide early work in this area.

Heat Transfer in Coolant Passages

The discussion will now turn to the many heat-transfer problems inside the curved cooling channels within the nozzle wall shown in figure II–8. This cooling prevents the hot propellant gas from burning up the wall of the nozzle. On the coolant side of the nozzle, there are problems similar to those on the hot gas side, plus a few more. One complicating factor in computing the heat transfer in the cooling passages is the rather unusual fluid state. In part of this passage the fluid is at its critical temperature but is generally above the critical pressure. In the region of the critical temperature and over an appreciable range of pressures above critical, the properties of hydrogen or any fluid vary sharply with small changes in temperature. These property variations make estimates of heat transfer difficult.

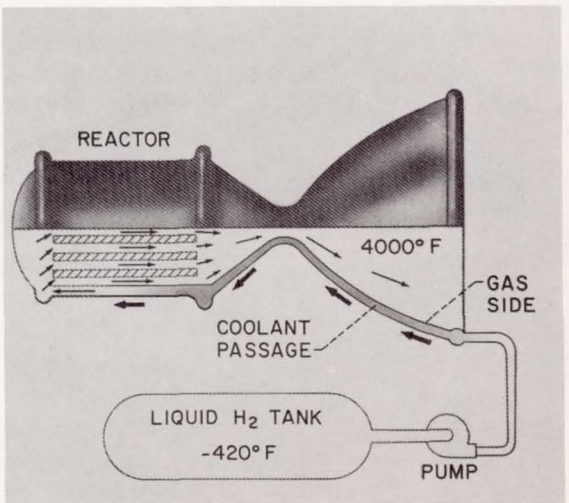

FIGURE II–8.—Coolant passages in rocket nozzle wall.

Earlier in the discussion it was mentioned that the convective heat-transfer coefficient is proportional to a product of density and velocity. Consequently, a value of fluid density has to be inserted in the convective heat-transfer correlation. However, as is shown in figure II–9, the density of hydrogen around the critical point varies sharply with temperature. This makes a selection of a characteristic density difficult. Actually the near-critical regime with very large property variations is the one primarily encountered during the startup or shutdown phases of operation for the nuclear rocket system. During full power operation, the fluid state within the nozzle lies considerably to the right of the critical point.

However, the prediction of the heat transfer during the startup transient is very important. Some technique is needed for analyzing situations in which density is extremely sensitive to temperature. An idea that has been used is to treat the near-critical fluid as if it were a mixture of light and heavy species. This is analogous to treating it as if it were a two-phase fluid, even though the equilibrium phase diagram indicates that the phase boundaries no longer exist. By this technique a film boiling correlation developed for the two-phase regime has been extended into the near-critical region.

Besides the correlation of the heat-transfer data, there are several bits of experimental evidence that justify this approach. One is some similitude in the appearance of heated hydrogen

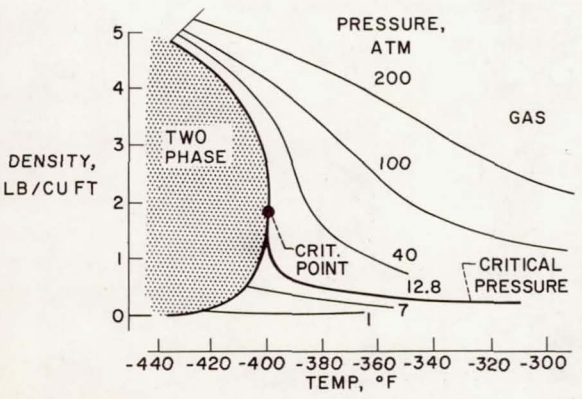

FIGURE II–9.—Density of normal hydrogen as function of temperature and pressure.

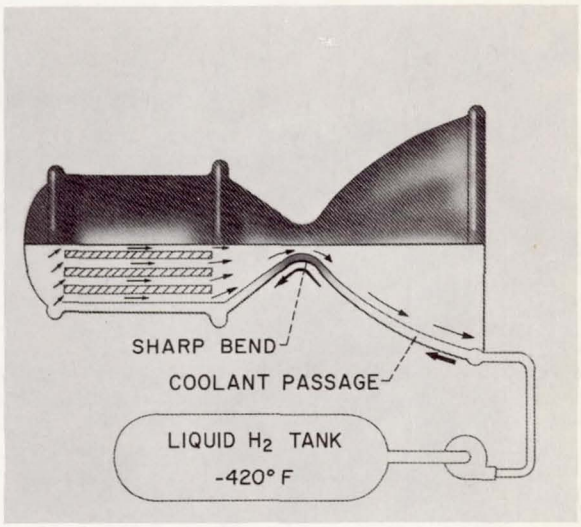

FIGURE II–10.—Sharp bend in coolant passage at nozzle throat.

for the film boiling and supercritical regimes. This was found by utilizing high-speed motion pictures to observe the heating of a pool of hydrogen. In film boiling large vapor patches rise through the liquid in a regular columnar pattern characteristic of this boiling regime. When the heating of supercritical hydrogen was observed, there was a columnar pattern of light agglomerates rising from the heater surface. It was apparent from the motion pictures that there were some similarities in the appearance of film boiling and the heating of supercritical hydrogen. In both cases there were discrete packets of lighter density fluid that rose in a columnar fashion. These packets for the near-critical fluid suggest an almost discontinuous change in density similar to that seen in a two-phase fluid. This visual evidence is one justification for treating the near-critical region in a fashion analogous to two-phase heat transfer.

Now that some of the fluid property effects have been discussed, a geometric effect will be considered. This effect is the increased heat transfer that results from the sharp turning of the fluid in the coolant passages at the nozzle throat as shown in figure II–10. The high-speed turbulent flow of the coolant must change direction very rapidly in passing around the sharp curve of the passage. This turning of the flow

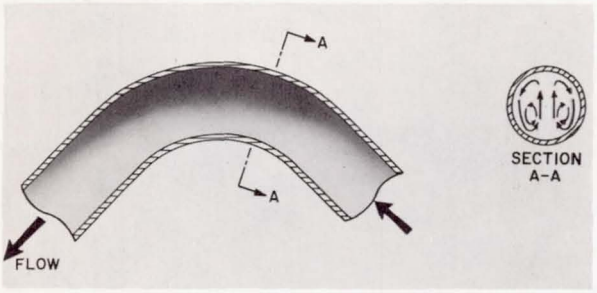

FIGURE II–11.—Density gradient and secondary flow in tube bend.

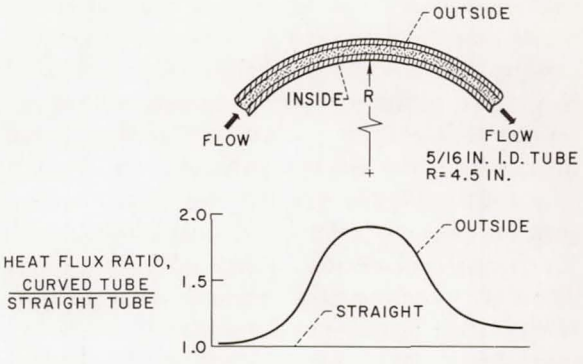

FIGURE II–12.—Experimental results for curved tube heat transfer.

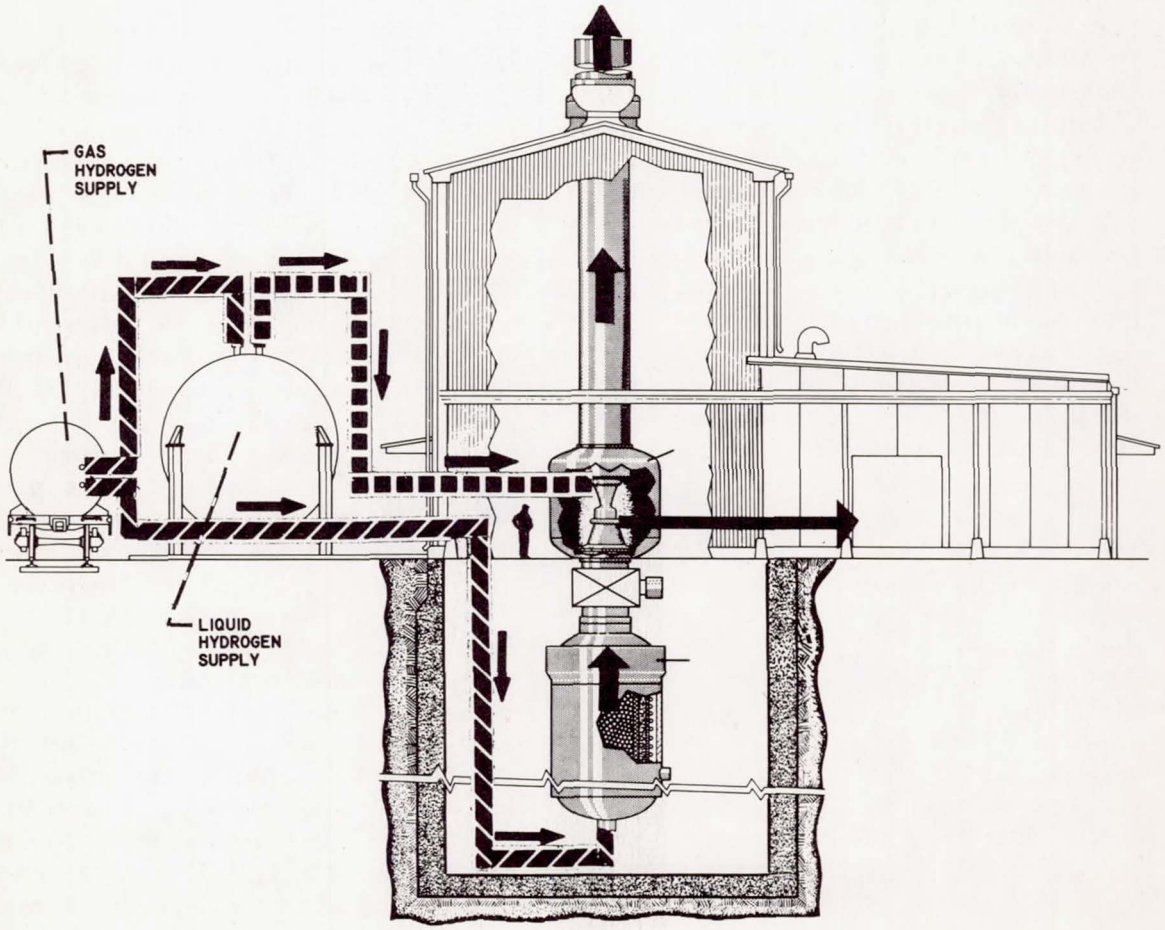

FIGURE II–13.—Rocket nozzle hydrogen heat-transfer test facility.

results in strong density gradients across the flow. Also, strong secondary flows are set up within the tube as shown in figure II–11. The combination of these effects would be expected to increase the heat-transfer coefficient of the coolant on the outer portion of the wall at the tube bend. The results of some experiments with electrically heated tubes using liquid hydrogen indicate that this is the case (see fig. II–12). With a $\frac{5}{16}$-inch-diameter tube and a radius of curvature of $4\frac{1}{2}$ inches, the outside of the bend of the tube had a heat-transfer coefficient about two times the value on the inside of the bend. The inside value was essentially equal to that for a straight tube. This enhancement effect in heat transfer on the outside of the bend of the tube can result in significant reductions in tube wall temperature at the throat of the rocket nozzle.

Full-Scale Testing

Since there is a 2-to-1 increase in the coolant heat-transfer coefficient at the throat because of the channel curvature and a 2-to-1 decrease in the hot gas side coefficient near the throat as discussed earlier, there is in total a 4-to-1 advantage over what was originally predicted. These measurements, however, were obtained under laboratory conditions; consequently, there is some question as to whether these lower nozzle cooling requirements can be relied upon in full-scale hardware.

To better determine just how severe the actual cooling problem is, a test program is planned with the use of a highly instrumented nozzle. These tests will be conducted with a new facility that is now under construction. This facility, illustrated in figure II–13, will be able to provide close simulation to the nuclear nozzle on both the hot gas and coolant sides. Simulation of the hot gas side of the rocket nozzle is provided by supplying the research nozzle with heated hydrogen gas. The gas is heated by a pebble heater 28 feet high and $5\frac{1}{2}$ feet in diameter. The bed is filled with $2\frac{1}{2}$-inch-diameter graphite balls. Heating of the bed is provided by electrical induction heating of a graphite susceptor that forms the wall of the bed. The hydrogen gas is supplied from an outside storage vessel. The gaseous hydrogen is directed into the bottom of the bed, passes up through the bed where it is heated, then through the research nozzle, and finally up through the stack to the atmosphere where it is burned off. Simulation on the coolant side of the nozzle is provided by directing liquid hydrogen through the coolant passages of the research nozzle. The liquid hydrogen is contained in a large vessel located outside of the building. The facility is capable of testing nozzles of approximately one-half the size of current nuclear rocket designs.

Auxiliary Cryogenic Heat Exchanger

In addition to problems on the gaseous and coolant sides of the rocket nozzle, interesting heat-transfer problems often arise during the design of auxiliary equipment for rocket engines. For an example of this, consider a particular heat exchanger, such as the one shown in figure II–14. When a water moderator is used in a nuclear reactor, such as in the tungsten water-moderated nuclear rocket, it picks up heat. A means of keeping the water cool must therefore be provided. Fortunately, a coolant is available in the form of the liquid hydrogen propellant. Before the hydrogen enters the rocket nozzle cooling passages, it is diverted to a heat exchanger to cool the water used for moderating the nuclear reaction. However, since the hydrogen is extremely cold, about 420° F below zero, there is danger that the water circulating through the

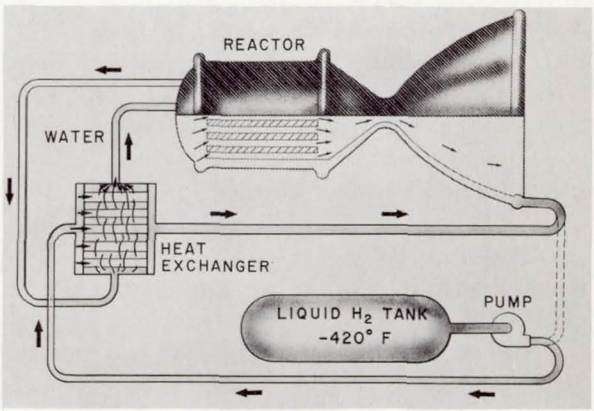

FIGURE II–14.—Liquid-hydrogen-water heat exchanger.

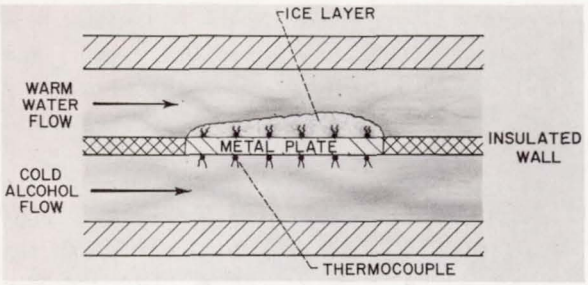

FIGURE II–15.—Experimental ice layer formation in flowing water.

exchanger will freeze. A similar situation exists when a car is driven out of a warm garage into very cold weather with only pure water in the car radiator. Will the water freeze solid in the radiator passages and block the flow or will it pick up enough heat in the engine to prevent the ice growth?

Before the ice buildup in the heat exchanger can be computed, there is a need for general information on what happens when a very cold surface is placed in a stream of flowing water. This seems like a rather common problem and yet there was hardly any information that could be found about it. The first thing that was done was to devise an experiment where a metal plate was imbedded in a plastic wall and instrumented to measure surface temperatures as shown in figure II–15. A stream of warm water flows over one side of the plate, and chilled alcohol is used as a convenient fluid to cool the other side. When the alcohol is turned on, the plate temperature drops rapidly; and, if the water is not too hot or flowing too fast, the plate will reach the freezing point. It would be expected that freezing would then start immediately, but it was found that it often does not. The warm water flow sweeps away the ice nuclei that start to freeze, and no ice layer forms. Finally when the plate is about 10° F below the freezing point, the ice will suddenly flash on the plate and begin to grow rapidly. As the ice grows it insulates the surface and this reduces the heat removed by the coolant. Finally the warm water is trying to melt the ice away as fast as the coolant is trying to freeze it. This produces an equilibrium condition and a steady-state thickness of ice is reached. This is not like freezing a lake—in that case there is no heat source in the form of a warm water supply, and ice will continue to form as long as the temperature remains below freezing.

An analysis was also made so that the experimental results could be correlated. The analysis involved solving the transient energy equation that governs the solidification process and heat conduction within the ice layer. The ice layer growth was predicted reasonably well for design purposes.

Some full-scale tests have also been run with a shell and tube heat exchanger with liquid hydrogen as the coolant. Figure II–16 shows some typical tubes in the exchanger. The cold hydrogen flows inside the tubes with water in crossflow on the outside. Ice formed in part of the exchanger, which cut down on the exchange efficiency since the ice provides an insulation layer on the tubes. Fortunately, the process is self-regulating. If there is sufficient pumping pressure to maintain the flow, the ice formation increases the local water velocity within the tube bundle as it cuts down on the flow cross section. The higher velocity tends to melt the ice away and helps to keep the exchanger from becoming completely blocked.

SPACE ELECTRIC POWERPLANT

The preceding discussion has dealt with some of the problems that originated in connection with the nuclear rocket engine: on the gas and coolant side of the rocket nozzle, and in one piece of auxiliary equipment. The second system to be considered is the space electric powerplant.

Powerplant Components

It is expected that, in the years to come, spacecraft will be larger and will be involved in longer and more complex missions. Therefore, they will require more and more onboard electrical power. Power will be needed for such things as communications, operation of life-support equipment, and propulsion by various electrically powered means for flight changes and

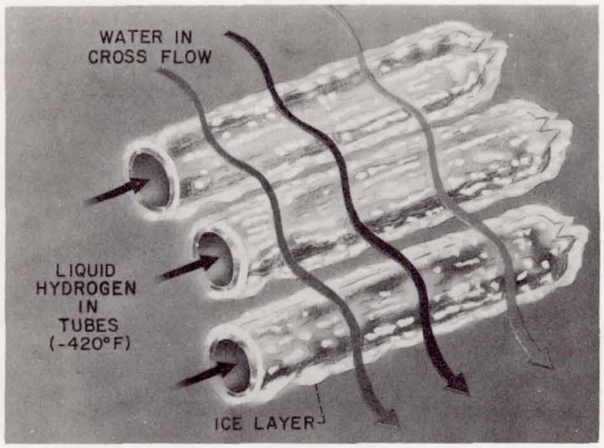

FIGURE II–16.—Ice formation on tubes in liquid hydrogen-water heat exchanger.

accelerations on missions of many months or years duration. The amount of electrical power output for such requirements can range from kilowatts to megawatts. In developing electrical power generation systems for use in space, more heat-transfer problems are encountered. What some of these new problems are and what NASA is doing to solve them will now be discussed. A pictorial concept of a large space power generation system is shown in figure II–17. The source of energy in this system is the nuclear reactor shown with its radiation shield. Reactor heat is transferred by a fluid in the primary pumped flow loop to the heat-exchanger-type boiler. Another fluid flowing through the boiler receives the heat and is vaporized. This vapor drives a high-speed turbine that turns an electric generator to provide power, in this case for an electric propulsion unit. The vapor that leaves the turbine is condensed and cooled in a radiator, and the liquid condensate is then pumped back into the boiler.

General Features of Space Boiler

The boiler is perhaps the best component of this system to illustrate some of the new heat-transfer problems. This section contains a discussion of boilers in some detail. Figure II–18 compares a space boiler with an older model conventional Earth-based boiler, which should be familiar to most people. The conventional boiler could be found in a central steam plant or a city electric powerplant. The Earth boiler shown is coal fired and has water inside miles of tubing that is heated by the hot combustion gases passing over the outside of the tubes. The water has a natural circulation cycle, rising in the slanting tubes, boiling along the way, and then flowing into the steam drum at the top; here the steam separates and flows out of the boiler, while the unevaporated water flows back down the vertical tubes by gravity and begins a recirculation cycle. Now consider the space boiler (fig. II–18(b)). It has an alkali metal fluid flowing from right to left through a compact bundle of tubes. This fluid is heated and vaporized in one pass through the boiler by the heat transferred from another liquid metal coming from the reactor and flowing in a surrounding annulus or shell in the opposite direction. The hairpin shape of the space boiler is a method of relieving thermal expansion problems. It is interesting to compare the sizes of these two boilers. The small space boiler in the upper right corner of figure II–18(b) is drawn to the same scale as the conventional boiler. (Newer Earth boilers are more compact and intricate than the one illustrated.) In the comparison in figure II–18, the heat transferred in the boiling process is the same for both boilers, that is, about 10 megawatts. The space boiler has approximately a 6-inch-diameter shell with tube lengths of 5 to 6 feet; the conventional boiler occupies the space

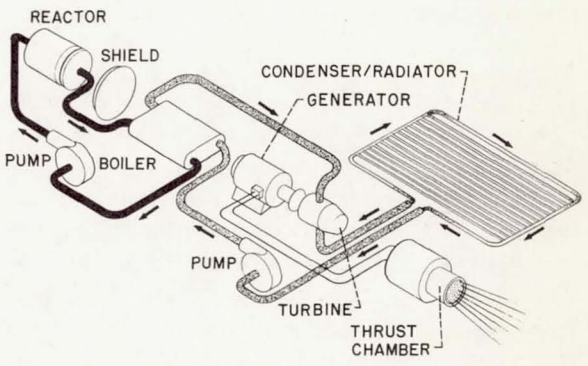

FIGURE II–17.—Nuclear-electric space power generation system.

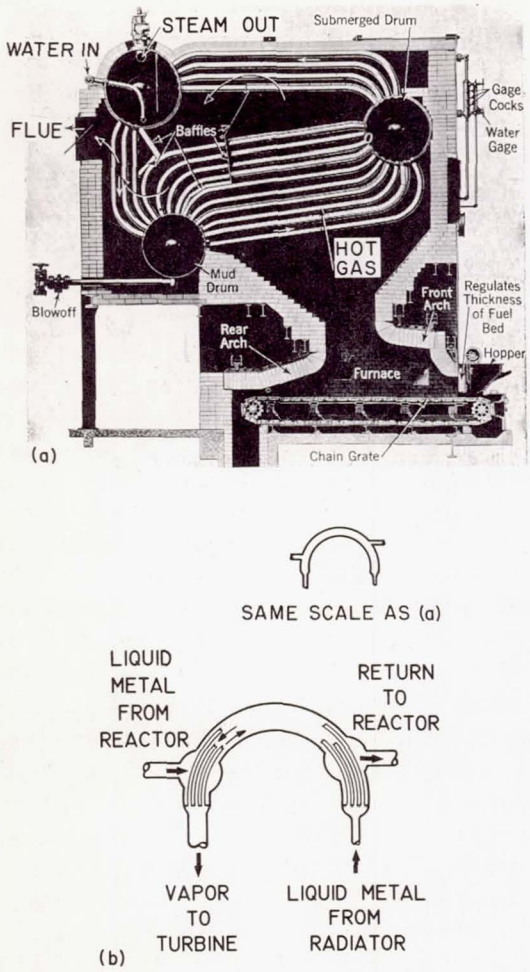

(a) Conventional gas-fired boiler.
(b) Liquid-metal boiler for space power generation.

FIGURE II–18.—Comparison of Earth-bound and space boilers.

of a 20-foot cube. Either boiler in a complete power generation system would produce slightly over 1 megawatt of electrical power.

How was this concept for a space boiler determined? Well, naturally for space flight, size and weight must be minimized as much as possible. This leads to very compact designs with high rates of heat flow and high fluid velocities. More important, perhaps, is the fact that for long periods of space flight the craft will be in a zero gravity, or weightless, condition. In zero gravity there is no buoyancy force to separate the vapor phase from the liquid, and both phases will "float" together as a mixture. So one problem in space is that gravity cannot be used to separate the vapor from the liquid as is done in the steam drum of the Earth-bound boiler.

The boiling difficulties encountered in zero gravity have been studied by taking high-speed motion pictures of pool boiling in reduced gravity fields by using free fall in a drop-tower facility. Because of the low buoyancy in a reduced gravity field equal to about 1 percent of Earth gravity, the bubbles do not leave the surface as readily as they do in Earth gravity. The bubbles for boiling water grow to much larger sizes than in ordinary boiling. When the bubbles in reduced gravity break away from the surface they move upward slowly. In zero gravity there would be no buoyancy to move the bubbles through the liquid and the vapor would tend to accumulate near the surface. The surface could quite easily become covered with vapor, which would drastically cut down the heat-transfer rate because of the poor heat-transfer coefficients to the vapor phase.

These observations have shown that a means for separating the vapor from the liquid would have to be provided in the case of a space boiler so that only the vapor would be passed into the turbine. Because of the lack of vapor separation from the liquid and the danger of blanketing the heater with vapor, it is clear that a free circulation boiler cannot be used for the zero gravity space environment. To overcome the lack of gravity in space power generation systems, a complication must be added to the boiling process. A "once-through" forced-flow system is utilized in which the fluid is pumped around closed-return pipe loops, even though it is undergoing boiling and condensing. Hence, within the boiler the problem of forced convection boiling must be dealt with. Forced convection boiling is often analyzed by adding the individual effects of forced convection and pool boiling. As yet, however, some basic aspects of pool boiling are still not well understood, so research is being conducted in this area.

There are two major categories of pool boiling —nucleate and film—as illustrated in figure II–19. Nucleate, as the name implies, involves

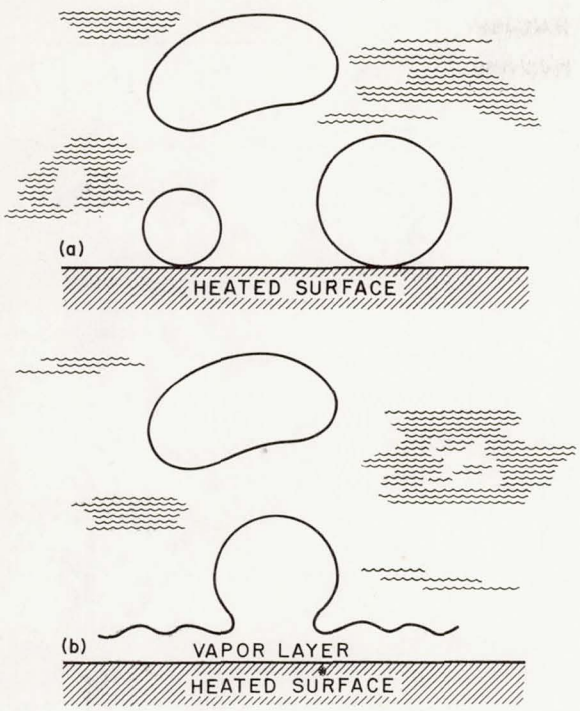

(a) Nucleate boiling.
(b) Film boiling.

FIGURE II–19.—Appearance of nucleate and film boiling regimes.

the production of bubbles at nuclei on the heated surface. This form of boiling is extremely efficient as a method of heat transfer. Film boiling denotes a condition where a blanket of vapor covers the heat-transfer surface and the heat transfer is not nearly as efficient as in nucleate boiling. One can differentiate nucleate and film boiling by the fact that liquid wets the heat-transfer surface in the nucleate condition while it does not generally wet the surface in film boiling. The fundamentals of both nucleate and film boiling are being studied at the Lewis Research Center. A few remarks concerning the theory of nucleate boiling are in order.

Various explanations have been offered as to why the heat-transfer rates in nucleate boiling are so high. One of the early explanations attributes the high rates to the amount of turbulence generated by the growth, movement, and collapse of bubbles. As shown in figure II–20, the bubble is pictured as a stirring agent. Another explanation, illustrated in figure II–21, portrays the bubble as a piston pumping superheated liquid away from the surface and admitting cooler liquid to the displaced volume near the surface. A recent explanation places emphasis on the evaporative process associated with the growth of the bubbles. A thin layer of super-

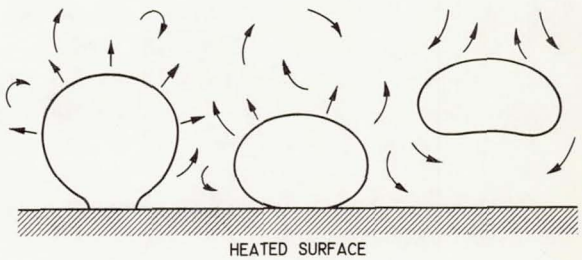

FIGURE II–20.—Bubble agitation mechanism in nucleate boiling.

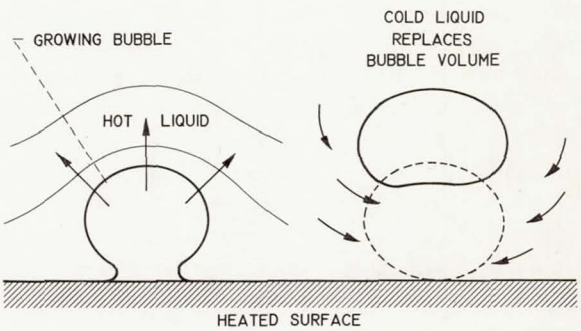

FIGURE II–21.—Vapor-liquid exchange in nucleate boiling heat transfer.

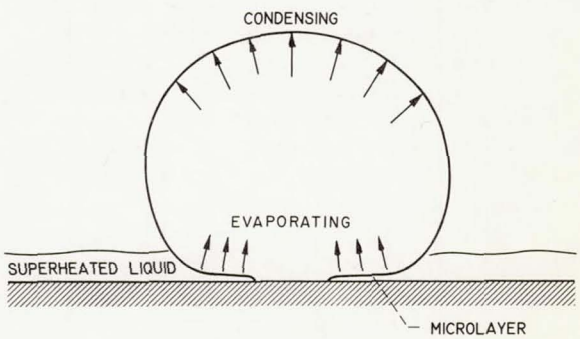

FIGURE II–22.—Microlayer evaporation heat-transfer mechanism.

heated liquid underneath a bubble as shown in figure II–22 acts as an evaporative surface, while condensation is occurring over the dome of the bubble. The kinetic theory of evaporation shows that these evaporation-condensation fluxes can be very high.

Each of these models appears to represent part of the overall boiling process and is contributing something to the overall heat flux. At Lewis, recent research supports the concept of evaporation from a liquid layer under the bubble as being very important. The physical presence of such a thin layer has been shown experimentally. It appears that, when evaporation is ocurring from more than 5 to 10 percent of the heating surface, it dominates the heat-transfer process, and the large heat fluxes in nucleate pool boiling can be attributed to the evaporation-condensation mechanism.

When forced flow is added to pool boiling, such as in the space boiler, much more complicated processes result, as shown in figure II–23. These processes are briefly reviewed so that some of the problems peculiar to space systems can be described. The boiling fluid flows within a tube and is heated by a second fluid that moves in a surrounding annulus. At the beginning of the boiler tube, the fluid is all liquid and is at a temperature below the boiling point. The graph in the lower part of the figure illustrates the heat flux being transferred into the boiler tube. In the "all-liquid" region the heat transfer is relatively low, since it occurs by ordinary forced convection. As the liquid is heated, the portion near the wall reaches the boiling point. Bubbles are then formed near the wall with the core of the fluid remaining liquid. Here the heat transfer begins to increase because of the boiling action. The next flow regime, "bubbly flow," is reached when the core of liquid approaches the boiling point and bubbles extend over the entire tube cross section. These bubbles begin to coalesce, forming large vapor masses. The result is the "slug flow" regime, with alternate portions of liquid and vapor. Liquid is still flowing along the wall and the heat transfer is very high. The vapor slugs then merge together and "annular flow" results, where an annulus of liquid flows along the tube wall, and vapor flows at high velocity down the center of the tube. The last regime is "mist flow," where the wall is essentially dry and the vapor is carrying entrained liquid droplets. Generally, most of the length of a space boiler tube is occupied with the annular and mist flow regimes, the mist droplets being difficult to evaporate completely. Somewhere along the tube, often in the annular region, the heat transfer experiences a transition and very abruptly decreases to a low heat flux rate. This is caused by the onset of a vapor binding condition where vapor rather than liquid is predominantly in contact with the tube wall. The convective heat transfer to the vapor phase is much lower than to a boiling liquid. A difficulty is that this transition point has the nasty habit of fluctuating up and down the boiler tube in a rapid uncontrolled manner, producing

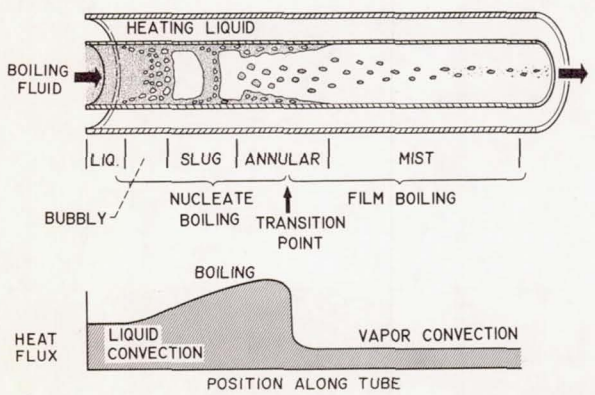

FIGURE II-23.—Two-phase boiling flow regimes.

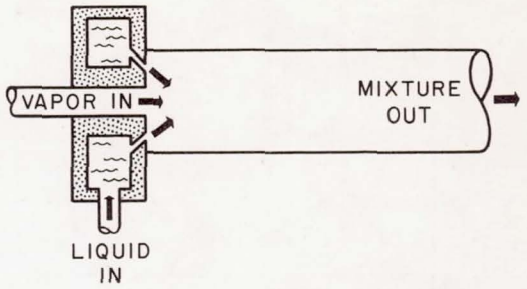

FIGURE II–24.—Jet mixing of liquid and vapor to demonstrate two-phase instabilities.

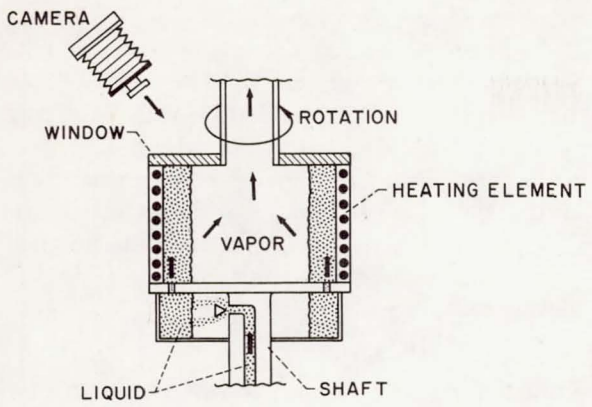

FIGURE II–25.—Rotating boiler experiment.

violent flow pulsations. This instability is one of the main problems in once-through boilers, and is now discussed.

Instabilities and Boiler Design

Boiler instabilities can have many complex forms. It is believed that the fluctuations in the transition to a vapor binding or film boiling condition are to a large degree caused by slug flow oscillations originating upstream where the liquid bulk temperature is still below the boiling temperature. Vapor created at the heated wall moves toward the center of the tube, where it tends to condense in the cooler liquid there. This creates alternate slugs of vapor and liquid, an inherently unstable condition. This slug flow has been studied in a simple device that also can create the various flow regimes described previously. As shown in figure II–24, vapor and subcooled liquid are caused to mix when steam enters the end of a tube as a central jet and impinges upon a conical jet of water. At the start of a typical test the water is cool and the steam forms a small bubbly cloud as it quickly condenses; elsewhere the flow is mainly liquid. As the water temperature is steadily increased with the flows remaining the same, the vapor cloud becomes longer, a distinct interface forms between vapor and liquid, and the interface starts to oscillate vigorously as slug flow develops. When the water temperature is further increased, the slugging flow moves further down the tube, leaving an annular flow in the test section.

Unstable flow excursions in the boiler can lead to serious difficulties in the space powerplant. For example, liquid may enter the turbine and damage the turbine blades. Consequently, this problem is being pursued along several paths. The mechanisms and the mathematics of such flow instabilities are being studied by using extensions of analyses of pipe line dynamics. An attempt is also being made to prevent these instabilities by various designs and devices.

One way to stabilize the liquid-vapor interface in weightless flight is to create an artificial gravity by rotating the parts of the flow system that undergo a phase change. Figure II–25 shows an apparatus in which boiling takes place in a rotating cup. The liquid enters at the bottom of the device through a hollow shaft. It passes through a regulating valve and then sprays out to the cylindrical walls, where it forms an annulus of liquid. The liquid passes up into the heated zone to replace the liquid that has boiled off. At the liquid-vapor interface, vapor leaves the liquid and flows toward the center of rotation and then out the top of the boiler. Photographs taken through a window on top of the rotating cup have shown that boiling can be quite stable at conditions of 75 times Earth gravity and at a heating rate of 250 watts per square inch (~120 000 Btu/(hr)(sq ft)). Under these conditions, bubbles form at the heated surface and quickly move inward through the liquid. At this point the bubbles break, and being quite numerous, they form a thin zone of bubbly froth at the interface. By increasing the rotation and generating 475 times Earth gravity, the bubbling was almost entirely eliminated, but the boiler could still transfer the same rate of heating by vaporization only at the interface, which was then a sharp steady boundary between clear liquid and vapor. The maximum heat that can be transferred to water by pool boiling at one gravity is about 650 watts per square inch; above this level film boiling sets in. However, at 400 Earth gravities 840 watts per square inch (30 percent more) have been transferred, and only a few patches of bubbles were actually formed in the process. Obviously, much higher heating rates and higher gravities are possible and could be very beneficial.

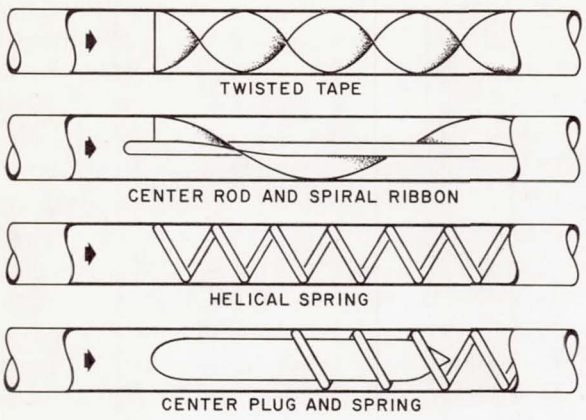

FIGURE II–26.—Centrifugal types of boiler tube inserts.

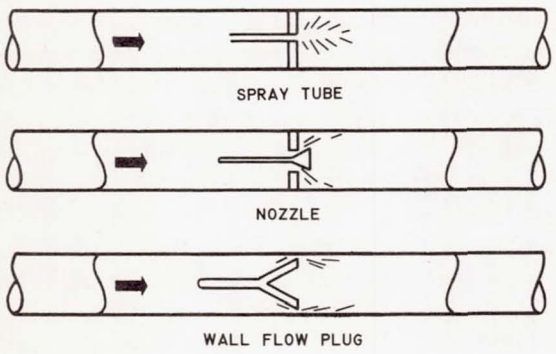

FIGURE II–27.—Pressure-drop types of boiler tube inserts.

Other ways of stabilizing a once-through boiling process are to design the stationary flow tubes to impart a swirl to the fluid as it passes through. Ideas as to how this may be accomplished are shown in figure II–26. The boiler tubes are shown with inserts such as twisted tapes, spiral ribbons, and helical wire springs to spin the fluid, thereby throwing the entrained liquid against the tube wall, and allowing vapor to flow down the center. Even a tube bend, as was shown in figure II–18(b) of the space boiler, will separate the phases in two-phase flow. The tube bend thus serves the dual purpose of relieving thermal stresses and aiding the boiling process.

Another technique to stabilize boiling, as shown in figure II–27, is to add an insert such as a short spray tube, a nozzle, or a conical plug to create a pressure drop at the point where the boiling temperature is approached. Vapor will be maintained downstream of the insert because of flashing, and thus oscillating slug flow will be eliminated. The flow will go from all-liquid upstream of the insert to annular flow downstream of the insert, with liquid on the wall. These techniques are being evaluated and hold promise for adding considerable stability to the forced flow boiling process.

Problems Arising From Vacuum Environments

In addition to zero gravity in space flight, there is another factor that forces the power generation systems to be different from Earth-based conventional designs. This factor is the vacuum or lack of atmosphere in space. Looking again at a sketch of the space power system (fig. II–28) recalls that the vapor leaving the turbine has to be condensed and cooled before being pumped back to the boiler. This represents heat that must be wasted in the thermodynamic cycle. In space, the only way to dissipate heat is by thermal radiation, since no atmosphere is available to convect heat away. At ordinary temperatures, the radiator would have to be colossal to dissipate the heat involved in the power cycle. Consequently, the temperature of the radiator is run as high as possible to utilize the fourth power temperature law of radiation. Work is being courageously done at temperature levels of 1400° F for the radiator, 2000° F for the boiler, and 2300° F for the reactor.

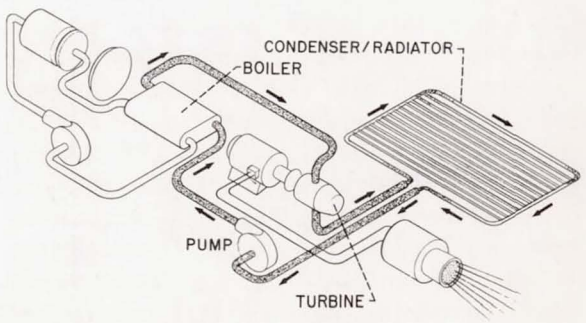

FIGURE II–28.—Condenser-radiator flow loop in space power system.

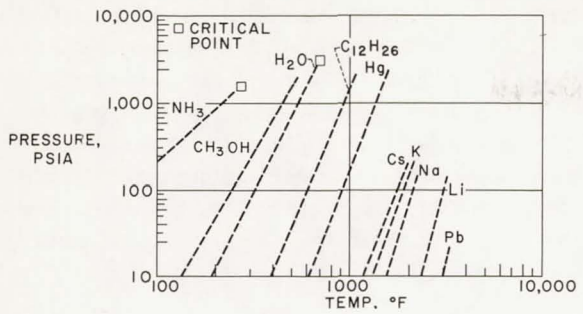

FIGURE II–29.—Boiling pressure and temperature for conventional fluids and liquid metals.

These high temperature levels place some rather special requirements on the fluids that can be used in the flow circuits. It was stated earlier that liquid metals are used. The reason for this can be found from figure II–29, which is a plot of the boiling pressure as a function of saturation temperature for several fluids. As a point of reference, water is shown to boil at 212° F at about 15 pounds per square inch pressure; at 1000 pounds per square inch absolute, it boils at a temperature of over 500° F. Other fluids shown are ammonia, alcohol, a hydrocarbon, and mercury. At temperatures near 2000° F, these conventional types of fluids are either supercritical or boil at excessively high pressures. At high temperatures, however, it is especially important to keep the pressures low because even the refractory metals have stress limits of only a few thousand pounds per square inch because of creep under extended service. Consequently, the preferred fluids for space use turn out to be the alkali liquid metals: lithium, sodium, potassium, rubidium, and cesium. Lead and other metals fall still higher on the temperature scale than the alkali metals. The alkali metal fluids generally have desirable heat-transfer properties. For example, they have large heats of vaporization, low viscosity, low specific heat, high thermal conductivity, good wettability, and a high volume ratio between vapor and liquid phases. However, the alkali metals have their problems too. They must be kept highly purified and away from all oxygen and water. They are caustic and toxic and freeze at ordinary temperatures. What is more, they often get into a metastable liquid state at a temperature far above the normal boiling temperature, because of a difficulty in nucleating bubbles within the liquid.

Bubble Nucleation in Boiling

The bubble nucleation problem in a liquid metal boiling loop can develop as follows: the fluid heats up from 100° to 300° F above its normal boiling temperature but still remains entirely liquid. Then, at some point, the liquid in the tube will suddenly break to form an interface and flash into vapor. This releases the energy that had been stored in the superheated liquid and the process can be quite violent. It produces pounding and bumping actions, with geysering and waterhammer consequences. The outrush of vapor may send a surge of flow and pressure around the flow loop, thereby forcing cooler liquid back into the boiler tube, refilling the tube with liquid and setting up another superheating and geysering cycle. This type of nucleation instability can keep a space powerplant designer quite unhappy. To better understand the reason for this behavior, some of the details of bubble nucleation are being investigated.

It has been noted in the literature and studies at Lewis also show that bubbles originate from pits and scratches on the boiling surface as illustrated in figure II–30. In a water system it is well known that a little vapor or gas must be present in the cavities to allow boiling. It has been found through experiments (fig. II–31)

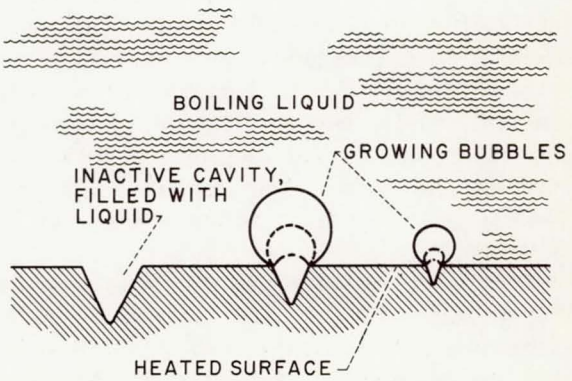

FIGURE II–30.—Bubble nucleation from surface cavities.

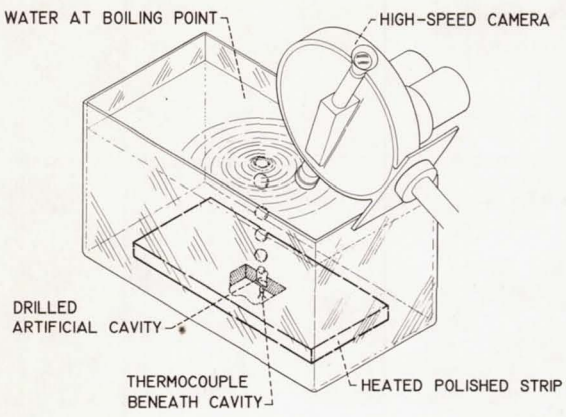

FIGURE II–31.—Experimental study of bubble nucleation from artificial cavities.

where high-speed magnified motion pictures were taken of bubbles growing from artificial nucleation sites of various sizes that boiling can be maintained from most sites with only a few degrees Fahrenheit of superheat. Figure II–32 shows the form of the results where the superheat required to maintain bubble formation is given as a function of the size of the surface cavity opening. For a certain optimum cavity size a minimum superheat is obtained. This minimum is of the order of a few degrees Fahrenheit in water, and theory shows this to also be true for liquid metals. However, these minimum values occur only under the most favorable circumstances. The cavities need to have gas or vapor already within them to provide a nucleus from which the bubbles can grow. The highly superheated state that can be encountered in the liquid metal boiler occurs because conditions for bubble formation are unfavorable. The liquid metal systems are highly degassed to help reduce corrosion and oxidation. This means there is no gas in the surface cavities. Also the alkali metals wet the surface so that they tend to fill up the cavities and render them inactive. This can lead to large liquid superheats and violent instabilities.

An obvious remedy to this problem is to get vapor somehow to the surface cavities before the tube is heated, so that the cavities will be active for bubble formation. One way this is accomplished is shown in figure II–33. A very short leg, or "hot finger," connected to the tube near the inlet is heated to a few hundred degrees Fahrenheit superheat. The vapor from this segment is carried downstream by the flow, and activates sites along the wetted area of the remainder of the heated tube. This continuous production of vapor prevents the metastable liquid superheat from building up in the boiler tube and greatly stabilizes the flow.

Containment Materials

One aspect of the high-temperature level used in these power generation systems that has not been mentioned yet is the need for special containment materials. Obviously, at 2000° F and

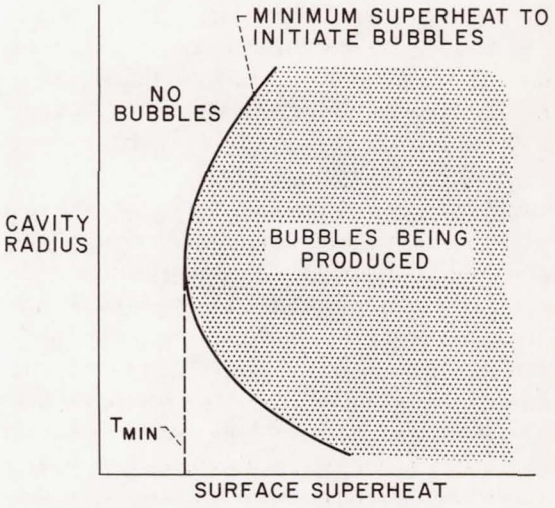

FIGURE II–32.—Incipience of boiling from artificial nucleation sites.

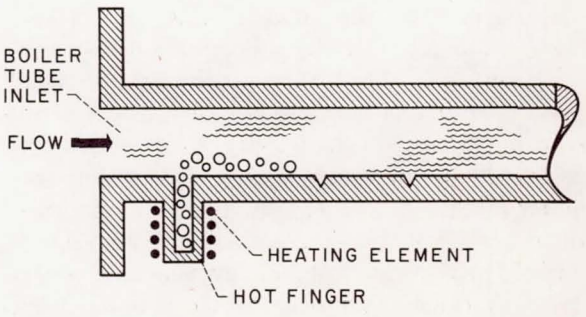

FIGURE II–33.—Nucleating device for liquid-metal boiler tube.

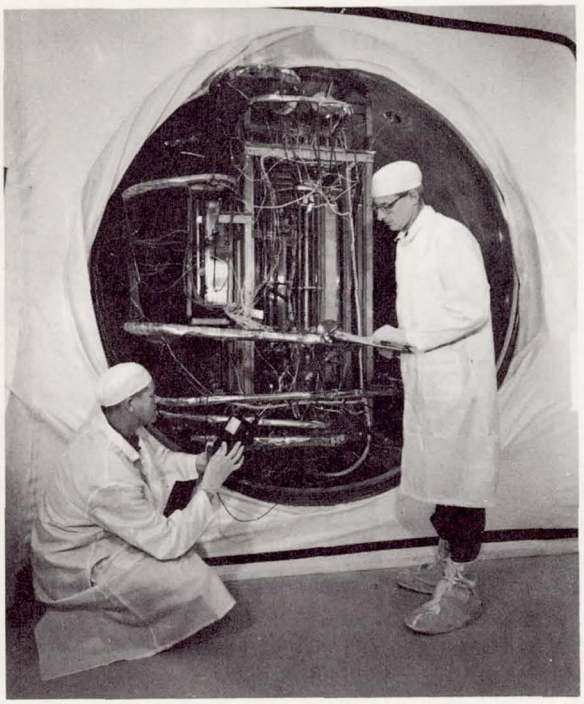

FIGURE II–34.—High-temperature alkali-metal boiling facility.

higher, refractory metals are needed, such as tantalum, columbium, and molybdenum. These metals are expensive, have severe corrosion problems, and must be kept free of oxygen at elevated temperatures. If not, oxygen will diffuse easily through grain boundaries and react with the metals to form a powdery oxide. In the vacuum of space, this is no problem, but for testing on Earth it is a different matter; cumbersome vacuum tanks must be used. Figure II–34 shows part of a columbium metal facility used for studying the boiling of sodium at temperatures over 1900° F. This is a highly instrumented, ultraclean, complex unit mounted in a deep vacuum vessel. Vacuums of the order of 10^{-7} millimeter of mercury have been achieved during operation. Use of an 8-foot-diameter by 18-foot-long vacuum tank for the study of a multitube condenser-radiator is shown in figure II–35. Potassium vapor enters the tubes at about 1400° F and condenses into liquid potassium by the time the flow reaches the dark area of the tubes. This photograph was taken with only the light given off by the hot radiator tubes.

Space Radiator

As was mentioned earlier, the radiator for a a space power system can be of colossal size. In fact, even at high temperatures it remains the largest and heaviest component in the system. This is illustrated in figure II–36, which shows a proposed design for an eight-man Mars mission. The radiator in this case is the size of two football fields! This large size arises because, to generate a certain amount of power, the system must reject a given amount of waste heat. Since radiation to space is the only effective way of doing this, look at the relations governing radiant heat loss. These show that radiator area depends directly on the heat rejected and the surface radiation properties, and inversely on the absolute surface temperature to the fourth power. High temperatures near the material limits are already being utilized, and surface properties are chosen to be as close as possible to that perfect radiator, the blackbody. This does not leave much room for further reducing radiator area.

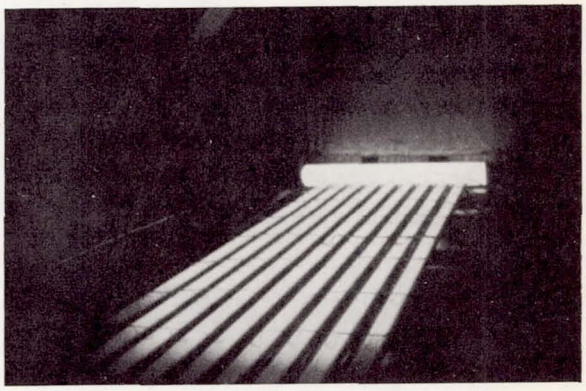

FIGURE II–35.—Condenser-radiator using potassium at 1400° F.

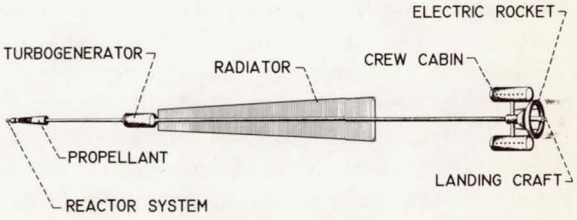

FIGURE II–36.—Space vehicle for eight-man Mars trip.

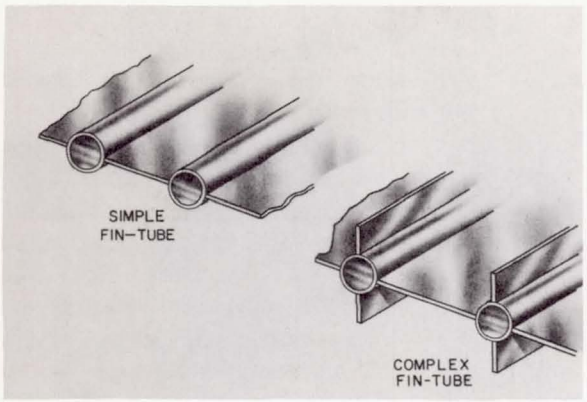

FIGURE II–37.—Fin tube configurations for space radiator.

In addition, the radiator must be constructed so that system fluid will not be lost through meteoroid punctures. The radiator must therefore be segmented, be armored, have its vulnerable area reduced, or have some combination of these protective methods. This further limits the designs. However, even a reduction in radiator weight of only a few percent would take off a large amount of vehicle weight at launch, so consider what can be done to reduce radiator weight. The first is a simple fin-tube arrangement (fig. II–37). This employs lightweight fins to radiate heat conducted from the tubes where the hot fluid is being condensed and cooled. The fins keep the area large while reducing radiator weight and reducing vulnerable area for meteoroid puncture. To minimize weight, large area fins and few tubes are utilized. However, at the center of the fin, the temperature is diminished and fin area here is not very effective. Since fins do provide some improvement, a few more might be added, as in the second concept shown in figure II–37. However, because of radiant interchange between the perpendicular fins, it is found that the gain in radiating efficiency is soon outweighed by the fin weight penalty and the efficiency cannot be increased any further.

Since the heat rejected by radiation is proportional to temperature to the fourth power, it is desirable to have the highest temperature possible over the whole radiator surface. This means that a uniform fin temperature is required. One design intended to do this is shown in figure II–38. The fin is built like a chamber and is partially filled with a secondary fluid whose boiling point is slightly below that of the condensing fluid. The secondary fluid is evaporated at the tube wall and carries heat to the fin surface, where the secondary fluid condenses. The secondary fluid is then returned to the hot tube surface by a capillary wick material. This Rankine evaporation-condensation cycle produces an effective thermal conductivity that can be about 200 times that of copper, so it is effective in keeping the temperature constant over the fin span. Such a design appears to offer some weight advantage over simple fin-tube arrangements, and as noted even small gains are important. Segmenting the wick compartments provides additional reductions in the probability of dangerous meteoroid punctures.

Use in Earthbound Powerplant

Some of the problems with space power systems have been pointed out in this discussion. If enough of the heat-transfer and stability problems of these space systems can be resolved, the concepts might some day be used in Earth-based electric powerplants. Nuclear reactor electric powerplants are already in use in many countries around the world. Higher efficiencies could be obtained in these systems by going to a high-temperature liquid metal forced flow system such as was discussed here. Perhaps also some advantages would be gained by utilizing high accelerations in a compact rotating unit that might contain the boiler, turbine, condenser, and pump elements in one close-coupled unit.

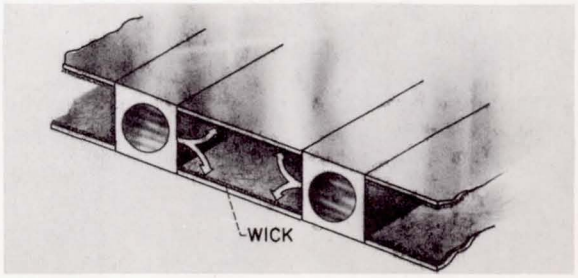

FIGURE II–38.—Use of secondary fluid to provide constant temperature fins.

CONCLUDING REMARKS

In conclusion it should be pointed out that only a limited number of heat-transfer problems have been discussed that have required further investigation for the development of space technology. In the discussion two systems have been chosen for purposes of illustration: the nuclear rocket engine, and a space electric power generation system. Although these are specific systems, their design requirements have led to many problems that are of a basic nature. These include such things as turbulent heat transfer with large flow accelerations, flow of near-critical fluids in curved channels, solidification of a liquid flowing over a cooled surface, and the many complexities of high-temperature forced flow boiling.

It is hoped that this discussion has provided a good indication of the scope of heat-transfer information which is available as a result of space programs.

BIBLIOGRAPHY

[Listed in order of discussion of subject matter in text.]

Nuclear Rocket Engine

SCHACHT, RALPH L.; QUENTMEYER, RICHARD J.; AND JONES, WILLIAM L.: Experimental Investigation of Hot-Gas Side Heat-Transfer Rates for a Hydrogen-Oxygen Rocket. NASA TN D-2832, 1965.

BOLDMAN, DONALD R.; SCHMIDT, JAMES F.; AND FORTINI, ANTHONY: Turbulence, Heat-Transfer, and Boundary Layer Measurements in a Conical Nozzle With a Controlled Inlet Velocity Profile. NASA TN D-3221, 1966.

RIBNER, H. S.; AND TUCKER, M.: Spectrum of Turbulence in a Contracting Stream. NACA TN 2606, 1952.

HENDRICKS, ROBERT C.; GRAHAM, ROBERT W.; HSU, YIH Y.; AND FRIEDMAN, ROBERT: Experimental Heat-Transfer Results for Cryogenic Hydrogen Flowing in Tubes at Subcritical and Supercritical Pressures to 800 Pounds Per Square Inch Absolute. NASA TN D-3095, 1966.

HENDRICKS, R. C.; AND SIMON, F. F.: Heat Transfer to Hydrogen Flowing in a Curved Tube. Multi-Phase Flow Symposium, Norman J. Lipstein, ed., ASME, 1963, pp. 90–93.

SIEGEL, R.; AND SAVINO, J. M.: An Analysis of the Transient Solidification of a Flowing Warm Liquid on a Convectively Cooled Wall. To be Presented at the Third International Heat Transfer Conference, Chicago, Ill., Aug. 1966.

Space Electric Powerplant

GUTIERREZ, O. A.; SEKAS, N. J.; ACKER, L. W.; AND FENN, D. B.: Potassium Condensing Tests of Horizontal Multitube Convective and Radiative Condensers Operating at Vapor Temperatures of 1250° F to 1500° F. Paper Presented at Rankine Cycle Space Power Systems Specialist Conference, AIAA, Cleveland, Oct. 26–28, 1965.

FENN, DAVID B.; COE, HAROLD H.; AND GUTIERREZ, ORLANDO A.: Steady-State Performance of a Modified Rankine Cycle System Using Water. NASA TN D-3333, 1966.

SIEGEL, R.; AND KESHOCK, E. G.: Effects of Reduced Gravity on Nucleate Boiling Bubble Dynamics in Saturated Water. AIChE J., vol. 10, no. 4, July 1964, pp. 509–517.

SIEGEL, ROBERT; AND KESHOCK, EDWARD G.: Nucleate and Film Boiling in Reduced Gravity From Horizontal and Vertical Wires. NASA TR R-216, 1965.

JEGLIC, FRANK A.; AND GRACE, THOMAS M.: Onset of Flow Oscillations in Forced-Flow Subcooled Boiling. NASA TN D-2821, 1965.

HILDING, WINTHROP E.; AND COOGAN, CHARLES H., JR.: Heat Transfer Studies of Vapor Condensing at High Velocities in Small Straight Tubes. NASA CR-124, 1964.

LEWIS, J. P.: Experimental Investigation of Forced Flow Boiling of Sodium. Paper Presented at Rankine Cycle Space Power Systems Specialist Conference, AIAA, Cleveland, Oct. 26–28, 1965.

HOWELL, J. R.; AND SIEGEL, R.: Incipience, Growth, and Detachment of Boiling Bubbles in Saturated Water from Artificial Nucleation Sites of Known Geometry and Size. To be Presented at the Third International Heat Transfer Conference, Chicago, Ill., Aug. 1966.

GOODYKOONTZ, JACK H.; AND DORSCH, ROBERT G.: Local Heat-Transfer Coefficients for Condensation of Steam in Vertical Downflow Within a §-inch-Diameter Tube. NASA TN D-3326, 1966.

KREBS, RICHARD P.; HALLER, HENRY C.; AND AUER, BRUCE M.: Analysis and Design Procedures for a Flat, Direct-Condensing, Central Finned-Tube Radiator. NASA TN D-2474, 1964.

HALLER, HENRY C.; LINDOW, BRUCE G.; AND AUER, BRUCE M.: Analysis of Low-Temperature Direct-Condensing Vapor-Chamber Fin and Conducting Fin Radiators. NASA TN D-3103, 1965.

Page intentionally left blank

III Hydrodynamics of Liquid Surfaces

EDWARD W. OTTO
Lewis Research Center

FOR THE LAST SEVERAL YEARS the Lewis Research Center has been studying the behavior of liquids and gases in a zero-gravity environment with respect to the management of propellants and liquids in space vehicles during coasting flight. The behavior of fluids in this environment is governed to a large extent by capillary forces that can often be neglected in normal gravity. These studies have contributed a great deal to the understanding of the dynamic behavior of liquids under the influence of capillary or surface tension forces such as would be encountered in small tubes, screens, porous materials, and similar geometries that are common to the petroleum industry. Therefore, a review of those hydrodynamic phenomena that are strongly influenced by surface tension forces is presented herein. Special emphasis is placed on description of the fluid behavior in terms of the fluid properties and other physical constants of the system and on the dimensionless scaling parameters that lead to a better understanding of the physical mechanisms governing the behavior.

ANALYTICAL CONCEPTS

The study of the change in basic mechanisms or fluid behavior between 1 and 0 g leads to the examination of the change in forces or force levels in going from one gravity field to the other. In general, the forces acting on a liquid are the inertial and the intermolecular forces that are exhibited in the form of the surface tension forces. Under 1 g, or Earth-bound conditions, a liquid in a container is restrained from accelerating freely in the gravity field. Under these conditions the inertial forces predominate, and only small effects of the surface tension forces are noticeable. Typically, the effects of dominant inertial forces are the shaping of liquids in tanks, the weight of the liquid, the hydrostatic pressure of liquid columns, the rise of vapor bubbles in liquid due to buoyancy, and the convection currents in liquids as a result of heat inputs. Although the surface tension forces are small in comparison with inertia forces at 1 g, their effects are still observable in the meniscus of liquids in contact with solid bodies and in the capillary rise or depression in small diameter tubes.

However, when a liquid or a system containing liquid and vapor is allowed to accelerate freely in the local gravity field, the inertia forces disappear and the surface tension forces remain. These forces are dominant in determining the equilibrium liquid configuration and the liquid configuration dynamics and play a larger role in the heat-transfer mechanics.

Early History

The history of the study of surface-tension phenomena can be traced as far back as Leonardo da Vinci and Sir Isaac Newton; however, it was Young who first established the theory by demonstrating how the principles of surface tension and contact angle can be used to explain a great many capillary phenomena. The theory was put on a firm mathematical foundation by Laplace and later Poisson. Further developments were made by Gauss, who applied the principle of conservation of energy to the system and obtained not only the equation of the free surface but also the conditions of the contact angle. Other early investigators include Duprè, Rayleigh, Gibbs, and Plateau, who utilized soap

bubbles and other devices to determine the equilibrium configuration of liquids. Later investigations were carried out by Langmuir and Harkins in the United States and Adam and Burdon in England.

Liquid Contact Angle

Consider a liquid in contact with a solid surface. The free surface energies at the solid-liquid-vapor interfaces may be represented by the surface-tension forces acting in the direction of the surfaces. The angle at which the liquid meets the solid surface, measured in the liquid, is the contact angle. A schematic diagram illustrating how these surface-tension forces act at the solid-liquid-vapor interfaces is presented in figure III–1.

For the liquid to be in equilibrium with the solid surface, the surface-tension forces at the solid-liquid-vapor interfaces must be in balance parallel to the solid surface. Therefore,

$$\sigma_{vs}=\sigma_{\ell s}+\sigma_{v\ell}\cos\theta \tag{1}$$

and

$$\theta=\cos^{-1}\frac{\sigma_{vs}-\sigma_{\ell s}}{\sigma_{v\ell}} \tag{2}$$

(Symbols are defined in the appendix.) Equation (1) is known as Young's equation. It is observed that the contact angle θ depends on the magnitudes of the three surface-tension forces. When $(\sigma_{vs}-\sigma_{\ell s}/\sigma_{v\ell}$ is between 0 and 1, the contact angle θ lies between 0° and 90°, and the common convention is to call the liquid a wetting liquid. If, however, $(\sigma_{vs}-\sigma_{\ell s})/\sigma_{v\ell}$ lies between 0 and −1, the contact angle θ will lie between 90° and 180°, and the liquid is said to be a nonwetting liquid.

From these considerations, it can be concluded that the contact angle should remain constant in any gravity field, including a weightless environment, because the intermolecular forces that are exhibited in the surface-tension forces are independent of the level of the gravity field.

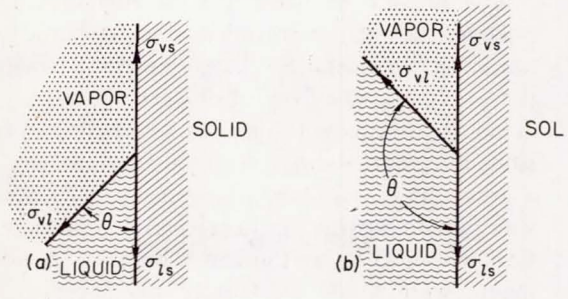

(a) Wetting liquid, $0° < \theta < 90°$.

(b) Nonwetting liquid, $90° < \theta < 180°$.

FIGURE III–1.—Surface energy and contact angle relation.

Pressure Difference Across Liquid-Vapor Interface

Although the property commonly referred to as surface tension is an energy, it behaves in every way like a tension and tries to make the surface as small as possible. Thus a drop of liquid tends to become spherical, and the tendency of the surface to contract increases the pressure inside the drop. Because the pressure everywhere inside the drop is the same, this pressure difference between the inside and outside of the drop is the pressure drop across the interface and is given by the following expression:

$$\Delta P=\frac{2\sigma}{R} \tag{3}$$

This expression is found everywhere in the literature and is simply derived by equating the surface-tension force acting along a meridan circumference to a pressure difference times the circular area enclosed by this meridan circumference. If the interface is not spherical, the pressure drop is given by the more general equation

$$\Delta P=\sigma\left(\frac{1}{R_1}+\frac{1}{R_2}\right) \tag{4}$$

Dimensionless Parameters

Dimensionless parameters have been employed in the field of fluid mechanics to describe behavior similarities between systems of different size and to define different behavior regions. For instance, Reynolds and Rayleigh numbers define the conditions required to obtain similar

flow and convection current characteristics, respectively, in different sized systems and also define regimes of different behavior. Other dimensionless parameters that have been found useful in the field of fluid mechanics are Grashof number, Prandtl number, Froude number, Nusselt number, Mach number, etc. These parameters are useful to the theorist in providing an insight into the basic behavior mechanism and to the engineer as an aid in studying the behavior of full-sized systems through the use of models.

Two dimensionless parameters that are useful in the field of capillarity are Bond number *Bo*, the ratio of gravitational or acceleration forces to capillary or surface-tension forces, and Weber number *We*, the ratio of pressure or inertia forces to surface tension forces. These parameters are defined in terms of the physical constants of the system as follows:

$$Bo=\frac{F_a}{F_c}=\frac{Ma}{\sigma L}=\frac{\rho L^3 a}{\sigma L}=\frac{\rho}{\sigma}L^2 a \qquad (5)$$

$$We=\frac{F_i}{F_c}=\frac{\text{(Pressure drop) (Area)}}{\sigma L}=\frac{\rho V^2 L^2}{\sigma L}=\frac{\rho}{\sigma}V^2 L \qquad (6)$$

The Bond number defines the acceleration or gravity regimes in which either acceleration or capillary forces dominate. For instance, when the Bond number is large (greater than one), acceleration forces dominate; whereas, when the Bond number is small (less than one), the surface-tension forces will be dominant in determining the fluid mechanisms. Bond number should also be useful in predicting the critical acceleration of the liquid gas interface.

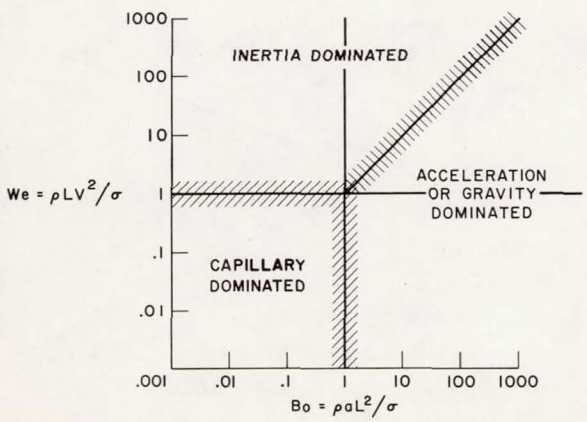

FIGURE III–2.—Hydrodynamic regimes.

The Weber number defines the behavior of the interface in the presence of flow forces. When the Weber number is large, the flow forces predominate and the capillary forces are insignificant; whereas, when the Weber number is small, the capillary forces will shape the interface. Rearranging the expression for Weber number gives an indication of the transition time for zero-gravity phenomena, such as interface formation or wave period:

$$We=\frac{\rho}{\sigma}V^2 L=\frac{\rho}{\sigma}\left(\frac{L}{t}\right)^2 L=\frac{\rho}{\sigma}\frac{L^3}{t^2} \qquad (7)$$

$$t=\left(\frac{\rho}{We\sigma}\right)^{1/2} L^{3/2} \qquad (8)$$

The value of the Weber number will be empirical depending on the specific configuration.

Reynolds (ref. 1) has portrayed the various hydrodynamic regimes as a function of Bond and Weber numbers as shown in figure III–2, which is taken from his work. This diagram provides a useful means of visualizing the several hydrodynamic regimes as defined by the several dimensionless parameters.

FACILITIES

The Lewis Research Center has utilized several zero-gravity facilities to obtain various periods of zero-gravity time. A diagram of the facilities and a comparison of their times is shown in figure III–3. Each of these involves the technique of free fall to obtain a zero-gravity, or weightless, environment.

Requirements on Time and Acceleration Level as Functions of Size

The study of the various aspects of fluid mechanics in zero-gravity requires zero-gravity facilities with different characteristics. For example, the bubble behavior produced by heat transfer is a high-speed phenomenon, and only a short-time facility, such as a drop tower, is required. However, if the heat-transfer charac-

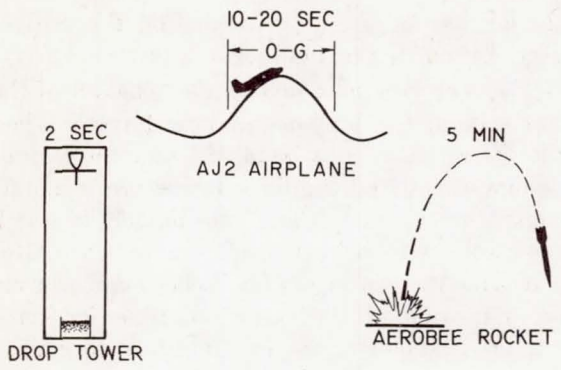

FIGURE III–3.—Zero-gravity facilities.

teristics in a system are being studied, as in a closed propellant tank, a facility offering several minutes of zero-gravity time is required, such as a ballistic rocket. The study of forced convection mechanics, or the behavior of evaporators or condensers, requires relatively short times such as available in drop facilities or airplanes. In these studies the interface is generally so small that small perturbations of the order of a few milli-g's are not important as indicated by the Bond number criterion; however, in studying the behavior of large liquid-vapor interfaces, as in models of propellant tanks, the acceleration level provided by the facility becomes important. The initial disturbance also becomes important; however, if the zero-gravity time is long enough for this disturbance to damp out or be negated by a collection and release maneuver, it becomes less of a consideration.

The expressions for Bond and Weber numbers can be used to provide an estimate of the zero-gravity time and maximum gravity level required in a facility to perform interface studies. A plot of the predicted interface formation time and allowable acceleration, or g-level, as a function of model size is shown in figure III–4. The allowable acceleration level results from the expression for Bond number using an experimentally determined Bond number near 1, where L corresponds to the radius. The interface formation time is obtained from the expression for time developed from the Weber number relation using an experimentally determined Weber number near 7, where L is again the radius. The most significant aspect of figure III–4 is the low acceleration, or g-level, required for interface experiments in the 2- to 20-inch range (the most desirable model range). This requirement also implies that the initial disturbance be low. These acceleration and disturbance requirements have prevented successful use of airplane facilities for interface experiments even though their 15-second time range has been very attractive.

Zero-Gravity Drop Tower

One-hundred-foot drop facility.—The Lewis Research Center zero-gravity drop-tower facility has a usable drop height of 85 feet that yields a free-fall time of 2.3 seconds. This tower is a 21-foot-square, eight-story structure shown schematically in figure III–5. In this particular facility air drag on the experimental package is kept to a minimum by allowing the experimental package to fall within a protective drag shield. The experimental package and the drag shield are unguided during the free fall.

A 3- by 5- by 6.75-foot-deep sandbox is located on the first floor of the building and serves as part of a deceleration device for the experiment. Adjacent to the sandbox is a sand storage hopper, which is used in aerating the sand. Sand aeration is accomplished by using an enclosed screw-type auger to pump sand from

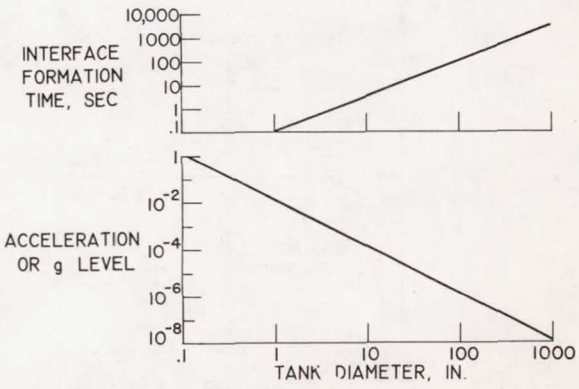

FIGURE III–4.—Effect of model size on facility and gravity-level requirements.

the sandbox into the hopper and then back into the sandbox through a strainer.

The fifth floor of the drop tower serves as a working and assembly area for handling the experiment before and after a test drop. In order to facilitate test operations, a cradle support for the drag shield is welded to a movable section of floor that can be rolled out of the way before each drop.

The eighth floor contains an electrically powered hoist used for lifting the experiment to its predrop position. Attached to a roof beam directly over the drop area is a combination wire support and release mechanism from which the experiment is hung. The release mechanism consists of a double-acting air cylinder with a hard steel knife edge attached to the piston. Pressurization of the air cylinder forces the knife edge to cut the wire against an anvil, thereby ensuring a smooth release.

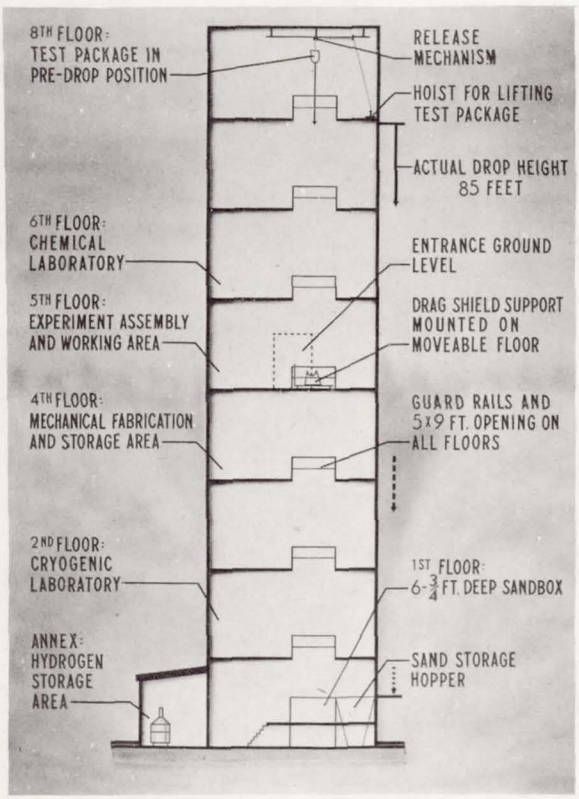

FIGURE III–5.—100-Foot zero-gravity drop tower.

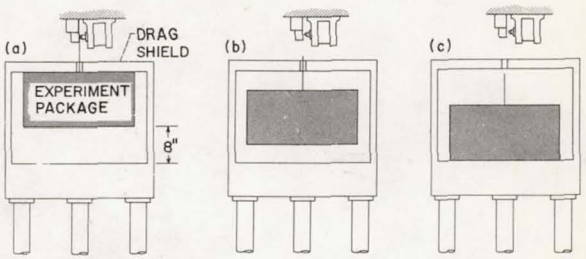

(a) Before test drop. (b) During test drop. (c) After test drop.

FIGURE III–6.—Zero-gravity drag shield.

Air resistance on the experiment package is kept below 10^{-5} g of deceleration by allowing the experimental package to fall within a 400-pound drag shield as shown in figure III–6. The ratio of weight to frontal area of the drag shield is kept high so that the deviation from a true free fall is kept to a minimum. Both drag shield and experiment package fall together during the test drop. Access to the inside of the drag shield is through two detachable side plates. Three maple spikes, 3 inches in diameter and 73 inches in length, are mounted in a row along the bottom. These serve to decelerate the drag shield and the experiment package upon impact into the sandbox. Attached to the bottom of the spikes are machined aluminum tips. The size of the aluminum tips is reduced after every drop to compensate for sand packing and thus to maintain a nominal decelerating force on the experiment of 15 g's.

Four-hundred-foot drop facility.—The Lewis Research Center is constructing a new drop facility, which will provide 5 seconds of zero-gravity time in a single-pass mode or 10 seconds in a double-pass mode. The double pass will be obtained by projecting the experiment from the bottom of the facility. A diagram of this facility is shown in figure III–7. It consists of a 30-foot-diameter concrete-lined shaft, somewhat over 500 feet deep. A 20-foot-diameter steel tube capable of being evacuated is mounted off center to allow for air ducts, services, elevator, etc. The projector or accelerator is mounted at

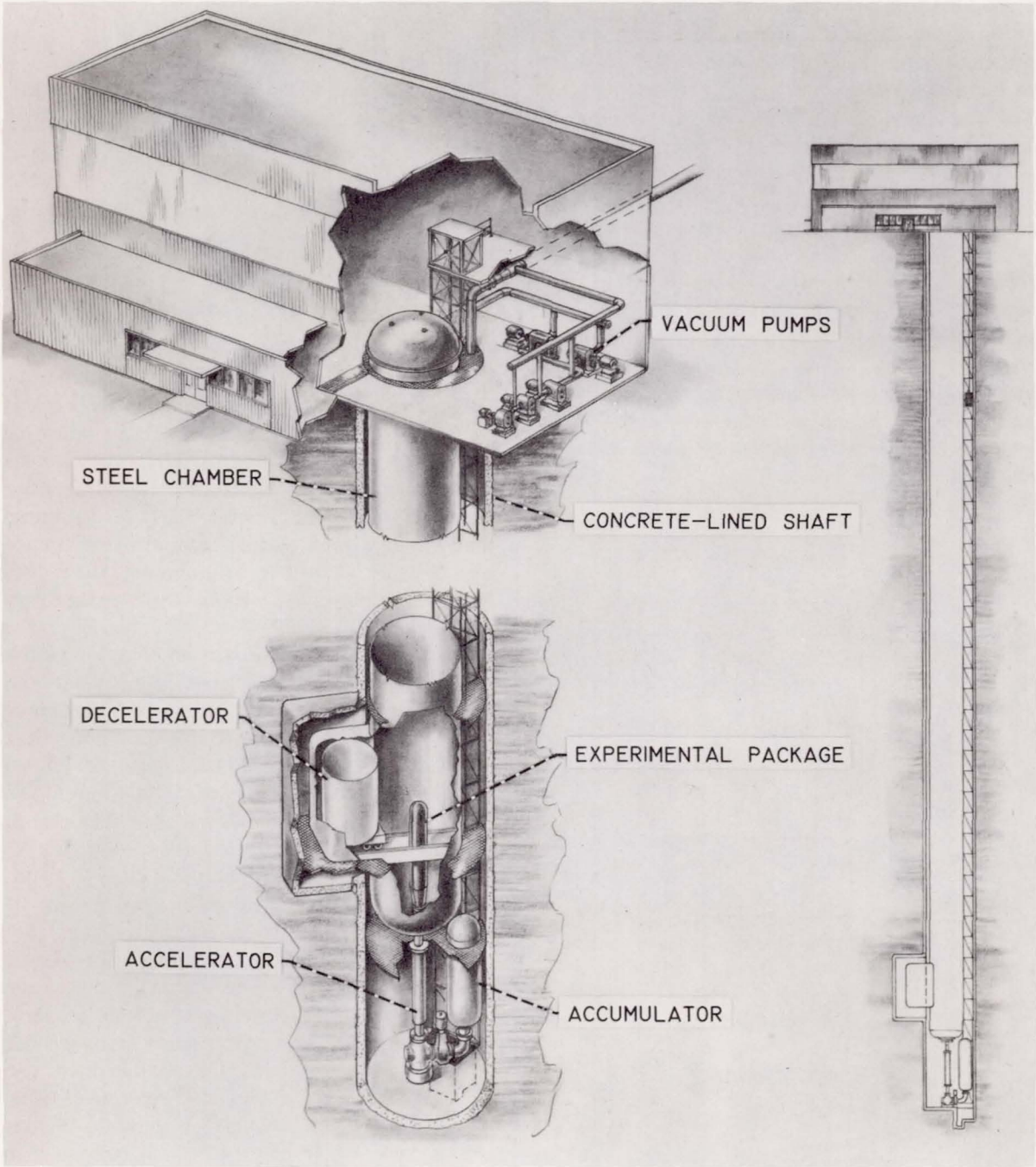

FIGURE III–7.—400-Foot zero-gravity drop facility (perspective cutaway view).

the bottom of this steel tube, and the deceleration device, which consists of styrofoam, is mounted in a pocket near the bottom of the steel tube. The decelerator rolls into place after the experiment is projected. Evacuation to 10^{-5} atmospheres allows experiments to be conducted without a drag shield; however, the accelerator and decelerator are designed to accommodate the weight of a drag shield if desired.

Airplane Zero-Gravity Facility

The Lewis Research Center operates an AJ–2 airplane as a zero-gravity facility that provides from 10 to 20 seconds of near zero-gravity time. The lower time figure is obtained when experiments are "free floated" and the gravity level is low; the initial disturbance, however, is high. The longer times are obtained for "tied down" experiments where the gravity level is higher (in the neighborhood of 0.01 to 0.05). As previously noted, the airplane facility has not been useful for interface studies because of the high initial disturbance.

Rocket Zero-Gravity Facilities

The Lewis Research Center has used various rockets as zero-gravity facilities providing extended times. The Aerobee sounding rocket has been used for a series of heat-transfer experiments. Atlas side pods have also been utilized for heat-transfer experiments. At the present time, the Center is developing the WASP, a two-stage solid-propelled sounding rocket for larger, heavier experiments.

FIGURE III–8.—Aerobee rocket zero-gravity facility.

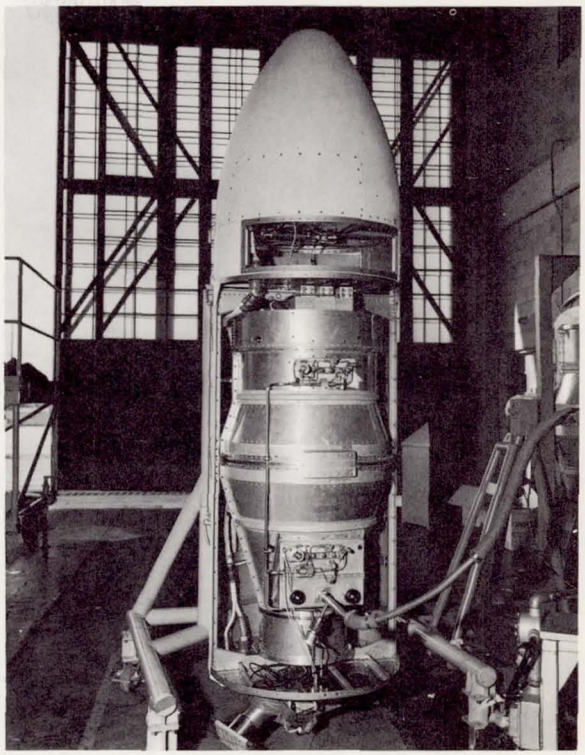

FIGURE III–9.—Atlas side-pod zero-gravity facility.

The Aerobee rocket shown in figure III–8 permits a payload size up to approximately 15 inches in diameter and a weight up to approximately 300 pounds. It will provide approximately 3 to 5 minutes of zero-gravity time for payload weights from 200 to 300 pounds. The gravity level is estimated to in the neighborhood of 10^{-4} g over most of the trajectory. The experiments flown on the Aerobee have involved sizable liquid-vapor interfaces, and because the Aerobee spins for stability, a despin table has been employed that holds the payload stationary. Data are obtained by telemetry, although in some experiments a camera was used; the film is recovered by parachute.

The Atlas side pod shown in figure III-9 permits a payload size up to approximately 30 inches in diameter and a weight up to approximately 400 pounds. It will provide 20 to 25

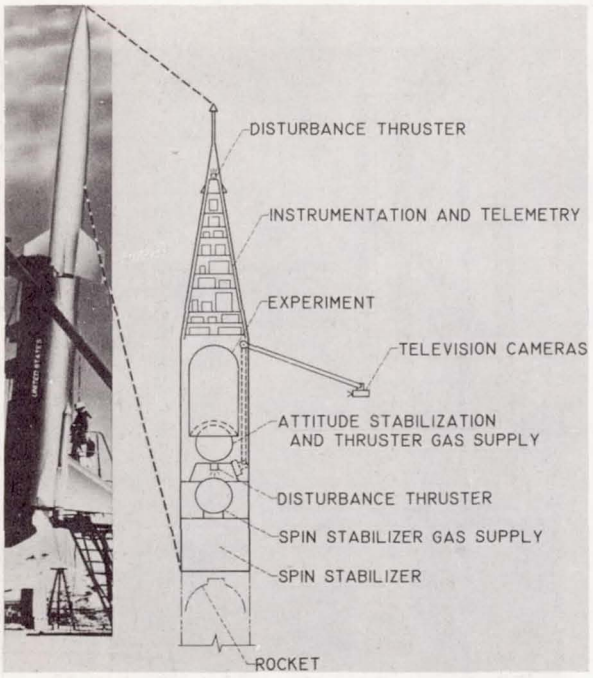

FIGURE III–10.—WASP rocket zero-gravity facility.

minutes of zero-gravity time with the capability of a very low gravity level because of the great height of the trajectory. The pod is ejected from the side of the Atlas after nose-cone separation and must be stabilized in angular rotation to realize this potential. The method employed by Lewis has been to extend weights at the end of arms to attenuate the angular rates. Data are obtained by telemetry.

The WASP rocket shown in figure III–10 permits a payload size up to approximately 30 inches in diameter and a weight up to approximately 1600 pounds. The zero-gravity time is from 7 to 11 minutes depending on payload weight, and the gravity level is estimated to be below 10^{-5} g over most of the trajectory. This rocket also spins for stability, and for those experiments employing a sizable interface a despin table is employed similar to that used in the Aerobee experiments. Data are obtained by telemetry although in the case of the fluid dynamics experiments it is intended to transmit pictures by means of television and a telemetry link.

INTERFACE STATICS

Interface Configuration in Cylinders and Spheres

The configuration of the liquid-vapor interface under weightless conditions has been studied analytically by several investigators. Benedikt (ref. 2) and Reynolds (ref. 1; Reynolds having indicated that he also found the calculations in the works of Rayleigh) calculated exact solutions for the configuration of the interface between parallel plates as a function of the gravity level or Bond number. From these calculations and the principles involved, they inferred the configuration of the interface in other geometries. Li (ref. 3) used the principle of the minimization of the free surface energies to predict the interface configuration in many geometries. All these analyses indicate that the interface

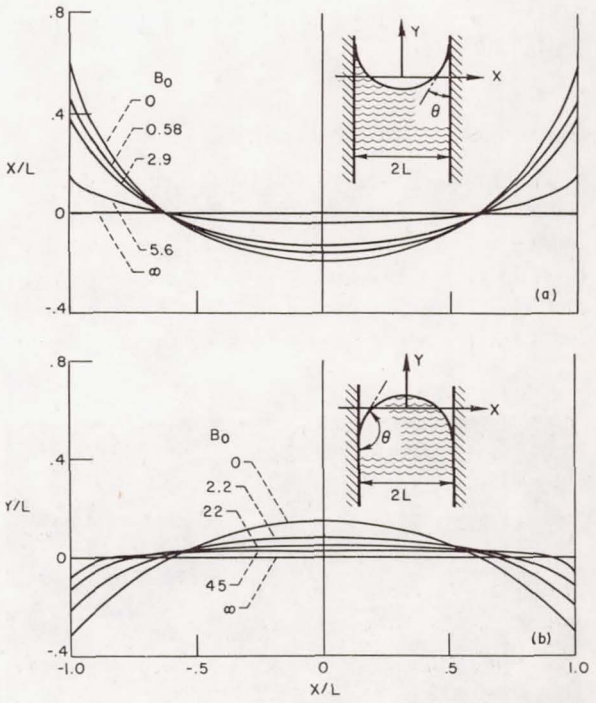

(a) Contact angle, 10°.
(b) Contact angle, 140°.

FIGURE III–11.—Calculated configuration of liquid-vapor interface between parallel plates for various Bond numbers and contact angles.

configuration is primarily dependent on the contact angle and that during weightlessness the liquid vapor interface tends to assume a constant curvature surface that intersects the tank wall at the contact angle.

The results of the calculations for the configuration of the interface between two parallel plates as obtained by Reynolds are presented in figure III–11. The calculations present the interface configurations for a relatively wetting liquid (contact angle, 10°) and a relatively nonwetting liquid (contact angle, 140°), each at a series of Bond numbers from zero (true weightlessness) to infinity (essentially representative of 1 g). At a Bond number of zero, the interface is a surface of constant curvature intersecting the wall at the contact angle. The contact angle determines whether the surface is concave or convex. The increased distortion of the surface from its constant curvature configuration as Bond number increases is apparent.

The results of the calculations for the two-dimensional case may be used to infer the configuration in three-dimensional geometries. Figure III–12 shows the predicted configuration for cylinders and for spheres as a function of the contact angle and for the volume fraction of liquid in spheres. These predicted configurations are for a Bond number of zero. Five general configurations are shown for spheres ranging from an imbedded vapor bubble for all fillings at zero degree contact angle to an imbedded liquid mass for all fillings at the hypothetical contact angle of 180°. The curved line indicates the combination of contact angles and fillings at which the interface is flat as depicted by the center diagram. The diagrams on either side of center are generally representative of the configurations obtained for the combination of contact angles and fillings in the surrounding area. The configurations predicted for cylinders do not show the end effects that would be encountered in tanks with normal ends. For tanks with hemispherical ends, the configurations may be inferred from the configuration for spheres.

Experimental verification of the predicted interface configurations has depended heavily on a suitable zero-gravity facility. The author and

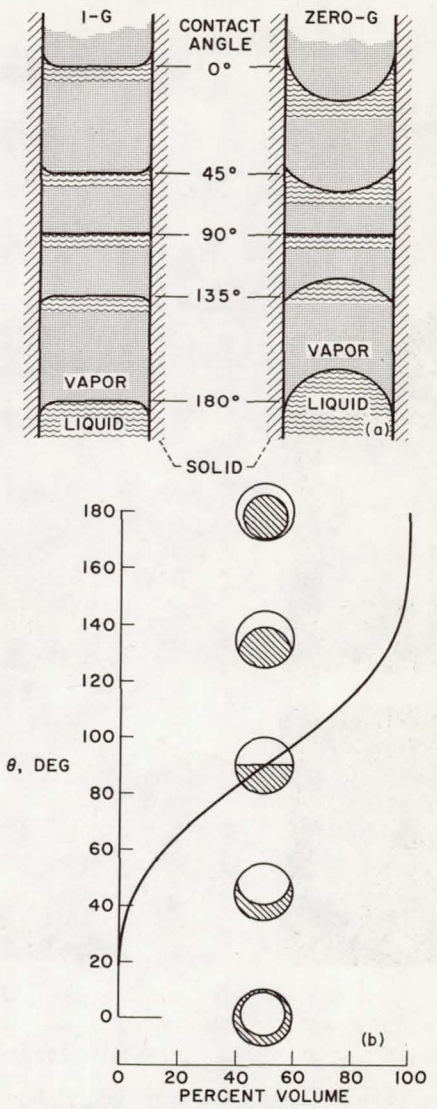

(a) Configurations in cylinders.
(b) Configurations in spheres.

FIGURE III–12.—Weightlessness configurations in cylinders and spheres.

his colleagues conducted a series of experiments (refs. 4 and 5) in the NASA Lewis Research Center 2.3-second drop-tower facility that verified the predicted configurations. These experiments were conducted with liquids with three different contact angles in spheres, cylinders, and cones at several different fillings. The results for the range of conditions can be represented by figure III–12; however, photographs of several

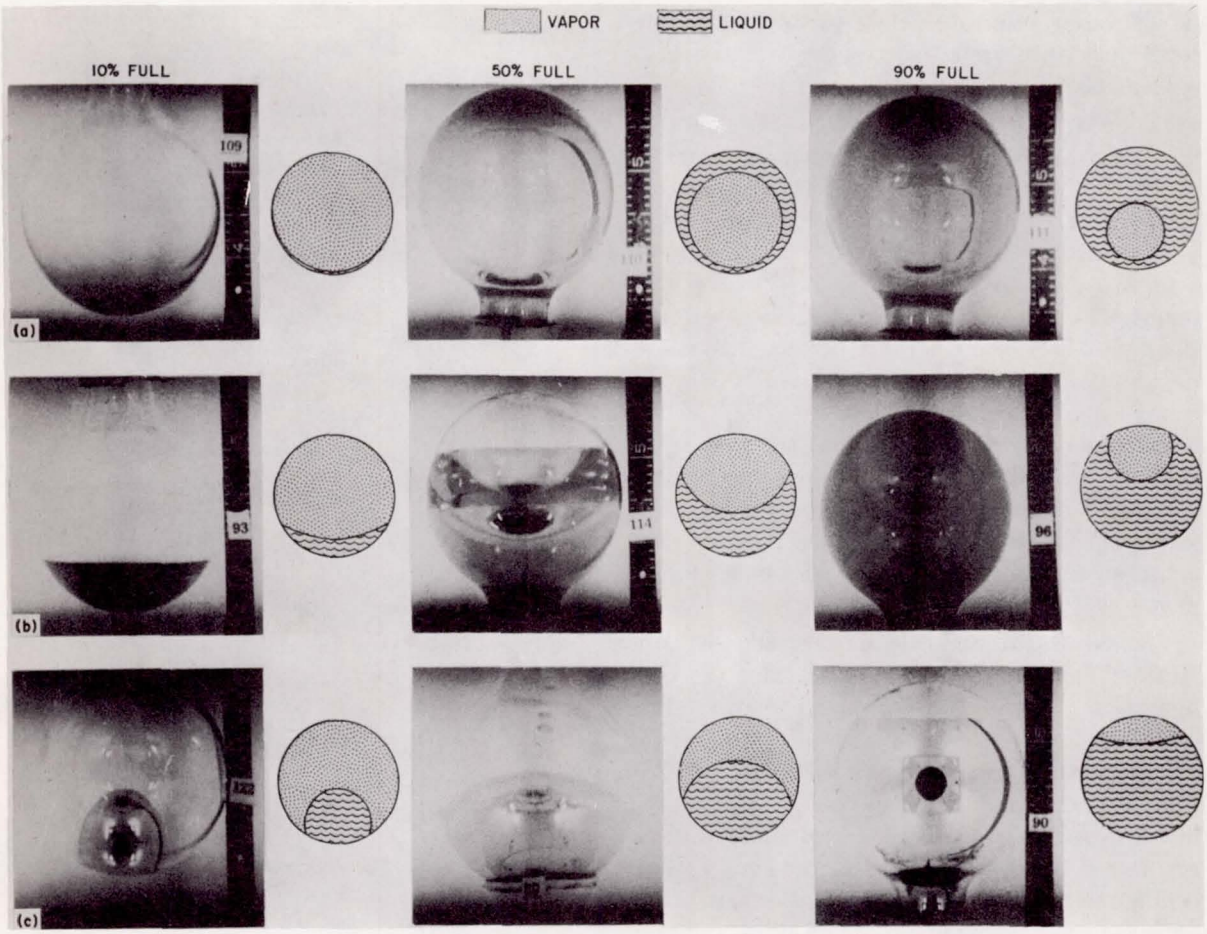

(a) Alcohol; contact angle, 0°.
(b) Tetrabromoethane; contact angle, 40°.
(c) Mercury; contact angle, 125°.

FIGURE III–13.—Configuration of liquid-vapor interface during weightlessness in spheres.

interface configurations are shown in figures III–13 and 14. Clodfelter (ref. 6) has recently used the 1.85-second drop facility at Wright-Patterson Air Force Base to confirm some of these results and has extended the work to show some interesting end effects in flat-bottomed cylinders.

Effect of Baffles

The analyses for defining the configurations of the interface indicated a reduction of system energy as the interface changed from its normal-gravity configuration to the zero-gravity configuration. Therefore, the study of the ability of tank geometries, which provide appreciable changes in surface energy to position the liquid and vapor in acceptable configurations, appeared promising. A simple configuration that probably has occurred to most investigators in the field and has been suggested and analyzed by Reynolds (ref. 1) is a tube mounted over the pump inlet concentric with the vertical centerline with holes around the bottom to allow fluid transfer

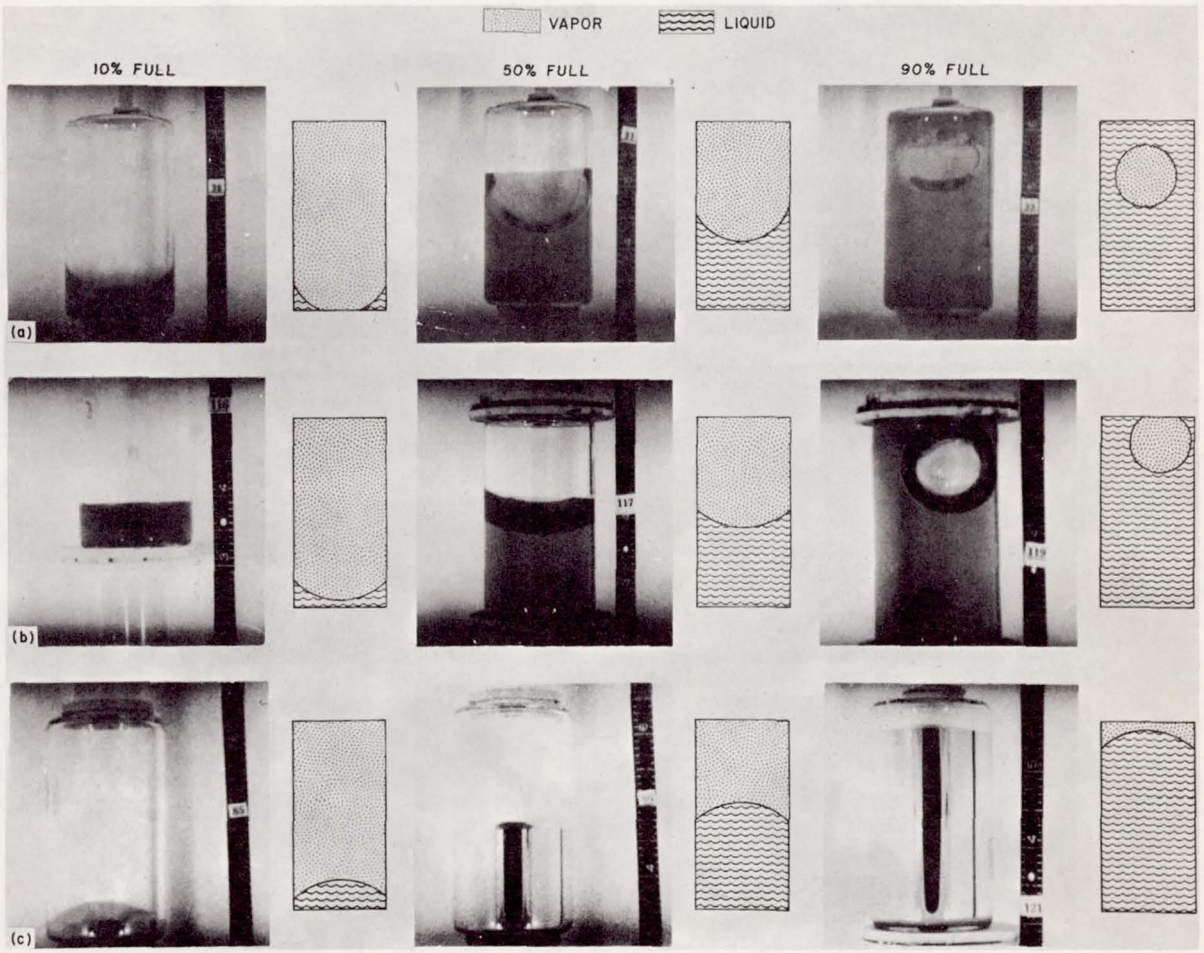

(a) Alcohol; contact angle, 0°.
(b) Tetrabromoethane; contact angle, 40°.
(c) Mercury; contact angle, 125°.

FIGURE III–14.—Configuration of liquid-vapor interface during weightlessness in cylinders.

between the tank and the tube as shown in figure III–15. An analysis that uses either surface energy or capillary pressure drop can be made, which shows that a wetting liquid should rise in the tube when the tube diameter is less than one-half of the tank diameter and fall if it is greater than one-half of the tank diameter. This behavior is a positive demonstration of the tendency of the surface energy to minimize (ref. 7). Because of this minimization of the surface energy, the liquid then takes the configuration in weightlessness shown in figure III–15. The liq-

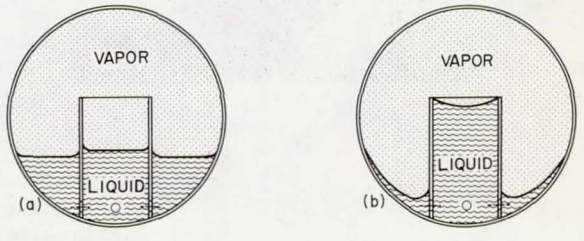

(a) 1-g configuration. (b) Zero-g configuration.

FIGURE III–15.—Capillary-type ullage control surface.

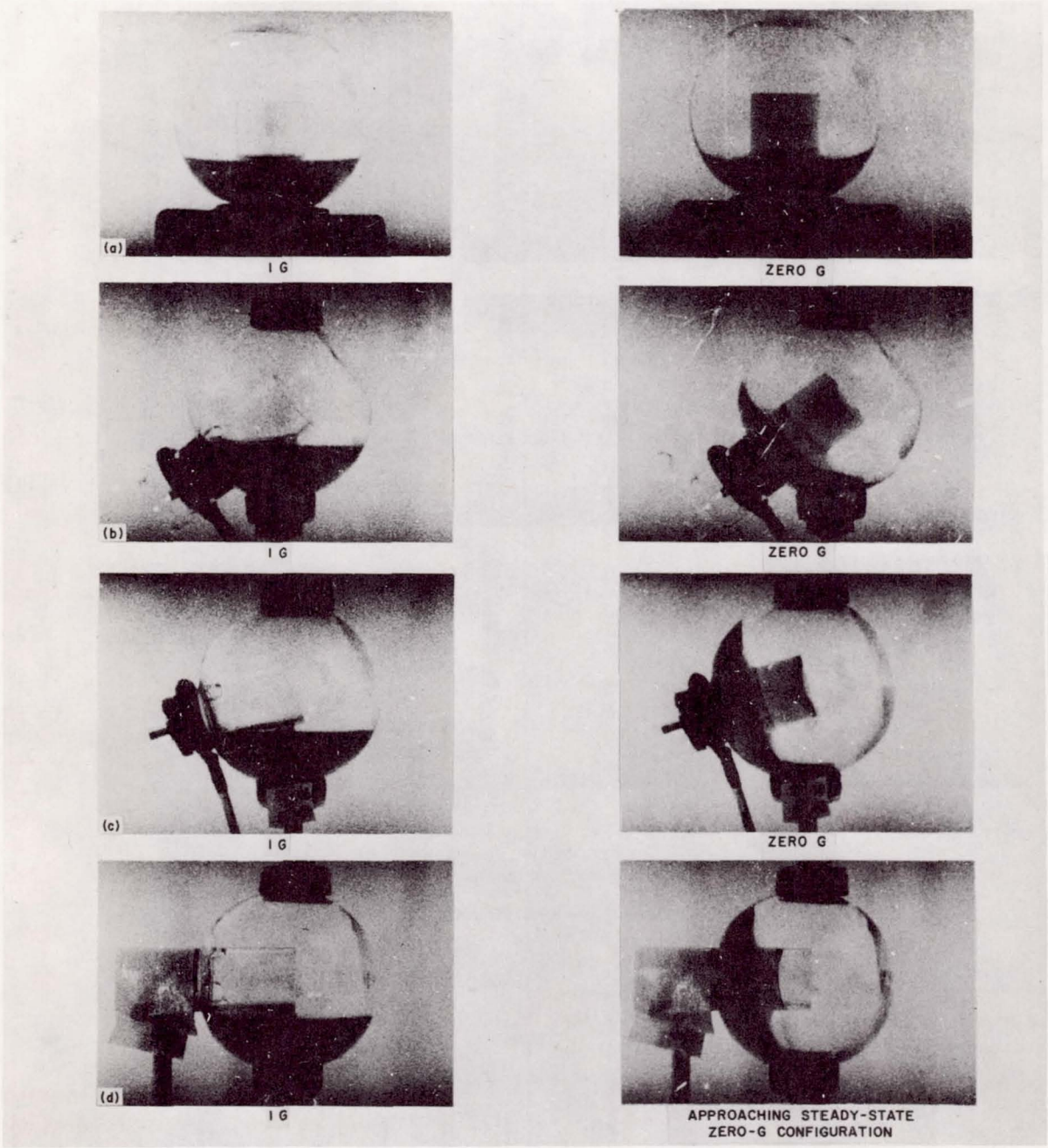

(a) Initial mounting angle, 0°.
(b) Initial mounting angle, 45°.
(c) Initial mounting angle, 75°.
(d) Initial mounting angle, 90°.

FIGURE III–16.—Drop-tower tests for range of initial mounting angles.

uid is maintained over the area of the pump inlet, while the vapor is maintained in the area of the vent.

The author and his colleagues have studied the performance of this geometry in a series of experiments in the drop tower (refs. 7 and 8) and in the Mercury Project MA–7 spacecraft (ref. 9). A desirable characteristic of this geometry in spheres and to some extent in cylinders is its ability to recapture the liquid following an excessive acceleration disturbance. This effect, which is shown in figure III–16, shows the results of drop-tower tests in which the standpipe baffle was at various initial angles to the gravity vector. For the 90° test, the time available was insufficient to allow complete filling of the baffle. The tendency of the baffle to fill with liquid was also noted at 180°, but again the time was insufficient to allow complete filling of the baffle. The most serious shortcoming of this baffle configuration is its inability to provide reliable positioning of the vapor bubble over the vent if the standpipe is more than 50 percent of the height of the sphere. If the tank is filled to more than 83 percent, the resulting ullage bubble will float free (ref. 8).

In an effort to overcome the shortcomings of the standpipe design, the geometry shown in figure III–17 was proposed (ref. 8). This design utilizes a sphere within the spherical tank somewhat offset in the direction of the pump inlet. The action is such that the vapor bubble tends to return to the location (over the vent) where it can become most nearly spherical (which represents the condition of minimum energy) after an excessive acceleration. For a geometry in which the inner sphere is 50 percent of the tank diameter and the offset is 10 percent of the tank diameter, the tank can be filled to 95 percent without the ullage bubble floating free. The tapering sections provide a stable interface position around the tank as it empties, and the geometry provides an excellent resistance to vapor pull through during pumping in addition to the capability of complete volume pumpout. Mounting the inner sphere on webs between it and the lower half of the tank creates an even stronger pumping geometry.

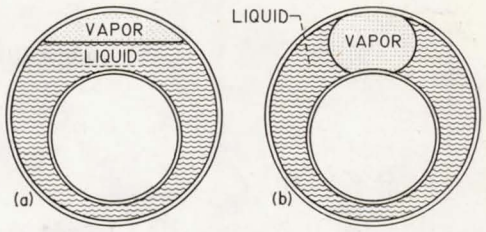

(a) 1–g configuration. (b) Zero–g configuration.

FIGURE III–17.—Application of tapered-section principle to spherical tank.

INTERFACE DYNAMICS

The previous discussion has been concerned mainly with the configuration of the interface, the location of the liquid and vapor, and the means of influencing the configuration or location under the condition of no external disturbances to the system. When disturbances such as attitude control accelerations or outflow disturbances are imposed, however, the established interface or fluid configuration will be distorted or disturbed. If the disturbance is sufficiently large, the established interface may break, and the liquid would move to a new position. The dynamic behavior of the interface in response to these disturbances is important because of its effects on various propellant management problems, such as pumping and venting operations, and on the stability of the attitude control system. The Bond and Weber numbers will be expected to be of significance in describing dynamic behavior because they incorporate the effects of acceleration, inertia, and surface energy.

Interface Formation Time Following Change in Acceleration Level

One phase of interface dynamic behavior that has been under study is the time required for the interface to form its zero-gravity configuration after release from a normal-gravity or high-acceleration field. Benedikt (ref. 10) derived an expression for the oscillation time of an initially deformed freely falling mass of liquid. Functionally, his expression is equivalent to the

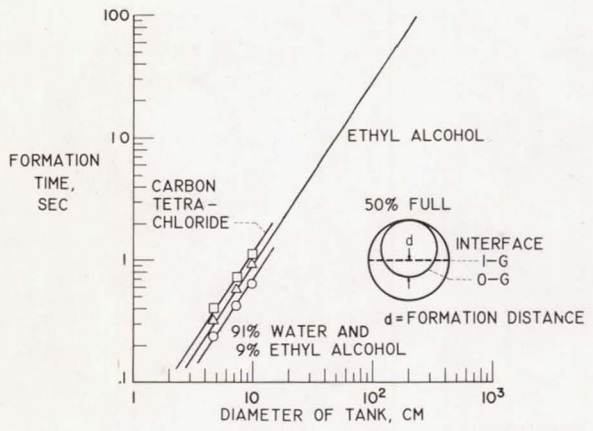

FIGURE III–18.—Effect of tank size and liquid properties on interface formation time in spheres after entering zero gravity.

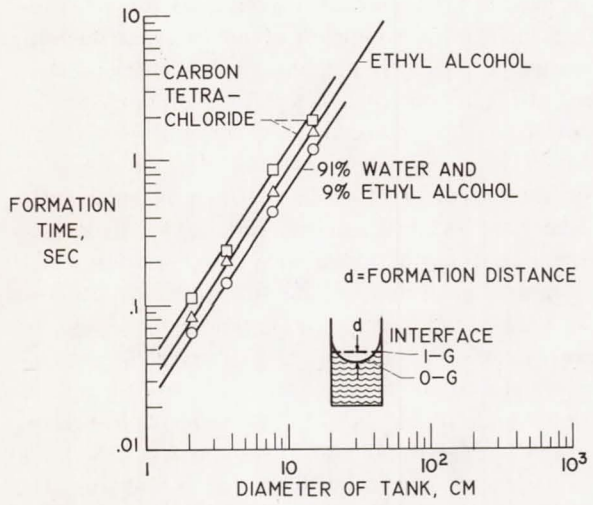

FIGURE III–19.—Effect of tank size and liquid properties on interface formation time in cylinders after entering zero gravity.

expression for Weber number; it indicates that the transition time is a function of the ratio of density to surface tension to the one-half power $(\rho/\sigma)^{1/2}$ and of a characteristic dimension of the interface to the three-halves power $D^{3/2}$. It is similar to an expression, derived by Rayleigh (ref. 11), for the oscillation frequency of a liquid jet issuing from a noncircular hole.

The author and his colleagues have conducted drop-tower experiments (ref. 12) in which the time required for the interface to form in spheres and cylinders after entering zero gravity was measured. These experiments confirmed the functional relation suggested by Benedikt. The results of these experiments are presented in figures III–18 and 19. The formation time given is that required for a point on the interface and on the vertical axis of the container to move from the 1-g to the 0-g position as depicted by the small diagrams.

The general expression for formation time as a function of fluid properties and dimensions of the system, derived from the Weber number by substituting a length divided by time, is rearranged as follows:

$$T=\left(\frac{1}{We}\right)^{1/2}\left(\frac{\rho}{\sigma}\right)^{1/2}(CD)^{3/2} \qquad (9)$$

Equation (9) indicates that formation time should vary with $D^{3/2}$ and with $(\rho/\sigma)^{1/2}$. The solid lines on figures III–18 and 19 are drawn at a three-halves-power slope. In each case the data fit the lines closely, which indicates a good correlation with theory. It was also found that the data correlate well with $(\rho/\sigma)^{1/2}$. If a Weber number of 1 is assumed, the term CD may be considered the characteristic dimension of the system. For spheres, the value of C was determined as 0.292 and for cylinders as 0.277. Although the size range is small as limited by the drop-tower time, good correlation with theory inspires confidence in the use of the Weber number expression to predict the time response in large vehicle tanks.

Interface Behavior During Outflow Disturbance

A large portion of the zero-gravity research work has been given to the determination of means to assure that liquid is located over the pump inlet prior to engine startup. Comparatively little work has been devoted, however, to a study of the effect of the outflow disturbance on the interface nearest to the outlet. There is an almost complete absence of literature reporting either analytical or experimental studies of

the phenomenon. A recent paper by Povitskii and Lyubin (ref. 13) analyzes the velocity along the free surface of the interface as affected by outflow velocity. The results of their analysis indicate that, for liquid depths greater than the diameter of the outlet tube, the free surface is not appreciably disturbed beyond a diameter corresponding to four times the depth.

Because the outflow velocity creates a velocity gradient in the liquid above the outlet that appears to carry through to the interface, the Weber number is expected to be the scaling relation useful in relating the distortion of the interface between various system sizes. For more severe velocity gradients and greater distortions, however, the viscosity may have an effect, so that the Reynolds number may also be required to scale the phenomenon properly.

Nussle (ref. 14) has conducted outflow experiments under zero-gravity conditions in the drop tower to study the behavior of the interface under this disturbance and to attempt to determine a scaling parameter. At the present time, experiments have been conducted only with flat-bottom cylinders and with initial liquid depths greater than one tank diameter. However, three ratios of outlet to tank diameter, a range of tank diameters from 2 to 16 centimeters, and the effect of baffles at the liquid outlet and gas inlet have been studied.

Photographs of the behavior of the interface during outflow under zero gravity are presented in figures III–20 and 21 for the condition of a high outlet velocity and no baffles. Note that although the outlet velocity is relatively high, the interface does not distort sufficiently to permit vapor blowthrough until it is relatively close (1 or 2 diam. of the outlet tube) to the bottom. The interface does distort considerably from the hemispherical equilibrium zero-gravity configuration with the result that considerable liquid is left on the walls at blowthrough. Also the interface shows considerable wave distortion apparently from the impingement of the outlet gas.

Schematic diagrams of the configuration of the interface at the moment of vapor blowthrough are presented in figure III–21 for a range of outflow velocities and for several inlet and outlet

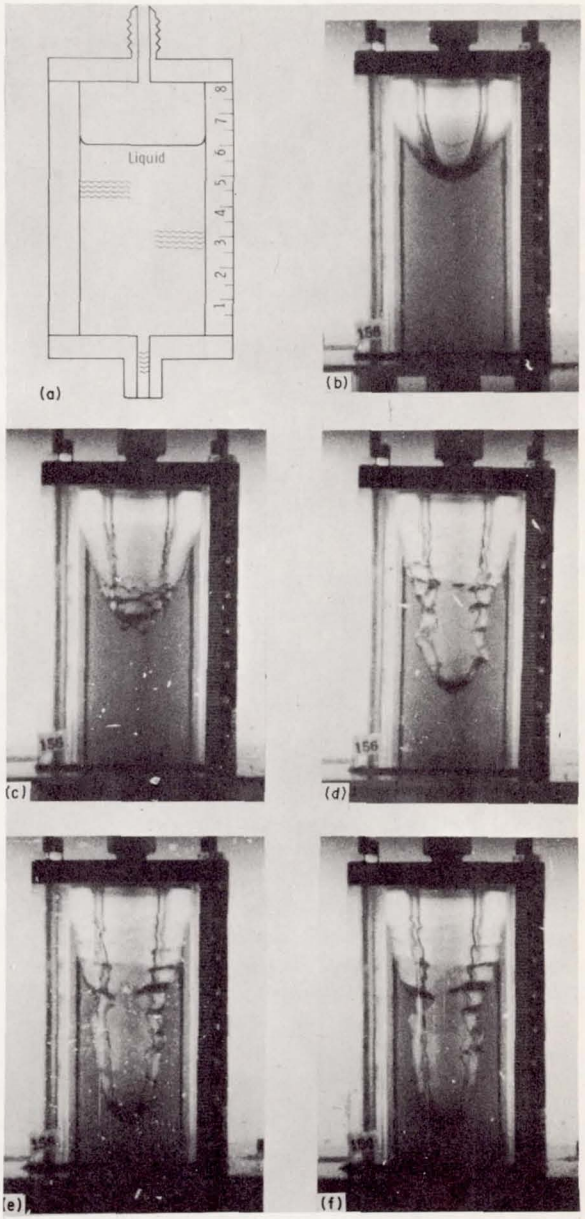

(a) 1–g configuration.

(b) Inception of pumping; time, 0 second

(c) Time, 0.03 second.

(d) Time, 0.07 second.

(e) Inception of blowthrough; time, 0.09 second.

(f) Vapor blowthrough; time, 0.10 second.

FIGURE III–20.—Interface configuration during outflow from cylindrical tank. Outlet velocity, 1408 centimeters per second.

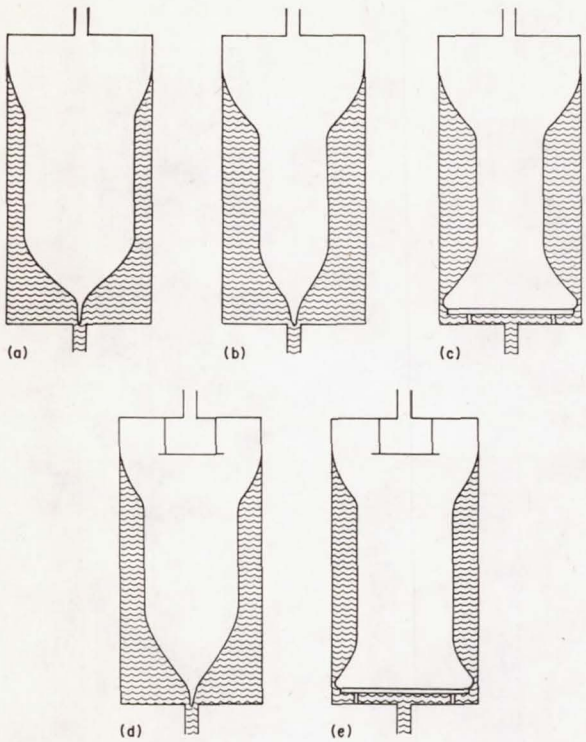

(a) Outlet velocity, 291 centimeters per second; expelled liquid, 47 cubic centimeters.
(b) Outlet velocity, 1408 centimeters per second; expelled liquid, 18.7 cubic centimeters.
(c) Outlet velocity, 1330 centimeters per second; expelled liquid, 26 cubic centimeters.
(d) Outlet velocity, 1427 centimeters per second; expelled liquid, 32 cubic centimeters.
(e) Outlet velocity, 1348 centimeters per second; expelled liquid, 45 cubic centimeters.

FIGURE III–21.—Schematic diagrams of interface configuration at vapor blowthrough during outflow from cylindrical tanks in weightlessness.

baffle combinations. These diagrams show that as the outflow velocity is increased, more liquid is left on the walls of the tank. The addition of the outlet baffle to direct the flow streamlines along the tank wall provides some improvement but not as much as might be expected. The use of a crude baffle over the gas inlet provides more improvement than might be expected, indicating that the impingement of the inlet gas is a primary cause of interface distortion. The combination of inlet and outlet baffles results in reducing the amount of liquid remaining on the wall almost to the amount left at low outflow velocities.

One of the objectives of these studies was to determine the effect of such parameters as outlet velocity, ratio of outlet to tank diameter, and absolute tank size on the interface distortion to enable prediction of allowable velocities for a nominal interface distortion in full-size vehicles. The results of these efforts are presented in figure III–22, where interface velocity on the tank centerline (which when compared with the average interface velocity is a measure of the distortion) is plotted as a function of outflow velocity for several ratios of outlet to tank diameter and a range of tank diameters from 2 to 16 centimeters. These experiments were run with a gas inlet baffle but no outlet baffle. Although the distortion of the interface does increase with average interface velocity, it is not severe even at very high average interface velocities. The average interface velocities in full-size vehicles are, in general, less than 10 centimeters per second. The effect of the ratio of outlet to tank diameter on interface distortion appears only through its effect on average inter-

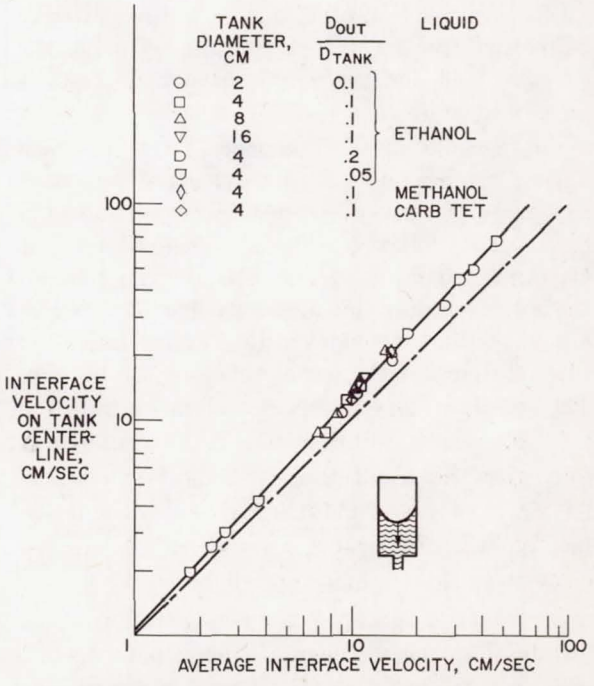

FIGURE III–22.—Liquid-vapor interface velocity during outflow in weightlessness.

face velocity. The most surprising result is that although the tank size was varied over a range from 8 to 1, no effect of size can be discerned. The results of these studies indicate, therefore, that no particular difficulties with interface distortion should be encountered in full-sized tanks for liquid depths equal to one tank diameter or greater. Data at low liquid depths are not yet available, although it appears from figure III–21 that simple baffles will satisfactorily solve any problems of vapor blowthrough.

Interface Behavior During Acceleration Disturbance

A number of acceleration disturbances will occur during the operation of space vehicles, such as those resulting from attitude-control-system operation, crew movement, docking jolts, and atmospheric drag. The acceleration perturbation may be intermittent, as in attitude-control operation, or steady as in drag or liquid collection by thrust before engine startup. These disturbances will occur at all angles to the vehicle thrust axis and will tend to move the liquid opposite (relative to the tank) to the direction of the acceleration. The surface-tension forces give the interface the ability to resist or be stable to a certain amount of acceleration, which is expected to be defined by the Bond number criterion (the ratio of acceleration to surface-tension forces). The study of interface behavior in response to acceleration disturbances may be divided for convenience into two phases: acceleration disturbances less than and acceleration disturbances greater than a critical value at which the stability limit of the interface is exceeded. The stability limit of the interface (i. e., the value of the acceleration at which the interface will break) is expected to be defined by the Bond number, which is called the critical Bond number. The various analyses in the literature quote values of critical Bond numbers from 0.15 to the value of 14.68 obtained by Maxwell. Recently, Masica (ref. 15) measured the critical Bond number in cylindrical tubes using the normal gravitational field as the acceleration disturbance. Some of his results are shown in figures III–23 to III–25 for different orientations of the acceleration field and position of the interface relative to the edge of the tube. The critical diameter is shown as a function of the specific surface tension σ/ρ. The left axis intercept of the solid line approximating the data is proportional to the critical Bond number and is computed as follows with figure III–23 as an example. The equation of the solid line that is drawn at a slope of $\frac{1}{2}$ is, after the critical diameter is converted to centimeters,

$$D=0.184\left[\frac{\sigma}{\rho a(0.01)}\right]^{1/2} \tag{10}$$

When arranged in the form of the Bond number expression (eq. (5)) and when the radius is substituted for the diameter, equation (10) becomes

$$\left[\frac{0.184}{(2)(0.1)}\right]^2=\frac{\rho}{\sigma}aR^2=0.84=Bo_{\text{critical}} \tag{11}$$

The Bond number (based on a radius) of 0.84 agrees with the value obtained analytically by Bretherton (ref. 16) and that obtained experimentally by Hattori (ref. 17) for this configuration and acceleration direction. A variation in Bond number dependent on the specific surface tension was observed for the situation in which the acceleration was directed normal to the axis of the cylinder as shown in figure III–24. The value was 1.12 for specific surface tensions less than 43 cubic centimeters per second squared

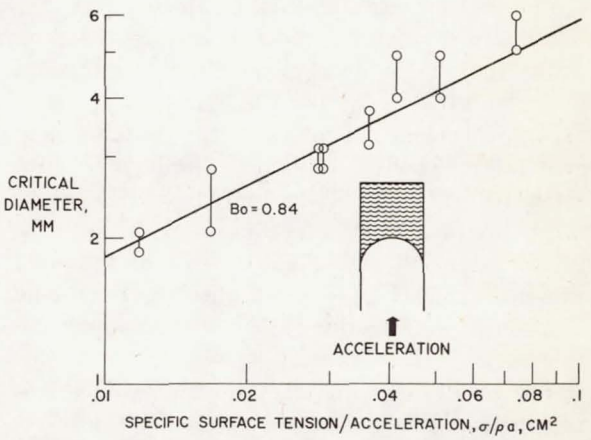

FIGURE III–23.—Stability characteristics in vertical cylinder. Acceleration, 980.2 centimeters per second per second.

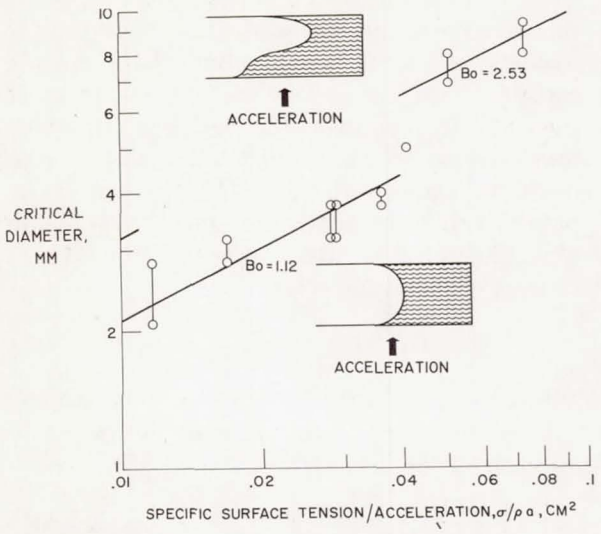

FIGURE III–24.—Stability characteristics in horizontal cylinder. Acceleration, 980.2 centimeters per second per second.

and 2.53 for specific surface tensions greater than 43 cubic centimeters per second squared. For the configuration in which the liquid was at the edge of the tube, as shown in figure III–25, a strong edge effect was noted: the Bond number was 3.37.

In these experiments, the specific surface tension was varied over a 6-to-1 range, thus establishing its functional relation in the Bond number expression. The experiments were performed, however, with only one acceleration disturbance, the normal gravitational field. Masica (ref. 18) has recently extended these studies in the drop tower to include acceleration fields equivalent to 0.1 and 0.01 g for the configuration of figure III–23. Acceleration forces on the container and gravitational body forces on the liquid were considered equivalent. The results of these experiments are presented in figure III–26. These data fit an extension at the same slope of the solid line in figure III–23 and establish the functional relation of acceleration in the Bond number expression.

The results of these experiments can be used to predict the critical accelaration for the interface in large vehicle propellant tanks. Figure III–27 presents the critical acceleration in g's as a function of tank diameter in inches for a specific surface tension of 28.28 cubic centimeters per second^2, which is representative of many propellants. The data obtained at 1, 0.1, and 0.01 g are shown. The critical acceleration for vehicles of 100 to 400 inches in diameter is indicated as 10^{-6} to 10^{-7} g.

Accelerations less than the critical value may be encountered in situations of low residual atmospheric drag, solar pressure, attitude control disturbances, or crew movements. Residual drag or solar pressure will result in a continuous acceleration, which will distort the interface in a generally predictable manner. The operation of attitude controls or crew movements, however, cause intermittent acceleration perturbations that may set up an oscillation of the interface. In high gravitational or acceleration fields (high Bond numbers), the frequency of oscillation is determined by the gravitational or acceleration forces. In a zero-gravity environment (zero Bond number), the surface tension forces, the only remaining restoring forces, determine the frequency. The damping of these oscillations is dependent on the viscosity for both high and low Bond number situations. It will be important to avoid these frequencies in attitude control systems.

There is extensive treatment in the literature concerning the dynamics of free surfaces but only for the condition of an unbounded surface

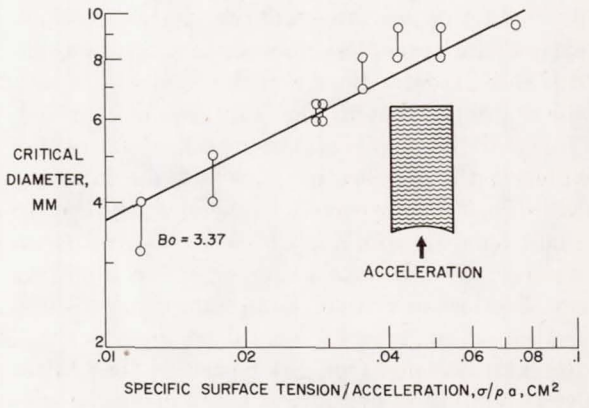

FIGURE III–25.—Stability characteristics at ground edge of vertical cylinder. Bond number, 3.37; acceleration, 980.2 centimeters per second per second.

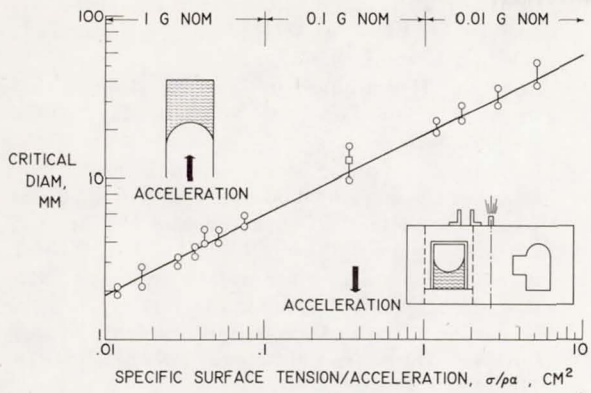

FIGURE III–26.—Stability characteristics in vertical cylinder for several acceleration fields.

for the case where contact angle effects can be ignored. Satterlee and Reynolds (ref. 19) have calculated the natural frequency of the surface at low Bond numbers for several contact angles and have obtained some experimental verification (best at low contact angles) of their analysis. Their results are presented in terms of a dimensionless frequency parameter, which is a linear function of the Bond number and has a finite value at zero Bond number.

For the situation in which an acceleration greater than the critical value is applied along the axis of the tank from the vapor to the liquid, as when the drag exceeds the critical value of the interface or during collection maneuvers, the work of Taylor (ref. 20), Bretherton (ref. 16), Hattori (ref. 17), and Goldsmith and Mason (ref. 21), which are studies of the motion of a bubble that fills the tube, can be applied. The results of some of these studies defining the velocity of the interface as a function of Bond number are given in figure III–28 together with some data by Masica (ref. 22) for high Bond numbers at 1 g and for low gravitational values. The data shown tend to establish the functional relation of the acceleration, the specific surface tension, and the size in the relation of the interface velocity parameter and Bond number. The results of these experiments can be used to predict the velocity on the tank axis of the penetration of the ullage vapor into the liquid during a collection thrust and thus allow a rough prediction of the time for vapor to reach the top of the tank for a situation in which the tank is partly full. Masica (ref. 23) has presented some data on the behavior of the liquid as it gathers in the bottom of the tank which shows that a geyser is obtained for collection Bond numbers greater than 10. The use of baffles was only partly successful in reducing or eliminating the geyser.

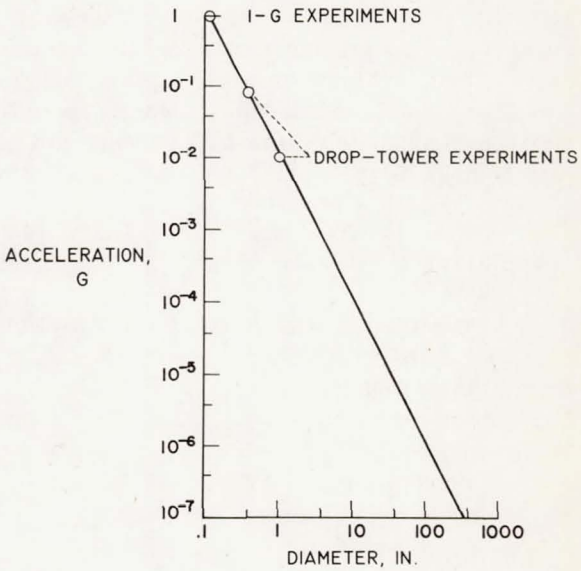

FIGURE III–27.—Interfacial stability as function of acceleration. Specific surface tension, 28.28 cubic centimeters per second.²

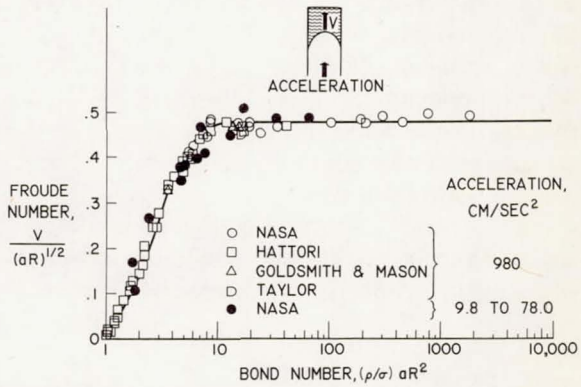

FIGURE III–28.—Penetration velocity of ullage vapor during collection. Specific surface tension, 11.8 to 74.12 cubic centimeters per second²; radius, 0.165 to 4.77 centimeters; acceleration, 9.8 to 980 centimeters per second per second.

CONCLUDING REMARKS

In summary, the results of research concerning the dynamic behavior of the surface of a liquid when influenced primarily by surface tension forces have been reviewed. Although our research has been directed primarily toward fluid behavior and management problems in space vehicles under zero-gravity conditions, a great deal of attention has been given to scaling parameters involving fluid properties and system geometry. The results are therefore widely applicable and can provide an insight into normal-gravity fluid behavior in such capillary-dominated systems as small tubes, screens, porous materials, and similar geometries common to the petroleum industry.

APPENDIX-SYMBOLS

a	acceleration (equals 1 g when at rest on Earth)
Bo	Bond number
C, K	constants
D	diameter
F	Force
F_a	acceleration force
F_c	capillary force
F_i	inertia force
Fr	Froude number
L	characteristic length
M	mass
P	pressure
R	radius
T	time
V	velocity
We	Weber number
θ	contact angle
ρ	liquid density
σ_{ls}	surface energy of liquid-solid interface
σ_{vl}	surface energy of vapor-liquid interface
σ_{vs}	surface energy of vapor-solid interface

REFERENCES

1. Reynolds, William C.: Hydrodynamic Considerations for the Design of Systems for Very Low Gravity Environments. Rep. No. LG-1, Stanford Univ., Sept. 1961.
2. Benedikt, E. T.: Epihydrostatics of Liquids in Vertical Tanks. Rep. No. ASG–TM–61–48, Norair Div., Northrop Corp., June 1961.
3. Li, Ta: Hydrostatics in Various Gravitational Fields. J. Chem. Phys., vol. 36, no. 9, May 1, 1962, pp. 2369–2375.
4. Petrash, Donald A.; Zappa, Robert F.; and Otto, Edward W.: Experimental Study of the Effects of Weightlessness on the Configuration of Mercury and Alcohol in Sperical Tanks. NASA TN D-1197, 1962.
5. Petrash, Donald A.; Nussle, Ralph C.; and Otto, Edward W.: Effect of Contact Angle and Tank Geometry on the Configuration of the Liquid-Vapor Interface During Weightlessness. NASA TN D-2075, 1963.
6. Clodfelter, Robert G.: Fluid Mechanics and Tankage Design for Low-Gravity Environments. Rep. No. ASD–TDR–63–506, Air Force Systems Command, Wright-Patterson AFB, Sept. 1963: (Available from DDC as AD-423554).
7. Petrash, Donald A.; Nelson, Thomas M.; and Otto, Edward W.: Effect of Surface Energy on the Liquid-Vapor Interface Configuration During Weightlessness. NASA TN D-1582, 1963.
8. Petrash, D. A.; and Otto, E. W.: Controlling the Liquid-Vapor Interface Under Weightlessness. Astronaut. Aeron., vol. 2, no. 3, Mar. 1964, pp. 56–61.
9. Petrash, Donald A.; Nussle, Ralph C.; and Otto, Edward W.: Effect of the Acceleration Disturbances Encountered in the MA-7 Spacecraft on the Liquid-Vapor Interface in a Baffled Tank During Weightlessness. NASA TN D-1577, 1963.
10. Benedikt, E. T.: General Behavior of a Liquid in a Zero or Near Zero Gravity Environment. Rept. No. ASG–TM–60–9Z6, Northrop Corp., May, 1960.
11. Rayleigh, Lord: On the Capillary Phenomena of Jets. Roy. Soc. (London), Proc., vol. 29, no. 196, May 15, 1879, pp. 71–97.
12. Siegert, Clifford E.; Petrash, Donald A.; and Otto, Edward W.: Time Response of Liquid-Vapor Interface After Entering Weightlessness. NASA TN D-2458, 1964.
13. Povitskii, A. S.; and Lyubin, L. Ya.: Emptying and Filling Vessels in Conditions of Weightlessness. Planetary Space Sci., vol. 11, 1963, pp. 1343–1358.
14. Nussle, Ralph C.; Derdul, Joseph D.; and Petrash, Donald A.: Photographic Study of Propellant Outflow from a Cylindrical Tank During Weightlessness. NASA TN D-2572, 1965.
15. Masica, William J.; Petrash, Donald A.; and Otto, Edward W.: Hydrostatic Stability of the Liquid-Vapor Interface in a Gravitational Field. NASA TN D-2267, 1964.
16. Bretherton, F. P.: Motion of Long Bubbles in Tubes. J. Fluid Mech., vol. 10, pt. 2, Mar. 1961, pp. 166–188.

17. HATTORI, SIN-ITI: On the Motion of a Cylindrical Bubble in a Tube and Its Application to the Measurement of the Surface Tension of a Liquid. Rep. No. 115, Aero. Res. Inst., Tokyo Imperial Univ.; Jan. 1935.
18. MASICA, WILLIAM J.; DERDUL, JOSEPH D.; and PETRASH, DONALD A.: Hydrostatic Stability of the Liquid-Vapor Interface in a Low-Acceleration Field. NASA TN D-2444, 1964.
19. REYNOLDS, W. C.; and SATTERLEE, H. M.: Dynamics of the Free Liquid Surface in Cylindrical Containers Under Strong Capillary and Weak Gravity Conditions. Rep. No. LG-2, Stanford Univ., May 1, 1964.
20. DAVIES, R. M.; and TAYLOR, GEOFFREY: The Mechanics of Large Bubbles Rising Through Extended Liquids and Through Liquids in Tubes. Roy. Soc. (London), Proc., ser. A, vol. 200, no. 1062, Feb. 7, 1950, pp. 375–395.
21. GOLDSMITH, H. L.; and MASON, S. G.: Movement of Single Large Bubbles in Closed Vertical Tubes. J. Fluid Mech., vol. 14, pt. 1, Sept. 1962, pp. 42–58.
22. MASICA, WILLIAM J.; and PETRASH, DONALD A.: Motion of Liquid-Vapor Interface in Response to Imposed Acceleration. NASA TN D-3005, 1965.
23. MASICA, WILLIAM J.; and SALZMAN, JACK A.: An Experimental Investigation of the Dynamic Behavior of the Liquid-Vapor Interface Under Adverse Low-Gravitational Conditions. Presented at Symposium on Fluid Mechanics and Heat Transfer Under Low Gravitational Conditions sponsored by the United States Air Force and Lockheed Missiles and Space Company, Palo Alto, Calif., June 24–25, 1965.

Page intentionally left blank

IV Surface Physics and Chemistry

ROBERT A. LAD
Lewis Research Center

SURFACES AS WE USUALLY KNOW THEM are covered with oxides, oil films, and adsorbed gases. Much of their behavior is dictated by the properties of the contaminants rather than by the structure of the substrate material. In some instances, continual interaction between the contaminants and the substrate material controls the surface behavior. Because most materials are normally exposed to the atmosphere, the engineering properties of contaminated surfaces are those of importance. The interest in truly clean surfaces has been of concern mainly for a few applications (e. g., catalysis) and for study of the fundamental aspects of surface chemistry and physics.

With the advent of space exploration and flight at very high altitudes, new interest in the properties of clean surfaces has developed. Materials and devices must survive in new environments—ultrahigh vacuum, extremely reactive gases, very high temperatures, very low temperatures, micrometeoroids, and a wide variety of radiations.

Many problems under study here at Lewis stem from our need to understand and to cope with these new environments. One program described in detail is that concerned with bearings, seals, and lubricants.

The subject discussed in this paper is one in which surface chemistry and physics are used to gain insight into the behavior of the whole solid.

Imperfections play a very important role in the behavior of solids. Dislocations provide the means by which slip occurs. Vacancies and interstitial atoms interact with dislocations and modify the ease with which they can move. Vacancies, interstitial atoms, and impurity atoms scatter electrons as they migrate through a crystal. Radiation damages solids by the creation of vacancies and interstitials. Imperfections are important ingredients of the active sites on a catalyst which cause it to perform its function of increasing the rate of chemical reaction. One of the objectives at the Lewis Research Center is to contribute to the understanding of these imperfections and their role in the behavior of solids.

While attention is mainly directed toward bulk behavior, some of the research on the structure of imperfections in oxides is directly related to catalysis. In fact, one study was prompted by the observation that ultraviolet-irradiated magnesium oxide has catalytic properties which the unirradiated material lacks. Earlier studies elsewhere had suggested that the catalytic site following irradiation involves the ferric ion formed from the ferrous ion existent as an impurity in the magnesium oxide.

Examination of the problem suggested that the ferrous to ferric reaction was only one of several possibilities; the others involved the generation or modification of vacancies or vacancy clusters. It was decided to use Electron Paramagnetic Resonance (EPR) to study the problem. Previous applications of this technique to the study of bulk imperfections in magnesium oxide suggested that it might also be useful for this *surface* problem.

The EPR technique is a form of absorption spectroscopy. It is particularly useful in solid state research because it makes possible the detection of certain kinds of atomic entities in a solid without destroying the specimen. With proper calibration, it also is possible to determine the amount of the species present. The species which respond to EPR are those which

interact with a magnetic field, namely, those with an odd number of electrons. These species are termed paramagnetic. These atoms or molecules behave like small magnets and respond to a magnetic field in much the same manner as a compass needle responds to the Earth's field. Examples are neutral atoms, like nitrogen and hydrogen; ions with partly filled inner electron shells, like iron or chromium; molecules having an odd number of electrons, like nitric oxide (NO) or the CO^{-}_{2} radical ion; and sites called color centers, which are formed in some solids by irradiation with ultraviolet light, X-rays, and other radiations.

In the EPR spectrometer (fig. IV–1) the specimen is subjected simultaneously to a constant high magnetic field and a rapidly alternating small field. The smaller magnetic field alternates at microwave frequencies, about 10 billion times per second. When the intensity of the constant magnetic field and the frequency of the alternating field bear a proper relation to each other, the paramagnetic species in the sample can absorb microwave energy. The usual experimental procedure is to maintain a constant microwave frequency and to vary the constant field intensity slowly. Measurement of the microwave energy absorbed then yields a spectrum. An example of such a spectrum is shown in figure IV–2. Theoretical quantum mechanical methods are available which permit the identification of a spectrum with structural details of

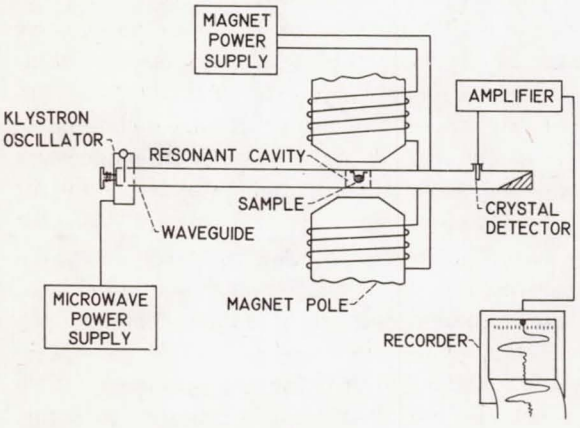

FIGURE IV–1.—Electron paramagnetic resonance apparatus.

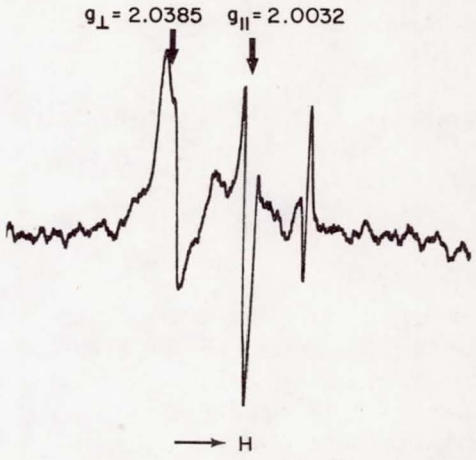

FIGURE IV–2.—Spin resonance curve of magnesium oxide catalyst degassed at 290° C in vacuum and given 2537 Å ultraviolet irradiation.

the paramagnetic species and its surroundings in the crystal lattice. The g values indicated on the spectrum are pertinent to this identification. After a correlation is made between a structure and a spectrum, the spectrum can be used as an indicator of the presence of the paramagnetic species and as a measure of their abundance. Studies at Lewis have used EPR in just this way.

The first experiments on irradiated magnesium oxide showed that the ferric ion is not in itself the catalytic site. While the effectiveness of the magnesium oxide (MgO) as a catalyst increased with irradiation, the ferric ion concentration actually *decreased*. Other sources were then examined for the catalytic activity.

Another change which occurs when magnesium oxide is irradiated for times of the order of tens of minutes is the formation of the paramagnetic V_1 center. Its EPR spectrum has been observed and identified. The V_1 center is depicted in figure IV–3. The crystal of magnesium oxide is a cubic array of positive magnesium ions and negative oxygen ions. Some lattice sites are vacant; two such vacancies are shown. A vacant site creates a local imbalance of electric charge. The local imbalances result in interesting effects. A missing magnesium ion results in an excess of electrons, which are the source of negative charges in the vicinity of the vacancy.

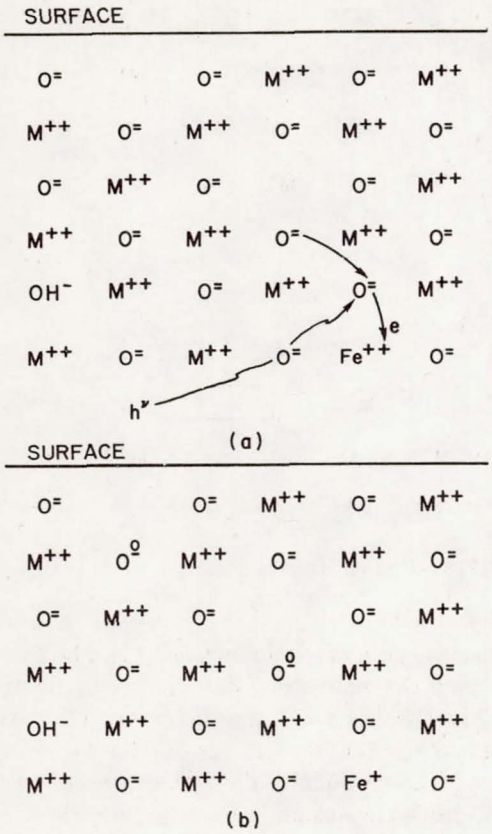

(a) Mechanism for formation of V_1 center by irradiation.

(b) Metal oxide with V_1 center.

FIGURE IV–3.—Metal oxide lattice showing V_1 center, electron trap, and charge compensating ion.

When the crystal is bombarded with ultra-violet light, it can free electrons from the oxygen ions. This, then, is a means for removing electrons from the regions where they are locally in excess, around magnesium ion vacancies. The electron that is freed must find a resting place, and one such place is on a ferrous ion (Fe^{+2}), which is an impurity in MgO. The Fe^{+2} is converted to Fe^{+1}. Impurity atoms in crystals often play an important role in the formation of centers of this sort. The process is called charge compensation. The net effect is reduction of the excess negative charge around the vacancy. When the charge is reduced, a paramagnetic center is formed.

A search was made for a correlation between V_1 center concentration and catalytic efficiency. The chemical reaction was the hydrogen-deuterium interchange, $H_2+D_2 \rightarrow 2HD$. A correlation was found, and some of the experimental results are shown in figure IV–4. The relative catalytic activity and the V_1 center concentration are plotted against time. Both quantities fall in time at rates which are dependent on temperature. The specimens were irradiated and then held at a particular temperature for various times. The changes in catalytic efficiency and V_1 center concentration were determined at these times. The results indicate a good correlation between the two quantities. The significance of these findings to the work at Lewis lies in the fact that the V_1 center can exist in close proximity to the surface. The significance to catalysis is that a structure has been identified that is either an active site or an intermediate form in the building of an active site.

The next project to be described is the first use of EPR to provide a complete description of an adsorbed molecule on a surface. If magnesium oxide is irradiated for long periods, of the order of several hours, the sample assumes a violet color and a new EPR spectrum appears (fig. IV–5). If the sample is exposed to carbon dioxide (CO_2), the spectrum in figure IV–5 gives way to the one in figure IV–6.

Analysis of the first spectrum and comparison with the literature led to the conclusion that it is representative of *another* kind of radiation-produced site, the S' center. This center is depicted

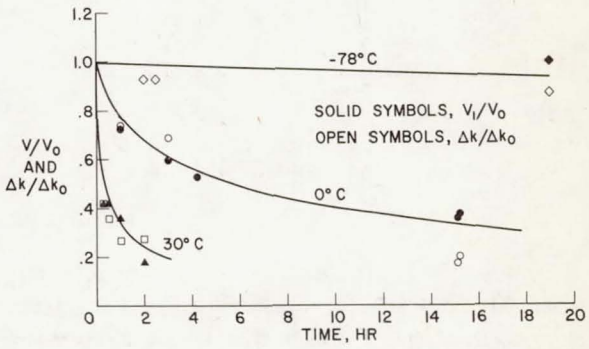

FIGURE IV–4.—Thermal decay at three temperatures following 2537 Å ultraviolet irradiation.

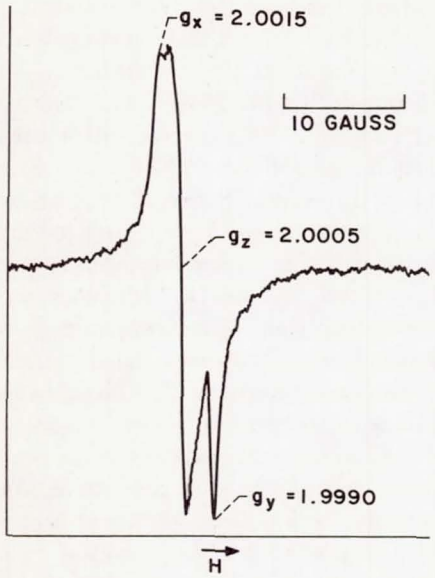

FIGURE IV–5.—*S′* spectrum of ultraviolet-irradiated magnesium oxide.

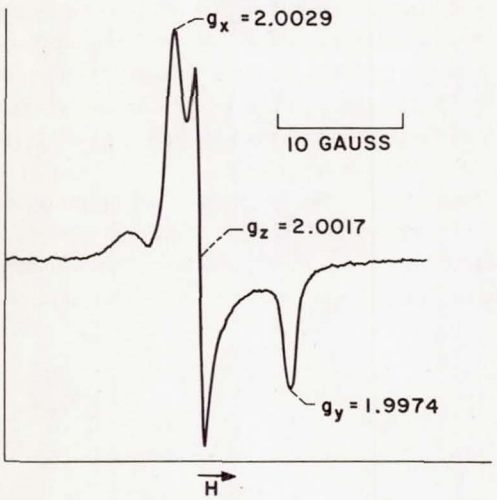

FIGURE IV–6.—EPR spectrum of carbon dioxide absorbed on ultraviolet-irradiated magnesium oxide.

in figure IV–7. It consists of a vacancy pair (one Mg and one O vacancy) and an electron. The extra electron makes the site paramagnetic.

If the adsorption of the CO_2 molecule, which is not paramagnetic, destroyed one paramagnetic species and created a new one, it can be concluded that the new site is as shown in figure IV–8. The CO_2 molecule has taken the electron from the *S′* center, and it resides on the CO_2 molecule. The CO_2 molecule is shown as having changed from the usual linear configuration to the nonlinear form because the EPR spectrum observed is just the one reported in the literature for the nonlinear CO^-_2 ion, which can be generated in solid sodium formate by γ-irradiation.

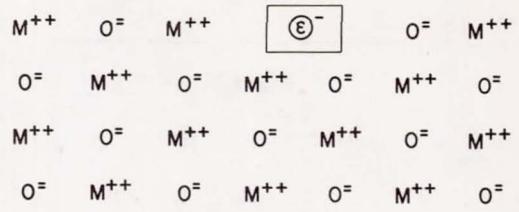

FIGURE IV–7.—*S′* center.

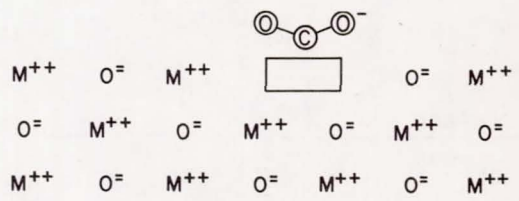

FIGURE IV–8.—Carbon dioxide adsorbed on *S′* center.

This work illustrates the usefulness of EPR in defining the detailed structure of an adsorbed molecule on a surface active site. It suggests that a tool is now available which might help the understanding of the mechanism of catalysis in new ways. Other methods, such as gas adsorption, of necessity yield information on the average behavior of large numbers of molecules and large areas of surface.

Interest in the interaction of solid surfaces with gases led to examination of other systems. One was carbon monoxide (CO) on MgO. The adsorbed CO molecule plays an important role in the Fischer-Tropsch process for the production of hydrocarbons from CO and hydrogen. Experiments at Lewis showed that some of the adsorbed CO forms a paramagnetic species. The analysis of the spectrum yielded information

which will aid in the understanding of CO adsorption, which has been previously studied extensively by infrared spectroscopy.

Attention is presently directed toward the identification of the state of adsorbed *oxygen* on magnesium oxide and on the semiconductor zinc oxide. This information is pertinent to the understanding of the interaction of surface oxide layers with atmospheric oxygen and to the process of oxidation itself.

Other work in progress at this center should also be mentioned. Methods are being studied for preparation of the high purity carbides and nitrides of metals like titanium and zirconium. These materials are of interest because they are among the highest melting materials known. The nature of the chemical bonding in them is unusual. In order to study it, it is necessary to have higher purity material than is commercially available. Another interesting property of these refractory compounds is their high electrical and thermal conductivity; it is almost as high as for metals. Their state of chemical bonding, which is neither ionic nor metallic, might make the pure materials interesting to investigate as catalysts.

Another investigation is concerned with diffusion in oxides. Figure IV–9 shows how atoms or ions move in magnesium oxide. The ions move by changing places with vacant sites in the lattice. In the case of oxygen ions, both the number of vacant oxygen sites and the driving force for their motion depend on the presence or absence of oxygen gas at the specimen surface. It is thus conceivable that changes in the catalytic behavior of oxides (which are commonly used catalysts) may come about because of surface layer diffusion when they are used in oxygen-deficient surroundings.

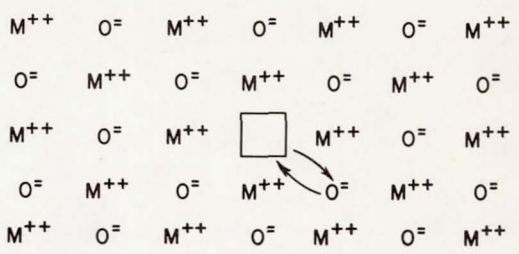

FIGURE IV–9.—Diffusion of oxygen in magnesium oxide.

In summary, several research programs have been described which have pertinence to catalysis. In a study of the structure of radiation-produced imperfections in magnesium oxide, information has been generated on their relation to catalytic behavior. The configuration of the carbon dioxide molecule adsorbed on an active site has also been described. Work on the chemical bonding in refractory compounds and on diffusion in oxides also suggests possible applications to catalysis.

Page intentionally left blank

V Magnetics and Superconductivity

EDMUND E. CALLAGHAN
Lewis Research Center

THE LAST DECADE has seen the ever wider development of electrical and electronic devices whose capabilities are dependent on low-temperature operation. Typical of such devices are masers (very low noise level radiofrequency amplifiers) and cryotrons (very high speed counters for computers). The development of elegant and unique low-temperature electrical gadgets has somewhat over-shadowed the considerable gains which have been made in the overall technology for the operation of electrical gear at low temperature as a means of overall power savings.

It is well known that the electrical resistance of most conductors decreases with decreasing temperature. What is not so well known is that advances in the knowledge of material properties at low temperatures and the development of efficient refrigeration techniques can be combined to give substantial savings in the overall power consumption of much common electrical hardware. The kind of changes in electrical resistivity which occur with temperature is illustrated in figure V–1. Good conductors such as copper or aluminum show a decrease in electrical resistance of four or five orders of magnitude between room temperature and temperatures near absolute zero. Absolute zero is defined here as that temperature at which all gross motion of the atoms ceases. There is a distinct leveling off of the resistance at very low temperatures, and there is a residual resistance of most materials close to absolute zero. There is a class of materials, known as superconductors, which show a sharp drop in resistance at very low temperatures. Lead and tin are two such materials. In fact, there are now an enormous number of

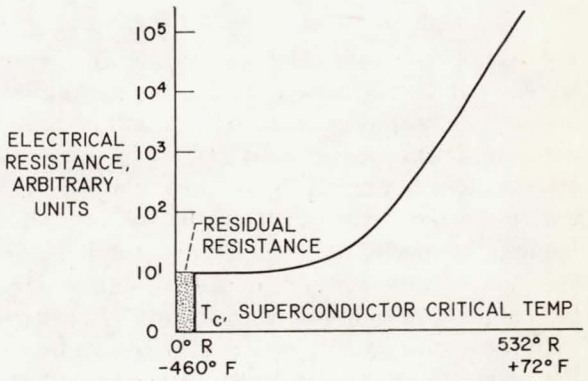

FIGURE V–1.—Resistance of conductors.

elements and alloys which have been found to have this property; at some critical temperature, dependent on the material, the resistance drops to a value so low as to be unmeasurable by any available technique.

There are, therefore, two distinct classes of conductors, those called normal conductors and those called superconductors. They are discussed separately herein, first, the matter of simply decreasing resistivity by going to low temperatures with normal conductors, and second, superconductors. An interesting sidelight here is that materials which are considered to be good conductors at room temperature, such as copper and aluminum, are either not superconductors at all or very poor ones. Other materials which are rather poor conductors at room temperature are rather good superconductors.

The whole value of applying cryogenic but nonsuperconducting techniques to electrical devices is to reduce the total power consumption of such a system as illustrated in figure V–2.

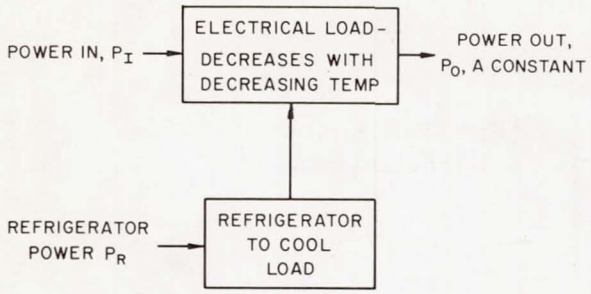

FIGURE V–2.—Application of cryogenic techniques to resistive devices. P_I (cold) $+ P_R < P_I$ (normal temperature).

For example, assume that an electrical device is required to perform a certain task, that is, that a fixed output is required. For normal temperature operation, a fixed output requires a certain input power. If the resistive losses of the device are significant, they can be substantially reduced by decreasing temperature, and hence the input power required for a fixed output can be reduced. Temperature reduction, however, requires a refrigerator, and it also is an absorber of power. Hence, in order to achieve a net saving, the sum of the input power (cold) plus the refrigerator power is required to be less than the power required to operate the device at normal temperature, that is, without refrigeration. The particular device of concern here at Lewis was a large cryogenic magnet, but the same principles apply to any electrical device which has a significant power loss, simply because of the resistance of the conducting material.

In general, then, the first problem is the choice of a conductor which will give the best possible characteristics at low temperatures. The equation $R = R_T + R_0 + R_M$ describes the characteristics of resistance of normal materials. The total resistance R is made up of three distinct components, the thermal resistance R_T, the residual resistance R_0, and the magnetoresistance R_M. The thermal resistance is a function of the temperature and really results from the activity of the atoms in the material. In order to visualize what happens, consider the atoms as being in a lattice structure tied together in a neat and orderly arrangement. An atom situated at any particular point moves up and down or crossways in the lattice and interferes with the motion of the current carrying electrons. As the temperature decreases, the atomic motion decreases and the electrons pass more easily through the lattice. The residual resistance merely reflects the fact that impurities and stresses tend to disorder the lattice structure.

Figure V–3 illustrates what can be expected of good conductors such as copper or aluminum. A resistance ratio is plotted as a function of temperature. The resistance is normalized simply by dividing by the room temperature resistance.

The most evident characteristic of the curve shown is that most of the change in resistance occurs at low temperature. This is as expected, for according to theory, resistance varies linearly with temperature at high temperatures and as the cube of the temperature at very low temperatures. The overall result is that the most significant decreases in resistance occur below 100° R, and therefore most cryogenic applications will occur below this temperature.

The value of the residual resistance shown here lies some five orders of magnitude below the normal room temperature resistance. This value is extremely sensitive to material purity and stress. A value such as shown here can only be achieved with extremely high purity, perhaps 99.999 percent, and fully annealed mate-

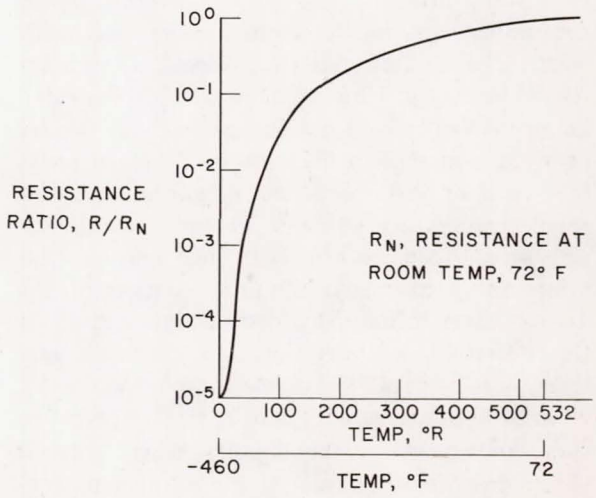

FIGURE V–3.—Resistance of copper.

rials. Less pure or stressed materials would have much higher residual resistances and might only be three or four orders of magnitude below room temperature resistance.

Magnetoresistance is probably a new term to many people, and it is a function of the magnetic field in which the conductor lies. Since magnetic fields are generated by electrical currents, it is impossible to build an electrical device which does not produce a magnetic field, and many large devices such as electrical generators produce quite large fields. Magnetoresistance is only significant at low temperatures, but it can result in very large effects. To visualize how magnetoresistance produces its effect, consider the simple picture of the lattice structure but filled with magnetic field lines. Since the current carrying electrons tend to be tied to the magnetic field lines, this also interferes with their ready passage through the lattice structure.

Detailed studies have been made of the magnetoresistance of a large number of conductors, and some typical results are shown in figure V–4. The particular data shown here are for aluminum and copper at 15° R. It is evident that aluminum is much better than copper for all cases where the magnetic field is significant, and in fact aluminum shows an interesting characteristic called "saturation"; that is, above a field of about 20 000 gauss there is no further increase in magnetoresistance. This is extremely advantageous when high fields are desired or merely exist.

Now consider the application of what has been discussed. Given a device which wastes considerable electrical power at room temperature

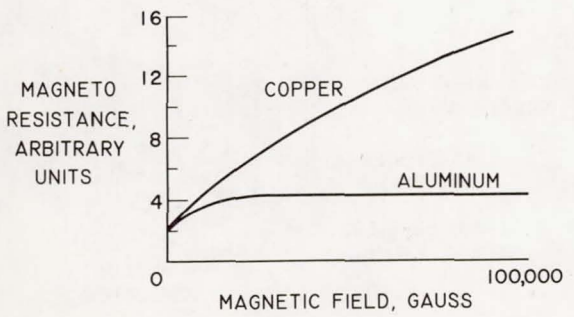

FIGURE V–4.—Resistance of conductors in magnetic fields. Temperature, 15° R.

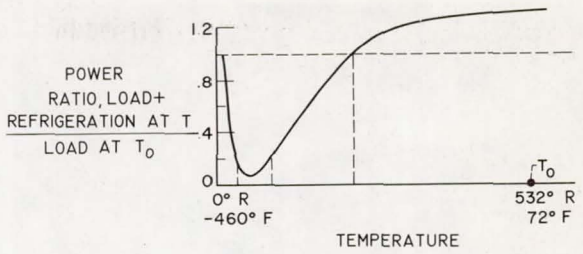

FIGURE V–5.—Power requirements of load and refrigeration plant.

simply because of electrical resistance, what advantages can be gained by going to low temperatures? Figure V–5 shows a particular case which was studied, a magnet that produced a field of 100 000 gauss and absorbed 3 megawatts of electrical power at room temperature. In figure V–5 is plotted the power ratio, that is, the total power of the magnet and its cooling or refrigeration plant divided by the power required to operate the magnet alone at room temperature. The power ratio goes from a value of about 1.2 at room temperature down to quite low values around 20° R.

The fact that the power ratio is greater than unity at room temperature merely reflects the inefficiencies in the refrigeration plant; it is interesting to note that the temperature must get down to 200° R before the value becomes unity. The minimum value was found to be between 20° and 50° R, and the minimum power ratio was found to be 0.04 or 4 percent at about 35° R. This is pretty much what might have been expected from the previous discussion of resistance. Very low temperatures are necessary to achieve the required reductions in resistance. The reason for the sharp rise in power ratio as very low temperatures are approached is the inefficiency of the refrigeration plant; in fact, it would take an infinite amount of power to achieve operation at 0° R.

The results shown in figure V–5 merely point out the large reduction in power losses which can be achieved by cryogenic techniques. Each separate case would have to be studied as to the best choice of conductor material and operating temperature.

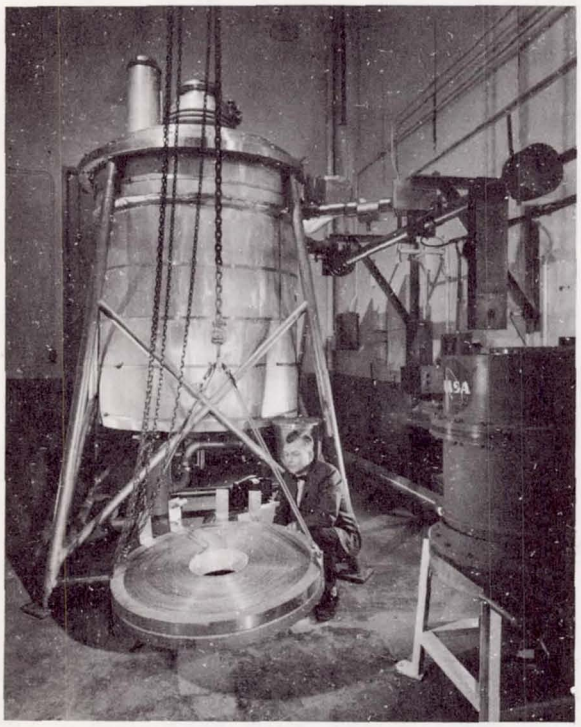

FIGURE V–6.—Cryogenic magnet.

Figure V–6 shows an actual cryogenic magnet which has been built for operation at liquid neon temperature, 50° R (−410° F). The magnet consists of 12 coils and can produce a field of over 150 000 gauss. The power consumption is about 1 megawatt, compared with 100 megawatts for operation at room temperature. The bore of the magnet is approximately 1 foot. The 12 coils are immersed in a bath of liquid neon and achieve cooling simply by nucleate boiling. The particular magnet shown is capable of fields in excess of 150 000 gauss, and a similar set of coils with a bore of approximately 5 inches has achieved a field of 200 000 gauss. The construction of the magnet is quite interesting. Very high purity aluminum is used as the conductor. Since the magnetic field is very high, the stresses are quite large. A magnetic field of 150 000 gauss is the equivalent of 14 000 pounds per square inch of gas pressure inside the magnet bore. Construction details are shown in figure V–7. To carry the high stresses involved, the aluminum strip is bonded by a mastic or glue to a stainless steel channel, which carries the loads out to the heavy retaining ring holding the assembly together. Many small spacers are provided between each turn to allow passage of liquid neon through the coil, and cooling is accomplished merely by submerging the coils in a bath of liquid neon and allowing it to boil off as power is run through the magnets.

Although it is quite evident that cryogenic techniques can result in very substantial savings, the question might well be asked, "Why bother, when superconductors can reduce power losses completely." The answer is that in the future superconductors may well be used, but at present cryogenic system technology is part way through the developmental process while superconductivity is still in the research stages. However, this research is vigorous and widespread and advancing at a tremendous rate.

In order to discuss superconductors, their uses, and their potential, their characteristics are first reviewed briefly.

The following characteristics are inherent in all superconducting materials: First, in the superconducting state, they have absolutely zero resistance. For example, a superconducting closed ring, immersed in liquid helium, has carried a

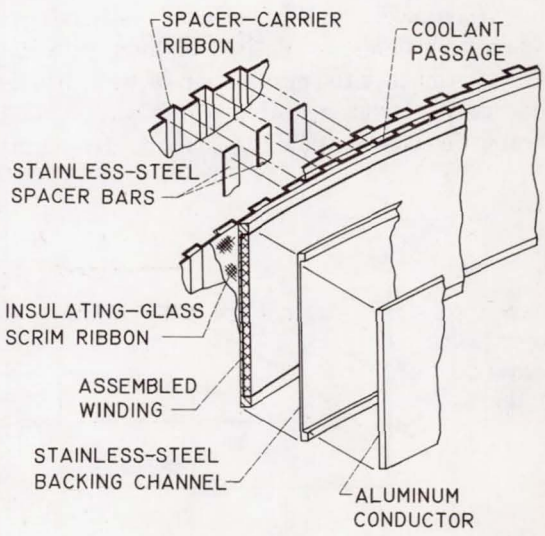

FIGURE V–7.—Construction of coils of cryogenically cooled aluminum magnet.

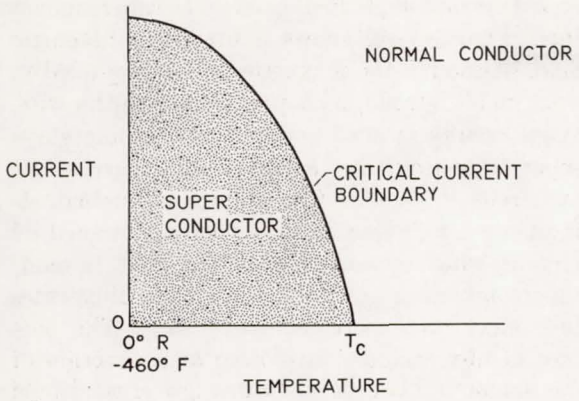

FIGURE V–8.—Critical current of a superconductor.

continuous current around the loop for several years. No measurable decrease in the current was observed, which indicates a resistance so low as to be effectively zero. Such a current set up in a normal conductor would cease almost immediately when the power source was withdrawn. Second, the region over which the superconducting property of any material exists is determined by temperature, magnetic field, and the electrical current flowing in the superconductor. In general, the superconducting domain is sharply defined; that is, a material is either superconducting or not, and a sharp jump in resistance is observed at the critical boundary between normal and superconducting states. Third, a superconductor excludes the magnetic field. This last characteristic is the one which most clearly differentiates between the older "soft" superconductors (type I) and the new high–field—high–current superconductors (type II). This difference will be examined in detail a little later, but the discussion of the first two items applies to all superconductors.

The region or domain over which superconductivity exists will now be examined in a little more detail. Figure V–8 shows the critical current as a function of temperature. Consider a superconducting wire through which a current can be put whose temperature can be controlled. If no current is flowing and the temperature is lowered to a value known as the critical temperature, the material suddenly becomes superconducting. For each value of current through the wire, there is a particular temperature at which there is a sudden jump from the normal to the superconducting state. For any point within the shaded area, the wire will remain superconducting, but outside the critical boundary the material is a normal conductor. The highest value of critical temperature is 33° R for an alloy of niobium and tin.

Exactly the same sort of behavior is exhibited in a magnetic field (fig. V–9), and the same sort of sharp jump is observed between the normal and superconducting states. The sharp boundary between the normal and superconducting states is exactly the property used to make cryotrons. The cryotron is merely a piece of superconducting wire with a small coil wrapped around it. Current flow in the wire can be stopped by energizing the coil and producing a sufficiently large magnetic field to force the superconducting wire into the normal state.

Consider now the third property of superconductors, exclusion of the magnetic field. It is this property that has probably caused the most consternation among physicists. When it was first discovered many years ago, it represented a greater difficulty in integration within the theory than did zero resistivity. Today many questions are still unanswered. To simplify the discussion, assume that there are essentially two kinds of superconductors. The first type gives complete field exclusion, as shown in figure V–10. Typical materials which exhibit this property are lead and tin. Consider a straight wire in a magnetic field. The end of the wire is the circle, and the wire runs into the paper. For most materials

CRITICAL FIELD OF A SUPERCONDUCTOR

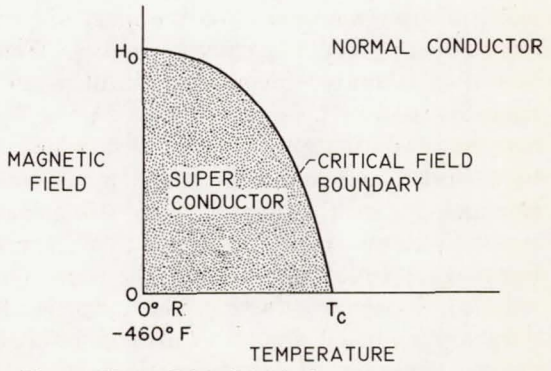

FIGURE V–9.—Critical field of superconductor.

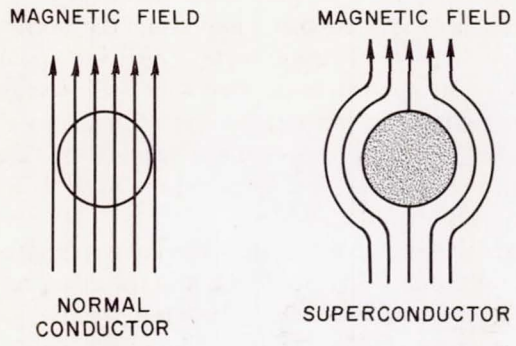

FIGURE V–10.—Magnetic-field exclusion (Meissner effect).

FIGURE V–11.—Magnet floating on its own field.

the magnetic field passes through the wire with no significant displacement of the flux lines. If the temperature is lowered and the wire becomes superconducting, the magnetic lines are totally excluded. The most obvious application of this characteristic is a superconducting bearing in which a shaft would float on the magnetic field. Such a bearing would be truly frictionless. Figure V–11 is a laboratory demonstration of magnetic field exclusion by a superconductor. A small bar magnet is floating above a lead dish which has been chilled in liquid helium and made superconducting. In the normal case, the magnet would lie in the dish and the flux lines from the bar magnet would pass through the dish. When the dish is superconducting, the magnetic flux lines are excluded from the dish and the bar magnet floats on its own magnetic field.

Consider now the characteristics of the new high–current—high–field or type II superconductors. Figure V–12 shows a wire in a magnetic field. Although the magnetic field is excluded in weak fields, strong fields penetrate into the wire. What results is a wire which as a whole stays superconducting, the current being carried by numerous threads or filaments of superconducting material. These filaments are surrounded by regions which are in the normal, that is, non-superconducting state. Figure V–13 illustrates this effect in a more definitive way. The percent of flux excluded is plotted as a function of the magnetic field. Below some low critical field $H_{c,1}$ all the flux is excluded just as in type I or soft superconductors. Above this field, flux gradually penetrates the conductor until at some higher field $H_{c,2}$ the material becomes completely normal and is no longer a superconductor. The

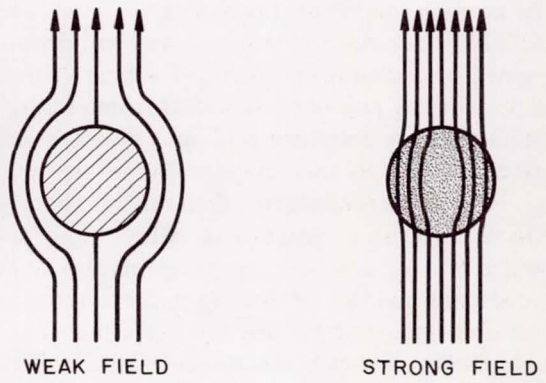

FIGURE V–12.—Magnetic field behavior of high-current—high-field superconductors.

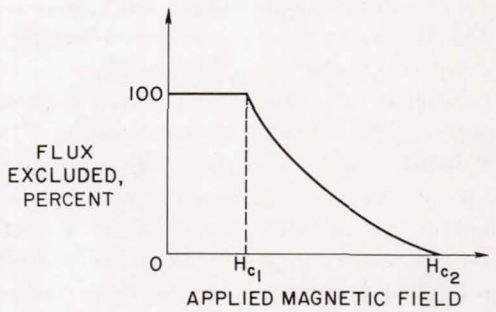

FIGURE V–13.—Flux exclusion as function of magnetic field for high-current—high-field superconductors.

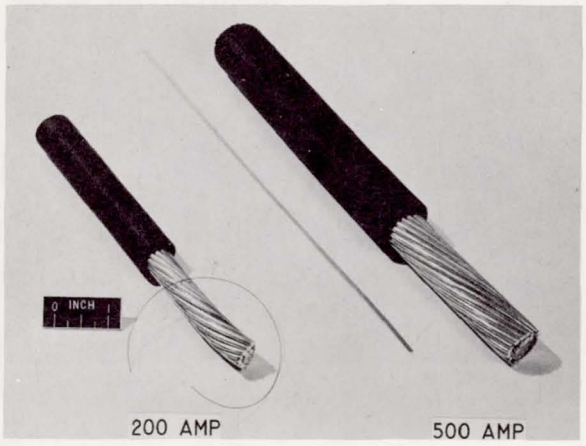

FIGURE V–14.—Current capacity.

older, type I, superconducting materials have critical fields of the order of a few thousand gauss, which are about the same as the lower critical fields of the new type II superconductors. The upper critical fields of the type II superconductors are of the order of 100 000 gauss or more, and hence these materials can carry usable currents in high magnetic fields. In the past this has been the biggest hindrance to the practical application of superconductivity.

Today many new superconducting materials carry enormous currents in the presence of high magnetic fields. In figure V–14 is a single superconducting wire of niobium-zirconium and its equivalent in a copper wire for room-temperature operation. The diameter of the copper wire is over 0.50 inch, while that of the superconductor is only 0.01 inch. Also shown is a very large copper wire over 0.750 inch in diameter and its equivalent in a superconducting ribbon of niobium-tin, which is 0.0025 inch thick and 0.125 inch wide. This is an indication of the kind of compactness that can be achieved in superconducting systems. A further illustration is a superconducting magnet. The magnet has a 2-inch bore and, when operated in the Dewar filled with liquid helium, produces a field of 60 000 gauss (fig. V–15). The magnet operates in a persistent mode without any power supply. The electric currents that produce the magnetic field simply go around in a closed patch through the

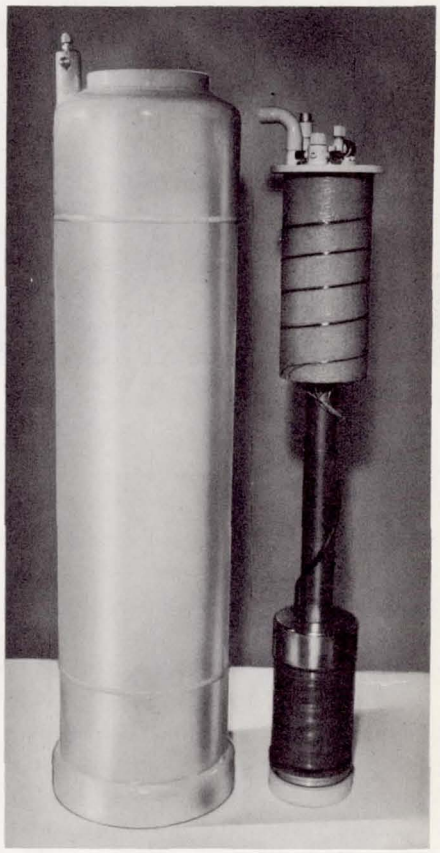

FIGURE V–15.—Superconducting magnet.

coil wires. It is, of course, necessary to supply the initial current to generate the magnetic field.

To achieve the field strengths discussed here by normal room-temperature techniques requires a considerable investment in equipment. Figure V–16 shows a water-cooled magnet built at Lewis which produces the same field over about the same volume. Notice the heavy bus bars required to bring the power to the magnet. This magnet absorbs about 1 megawatt of electric power. A whole room full of electric power equipment is needed to operate the magnet, and about one-half of it is shown in figure V–17.

The superconducting magnet is immersed in liquid helium, and although no heat is generated by the magnet, there are small losses just due to heat leakage into the system. To replace the helium boiloff due to leakage requires about

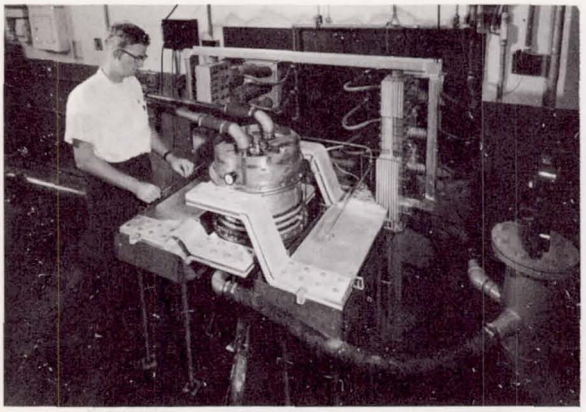

FIGURE V–16.—Water-cooled electromagnet.

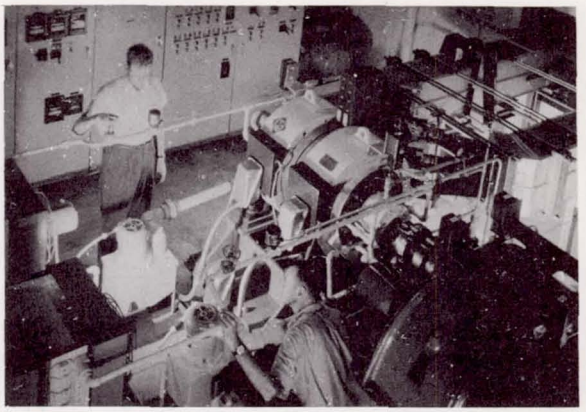

FIGURE V–17.—Magnet power supply.

2 kilowatts as compared with the 1 megawatt required for the water-cooled magnet.

Numerous studies have been made of the application of the new superconducting materials to all manner of electrical devices, and even such prosaic and well-developed items as transformers can possibly be improved. Such systems might be greatly reduced in size, by factors of 10 to 100. For example, detailed studies have shown that the normal electrical substation which now occupies one-quarter or one-half a city block would be compacted into a unit about the size of an office. This certainly would be of great value in downtown areas of large cities.

Another application of superconductors is energy storage. Very large amounts of energy can be stored in the magnetic fields of superconducting magnets, and this energy can be drawn off as electricity. So far studies at Lewis show that such devices can possibly be much better for certain applications than ordinary battery power.

Another interesting application is an ac-dc rectifier. A device has been built by using two cryotrons or gates. These gates operate alternately at 60 cycles per second, and 1 ampere of alternating current has been pumped up into 500 amperes of direct-current stored in a magnet. The whole device is about as large as a man's fist. The usual techniques would require a solid state converter about 100 times as big.

The future of the whole field of superconductivity is extremely bright, and it will most likely have a marked effect on industry.

VI Pump Technology

I. Irving Pinkel, Melvin J. Hartmann, Cavour H. Hauser, Max J. Miller, Robert S. Ruggeri, and Richard F. Soltis
Lewis Research Center

Attention is focused in this discussion on some of the technological advances in turbomachinery research and development which the petroleum industry, with its widely diverse technology, might find useful. The research and development on turbomachinery being conducted by the NASA Lewis Research Center and supported by this center through contract to industry and universities include effort on such components as compressors, turbines, and pumps and on materials used in their construction. Because of the large total effort involved, the following discussion is limited to only a selected portion of the overall effort in order that the work can be described in sufficient detail to reveal its scope and quality.

The subject chosen is that of high-performance pumps and the role of cavitation in defining pump performance limits. NASA interest in this subject stems from the need to minimize the structural weight of space vehicles to provide a corresponding increase in payload capability. The dependence of payload capability on pump performance can be illustrated by considering the principal components of a typical upper stage of a space vehicle shown in figure VI–1. The largest components by far are the propellant tanks, the wall thickness of which is determined primarily by tank pressure, although other factors are involved. For space vehicles in which the tank wall thickness is determined by propellant pressure, lower tank pressures allow lower vehicle weights.

In order to prevent propellant boiling, the tank pressure must be greater than the vapor pressure of the propellant. Propellants that have a high vapor pressure, for example, liquid hydrogen, are often carried at a tank pressure only a few pounds per square inch greater than the vapor pressure. Under these conditions, the propellant is in a near-boiling state.

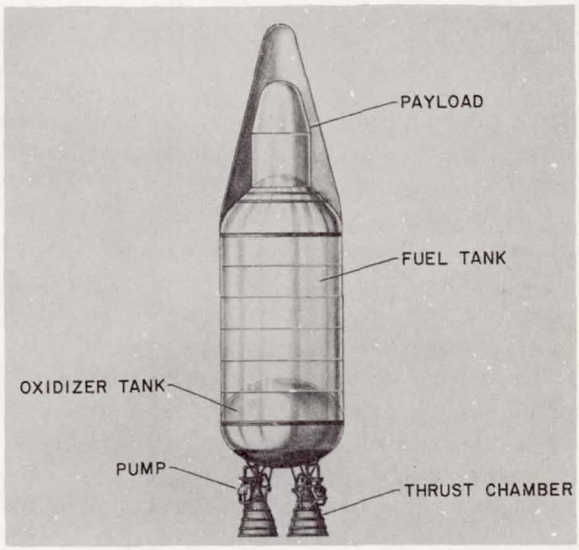

Figure VI–1.—Liquid-fueled rocket vehicle.

The difficulty in pumping a near-boiling liquid can be described by use of a simplified diagram of a rocket stage, as illustrated in figure VI–2, which shows one propellant tank, the thrust chamber, and the pump which delivers the propellant from the tank to the thrust chamber. A portion of a typical centrifugal pump rotor (and blading) often used in liquid rocket systems is also shown. The propellant tank is assumed to contain a near-boiling liquid. The

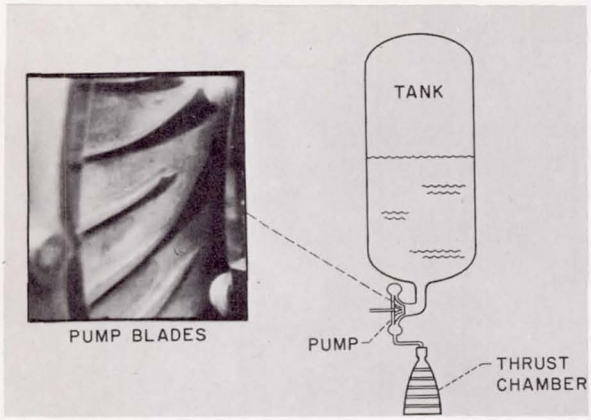

FIGURE VI–2.—Pump in liquid rocket system.

static pressure drop experienced by the liquid as it flows from the tank to the pump and into the pump passages usually causes a portion of the liquid to flash to vapor (boil) within the pump passages. This vapor formation, called cavitation, if sufficiently extensive, can cause a loss in pump performance. In rocket systems, this loss in pump performance can be catastrophic.

The degree of flow disturbance that can be produced by cavitation is illustrated in figure VI–3, which shows a pump operating under cavitating conditions. The photograph was taken through a transparent pump housing with the pump operating at a speed of 3000 rpm. Pump cavitation can be categorized into two basic types according to location, blade-tip cavitation and blade-surface cavitation. The first type is vapor formation that occurs because of flow through the clearance region between the blade tip and the pump casing (fig. VI–3). In general, blade-tip cavitation does not appreciably affect pump performance; however, blade-surface cavitation can degrade pump performance severely. The blade-surface cavitation shown in figure VI–3 disturbed the flow in the carefully designed flow passages of the pump sufficiently to degrade pump performance severely.

The requirement that rocket propellants be pumped under the conditions of lowest possible tank pressure (i. e., in a near-boiling state) can be discussed with reference to the Centaur space vehicle shown in figure VI–4. Centaur will be used as an upper stage on an Atlas booster to lift Surveyor to the Moon. Surveyor is designed to soft-land an instrumented package on the Moon to sample and to analyze the surface of the Moon and to make other measurements in preparation for manned landing a few years hence. The Centaur vehicle is 10 feet in diameter and about 16 feet long (cylindrical portion only) and uses liquid hydrogen as fuel. The fuel tank pressure is only 2.0 pounds per square inch greater than the vapor pressure of liquid hydrogen. This additional pressure above the vapor pressure is provided by the injection of helium gas at the top of the tank. Helium is used because it does not liquefy at the very low temperature of liquid hydrogen (about −423° F). The helium is carried separately in heavy high-pressure spheres at the bottom of the vehicle (fig. VI–4). If the tank pressure had to be raised an additional 2.0 pounds per square inch to avoid pump cavitation and assure good liquid-hydrogen pump performance, the extra thickness of tank wall required to support the added pressure and the additional helium plus the helium system would raise the structural and system weight several hundred pounds. This extra weight would reduce the payload by an equal amount and make it too low for the Surveyor mission.

The discussion presented herein, therefore, deals with the problems of pumping near-boiling liquids with modern high-performance pumps.

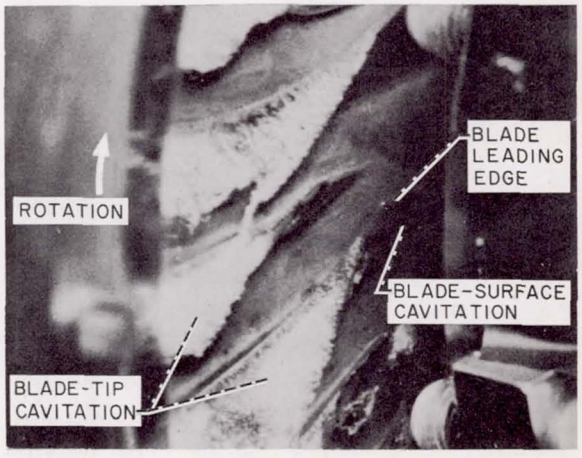

FIGURE VI–3.—Pump cavitation.

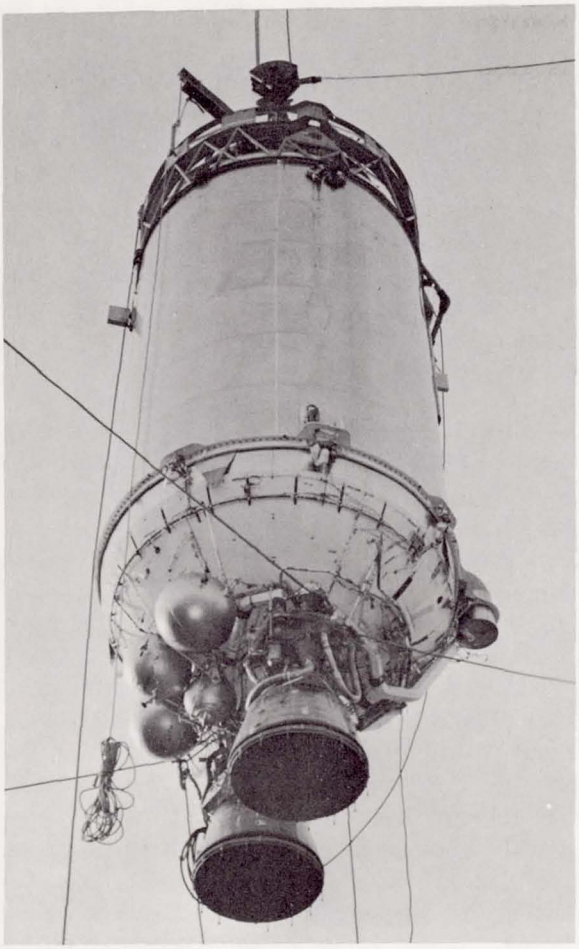

FIGURE VI–4.—Centaur space vehicle.

Subjects covered include the limiting effects of cavitation on pump performance, the approach to pump design that helps to overcome some of these limitations, methods for predicting pump performance under cavitating conditions for various liquids, cavitation damage, and pump flow instabilities with and without cavitation.

TYPES OF ROCKET PUMP

One of the two principal types of pumps used for handling rocket propellants is the centrifugal pump shown in figure VI–5. Basically, the centrifugal pump consists simply of a set of blades mounted on a rotating hub or rotor which is supported by a shaft and bearings and is generally driven by a turbine. Pumping work is done on the fluid by the rotor as the fluid flows radially outward through passages between the blading. The fluid is collected in a volute and delivered at high pressure.

Within limits, the work done on the fluid and thus the pressure at the discharge can be increased by increasing the rotational speed of the pump. If the desired pressure is higher than that which can be achieved by a single rotor, it is necessary to pass the propellant through additional rotor stages. Staging centrifugal pump rotors, however, requires elaborate ducting and an increased number of bearing supports, and heavy pumps result. A sketch of a typical multistage centrifugal pump is presented in figure VI–6. Thus, when the required discharge pressure is greater than can be attained by use of a single

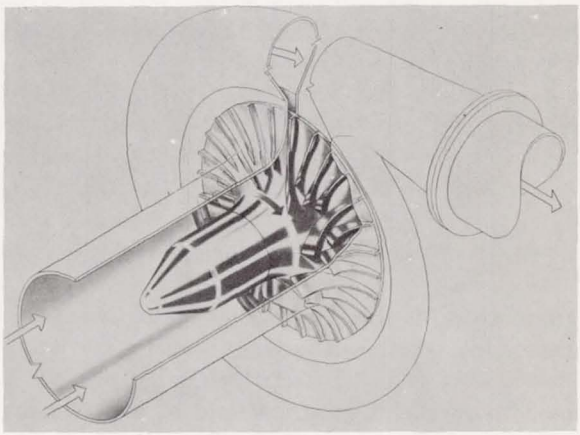

FIGURE VI–5.—Centrifugal pump.

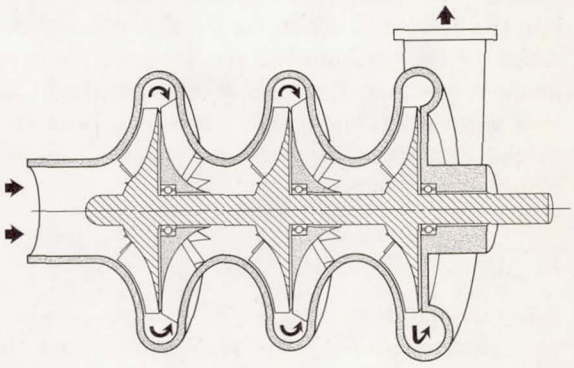

FIGURE VI–6.—Multistage centrifugal pump.

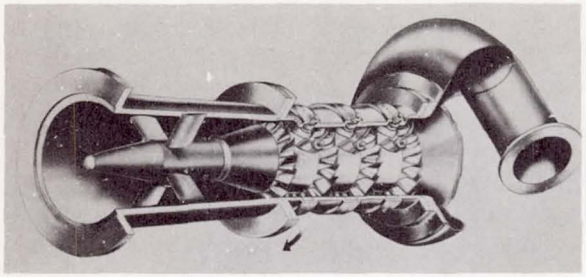

FIGURE VI–7.—Multistage axial-flow pump.

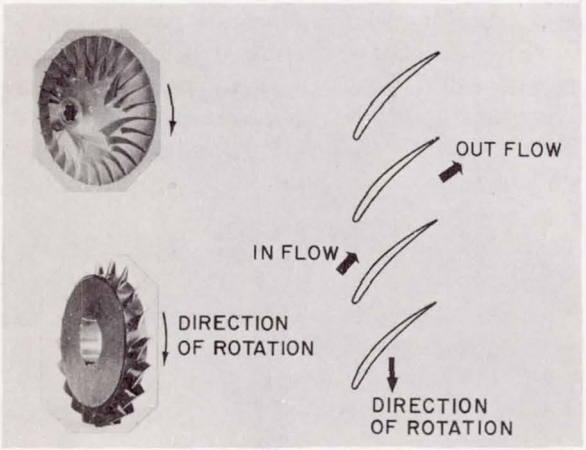

FIGURE VI–8.—Pump blades.

rotor, it is often advantageous to use an axial-flow pump, which can be easily staged. The axial-flow pump (fig. VI–7), which is also used in modern rocket engines, consists of a succession of rows of rotor blades and stator blades. The rotor blades, all of which are mounted on the same rotating drum, do work on the fluid being pumped, and the stator blades turn the flow into the desired direction for the next rotor stage. Although the pressure rise per stage of the axial pump is less than that of a centrifugal stage, the ease with which successive stages can be added to the axial-flow type allows a more compact high-pressure pump.

PUMP-FLOW ANALYSIS

Before the discussion of the manner in which cavitation degrades pump performance and the approach to design that is used to achieve a high degree of cavitation tolerance in pumps, it may be appropriate to review the manner in which pumps do useful work on the fluid to produce flow and pressure rise.

Rotors from the two types of pumps are shown in figure VI–8, centrifugal in the upper left and axial flow in the lower left. The sketch at the right of the figure represents a two-dimensional view of the blades for either type pump as they would appear unwrapped from the hub and viewed from the blade tips. The similarity to a series of aircraft wings can be noted. On conventional aircraft (fig. VI–9), the wing is so shaped that the air flowing immediately under it is slowed to less than flight speed and, consequently, experiences a rise in pressure with respect to that of the approaching air, as denoted by plus signs. The air adjacent to the top surface of the wing experiences a drop in pressure with respect to that of the approaching air, as denoted by minus signs. This difference in pressure on the upper and the lower wing surfaces produces the lift force that supports the aircraft.

The flow around pump blades is similar to that around a wing, as shown schematically in figure VI–10. The pressure variation along the surfaces of a typical pump blade is also presented. The differences in pressure existing on the upper and the lower blade surfaces result in a force on the blade which is proportional to the area between the pressure distribution curves. Conversely, an equal reaction force is exerted on the fluid by the pump blade, and, because the blade moves in the direction of force, work is done on the fluid. This work produces flow and a pressure rise across the blade row.

It is important to note that smooth flow must exist over the entire blade surface to produce the desirable large pressure differences. On the high-pressure side (lower surface), smooth flow can

FIGURE VI–9.—Wing analogy.

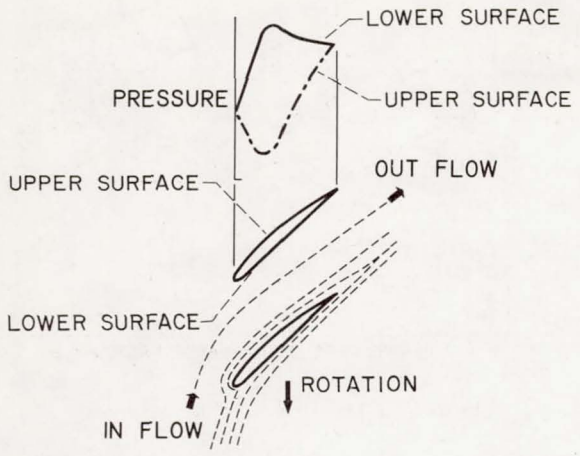

FIGURE VI–10.—Typical pump blade pressure distribution.

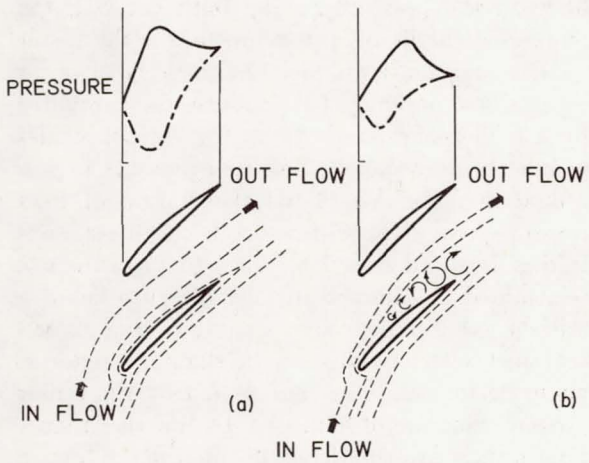

(a) Normal flow. (b) Separated flow.

FIGURE VI–11.—Pump blade pressure distribution for normal and separated flow.

be easily maintained, because this surface faces the oncoming flow which must stream around it. Maintaining smooth flow over the upper surface of the blade, however, is a critical matter. The flow adheres to the upper surface under the influence of low pressures, or suction, which exist on this surface. The flow over the upper surface of a pump blade can be easily disturbed and may detach, or separate, from the surface, as illustrated in figure VI–11. The desired suction on the upper surface is then partly lost over that portion of the blade where separation occurs. This loss is reflected by a change in the pressure distribution diagram. A comparison of the pressure distribution diagrams of figure VI–11 for smooth flow and separated flow shows that the area within the diagram is always less with flow separation. Because the suction on the top surface of the blade accounts for about half the force on the blade, partial loss of this suction reduces the blade force; hence, the pump work capability of the blade decreases. This decrease in pump work appears as a lowered pressure rise across the pump. Because flow separation disturbs the entire flow within the pump passage, the pressure distribution on the pressure surface of the blade is also affected, as noted in figure VI–11.

PUMPING NEAR-BOILING FLUIDS

As mentioned previously, the presence of extensive amounts of vapor (cavitation) in the pump limits pump performance. This problem of cavitation and its effect on pump performance becomes increasingly more critical as the fluid entering the pump approaches the near-boiling condition. In order to illustrate the effects of cavitation on flow conditions about pump blades, blade pressure distributions with and without cavitation are compared in figure VI–12. The

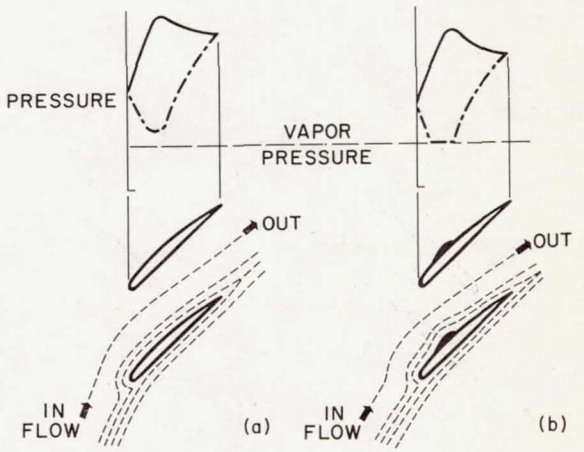

(a) Noncavitating. (b) Limited cavitation.

FIGURE VI–12.—Blade pressure distributions with and without cavitation.

horizontal dashed line represents the vapor pressure of the incoming fluid. If the inlet pressure is sufficiently high, the blade surface pressures are everywhere greater than the liquid vapor pressure. However, if inlet pressure is reduced sufficiently, local pressures on the suction surface of the blade are reduced to the fluid vapor pressure, and cavitation occurs. Because the pressure on the suction surface of the blade cannot be less than the vapor pressure of the liquid immediately adjacent to the vapor cavity, a loss in blade force results. This loss corresponds to the reduced area of the pressure distribution diagram, as illustrated by the right-hand diagram of figure VI–12.

As inlet pressure is further reduced, the cavitated region on the suction surface of the blade grows until the flow adjacent to the vapor cavity can no longer follow the sharp curvature at the downstream end of the vapor cavity, as illustrated by the right-hand diagram of figure VI–13. As noted in the figure, the flow separates from the blade, and a large part of the highly desirable suction is lost. The presence of cavitation causes a decrease in blade pressures on the lower surface because of disturbed flow in the channel between blades, as was the case for separated flow without cavitation (fig. VI–11). The greatly reduced area of the pressure diagram is

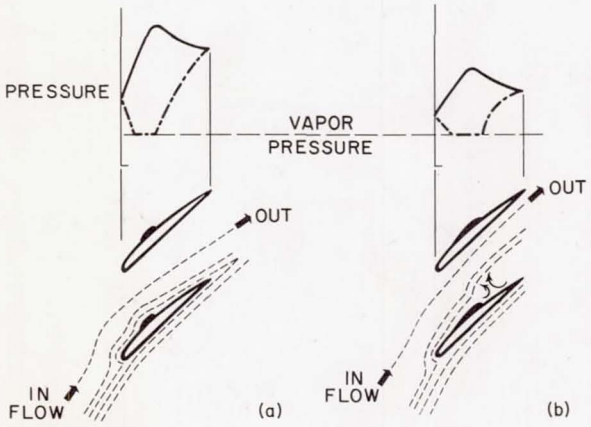

(a) Limited cavitation. (b) Severe cavitation.

FIGURE VI–13.—Blade pressure distributions with two degrees of cavitation.

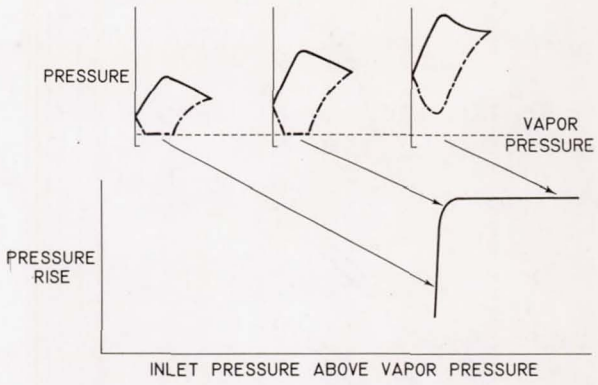

FIGURE VI–14.—Pump performance.

indicative of the large decrease in pumping work that can occur with extensive cavitation.

For fixed operating conditions, the difference between the pressure of the fluid entering the pump and the liquid vapor pressure is the factor which determines whether cavitation will occur in a given pump. The pressure rise provided by a high-performance pump for various values of inlet pressure above the vapor pressure is presented in figure VI–14. If the margin of inlet pressure above vapor pressure is adequate, cavitation is avoided and the desired pressure rise is attained. Reduction in inlet pressure below a critical value first produces cavitation of an extent just sufficient to cause a slight decrease in pump performance, as represented by the center pressure diagram of figure VI–14. Further reduction in inlet pressure leads to rapid deterioration of pump performance because of extensive cavitation and accompanying flow separation from the suction surface of the blade.

Photographs of pump flow corresponding to the three regimes of operation depicted in figure VI–14 are presented in figure VI–15. Cavitation-free flow, moderate cavitation at the point of performance dropoff, and extensive cavitation associated with a large performance loss are illustrated in figures VI–15(a), (b), and (c), respectively. With moderate cavitation (fig. VI–15(b)) where the pump operated just above the point of severe performance falloff, both blade-tip cavitation and suction-surface cavitation are evident. Although the blade-tip cavitation is quite prominent, it had no appreciable effect on

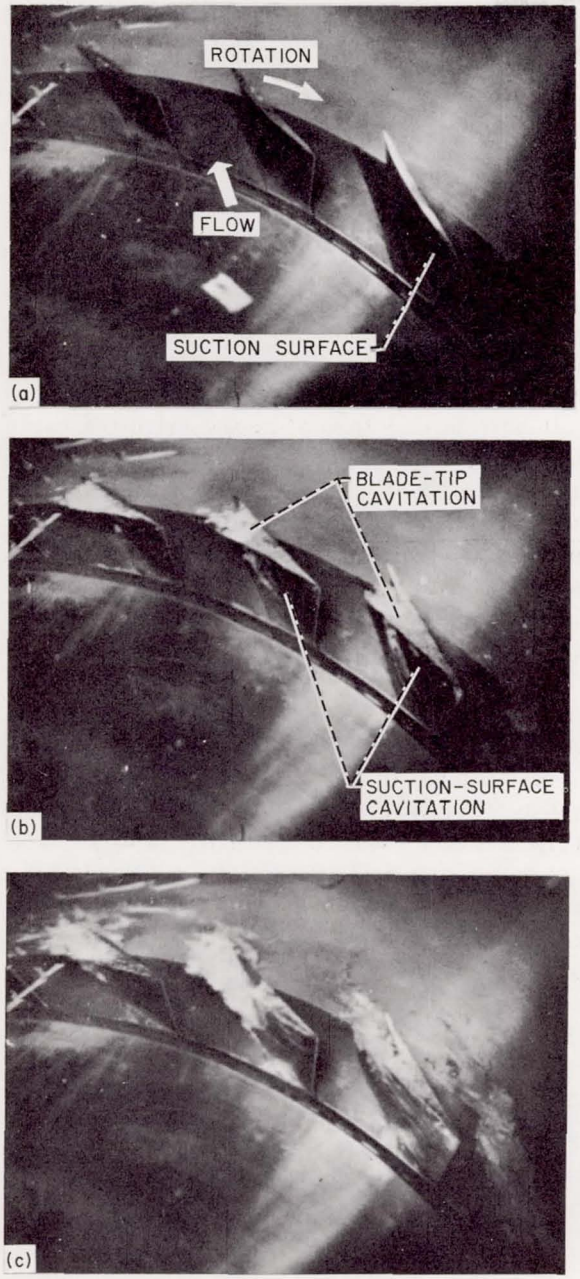

(a) Cavitation-free flow.
(b) Moderate cavitation.
(c) Extensive cavitation.

Figure VI–15.—Various degrees of cavitation.

pump blade performance. As inlet pressure was reduced, blade-surface cavitation continued to grow, as shown in figure VI–15(c). With this large amount of vapor present on the suction surface, the pump no longer operated effectively.

Unfortunately, for high-pressure-rise, high-speed pumps, the falloff in performance with extensive cavitation occurs at pump inlet pressures considerably greater than the low tank pressures required for some rocket applications.

INDUCERS

The problem of pumping from low-pressure tanks (i. e., near-boiling fluids) has been alleviated to a large extent through the design of a prepumping stage, which operates satisfactorily even under conditions of extensive cavitation. Such a prepumping stage is called an inducer. A typical inducer is presented in figure VI–16. The three exceptionally long blades are mounted on the hub in a manner approximating a helix. Inducers are generally located immediately upstream from the main pump and rotate on the same shaft as the main stage rotor. A typical inducer—axial-flow-pump combination is shown in figure VI–17 and the pressure rise through the various stages is illustrated schematically in figure VI–18. The inducer is only required to produce a pressure rise sufficient to allow the first axial-flow stage to operate free of cavitation.

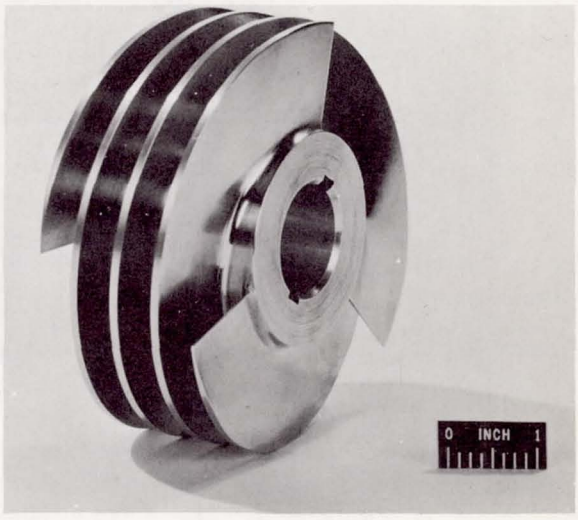

FIGURE VI–16.—Inducer.

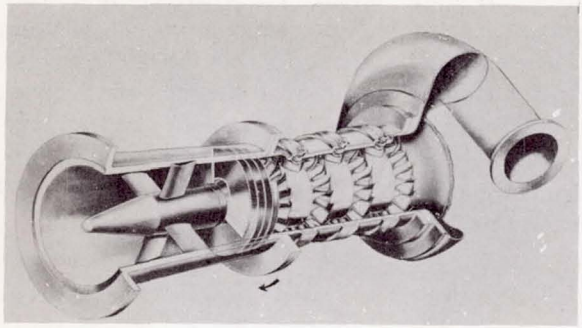

FIGURE VI–17.—Axial-flow pump with inducer.

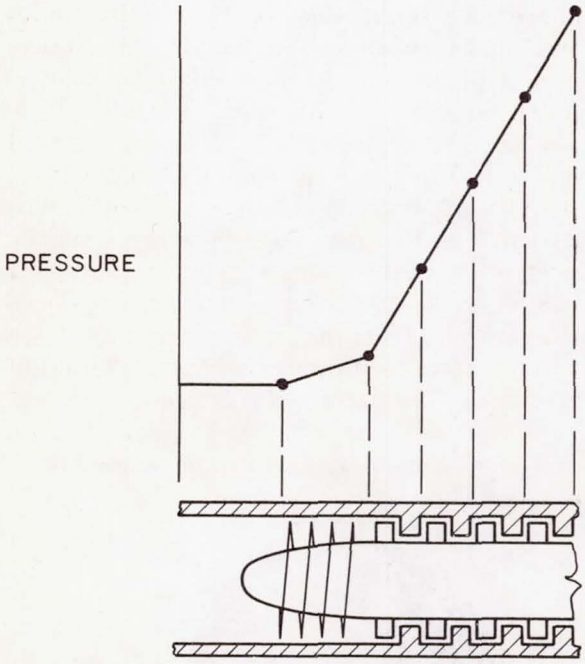

FIGURE VI–18.—Pressure rise in axial-flow pump with inducer.

The basis for the large cavitation tolerance of the inducer is illustrated qualitatively in figure VI–19. The long blades are shown in simplified form. The noncavitating pressure distribution indicates that with proper design the pressures on the suction side of the blade do not dip very deeply; the inlet pressure is thus allowed to approach close to liquid vapor pressure before cavitation is encountered. The diagram also shows that the largest pressure differences exist on the forward portion of the blade; thus, when operating without cavitation, the forward part of the blade does most of the pumping work. At low inlet pressures, cavitation and flow separation occur on the forward portion of the blade, but, because of the length and the hydrodynamic design of the blades, the separated flow reattaches to the blade surface behind the cavity to reestablish the desired blade force. Although the pressure forces on the forward portion of the blade have decreased, the forces exerted by the rear portion of the blade have increased. This compensating effect results in the same total area within the pressure diagram, denoted by the crosshatched areas; hence, blade pumping performance is maintained despite extensive cavitation. In order to illustrate the performance gains realized by use of an inducer, a comparison of the cavitation performance limit of a pump with and without an inducer is presented in figure VI–20. The addition of an inducer lowered the inlet pressure requirement for the pump to a value much closer to the liquid vapor pressure. Like the pump, however, the inducer is also limited by cavitation, as shown by the drop-off in performance.

An example of the amount of cavitation an inducer can tolerate with no appreciable loss in performance is shown in figure VI–21. The cavitation-free flow noted in the rearward channels between blades is associated with the pressure rise through the inducer, which causes the vapor to condense. In most cases, the use of

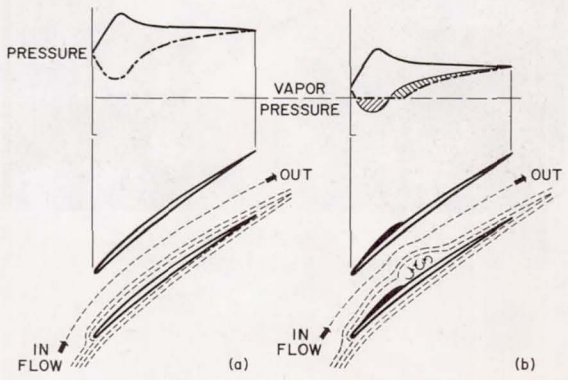

(a) Noncavitating. (b) Cavitating.

FIGURE VI–19.—Inducer blade pressure distributions.

inducers in rocket-engine pumps has allowed a reduction in propellant tank pressure sufficient to permit reasonable structural weights.

TYPICAL ROCKET PUMPS

Pump technology has made great strides in recent years. The liquid-hydrogen rocket-engine pump shown in figure VI–22, for example, provides a flow rate of 8000 gallons per minute and a pressure rise of 1400 pounds per square inch

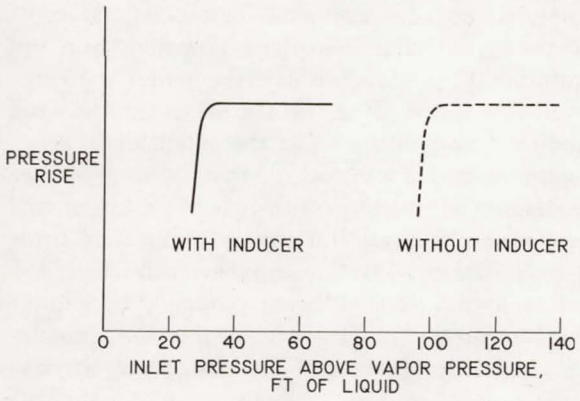

FIGURE VI–20.—Pump performance.

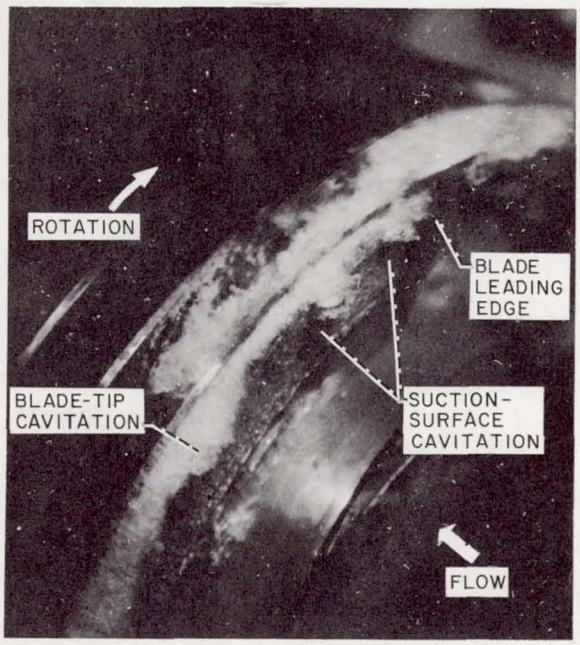

FIGURE VI–21.—Cavitating inducer.

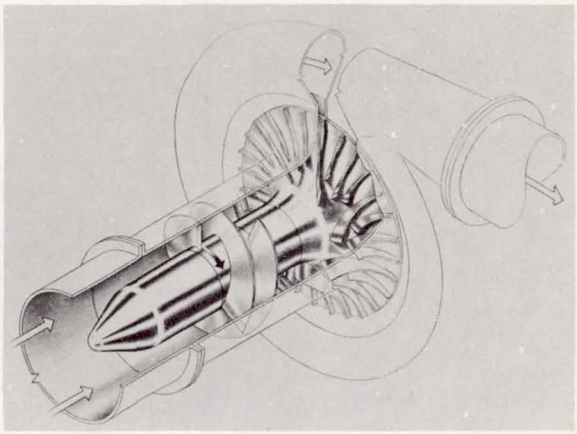

FIGURE VI–22.—Centrifugal pump with inducer.

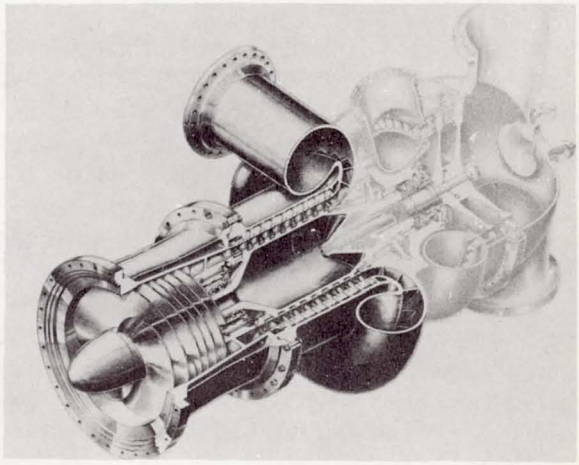

FIGURE VI–23.—Axial-flow liquid-hydrogen pump.

and requires about 9000 horsepower. The pressure rise across the pump is equivalent to raising the hydrogen to a height of over 50 000 feet. The technical sophistication of this pump can be realized from the fact that the 9000 horsepower is absorbed in useful work by a pump rotor that is about 8 inches in diameter and 8 inches long.

An axial-flow rocket pump for handling liquid hydrogen is shown in figure VI–23. This pump, developed for an advanced 1.5-million-pound-thrust engine, consists of an inducer and several axial-flow stages and is about 17 inches in diameter. It pumps 65 000 gallons of liquid hydrogen per minute to a pressure in excess of 1500

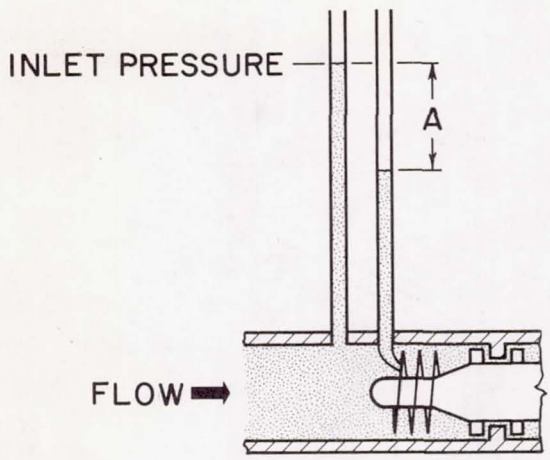

FIGURE VI–24.—Schematic pressure measurements.

pounds per square inch. The drive turbine, which produces over 90 000 horsepower, is directly connected to the pump shaft. If a cavitating inducer of the type shown could not be utilized, the pump rotational speed would have to be substantially reduced, and many more stages would have been required to obtain the desired discharge pressure. In addition, the pump diameter would have had to be increased to about 5 feet. Because the pump would have been required to rotate more slowly than the drive turbine, a massive speed-reduction gear box capable of transmitting 90 000 horsepower would have been required.

EFFECTS OF FLUID PROPERTIES ON CAVITATION PERFORMANCE

The aerospace program has provided high-performance pumps that operate well when near-boiling fluids are handled. For the most part, these pumps were proven with the use of rocket propellants such as kerosene, liquid oxygen, liquid hydrogen, and liquid fluorine. Because the cavitating performance of a pump can change with the liquid being pumped, the industrial designer is faced with the problem of having to determine cavitating performance with other liquids, that is, liquids of his interest. Specifically, the problem is that of predicting the lowest possible inlet pressure that can be established at the pump inlet while maintaining good pump performance.

The Lewis Research Center is presently engaged in several experimental and theoretical studies directed toward solving this prediction problem. Before the results of these studies are discussed, some basic observations with regard to pumps which handle different liquids under cavitating conditions should be noted in the interest of clarity.

Consider the schematic diagram of figure VI–24, which shows an inlet, pump inducer, and main pump of either axial or centrifugal type. It is assumed that the volume flow and the pump rotational speed for which the pump performs well are specified. It is also assumed that the inducer is operating under the condition of maximum tolerable cavitation; that is, any further reduction of inlet pressure would result in unacceptable pump performance. Pump inlet pressure is measured by a manometer containing the same liquid as that being pumped. A similar manometer symbolically measures the pressure on the suction surface of the blade in the cavitation zone. The basic observation is that the difference in level A between the two manometers shown is the same for all liquids for a given pump operating under the conditions specified. This observation is supported by theory and experience with cavitating pumps in which liquids of widely diverse physical properties were used. Once the pressure head difference A is established by some prior experience with the pump, it can be considered known.

Because the manometer on the inducer is in the cavitation zone, it measures the vapor pressure of the local liquid. For some liquids, this vapor pressure is essentially the same as the vapor pressure of the liquid entering the pump, which is known. For this case, the inlet pressure required is simply the sum of the head difference A and the known liquid vapor pressure. With some fluids, however, there is a beneficial effect, which is derived from the local cooling of the fluid adjacent to the cavitation zone. This cooling allows lower than expected inlet pressure requirements for these fluids. The difference in inlet pressure requirements with and without cavitation cooling is illustrated in figure VI–25.

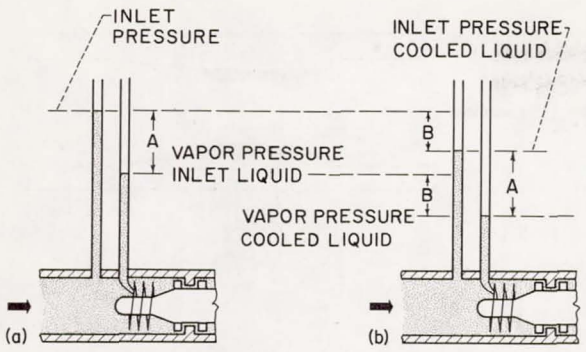

(a) No cavitation cooling. (b) Cavitation cooling.

FIGURE VI–25.—Cavitation cooling effect on pump inlet pressure.

Since the vapor pressure decreases with the lower temperature, the manometer on the inducer would read a vapor pressure which is lower than that of the incoming liquid by an amount B. Under these conditions, the inlet pressure can be lowered a corresponding amount, since it is sufficient to maintain the fixed pressure head differential A greater than the vapor pressure of the cooler liquid.

The cooling that occurs with cavitation present on the suction surface of an inducer blade is illustrated in figure VI–26. Heat is required to generate the vapor that fills the cavity, and this heat must be drawn from the surrounding liquid. Because of the high fluid velocities involved, the time required for the liquid and the vapor to traverse the cavitated region on the blade is very short. As a result, the amount of liquid which supplies the heat to form vapor is actually confined to a thin liquid film adjacent to the cavity, as shown. Because the amount of liquid involved is relatively small, a substantial cooling of the liquid film can occur in some cases. This cooling causes a drop in the vapor pressure of the liquid and a corresponding drop in the cavity pressure. As the temperature is decreased from that of the bulk liquid to that of the cooled film, a vapor-pressure drop occurs, as shown in the vapor-pressure—temperature curve of figure VI–26.

The magnitude of the vapor-pressure drop can be estimated by setting up a heat balance between the heat required for vaporization and the heat drawn from the surrounding liquid film, as follows:

Heat required for vaporization = Heat drawn from liquid film

$$\rho_v V_v L = (\Delta T)\, A h \rho_L C_L \qquad (1)$$

$$\text{Vapor-pressure drop} = K \left(\frac{\rho_v}{\rho_L} \frac{L}{C_L} \frac{dp}{dT}\right) \left(\frac{\rho_L C_L}{k}\right)^m U^n \qquad (2)$$

The mass of vapor generated is the product of the vapor volume V_v and vapor density ρ_v. This product multiplied by the heat of vaporization L is the heat required for vaporization. The heat drawn from the liquid film is equal to the mass of the film, given by the film area A, its average thickness h, and liquid density ρ_L, multiplied by its specific heat C_L and the film temperature drop ΔT.

The average thickness of the cooled liquid film depends on the heat-transfer process and can be expected to change with fluid properties and flow conditions. By introducing these heat-transfer effects and expressing the temperature drop ΔT in terms of a vapor-pressure drop through the vapor-pressure—temperature relations, equation (1) can be expressed as in equation (2). The term K is a proportionality constant that depends on the hydrodynamic characteristics of the flow device, such as a pump or inducer. The term dp/dt is the slope of the vapor-pressure—temperature curve at the bulk liquid temperature of interest. The last two terms are heat-transfer factors. The first of these is the inverse of the liquid thermal diffusivity and contains the ther-

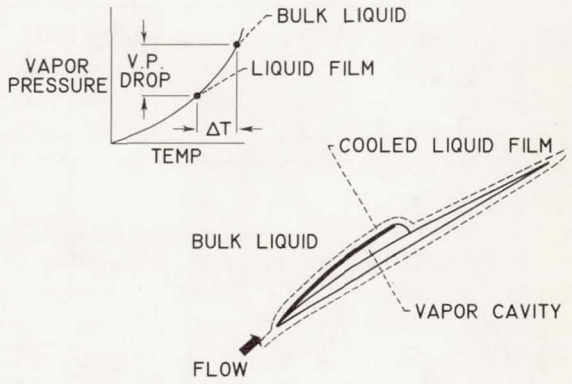

FIGURE VI–26.—Cavitation cooling.

mal conductivity of the liquid k, liquid density, and specific heat. The term U is a characteristic velocity, which can be the average velocity of the liquid relative to the blade. The exponents m and n depend on the heat-transfer process accompanying cavitation.

Because the minimum volume of vapor necessary to cause performance dropoff for a given pump is essentially the same for all liquids, comparisons of vapor-pressure drop are made on the basis of the same cavity size. For this case, a fixed relation exists between vapor volume V_v and film area A over which vaporization occurs. The terms V_v and A, therefore, do not appear explicitly in the vapor-pressure drop equation but are included in the constant K. Except for the constant K and velocity U, all terms are fluid properties.

In order to check the validity of this theoretical equation, it was necessary to conduct cavitation studies in such a way that the pressures and the temperatures within the cavitated region of various liquids could be measured directly. Because of the difficulty of making such measurements on a rotating pump blade, a venturi was used (fig. VI–27). The inside walls of the venturi are shaped to approximate the suction surface of a pump blade. With noncavitating flow, the pressure distribution on the venturi wall (lower part of fig. VI–27) is a useful approximation of the distribution on a pump blade. When the inlet pressure is lowered sufficiently to cause cavitation, vapor cavities are formed in the region of lowest pressure; the

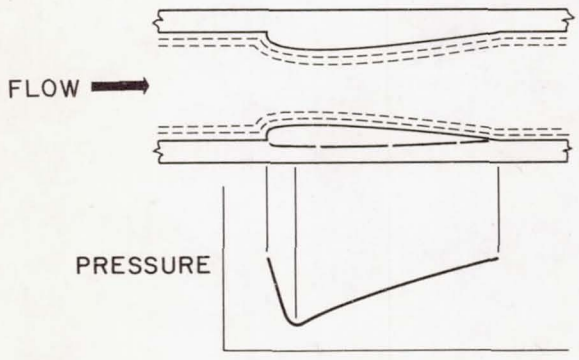

FIGURE VI–27.—Venturi.

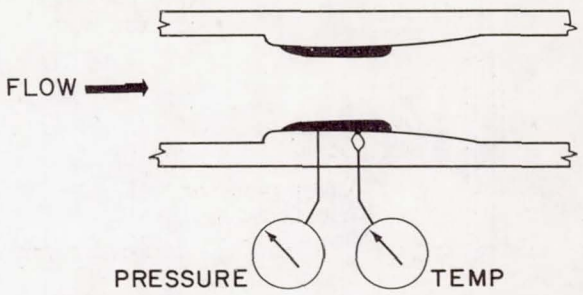

FIGURE VI–28.—Venturi with cavitation.

cavities then collapse downstream where the pressure increases, as shown schematically in figure VI–28. Temperatures and pressures within the annulus of vapor formed under cavitating conditions were measured simultaneously by means of thermocouples that protruded into the cavity and pressure taps located on the adjacent wall.

The fluids used in these studies were Freon 114, liquid nitrogen, and water in order to provide a wide spread in physical properties of the test fluids. Each fluid was studied over a range of flow velocity, temperature, and cavity length. Cavity length was determined by direct observation through the transparent walls of the venturi.

For all conditions studied, the measured cavity pressures corresponded to the vapor pressure at the measured temperatures. Cavity pressures as much as 6 pounds per square inch less than the vapor pressure of the incoming fluid were measured. This drop in vapor pressure corresponded to a 10° F drop in temperature accompanying cavitation.

Some of the measured vapor-pressure-drop data obtained with Freon 114 in the venturi study were used to evaluate the exponents and the constant K in the theoretical vapor-pressure-drop equation. The experimentally determined values for m, n, and K, respectively, are 0.5, 0.85, and 0.008; thus, the vapor-pressure-drop equation for the venturi is

$$\text{Vapor-pressure drop} = 0.008\left(\frac{\rho_v}{\rho_L}\frac{C_L}{L}\frac{dp}{dT}\right)\left(\frac{\rho_L C_L}{k}\right)^{0.5} U^{0.85} \quad (3)$$

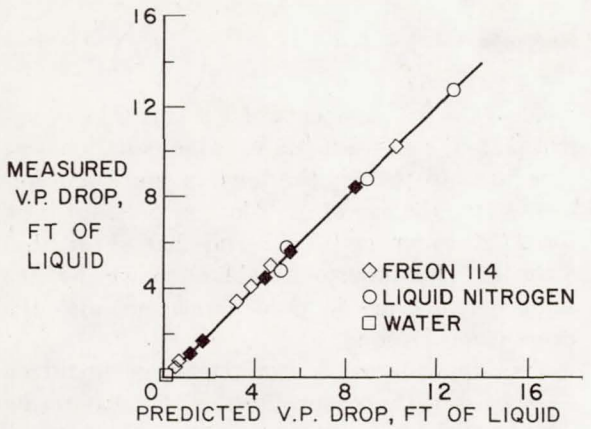

FIGURE VI–29.—Prediction of vapor-pressure drop.

With m, n, and K established by experiment, the vapor-pressure drop in the cavity can be computed for any liquid, the physical properties of which are known. The equation was used to predict the vapor-pressure drop for liquid nitrogen, water, and Freon 114 at different values of flow velocity and liquid temperature for the venturi. Some typical results are presented in figure VI–29, which compares the measured and the predicted vapor-pressure drops from equation (3). Some measured values of cavitation vapor-pressure drop for Freon 114 and liquid nitrogen at various temperatures, and flow velocities are listed in table VI–1. All the values listed are for a fixed cavity size. For conditions studied, room-temperature water showed essentially no vapor-pressure drop. In fact, all the water data obtained covering the temperature range from 40° to 120° F can be represented by the single datum point shown at the extreme low end of the curve (fig. VI–29). The solid symbols are representative Freon 114 data used to evaluate the unknowns in the equation. These points, of course, fall on the curve. The good agreement obtained between predicted and measured values indicates the equation, with the experimentally determined exponents of 0.5 and 0.85, to be quite general. The constant K, however, must still be evaluated for each different flow device.

TABLE *VI–1.—Measured Vapor-Pressure Drop*

Liquid	Temperature, °F	Flow velocity, ft/sec	Measured vapor-pressure drop, ft of liquid
Freon 114	6	32	0.9
Freon 114	28	32	1.8
Freon 114	59	32	5.1
Freon 114	79	32	8.5
Nitrogen	—320	32	8.8
Freon 114	78	44	10.2
Nitrogen	—320	42	12.5

The equation was used to predict the cavitation vapor-pressure drop for other liquids (fig. VI–30). The bar graph shows predicted vapor-pressure drops for several liquids, computed for the liquid temperatures shown. The 75° F water and the liquid-nitrogen results are repeated from figure VI–29 for comparative purposes. Although room-temperature water showed essentially no vapor-pressure drop, and drop for 450° F water is quite large, about 130 feet of water. This drop is due primarily to the large increase in vapor density and slope of the vapor-pressure —temperature curve at the higher temperatures. The vapor-pressure drop for two commercial liquids, liquid methane at the normal boiling point and methyl alcohol at 180° F, is about the same as for nitrogen. Liquid hydrogen, which is of interest as a rocket fuel, shows large vapor-pressure drops; from 130 feet of hydrogen at its normal boiling point of −423° F (37° R) to more

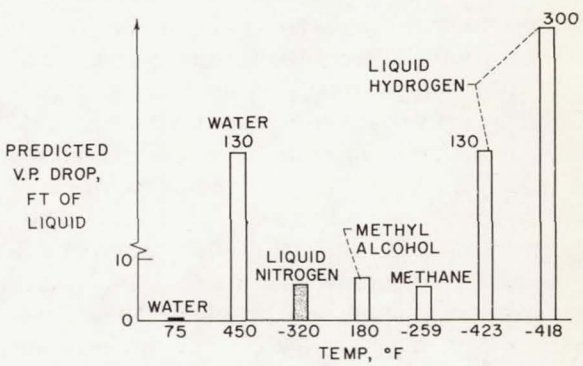

FIGURE VI–30.—Predicted vapor-pressure drops for Venturi.

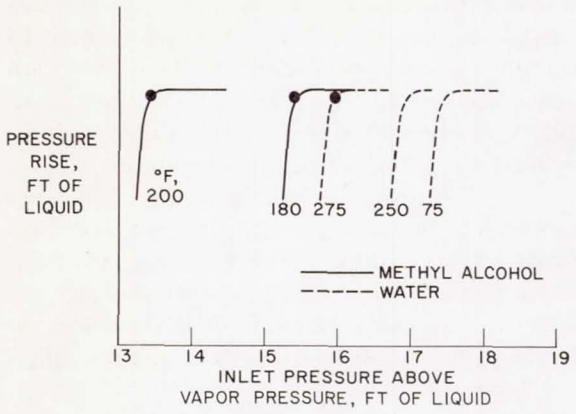

FIGURE VI–31.—Pump performance with water and methyl alcohol.

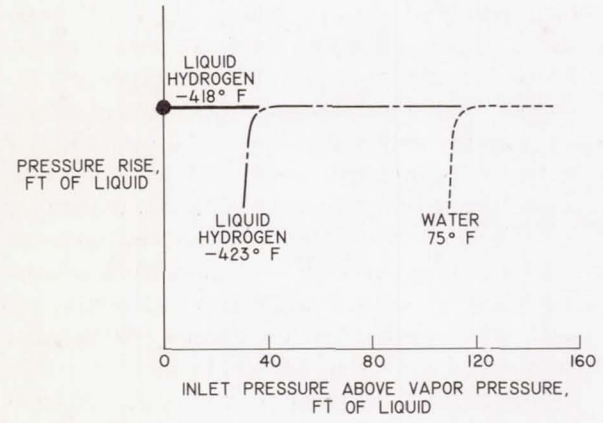

FIGURE VI–32.—Pump performance with water and liquid hydrogen.

than 300 feet of hydrogen at −418° F (42° R), an increase in temperature of only 5° F.

The utility of the vapor-pressure-drop equation for pumps was checked by using it to predict the cavitating performance limit for a small centrifugal pump handling hot water and methyl alcohol. A comparison of pump performance obtained with these liquids at various temperatures but for the same operating conditions is presented in figure VI–31, which shows pump pressure rise plotted as a function of inlet pressure above vapor pressure. The performance data obtained for the pump operated at 75° and 250° F water were used to evaluate the constant K in the equation

$$\text{Vapor-pressure drop} = K\left(\frac{\rho_v}{\rho_L}\frac{L}{C_L}\frac{dp}{dT}\right)\left(\frac{\rho_L C_L}{k}\right)^{0.5} U^{0.85}$$

which uses the exponents of 0.5 and 0.85 established in the venturi study. This equation was then used to predict the inlet pressure requirements (for the same small loss in pressure rise) for 275° water and 180° and 200° F methyl alcohol. The predicted values, shown by the solid symbols, are in good agreement with the experimental results.

The vapor-pressure-drop equation predicted a large drop in vapor pressure for cavitating liquid hydrogen as compared with room-temperature water (fig. VI–30). Figure VI–32 shows the performance of a pump operated at the same flow conditions in both water and liquid hydrogen. As anticipated from the cavitation-cooling studies, the margin of inlet pressure above vapor pressure at which the pump performance declined is much lower for the liquid hydrogen than for the cold water. For the same rotational speed and flow rate, the analysis also predicted that an increase of only 5° F in liquid-hydrogen temperature (from −423° to −418° F) would enable satisfactory operation of this pump at zero margin of inlet pressure above vapor pressure, that is, with the incoming liquid at its boiling point. This predicted point is indicated by the solid symbol. When the pump was operated under these conditions, pump performance was sustained when the hydrogen entering the inlet was boiling, as indicated by the solid line. Measured and predicted pump performance are thus in good agreement.

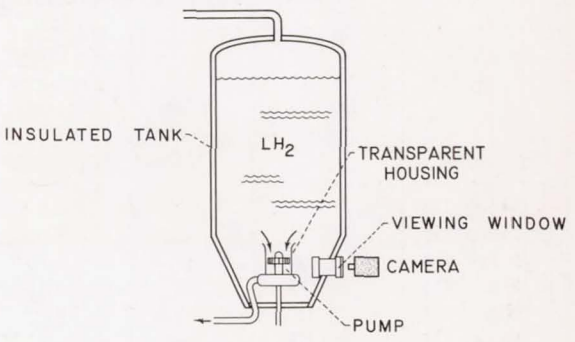

FIGURE VI–33.—Hydrogen-pump test arrangement.

Photographs of the pump operating at 20 000 rpm under cavitating conditions in −418° F liquid hydrogen were obtained with the experimental arrangement shown in figure VI–33. The pump, encased in a transparent housing, was photographed through an evacuated window tube, which was directly immersed in the tank of liquid hydrogen. Figure VI–34(a) shows the pump operating with a moderate degree of cavitation. It was impossible to obtain good photographs of inducer cavitation for the condition of zero margin of inlet pressure above vapor pressure. As the tank pressure (or pump inlet pressure) is progressively reduced, the tank pressure reaches the vapor pressure of the hydrogen,

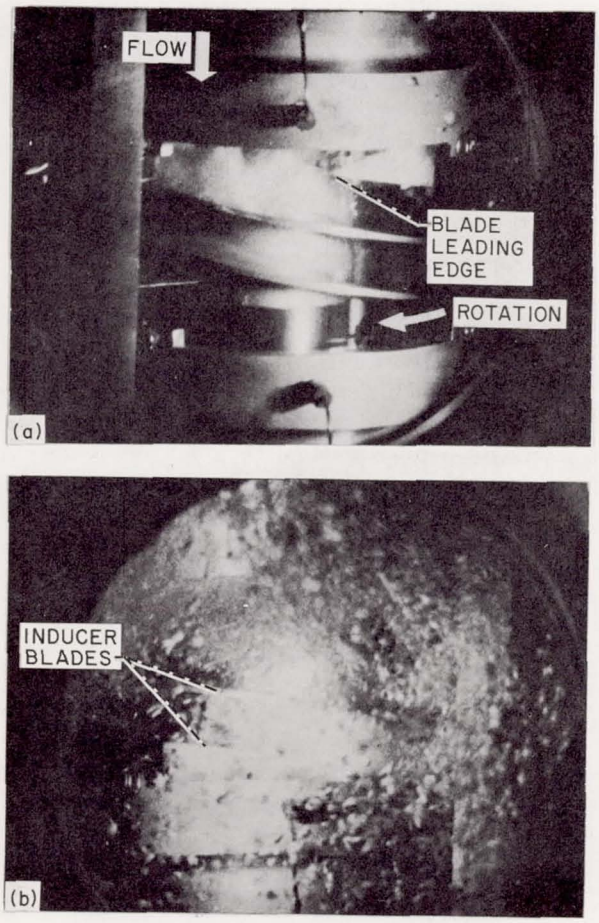

(a) Moderate cavitation.
b) Operation with boiling liquid hydrogen.

FIGURE VI–34.—Inducer cavitation in liquid hydrogen at −418° F.

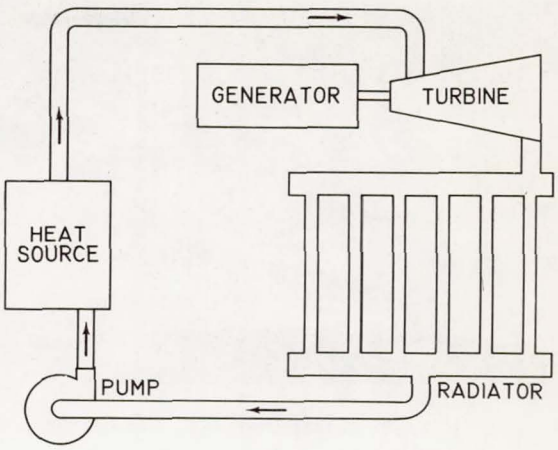

FIGURE VI–35.—Turbogenerator space power system.

and the liquid boils throughout the tank. The resulting vapor bubbles occurring between the window and the pump housing restrict the view of the inducer as shown in figure VI–34(b). Under the conditions shown in figure VI–34(b), the pump continued to produce a satisfactory pressure rise (fig. VI–32).

The present method for predicting pump cavitation performance for various liquids has been examined with only a limited number of liquids; however, because the test liquids had widely diverse physical properties, the general utility of the method is regarded with confidence. Present Lewis programs are exploring this subject further.

CAVITATION DAMAGE

Another and perhaps more familiar aspect of cavitation in industrial pumps is the structural failure that it can cause. In pumps used for rocket engines, cavitation damage is not a problem because the duration of the engine operation is so short. Pumps used in turbogenerator electric power systems on space vehicles, however, will be required to operate continuously unattended for a year or more. A schematic diagram of such a system is shown in figure VI–35. The system generates electrical power by means of a turbine-driven generator and uses a metal vapor, such as sodium or potassium, as the working fluid. After leaving the turbine, the

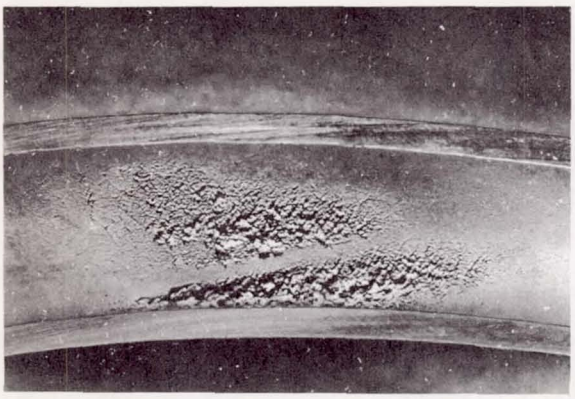

FIGURE VI–36.—Pump blade cavitation damage.

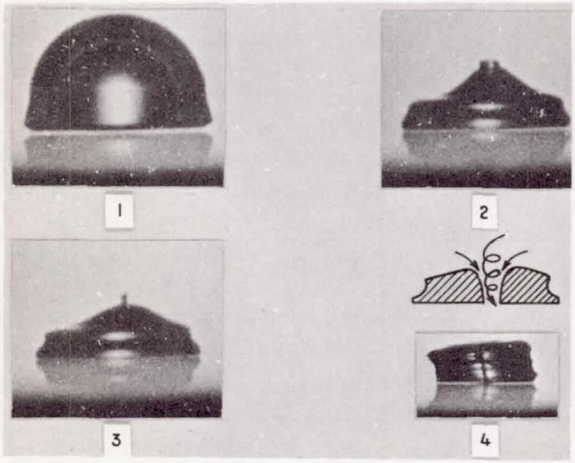

FIGURE VI–37.—Vapor bubble collapse mode. (Courtesy A. T. Ellis, California Institute of Technology, and T. B. Benjamin, University of Cambridge.)

spent vapor is condensed in the radiator. The condensate is returned to the boiler by a pump. Since this condensate is in a near-boiling condition, a cavitation problem also exists with liquid sodium or potassium. That a cavitation-damage problem exists is evident from the photograph of a pump blade presented in figure VI–36. The view shows the blade surface near the outlet of a mixed-flow impeller. The pump was tested at the Pratt & Whitney CANEL installation under cavitating conditions in liquid potassium at a temperature of 1400° F for 350 hours. If the severe pitting shown had been allowed to continue, blade failure would have eventually resulted. The need for cavitation damage research is clear.

Cavitation damage occurs on a fluid-containment surface, such as a pump blade, where adjacent vapor cavities rapidly collapse. Although various studies have shown that pure vaporous cavities can collapse rapidly and at high energy levels, the basic mechanics of damage by imploding vapor bubbles is not clearly established. Recent research, however, has revealed one way in which cavitation damage occurs. Figure VI–37 shows the successive phases of an imploding cavitation bubble near a solid surface. The first photograph shows a cavitation bubble adjacent to a surface somewhat as it would appear moving along the suction surface of a pump blade. As the bubble moves into a zone of higher pressure, the vapors within condense rapidly. The collapsing bubble takes odd shapes. In collapsing (photographs 2, 3, and 4), a jet of liquid is formed, which pierces the bubble and impinges on a small area of the adjacent blade surface. Careful scrutiny of the photographs of the impinging jet suggests that the jet is in rapid rotation. The center of the jet appears in the photographs as a dark core which extends above the bubble.

Lewis has sponsored research on materials that resist cavitation damage. Studies of cavitation damage with the use of alkali-metal pumps are supplemented by work with a magnetostrictive vibratory device which closely simulates pump-blade damage. This device (fig. VI–38) consists of two principal parts, a magnetostrictive vibrator, and a test specimen which is driven by the vibrator. Cavitation damage is produced on the

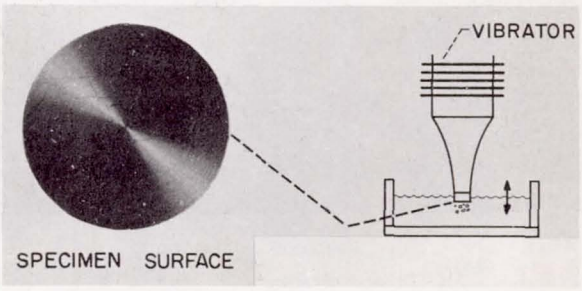

FIGURE VI–38.—Magnetostrictive cavitation damage apparatus.

surface of the 0.5-inch-diameter circular specimen, which is submerged in liquid and caused to vibrate at high frequency. On each upstroke, vapor bubbles are formed near the surface of the specimen. These bubbles collapse with high energy on the ensuing downstroke. The device provides a practical method for making rapid, accurate, and detailed measurements of the rate of weight loss for a given material.

The cavitation erosion rates for a number of materials, tested over a range of conditions, are presented in figures VI–39 and VI–40. Rate of weight loss in milligrams per hour is plotted as a function of exposure time in hours. The curve of figure VI–39 is for 304L stainless steel tested in 80° F water; the curve of figure VI–40 is for 316 stainless steel tested in 400° F liquid sodium. The curves are similar in that the damage rate is small initially, rises sharply, and then falls off to a constant, steady-state rate. Comparisons between various materials are made in the steady-state zone. The damage rate differs for the various materials. In water, for example, soft aluminum is eroded by cavitation about 60 times faster than stainless steel. The resistance of several refractory alloys, TZM, T–222, and columbium 132M has been studied in liquid sodium. These alloys maintain their strength at the high temperatures of interest in space power systems. In 400° F sodium, the resistance of these materials to cavitation damage (based on steady-state values) is comparable with that of 316 stainless steel. Stellite 6B, a cobalt-base alloy, is remarkably resistant to damage. After 14 hours

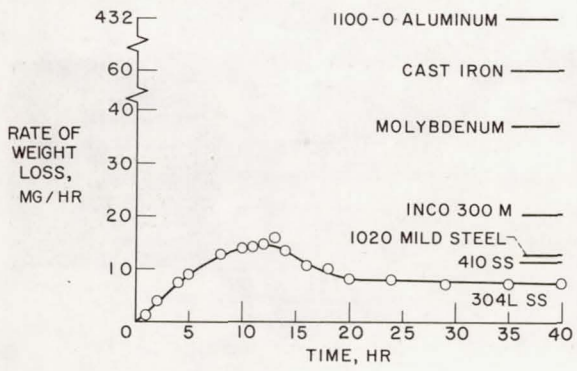

FIGURE VI–39.—Cavitation damage rate in water at 80° F.

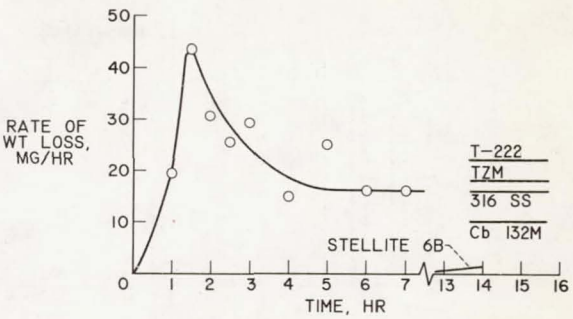

FIGURE VI–40.—Cavitation damage rate in liquid sodium at 400° F.

of exposure, weight loss was only beginning to become measurable. Because of its high cost and difficulty of fabrication, it is impractical to fabricate an entire pump rotor of Stellite. An inlay of Stellite in the most damage-prone area of the blading, however, might greatly extend pump life.

In order to determine which physical properties of the material are important in determining the resistance to cavitation damage, it is important to consider the mechanism of damage. Basically, the containment material is exposed to the jet impingement and pressure shock waves of imploding bubbles on or very near its surface. Damage resistance, then, is a measure of the capacity of a material to absorb this mechanical attack before fracture or pitting occurs. Thus, high values of yield strength, ultimate tensile strength, hardness, and ductility (percentage of elongation to fracture) are beneficial in providing resistance to cavitation damage.

In space powerplant systems, operation at high temperature levels is desirable; thus, it is important to consider the effect of fluid temperature on the rate of cavitation damage. The rate of damage for three materials immersed in liquid sodium at temperatures of 400°, 1000°, and 1500° F are compared in figure VI–41. All the data presented were obtained with the liquid sodium at atmospheric pressure. The greatly reduced rate of damage observed at 1500° F occurs despite the fact that the specimen materials have less strength at this higher temperature. This reduced damage is attributed to the high vapor pressure of sodium at 1500° F, which causes the

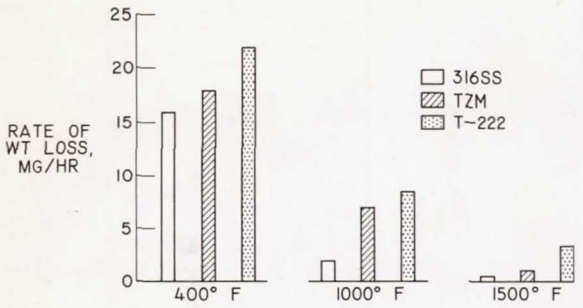

FIGURE VI–41.—Effect of temperature on cavitation damage rate in liquid sodium.

cavitation bubbles to collapse with less violence. For space power systems, it may be desirable to pump sodium at 1500° F or greater; thus, the reduced damage rate at high temperature is favorable.

Cavitation-damage data obtained thus far allow the arrangement of materials in the order of their resistance to cavitation damage with some degree of confidence. Further studies are being conducted to obtain a better understanding of the basic phenomena as well as the practical problems associated with cavitation damage.

FLOW INSTABILITY

Cavitation can cause pump damage in an entirely different manner; it can lead to flow instabilities, which produce strong pressure fluctuations in the pump. These pressure fluctuations can vibrate some of the pump parts to failure.

Photographs of flow oscillations induced by cavitation in a pump inducer (operating in water) were obtained by use of the arrangement shown in figure VI–42. The inducer was encased in a transparent housing, and nylon tufts attached to the housing wall were used to indicate local flow direction. A photograph showing the arrangement of tufts and inducer blading is also shown in the figure. Under normal flow conditions, the tufts ahead of the rotor indicate flow directly into the inducer. Tufts in the rotor area indicate the flow turned in the direction of inducer rotation. Flow oscillations that can occur with cavitation are presented in figure VI–43. With the inducer operating at a tolerable level of cavitation (fig. VI–43(a)), steady flow is indicated. As inlet pressure is reduced (fig. VI–43(b)), cavitation becomes more severe and the flow unsteady, as indicated by oscillations of those tufts ahead of the rotor. A further reduction of inlet pressure results in extreme cavitation (fig. VI–43(c)), and the entire flow pulses violently. In some instances, periodic flow reversals were indicated by all the tufts.

Figure VI–44 shows an inducer blade failure which occurred after a few minutes of operation in the presence of severe flow instability. These studies indicate that while inducers can operate satisfactorily with some degree of cavitation, flow instabilities caused by extreme cavitation can result in pump failure.

Pump instabilities can also occur in the absence of cavitation, and in some instances, these instabilities may lead to an erroneous diagnosis of difficulties in pumping systems. The manner in which these instabilities arise in cavitation-free flow can be illustrated by an examination of the flow in the channels between pump blades. Diagrams of the flow streamlines and the velocity profile in the flow channels of a centrifugal pump are presented in figure VI–45. The advancing face of the blade is the pressure surface (denoted by +), and the trailing face is the suction surface (denoted by −); thus, the pressure varies across the flow channel. A corresponding variation in flow velocity across the channel exists as diagramed with the highest velocities corresponding to the lowest pressures. The velocity distribution shown is for a well-designed pump

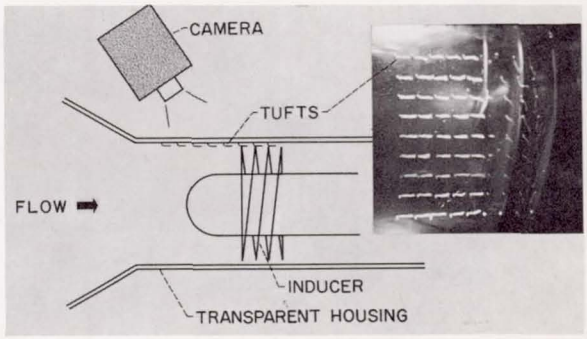

FIGURE VI–42.—Experimental arrangement for flow instability study.

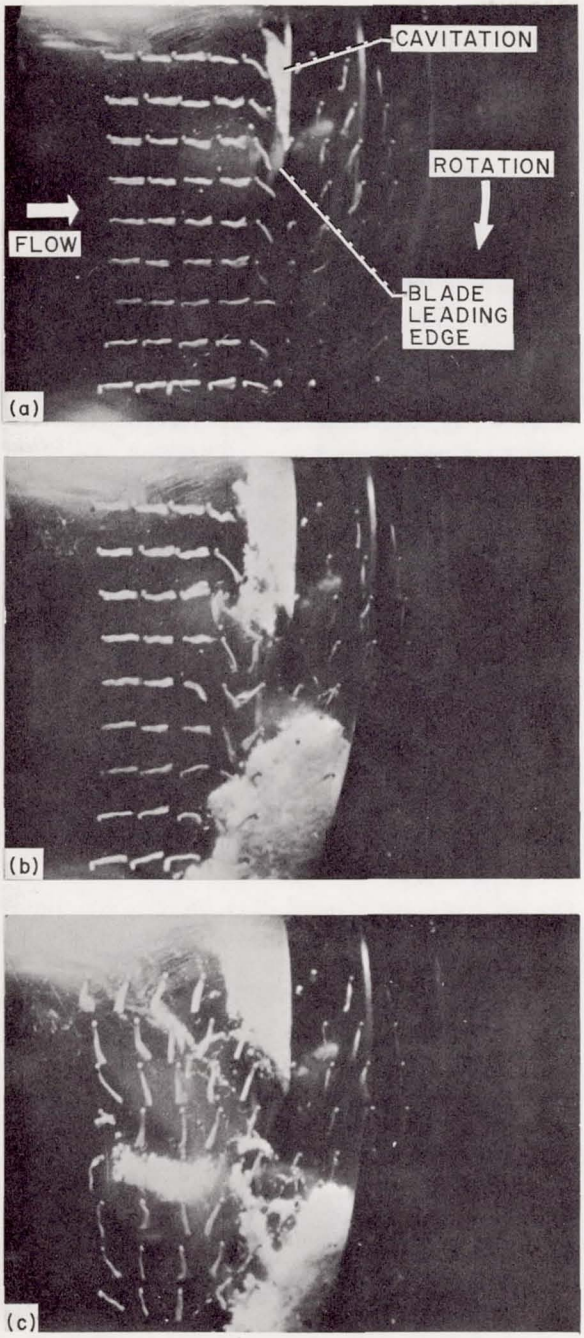

(a) Mild cavitation.
(b) Severe cavitation.
(c) Extreme cavitation.

FIGURE VI–43.—Cavitation-induced flow instability.

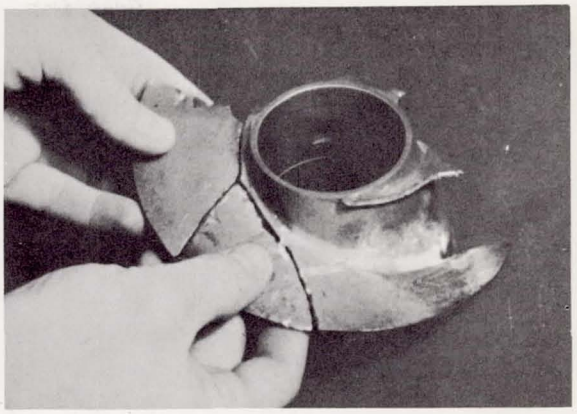

FIGURE VI–44.—Inducer blade failure.

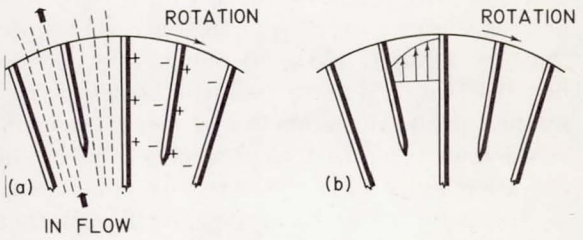

(a) Flow streamlines. (b) Velocity profile.

FIGURE VI–45.—Flow between pump blades.

operated at design conditions. Velocity distribution can be controlled by varying the hub contour, blade height and thickness, circumferential spacing, and blade curvature.

In a pump of poor design, the flow velocity may drop to zero or even become negative on the high-pressure side of the flow passage, as shown in figure VI–46. A negative velocity means that the local flow is opposed to the main stream direction. These local flow reversals produce a whirling eddy, which disturbs the flow, as indicated by the marked distortion of the streamlines. Unfortunately, these eddies are unstable. Eddies are continually generated, grow as they move outward through the blade passage, and are then washed downstream to produce a rhythmic fluctuation in pump delivery pressure and flow rate. Such oscillations can build to destructive magnitudes in pumps and associated plumbing systems.

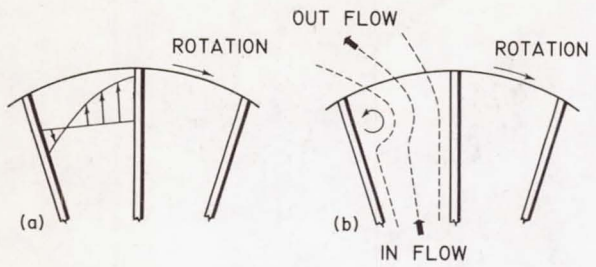

(a) Velocity profile. (b) Flow streamlines.

FIGURE VI–46.—Eddy flow.

Instabilities can also occur in a well-designed pump, if it is operated too far below the design flow rate. At low flow rates, eddies form and flow oscillations occur in a manner similar to that for a poorly designed pump. The stream flow field within a pump rotor can be determined by theoretical calculation procedures. Such a calculation can be used to determine the useful operating range of a well-designed pump; that is, the point of onset of flow oscillation that may occur as the flow is throttled can be predicted.

This analytical prediction technique has been programed in FORTRAN language for digital computing. Some pump manufacturers have obtained this program from Lewis and have used it to design and analyze the flow conditions within their pumps. The computer deck and necessary instructions are available upon request. It is referred to as a "Quasi-three-dimensional flow solution for centrifugal pump impellers." The analytical program is sufficiently flexible to allow calculation of velocity distributions in other internal flow devices, such as inlets, diffusers, or elbows.

CONCLUDING REMARKS

The foregoing discussion of the role of cavitation in defining pump performance treats one phase of NASA work on high-performance pumps. Companion work includes studies on the design of high pressure-rise blading for centrifugal and axial-flow pumps and high-work turbines for driving these pumps. These studies make extensive use of the compressor and turbine technology developed earlier for jet engines. Most of this work is documented in NASA reports dating from 1958.

Present NASA work on rotating machinery extends from large components for aircraft jet engines to small, high-speed turbines and compressors suited for turbogenerated electrical power systems in space that use gases such as argon and neon as the working fluid. The high efficiencies attained in turbines and compressors ranging in size to one as small as 3 inches in diameter represents a new advance in the technology of these machines. The wide range of information developed should include many areas of interest to the machine designers who serve the petroleum industry.

BIBLIOGRAPHY

Pumps and Inducers

CROUSE, JAMES E.; MONTGOMERY, JOHN C.; AND SOLTIS, RICHARD F.: Investigation of the Performance of an Axial-Flow-Pump Stage Designed by the Blade-Element Theory—Design and Overall Performance. NASA TN D–591, 1961.

CROUSE, JAMES E.; SOLTIS, RICHARD F.; AND MONTGOMERY, JOHN C.: Investigation of the Performance of an Axial-Flow-Pump Stage Designed by the Blade-Element Theory—Blade-Element Data. NASA TN D–1109, 1961.

HARTMANN, MELVIN J.; AND BALL, CALVIN L.: New Problems Encountered with Pumps and Turbines. Proceedings of the NASA-University Conference on the Science and Technology of Space Exploration, Vol. 2, NASA SP–11, 1962, pp. 23–35.

OSBORN, WALTER M.: Noncavitating and Cavitating Performance of a Liquid-Fluorine Pump Designed by Stream-Filament Method. NASA TM X–722, 1963.

SANDERCOCK, DONALD M.; SOLTIS, RICHARD F.; AND ANDERSON, DOUGLAS A.: Cavitation and Noncavitation Performance of an 80.6° Flat-Plate Helical Inducer at Three Rotational Speeds. NASA TN D–1439, 1962.

SOLTIS, RICHARD F.: Some Visual Observations of Cavitation in Rotating Machinery. NASA TN D–2681, 1965. (Technical Film Supplement C–239 available on request.)

SOLTIS, RICHARD F.: ANDERSON, DOUGLAS A.; AND SANDERCOCK, DONALD M.: Investigation of the Performance of a 78° Flat-Plate Helical Inducer. NASA TN D–1170, 1962.

Cavitation

JACOBS, ROBERT B.; MARTIN, KENNETH B.; AND HARDY, RICHARD J.: Direct Measurement of Net Positive Suction Head. Rep. No. 5500, National Bureau of Standards, July 18, 1957.

RUGGERI, ROBERT S.; AND GELDER, THOMAS F.: Cavitation and Effective Liquid Tension of Nitrogen in a Tunnel Venturi. NASA TN D–2088, 1964.

STAHL, H. A.; AND STEPANOFF, A. J.: Thermodynamic Aspects of Cavitation in Centrifugal Pumps. ASME Trans., vol. 78, Nov. 1956, pp. 1691–1693.

WILCOX, W. W.; MENG, P. R., AND DAVIS, R. L.: Performance of an Inducer-Impeller Combination at or Near Boiling Conditions for Liquid Hydrogen. Vol. 8 of Advances in Cryogenic Eng., K. D. Timmerhaus, ed., Plenum Press, 1963, pp. 446–455.

Cavitation Damage

KULP, ROBERT S.; AND ALTIERI, JAMES V.: Cavitation Damage of Mechanical Pump Impellers Operating in Liquid Metal Space Power Loops. NASA CR–165, 1965.

THIRUVENGADAM, A.; PREISER, H. S.; AND RUDY, S. L.: Cavitation Damage in Liquid Metals. Tech. Prog. Rep. 467–3, Hydronautics, Inc. (NASA CR–54459), 1965.

Page intentionally left blank

VII Lubricants, Bearings, and Seals

EDMOND E. BISSON, WILLIAM J. ANDERSON, ROBERT L. JOHNSON, ERWIN V. ZARETSKY, AND LAWRENCE P. LUDWIG
Lewis Research Center

AEROSPACE APPLICATIONS require lubrication under difficult or even hostile environments such as (1) extremely low and high temperatures, (2) vacuum, and (3) chemically active fluids. Some examples of these environments are found in the high-performance vehicle shown in figure VII–1. The high-energy propellants (the cryogenic liquids, hydrogen, oxygen, or fluorine) used in these vehicles expose bearings and seals to extremely low temperatures. For instance, the temperature of liquid hydrogen is −423° F. Similarly, there are mechanisms exposed to temperatures ranging from 600° to 2000° F or to vacuums ranging from 10^{-6} to 10^{-13} millimeter of mercury. As an example, the gimbal bearing of the rocket engine, which permits the engine to change its orientation, is exposed to both high temperatures and the vacuum of space. Environments found in space electric power generation systems include liquid alkali metals such as sodium (to 1640° F) and chemically inert gases such as argon (to 1500° F). These electric generating systems will be required to operate 1 to 3 years unattended.

Bearings, seals, and other components with rolling and/or sliding contacts must operate in these difficult environments with a high degree of reliability to preclude failure of an expensive and complex space mission. Inherent in reliability is the type of lubricating film separating surfaces in rolling and/or sliding contacts. Also of importance are the friction and wear characteristics when contacting surfaces touch under heavy overloads or at startup or shutdown.

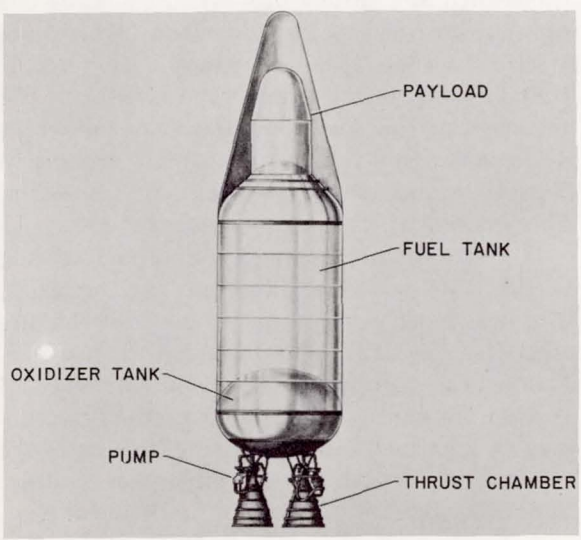

FIGURE VII–1.—Liquid-fueled rocket vehicle.

FILMS IN LUBRICATION

Hydrodynamic Films

Positive surface separation by hydrodynamic films precludes surface damage due to sliding contact. This widely used principle is illustrated in the hydrodynamic journal bearing schematic drawing (fig. VII–2). For purposes of illustration, the clearance between the journal and the bearing has been exaggerated. Typical clearances are of the order of 0.001 inch per inch of diameter. Under the action of a load W, the journal is displaced so that the bearing center and the journal center are no longer coincident. The result is a film of nonuniform thickness. As the journal rotates, fluid is dragged into the converging portion of the film because of the vis-

cosity of the fluid. As a result, the pressure in the film rises to produce the pressure pattern shown in figure VII–2. The higher the journal speed and the more viscous the fluid, the greater the pressure rise and, thus, the higher the load capacity. A fundamental characteristic of a hydrodynamic bearing is that it generates load capacity by a pumping action (drag induced flow) within the bearing clearance space.

This same principle is found in slider bearings (fig. VII–3). Relative motion of the slider parallel to the base generates pressure between the converging surfaces and produces an upward lift which can support load. Motion perpendicular to the base will also cause a pressure buildup between the surfaces, and the result is called the "squeeze" film.

Hydrostatic Films

In applications where the fluid viscosity is very low or where there is not sufficient relative motion to develop adequate load supporting pressure, hydrostatic bearings can be used. In hydrostatic bearings, the film is developed by external pump pressurization and, therefore, can be used to support surfaces having no relative motion. The film again is usually several thousandths of an inch thick. Film thickness is a function of external pump capacity, load, and surface flatness. Many fluids besides oil can be used in hydrostatic lubrication because the load capacity does not depend on fluid viscosity. A graphic

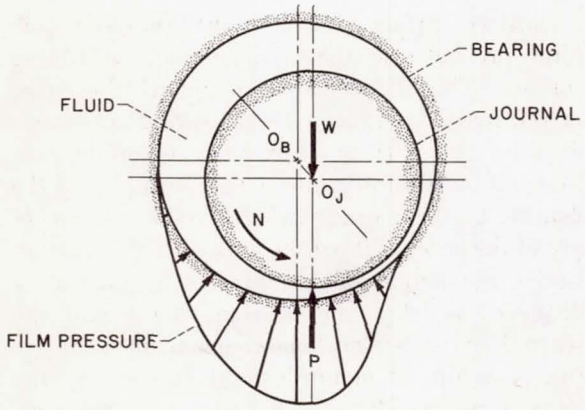

FIGURE VII–2.—Journal bearing under load.

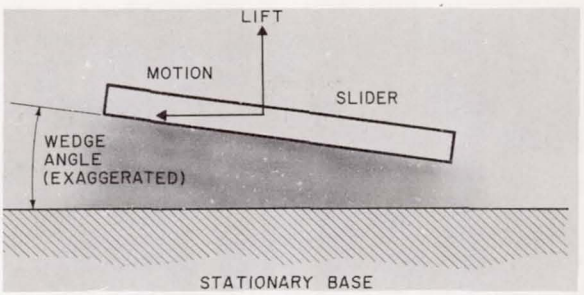

FIGURE VII–3.—Slider bearing wedge film.

example of a hydrostatic film is the 12-inch-diameter flat-plate bearing shown in figures VII–4(a) and (b). By application of lung pressure alone, 100 pounds is supported and floated freely across a flat surface.

Boundary Lubrication Films

Under normal operating conditions, hydrodynamic and hydrostatic films keep the surfaces in relative motion completely separated. At startup and shutdown or under momentary overloads, however, some contact of the sliding surfaces may occur. Under these contacting conditions, boundary-lubrication characteristics will determine the extent of surface damage.

Boundary-lubrication protection of surfaces is provided in a variety of ways. First, most oils contain so-called polar compounds which are adsorbed on surfaces to produce a microscopic boundary film of lubricant (fig. VII–5(a)). The thickness of this film is measured in millionths of an inch. Under light, momentary contact as between a journal and bearing, such adsorbed films prevent true metal-to-metal contact.

If heavy contact between journal and bearing occurs, this adsorbed film may be breached. The next layer of protection is an antiweld surface film (fig. VII–5(b)) which is a few millionths of an inch thick. This solid antiweld film is often an oxide, such as that normally occurring on a journal or bearing metal because of the presence of oxygen in our atmosphere. Other antiweld solid films are formed by chemical reaction between the bearing metals and chemical agents incorporated in the normal lubricant just

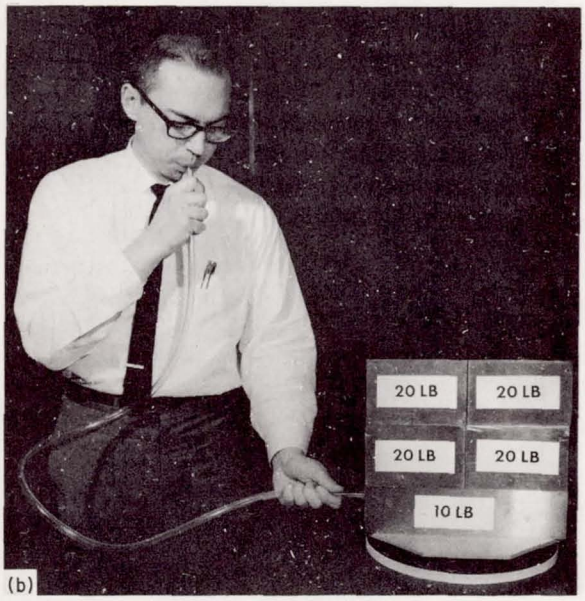

(a) Thrust bearing face showing grooving.
(b) Thrust bearing supporting load by lung pressure.

FIGURE VII–4.—Hydrostatic bearing.

for this purpose.

In the last resort, when boundary surface films can no longer provide a protective layer, contact between base metals must be expected and formation of surface welds is likely (fig. VII–5(c)). For instance, if the surfaces of the journal and bearing were absolutely clean of all films, the metal of the journal would weld to the metal of the bearing at the microscopically small contacting asperities that form the real area of contact (fig. VII–5(c)). Rotation of the shaft would tear these welds with obvious damage to the surface. High friction would result and abrasive wear particles would be created.

This cold-welding of metal surfaces can be demonstrated by sliding a clean indium surface on another clean indium surface. (Nascent indium surfaces can be produced by scraping off surface films.) The sequence in figure VII–6 demonstrates the strong adhesion and welding produced when sliding indium on indium. The weld does not break when the assembly is used as a hammer, although the force is great enough to bend the rod. This type of welding and adhesion is illustrative of that which is obtained with any clean pair of metal surfaces.

In order to prevent catastrophic surface damage, it is important to utilize materials that can experience film failure in nonlubricated rolling and sliding contact for at least short periods of time without gross surface welding. This choice of materials is particularly important to lubrication in vacuum in which many space mechanisms must operate.

Solid Lubricant Films

Solid lubricant films are widely used to provide low friction and surface protection. The thickness of these films ranges from a few millionths

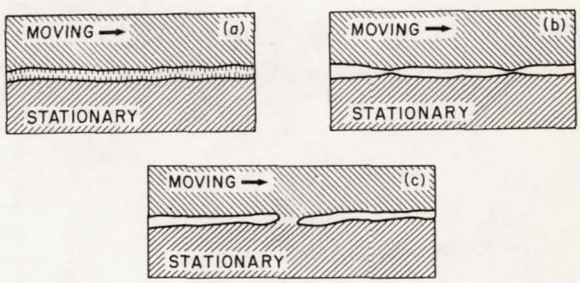

(a) Absorption films, 10 millionths inch.
(b) Oxide, reaction, or deposited films, 10 millionths inch.
(c) Weld, film failure.

FIGURE VII–5.—Boundary films.

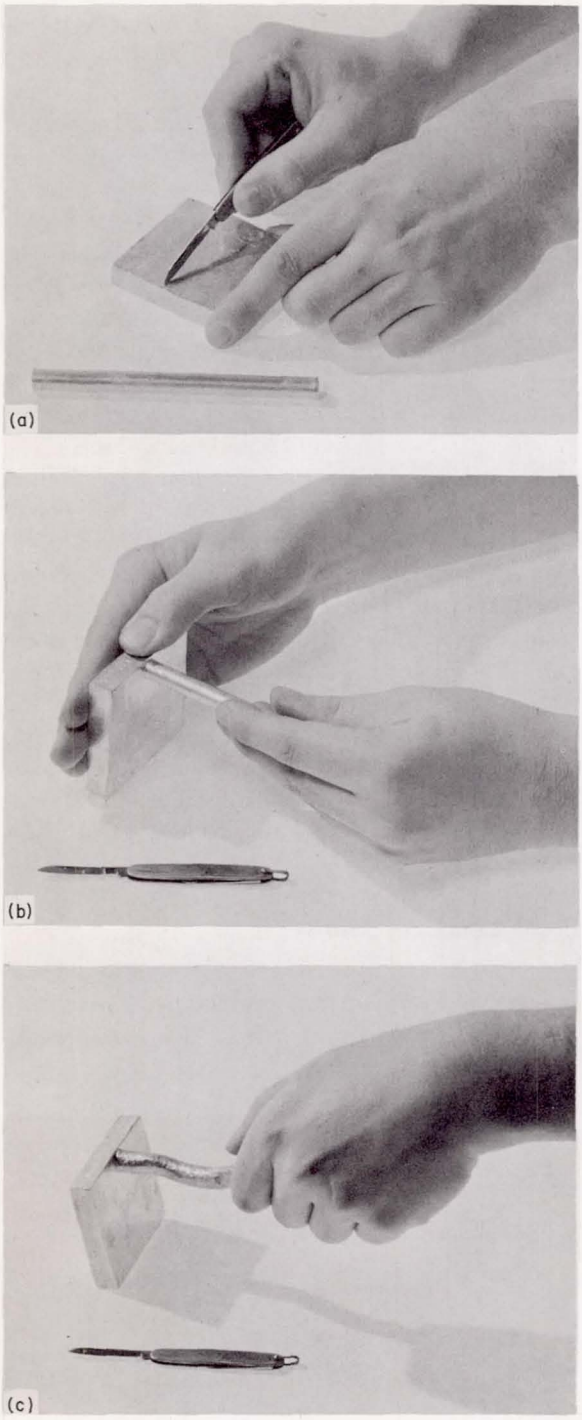

(a) Indium rod and block cleaned by scraping.
(b) Sliding indium on indium.
(c) Demonstrating force of adhesion.

FIGURE VII–6.—Cold welding of indium.

to several thousandths of an inch. Typical solid lubricant materials are molybdenum disulfide, graphite, lead oxide, and calcium fluoride. Important considerations in selecting solids for lubricants are crystal structure, adherence to surfaces, and chemical stability in the various environments. In ball bearings, the solid materials are commonly used as bonded solid films on the cage to provide transfer films to the races. Also, experience has shown that the dry powders can often be used directly. These dry powders are flowed into the bearings as smokes (suspensions of powders in gases). Further, solids are used in slurries in the same way. The liquid carrier in the slurry evaporates entirely to leave behind a fine layer of solid lubricant on the bearing surfaces.

The various temperature limits for operation with typical solid lubricants are shown in figure VII–7. At the low extremes, Teflon functions well, even at liquid-hydrogen temperatures. Molybdenum disulfide and graphitic carbons with additives are useful over the broad temperature ranges indicated. Inert environments can extend the useful temperature range of these latter two materials. The use of lead oxide is mostly intended for the temperature range of 500° to 1250° F. At the high extreme, calcium fluoride functions well at even higher temperatures than indicated and is so stable chemically that it can be used in most environments. For example, calcium fluoride was fused to a metal surface in a thin film; this surface was immersed in liquid

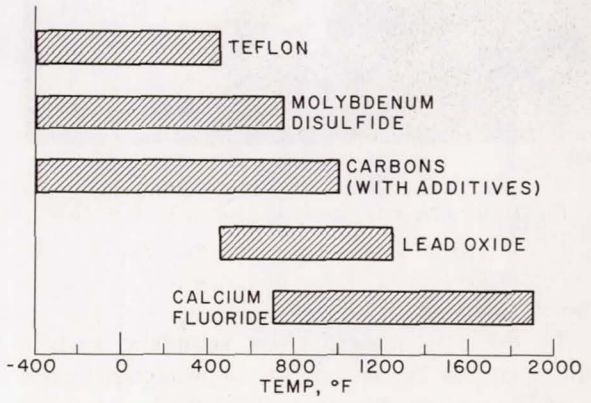

FIGURE VII–7.—Useful temperature ranges of self-lubricating materials.

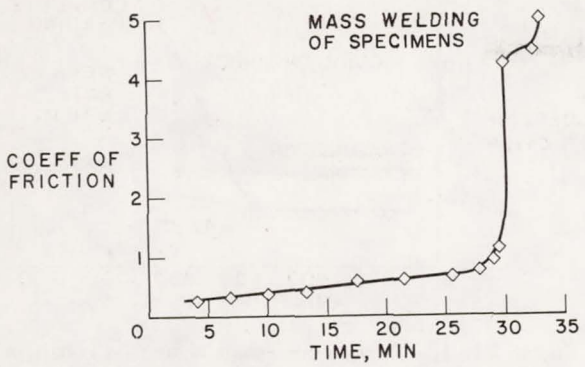

FIGURE VII–8.—Friction of SAE 52100 steel sliding on SAE 52100 steel in vacuum (10^{-7} mm Hg). Load, 1000 grams; sliding velocity, 390 feet per minute.

sodium at 1000° F to study friction and wear. These studies showed that the calcium fluoride film is capable of protecting surfaces from failure during sliding in this most difficult environment.

Vacuum Lubrication

In vacuum it is difficult to maintain the surface films needed for lubrication because lubricants evaporate and surface oxide films, which were present originally, do not reform when worn away. The types of surface failure that occur in vacuum are similar to those observed in most conventional lubrication when protective films are disrupted. As an example of the importance of the oxide film, figure VII–8 shows friction measurements made with SAE 52100 (a common bearing steel) sliding on SAE 52100 in vacuum.

As the protective oxides were worn away, friction increased and complete surface welding occurred. The friction coefficient obtained in vacuum is 10 to 100 times that normally found with metals sliding in air, and the extent of failure is greater in vacuum since complete surface welding and catastrophic surface damage occurs more readily because protective oxide films do not reform. From both a fundamental and practical standpoint, therefore, friction and wear experiments in vacuum provide a severe test of the utility of solid materials to be used in sliding contact.

Studies have shown that low friction and wear in vacuum can be achieved through the use of solid lubricants incorporated as "built-in" lubricants in the structure of cast or powder metallurgy solids. Also, recent work in vacuum lubrication indicates a marked difference, in friction and wear, between metals of the cubic and hexagonal crystal structure.

Figure VII–9 shows the atomic arrangement in typical face-centered cubic and hexagonal crystal lattices. Metals are agglomerates of crystals having these basic forms. When welding occurs between two metals, the weld may be made up of these crystals. When the crystals in the welds shear, they do so along distinct planes in the crystal and the required shear force depends on the plane being sheared. Shear forces in cubic crystals are normally greater than corresponding shear forces in hexagonal crystals. In hexagonal crystals, shear forces are usually least on the basal plane, that is, when shear occurs in a plane parallel to the hexagons. This shearing process is illustrated in figure VII–10 which shows the top hexagonal plane of the crystal displaced from the normal axis during the shear deformation process. As surfaces are moved with respect to one another, deformation, shear separation, and recrystallization occur as a continuing process.

The data in figure VII–11 show the difference in force required to shear metals of cubic and

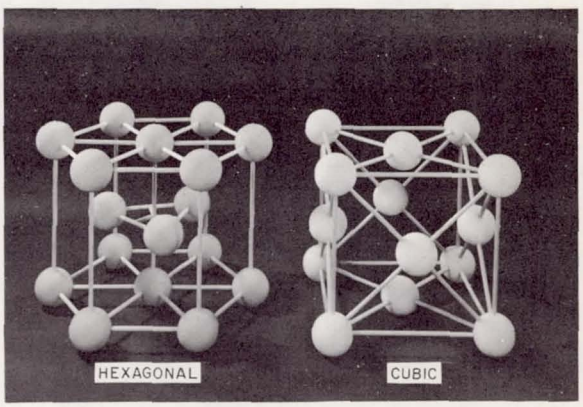

FIGURE VII–9.—Metallic crystal models.

hexagonal structures. It is known that cobalt transforms from the hexagonal to the cubic structure when heated above 750° F. A marked increase in friction is shown to accompany this crystal transformation (fig. VII–11). The transition is shown at less than 750° F because frictional heating caused the surface temperatures to be somewhat higher than the bulk metal temperatures measured. In addition, wear rate was about 100 times greater for the cubic cobalt than for the hexagonal cobalt as indicated by the two wear rates (fig. VII–11). Furthermore, at the highest temperature, complete welding of the specimens occurred. These data suggest that metals should be used in the hexagonal crystal form over the entire operating temperature range.

Additional inquiry showed that the shear force in hexagonal crystals varies with the relative spacing of the atoms in the crystal. In particular, the shear force is controlled by the ratio of the distance c, the spacing between hexagonal planes, to the distance a, the spacing between adjacent atoms in the hexagon. Various metals with hexagonal crystal structures have different values of c/a; figure VII–12 shows the variations in friction in vacuum for some of these metals. The coefficient of friction declines with increasing c/a, and those metals that showed low friction gave no evidence of gross surface welding.

Of the various metals in this study, cobalt and titanium are more commonly used and available and, hence, are of the greatest practical interest. Titanium is well known as a metal subject to surface welding or galling and otherwise having very poor friction properties. On the other hand, cobalt alloys have been used in bearings but usually in alloys with predominantly cubic structure. The preceding studies suggested that improved friction and wear properties could be obtained if cobalt and titanium were alloyed in such a way as to stabilize the hexagonal structure over greater ranges of temperatures and to increase the c/a lattice ratio.

Simple binary alloys of titanium with either tin or aluminum were found to provide the desired structural characteristics. Figure VII–13 shows friction and lattice ratio for a series of titanium-aluminum and titanium-tin alloys. Increasing the percentage of aluminum or tin produced a number of results: (1) higher c/a ratios, (2) greatly reduced friction, and (3) minimized surface failure tendencies.

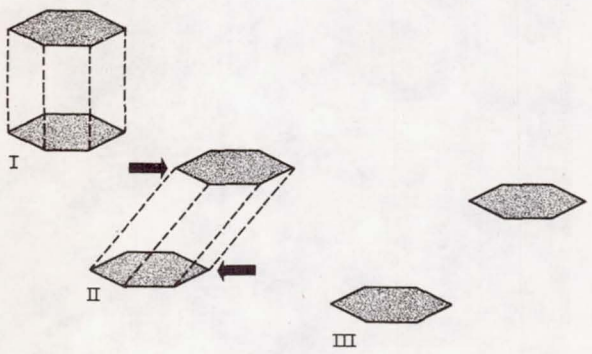

FIGURE VII–10.—Displacement of planes in hexagonal crystals with shear.

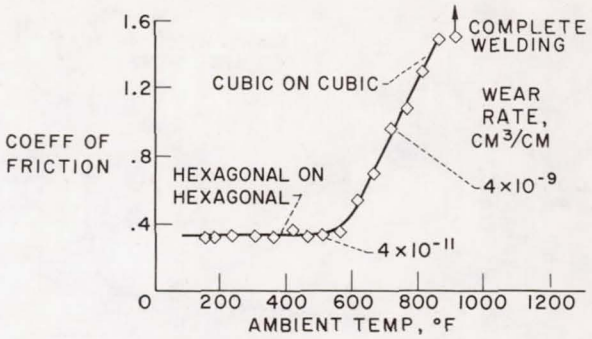

FIGURE VII–11.—Friction for cobalt sliding on cobalt in vacuum (10^{-9} mm Hg) at various temperatures. Load, 1000 grams; sliding velocity, 390 feet per minute.

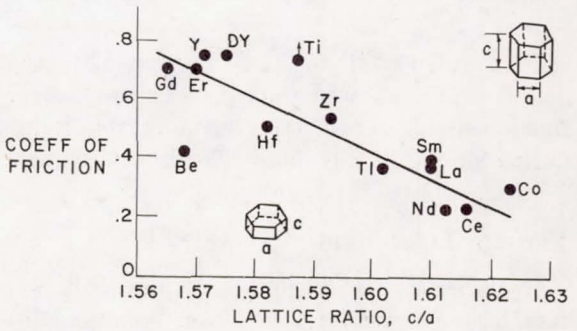

FIGURE VII–12.—Friction of various hexagonal metals on 440–C steel. Load, 1000 grams; sliding velocity, 390 feet per minute; pressure, 10^{-9} millimeter of mercury.

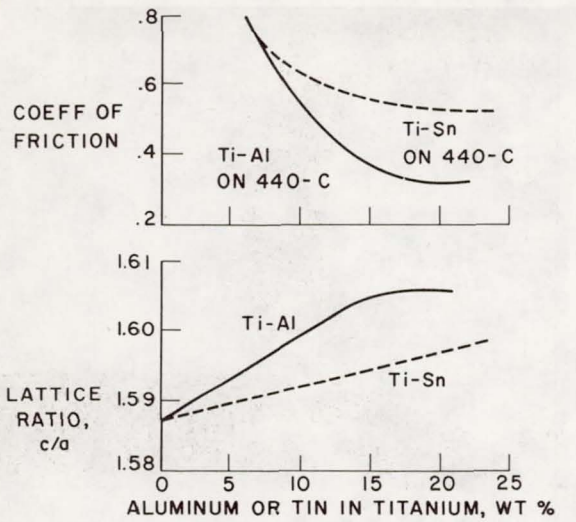

FIGURE VII–13.—Friction and lattice ratio (c/a) for titanium alloys. Load, 1000 grams; sliding velocity, 390 feet per minute; pressure, 10^{-10} millimeter of mercury.

Studies have also shown that the cobalt hexagonal form can be stabilized over greater temperature ranges by alloy additions of tungsten and molybdenum. This crystal structure stabilizing principle is potentially useful in many fields besides aerospace. As an example, in the medical field, Vitallium (a cobalt-base alloy) has been found compatible with the human body and is used in artificial human joints such as the ball and socket of the hip. NASA studies have shown a significant difference in friction and wear between the Vitallium alloy and a hexagonally stabilized cobalt-molybdenum alloy. The coefficients of friction were 0.22 for Vitallium and 0.15 for the NASA developed cobalt-molybdenum alloy. Further, the wear was much greater for the Vitallium than for the cobalt-molybdenum alloy. In this study, both alloys (Vitallium and cobalt-molybdenum) were lubricated with heptane in order to exclude oxygen and preclude formation of surface reactant films. (The synovial fluid of animal joints could not be used as the lubricant because it decomposes on contact with air.) Since the cobalt-molybdenum alloys have lower friction than Vitallium and are chemically similar, these cobalt-molybdenum alloys may provide artificial joints of improved friction and wear characteristics.

ROLLING ELEMENT BEARINGS

The ball bearing in figure VII–14 illustrates a typical rolling element bearing. The inner race is fastened to and rotates with the shaft, while the outer race is usually encased in a fixed housing. A number of balls in the annular space between the inner and the outer races are equally spaced by a cage (sometimes called a retainer or separator). In a ball bearing, the cage slides on its locating race and the balls slide in the pockets against the cage. The contact that takes place between the balls and the races is partly rolling and partly sliding. Lubrication is required at all these rolling and sliding contacts.

Rolling Element Bearing Lubrication

In contrast to the close fitting bearing and journal, a ball in a race groove has a small contact area, high contact pressure, and an extremely thin separating film—on the order of a few millionths of an inch. Basically, oil that wets the races and balls is trapped between the rolling surfaces and takes time to escape. During this time the load is distributed by the high pressures developed in the oil film between ball and race and by the elastic deformation of the ball and race surfaces. Greater viscosity increases the time for the fluid to escape and, therefore, helps to maintain a fluid film. Similarly, higher speeds result in less time for escape of the fluid from the pressure zone. The fact that extremely thin films (on the order of a few millionths of an inch in the contact areas between the balls and

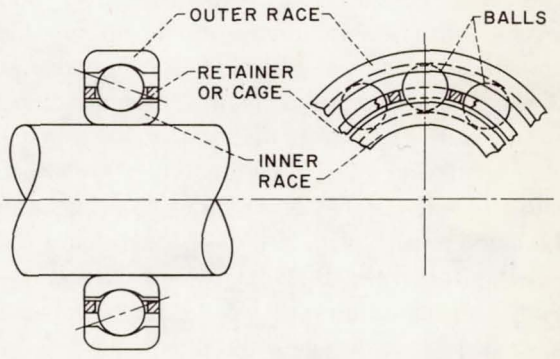

FIGURE VII–14.—Ball bearing components.

races) afford adequate surface protection is an important characteristic of rolling bearings. This means that only minuscule quantities of lubricant are required in rolling bearings provided a coolant is available to remove the frictional heat generated in the bearing.

Lubrication at low temperatures.—At the temperature extremes found in aerospace applications, normal lubricants cannot be used. For example, bearings for pumps operating at liquid hydrogen temperature (−423° F) cannot be lubricated with normal liquid lubricants because this temperature is far below their pour point and oils and greases become brittle solids.

Liquid-hydrogen lubricated journal bearings cannot be used because the fluid viscosity is too low to generate the required load capacity (e.g., the viscosity of liquid hydrogen is one ten-thousandth that of an ordinary lubricant at 100° F.) Further, the hydrogen reduces protective surface oxides which results in catastrophic surface welding when contact occurs.

The alternative is to use rolling element bearings that contain a solid lubricant to provide the lubricating function. Liquid hydrogen is a good coolant; therefore, it can be used effectively to remove the frictional heat generated in the bearing, but a solid lubricant is still required. Rolling element bearings are a natural for such an application because they require only minuscule amounts of lubricant. One of the solid lubricants that has been found to work well in rolling bearings is Teflon. In bearings for operation in liquid hydrogen, the standard cage is replaced by a Teflon cage shown in figure VII–15. This cage is reinforced with glass fiber and covered with an aluminum shroud to provide strength and stiffness. Lubrication is provided at all the rolling and sliding points either by direct contact with the Teflon material or by transfer films of Teflon. The films of Teflon are wiped onto the balls as they rub against the cage, and the balls, in turn, wipe a film of Teflon onto the races as they roll. Boundary lubricating transfer films ranging upward from a few millionths of an inch thick develop from plastic flow of the lubricating solid (Teflon) into the imperfections

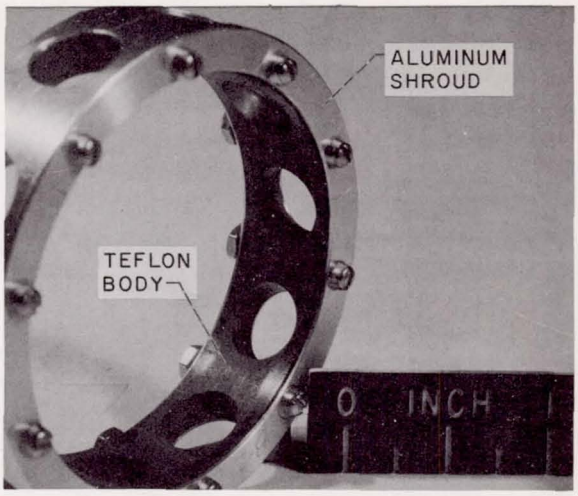

FIGURE VII–15.—Teflon—glass fiber reinforced cage.

of the mating surface. These films adhere by simple mechanical bonding.

In cryogenic turbopump machinery, which rotates at very high speed, the life of Teflon lubricated bearings is of the order of 10 hours, which far exceeds the required life of rocket engine turbopump bearings.

Lubrication at high temperatures.—There are many practical applications where lubrication is required at temperatures from 600° to 2000° F. This temperature range is above the limits for ordinary liquid lubricants in conventional systems. There are two modes of high-temperature degradation if liquid lubricants, namely, oxidation and thermal decomposition. If the lubricant system can be inerted so that the available oxygen is decreased, the oxidation of the lubricant is less and the temperature limit may be greater. Also, synthetic lubricants with improved thermal stability are available. For the upper end of the high temperature range, however, we must look to materials of even greater thermal stability, such as solids.

Studies have shown that solid films of lead oxide (PbO) are effective lubricants to 1250° F. The sequence in figure VII–16 shows a ball bearing before test and after test at 1250° F. The bearing cage was coated, prior to test, with lead oxide ceramic bonded coating (fig. VII–16 (a)). After test at 5000 rpm, disassembly re-

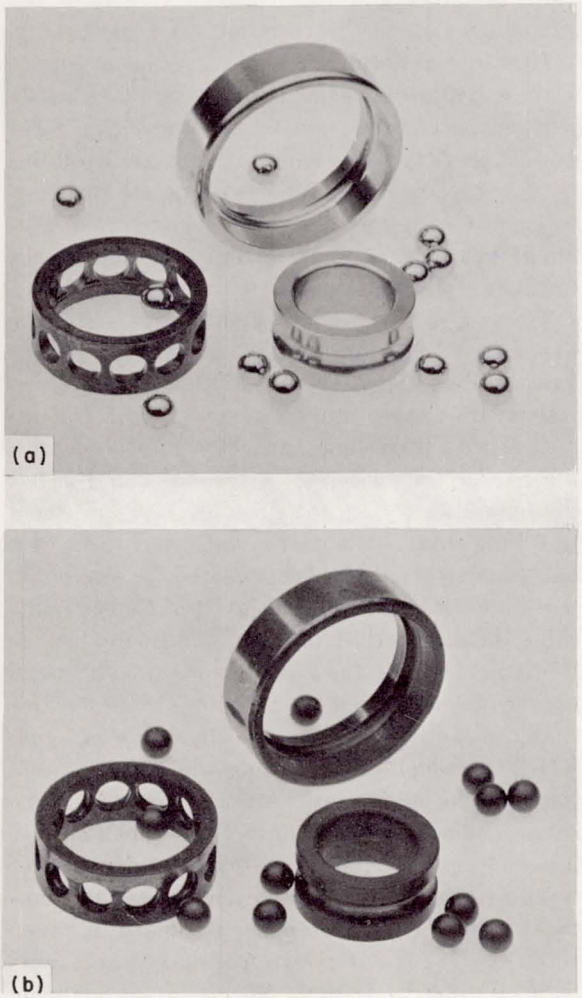

(a) Before test.
(b) After test (to 1250° F).

FIGURE VII–16.—Ball bearing with lead oxide coated cage.

vealed little or no wear to any of the bearing parts and the ball and races were highly polished (fig. VII–16(b)). This indicates that transfer films have been established on the balls as a result of the wiping action against the cage. Ball bearings with lead oxide coated cages have been run at 1250° F at speeds from 6000 to 23 000 rpm for time periods over 65 hours without failure.

Fatigue in Rolling Element Bearings

The failure mechanism of rolling element bearings operating at either of the temperature extremes discussed is primarily one of wear. That is, wear takes place because of film failure. Provided that the protective film between the wearing surfaces can be maintained in a rolling element bearing, fatigue becomes the primary mode of failure rather than wear.

Fatigue, also known as "spalling" or "flaking" occurs when a part is subjected to fluctuating loads until the part breaks. In a rolling contact bearing, these fluctuating loads appear on the races as each succeeding ball passes over a given point on the race. The load from each ball creates a high stress in the material and eventually a crack forms at the weakest point under stress. This crack spreads with successive load applications until a piece of material breaks off; this is called a fatigue spall. A typical fatigue spall is shown in figure VII–17. A piece of material, roughly circular in shape and limited in depth, has fallen out of the race groove.

Research on fatigue has shown that many fatigue cracks originate at hard inclusions or foreign particles in the zone where stresses are most damaging. This zone is a few thousandths of an inch below the surface so that fatigue cracks usually originate subsurface. Figure VII–18 shows a typical subsurface inclusion at which a fatigue crack has started. The inclusion is located in a region where stresses are high—

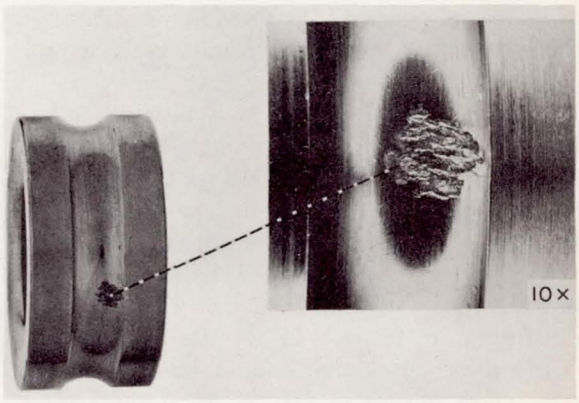

FIGURE VII–17.—Typical fatigue spall.

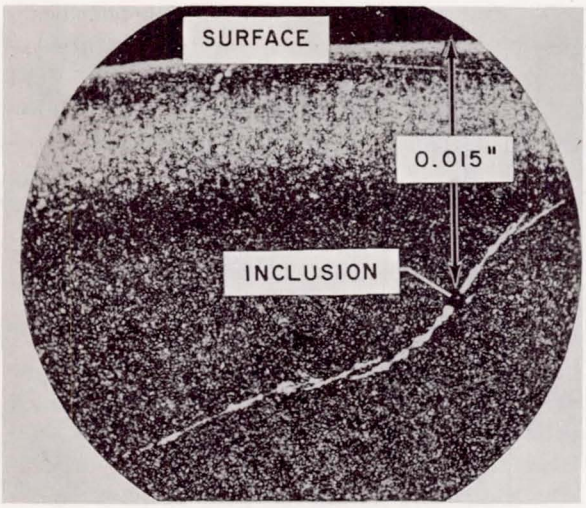

FIGURE VII–18.—Fatigue crack originating at an inclusion.

about 0.015 inch below the surface. Although this is considered to be a large inclusion, the inclusion itself is quite small—about 0.0005 inch in diameter. Even in the absence of an inclusion, fatigue will ultimately occur. The worst combination is to have an inclusion located at the point of maximum stress.

One method by which the fatigue life of bearings can be increased is by avoiding inclusions in the bearing materials. These materials are complex alloys containing several metals and carbon. Ordinarily, when the alloy is in the molten state during formation, some of the alloying elements react with oxygen in the atmosphere to form hard oxides. To avoid this type of inclusion, bearing alloys are now prepared by the consumable electrode vacuum melting process.

A second method by which bearing fatigue life can be improved is through better manufacturing. Whenever a material is shaped by rolling, forging, or extrusion, the metal grains take on a string-like pattern, resembling fibers, thus, the term fiber flow. The fiber flow in a bearing race that has been cut from tubing is illustrated in figure VII–19. Research at the NASA Lewis Research Center has shown that metals are weaker in fatigue when the ends of the fibers are exposed at the stressed surface than when the fibers are parallel to the surface. Note the fiber ends, which are exposed to the stressed region in the race cut from the tubing.

If a special forging technique is used, a race with essentially parallel fibers in the highly stressed ball groove can be produced (fig. VII–19). Experience has shown that significant increases in bearing fatigue life can be obtained when care with fiber orientation is exercised. Premium bearings are now made with due regard for fiber orientation.

Turning to another aspect of fatigue life, the Lewis Research Center and the bearing industry have studied the effect of material hardness on fatigue life; these studies revealed that life increases with increasing hardness. In other words, the harder the material of the balls and races, the longer its rolling fatigue life. It would seem to follow from this that the balls and races of a ball bearing should be heat-treated for maximum hardness. Recent research at this Center indicates, however, that maximum bearing fatigue life is achieved if the balls are made two points harder (as measured on the Rockwell-C scale) than the races. These results are shown in figure VII–20 in which relative life is plotted as a function of the difference in hardness ΔH. The shaded band represents data from bench studies in a five-ball fatigue rig tester; the curve represents data from full-scale bearing tests. It is apparent that fatigue life can be reduced as much as 80 percent if ΔH between the balls and races is much different from 2. Normal manufacturing variation is as much as ± 3 points on the races

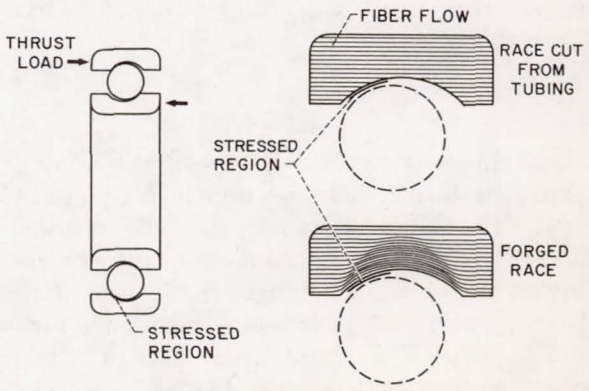

FIGURE VII–19.—Fiber flow in bearing races.

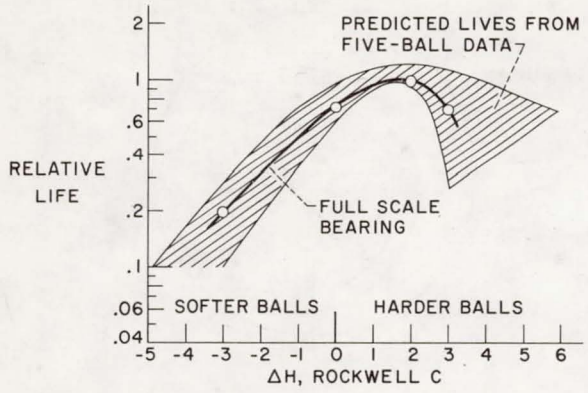

FIGURE VII–20.—Relative bearing life as function of hardness difference between balls and race, ΔH.

and ± 2 points on the balls or rollers. With such hardness variations, no improvements in fatigue life would be expected by specifying ΔH. This illustrates the importance of specifying not only the proper ΔH but of closely controlling component hardnesses so that the desired ΔH is *actually* achieved. This may require more careful manufacturing control and selection of matched sets of balls and races.

Ordinarily, a plot of bearing fatigue life for a batch of identical bearings shows considerable scatter as illustrated in figure VII–21. The plot shows the percent of bearings failed as a function of time to failure (bearing life measured in inner race revolutions) for a set of bearings having a $\Delta H \approx 0$ and for bearings having a $\Delta H \approx 2$. As illustrated, the bearings having a $\Delta H \approx 2$ not only show better fatigue life, but the greatest life increase is obtained in the early failure region. This improvement is extremely important in aerospace applications since the prime interest is in avoidance of early failures.

Another factor which affects bearing fatigue life is lubricant type and rheology. Lubricants form elastohydrodynamic films during bearing operation. These films affect the stress distribution on the races and balls as illustrated in figure VII–22. In essence, the lubricant film reduces the maximum stress from that calculated for a dry static contact. A plot of stress against life is shown. As illustrated, a reduction as small as 10 percent in stress can mean more than a two-fold increase in fatigue life. In general, bearings run with higher viscosity fluids produce the highest fatigue lives. Additionally, bearings run with lubricant base stocks exhibiting high increases in viscosity under increased pressure will also give high fatigue lives.

To sum up the fatigue discussion, a number of techniques have been devised to improve bearing fatigue life. These include the following:

(1) Avoidance of material inclusions through vacuum melting

(2) Better material fiber orientation by means of new forging techniques

(3) Higher material hardnesses

(4) Proper control of bearing component hardnesses such that $\Delta H = 2$

(5) Selection of lubricants having high viscosities and high increases in viscosity at increased pressure

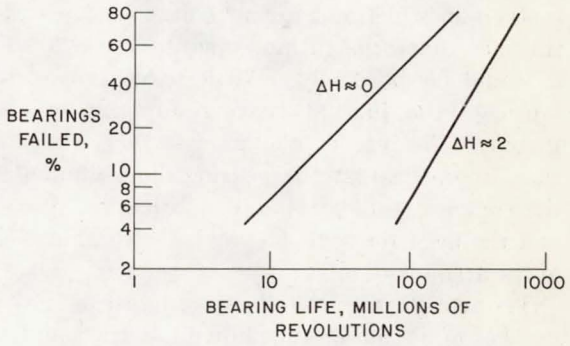

FIGURE VII–21.—Effect of hardness difference between balls and race, ΔH, on bearing fatigue scatter.

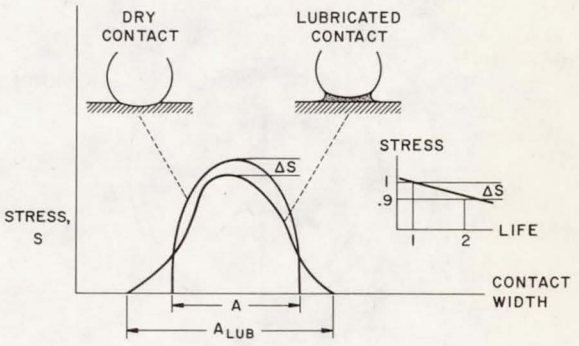

FIGURE VII–22.—Effect of lubricant film on stress distribution and fatigue life.

Utilization of all these techniques in the manufacture of rolling bearings and proper lubricant selection should result in a bearing life of at least 10 times greater than that of a decade ago.

GAS BEARINGS

In spite of all the advances made in solid lubricants, protective films, and improved bearing materials for use in difficult environments, bearings that operate in solid contact between running parts have limited life. This limited life is suitable for many machines, but when extra long bearing life at high temperature is required, fluid film bearings must be used. Fluid film bearings, such as a journal bearing, can utilize a gas as well as a liquid as the lubricant to provide a film of separation between the shaft and the bearing.

One space related application for gas bearings appears in turbogenerator electric power systems in which hot argon is used to drive the turbine. Since the turbine operates at 1700° F, it would be extremely difficult to use an oil to lubricate the journal bearing adjacent to the turbine. The use of the process fluid (in this case, argon gas) as the bearing fluid eliminates the complexity of a separate lubrication system and the need for seals to prevent contamination of the argon with oil.

The use of gas as the bearing lubricant has a number of advantages including low friction, low noise, cleanliness, and tolerance to radioactivity.

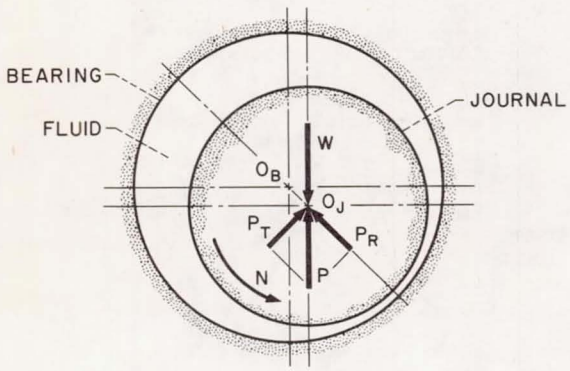

FIGURE VII–23.—Fluid film force components of journal bearing.

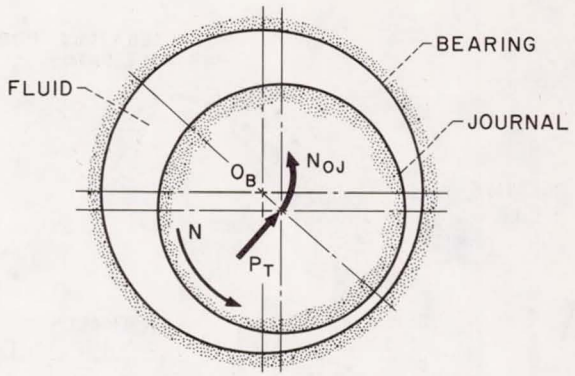

FIGURE VII–24.—Whirl instability due to unbalanced film force.

A disadvantage of gases is that they have low viscosities, which result in low bearing load capacity. In space applications, however, low load capacity is not the major problem. The major problem with gas bearings in space power systems arises from the fact that these machines must operate in the zero-gravity environment of space. Hence, the bearings are under extremely light loads since the bearings do not support the weight of the rotating machinery. Gas bearings which operate at high speeds and very light loads are subject to a severe form of mechanical instability known as half-frequency whirl. This instability can destroy the bearing.

As shown in figure VII–2, when a load is applied to the journal, the journal center does not move in the direction of the applied load. This characteristic of journal bearings is related to the development of half-frequency whirl. The film pressure force P (which is equal and opposite to the load W) is shown divided into two components in figure VII–23. One component P_R along the line of centers passes through the bearing center O_b, while the component P_T perpendicular to the line of centers has a moment about the bearing center O_b. Under steady-state conditions both P_T and P_R are balanced by components of W so that equilibrium is maintained.

Suppose that the bearing is running under a very light load W and the load is suddenly removed. An unstable condition may arise if there is no force to completely balance P_T as illustrated in figure VII–24. The journal center O_j will

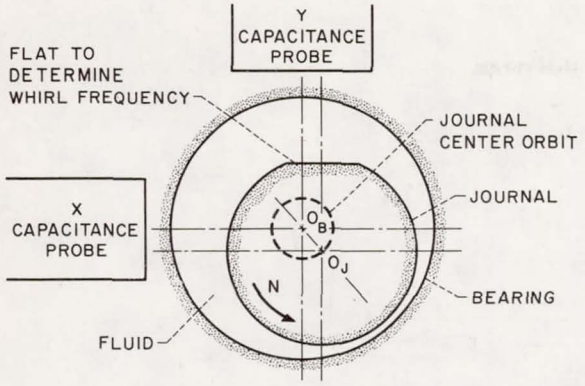

FIGURE VII–25.—Instrumentation for studying bearing whirl.

start to orbit about the bearing center O_b. As the orbital frequency N_{oj} increases, the tendency is to increase the amplitude of the orbit unless there is enough viscous damping present in the film. In gases this is often not true and the instability grows in amplitude until a catastrophic failure occurs.

The frequency of self-excited whirl N_{oj} is about one-half the rotational frequency N of the journal about its own center. Therefore, instabilities excited by the film are easily differentiated from the common synchronous whirl or shaft whipping caused by shaft unbalance.

A rotor supported on two gas-lubricated journal bearings was used to study and observe fluid film whirl. Instrumentation which detects shaft position as a function of time was employed. Two capacitance probes, located 90° to each other, are used in conjunction with an oscilloscope to display the shape of the orbit described by the journal center. The setup is illustrated in figure VII–25. Shown are the two probes, the bearing inside surface, the journal surface, and the flat on the journal which is used to determine the whirl frequency. Each time the flat on the journal passes a probe it produces a blip on the oscilloscope screen. If the bearing operates stably with a perfectly balanced rotor, we merely see a dot on the oscilloscope screen. There is always some unbalance in a rotor, however, which produces a small rotating load on the bearings. In response to the unbalance load, the journal center describes a circle of small amplitude, which is seldom harmful to the bearing. This is the small circle shown in figure VII–26(a) which represents the journal center motion when the rotor speed was 22 000 rpm. When the bearing becomes unstable, the amplitude of journal center motion continually increases until the journal rubs against the bearing. This mode of operation would result in bearing failure if allowed to continue. The journal center motion under these conditions is indicated in figure VII–26(b). This half-frequency whirl occurred at 56 000 rpm.

While this discussion has been concerned with machinery operating under zero gravity, the trend in ground-based machinery is also toward conditions leading to instability. This trend is toward smaller, more compact high-speed ma-

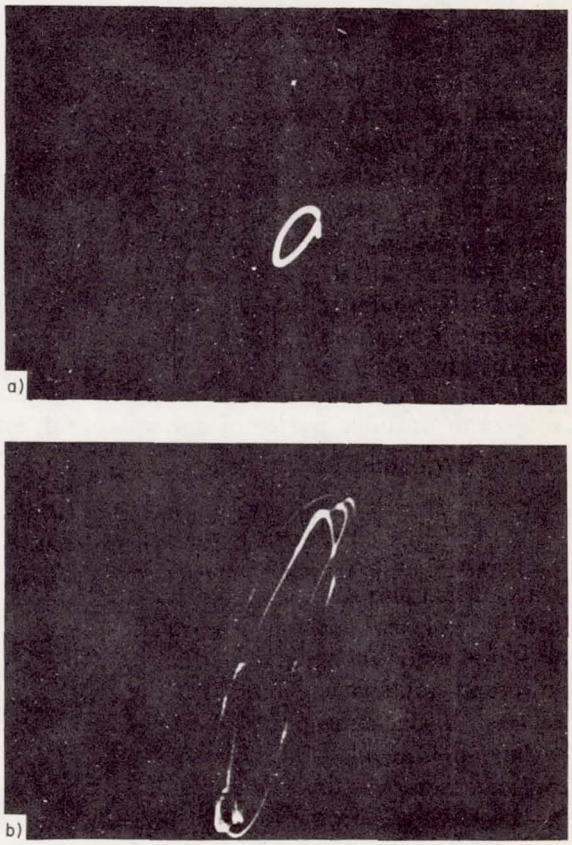

(a) Stable operation, 22 000 rpm.
(b) Half-frequency whirl, 56 000 rpm.

FIGURE VII–26.—Gas bearing journal center motion.

chines in which the bearings must operate under conditions of very light loads and high speed.

Since the instability problem arises because of light external loads, the solution to this problem involves bearing designs which apply loads *internally*. Figure VII–27 shows a bearing design which applies load internally. This bearing utilizes four shoes, each free to pivot. When the journal is running in the center of the bearing, a wedge-shaped film exists between each shoe and the journal, similar to that in an ordinary journal bearing under high load. Each shoe thus exerts a force on the journal to keep it centered. In this way bearing whirl is avoided.

Present-day gas-bearing technology is at the point where gas bearings are finding use in a rapidly expanding variety of commercial machines. These include air blowers and gas compressors (ranging from fractional horsepower to several hundred horsepower), turboexpanders, high-speed grinding spindles, alternating-current motors and converters, gyros, and medical diagnostic instruments such as the ballistic cardiogram. A home refrigerator, which can be floated on a hydrostatic air bearing supplied with air from the discharge of a vacuum cleaner, is also available.

To summarize, fluid film bearings utilizing the process fluid can be used to advantage in many types of machinery with a resulting significant reduction in design complexity. Bearings that operate at high speeds under light loads are subject to unstable modes of operation that can result in their destruction unless careful design procedures are used to eliminate bearing instabilities.

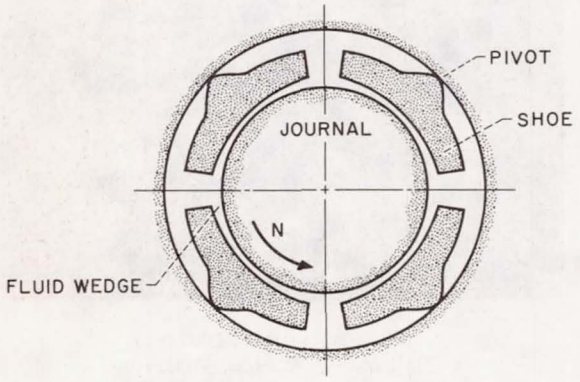

FIGURE VII–27.—Pivoted shoe bearing, preloaded.

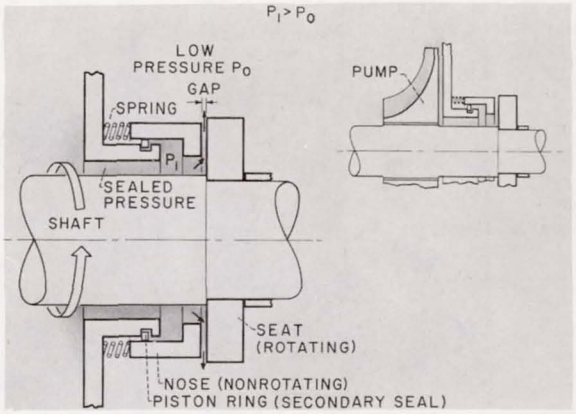

FIGURE VII–28.—Face contact seal.

FACE CONTACT SEALS

Often the rotating machinery, like the pumps for which bearings are provided, contain process fluids at pressures different from the surrounding space. Examples of such process fluids are cryogenic liquids, liquid metals, hot and cold gases, and lubricating oils. Intolerable leakage of the process fluid along the drive shaft is avoided by means of dynamic seals on the shaft.

Face contact seals, which are most commonly in use today, exist in a variety of forms, but most have the essential arrangement shown in figure VII–28. The sketch in the upper right corner shows the location of a seal on a pump shaft sealing pump outlet pressure P_1. The seal consists of two main parts—a seal seat which is fixed to the shaft and rotates with it, and a nosepiece flexibly attached to the stationary shaft housing. A piston ring secondary seal permits axial movement of the nosepiece. A sealing dam is formed by the nonrotating nosepiece which is held, by a force from the spring and the sealed fluid pressure, in rubbing contact or close proximity to the rotating seal seat. The sealing gap is shown exaggerated, and leakage is outward to the surrounding low pressure P_o. (The main seal components are also shown in figure VII–29.)

Sealing Gap

The sealing gap is the wearing surface, and the success of the seal is determined largely by what occurs at this gap. For most applications, the gap is very small, 10 to 500 millionths of an inch; for comparison, journal bearings previously discussed have film thicknesses of 500 millionths and greater.

Leakage rate through the gap is very largely dependent on sealing gap height; if the sealing gap increases by a factor of 10, say from 10 to 100 millionths of an inch, the leakage increases by a factor of 1000. Even with positive face separation, however, the leakage can be very low providing the gap is small. For instance, for water at 100 pounds per square inch and a sealing gap of 10 millionths, the leakage would be less than 10 pounds per year for a 3-inch-diameter face seal. The fact that the sealing gap is very small means that small variations and distortions in the sealing faces become significant.

Seal wear occurs when the nosepiece rubs on the seal seat. For long seal life, the seal must necessarily have positive face separation, which is maintained by the pressure in the fluid leaking across the face. Contact between the nosepiece and seat occurs only during start and stop, or during brief periods of severe overloads. Positive face separation with acceptable leakage is inherently tied to balance of hydraulic forces acting on the seal nosepiece.

Pressure Balancing

Pressure balancing is illustrated in figure VII–30, which shows the forces acting on a cylindrical nosepiece. The sealed pressure force on the nosepiece is represented by the rectangular area; the gap pressure force is represented by the triangular area, since the pressure decreases linearly across the gap from inside to outside. If the secondary seal piston ring is placed on the nosepiece outer diameter (fig. VII–30(a)), the sealed pressure force behind the nosepiece exceeds the gap pressure force and the nosepiece is forced against the seal seat. This is a pressure-loaded seal and has high face loads that can produce high wear rates. If the piston ring is located at the inner diameter (fig. VII–30(b)), the sealed pressure no longer acts behind the nosepiece. Therefore, the gap pressure opens the seal. This seal is pressure unloaded and, of course, leakage is very high. However, a diameter can be selected for the piston ring (as shown in fig. VII–31) such that sealed pressure force behind the nosepiece exactly balances the gap pressure force. This is a 100-percent pressure balanced seal, and only light spring loads hold the nosepiece in position.

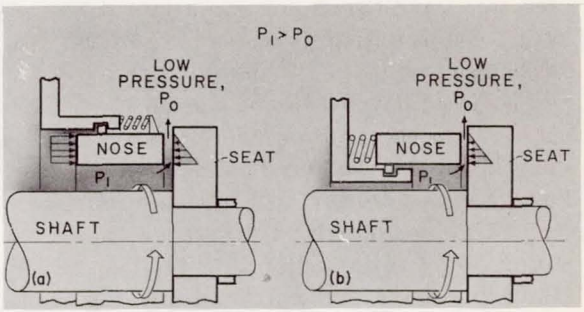

(a) Pressure loaded. (b) Pressure unloaded.

FIGURE VII–30.—Unbalanced face contact seals.

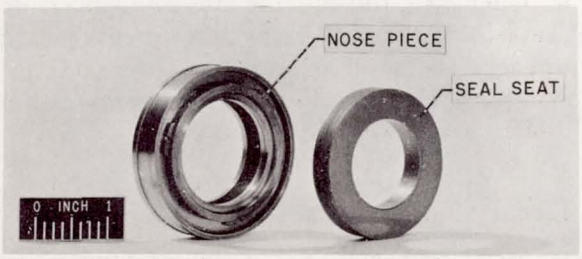

FIGURE VII–29.—Face contact seal components.

Compensating Pressure

Positive gap control is obtained by having the sealing gap perform as a hydrostatic thrust bearing. As shown in figure VII–32, the seal design is similar to figure VII–31 except that a recess and a series of orifices have been added to the nosepiece face. Some of the leakage through the seal takes place through the orifices arranged circumferentially around the seal. The

leakage flow through the orifices produces a pressure drop from sealed pressure P_1 to the recess pressure P' and the sealing gap height is controlled by compensation in recess pressure P'. The mechanism works in the following way: If the gap is closed down for some reason, the leakage out is reduced, that is, the pressure drop in the orifice is low because of leakage flow; therefore, recess pressure P' will increase, approaching sealed pressure P_1, and produce a net restoring force to maintain design gap height. Similarly, if the gap opens beyond the design point, the inverse process takes place. In effect, the gap is maintained by automatic compensation in the recess pressure P'. The designer can select the operating seal gap height through proper selection of the recess and orifice sizes.

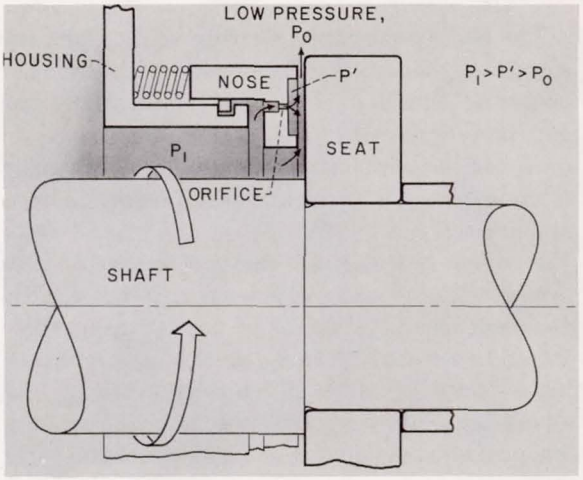

FIGURE VII–32.—Pressure compensated seal.

Wear Effects

Using the smallest closing loads that can maintain thin film separation in a seal is important. When contact occurs, wear and wear particle size increase with load. The wear particles can easily be larger than the normal sealing gap. Thus, wear particles between the surfaces can increase the thickness of the leakage gap. Ironically, if, in an attempt to reduce leakage, the spring force is raised, an increase is obtained in both wear and wear particle size; hence, leakage will be increased.

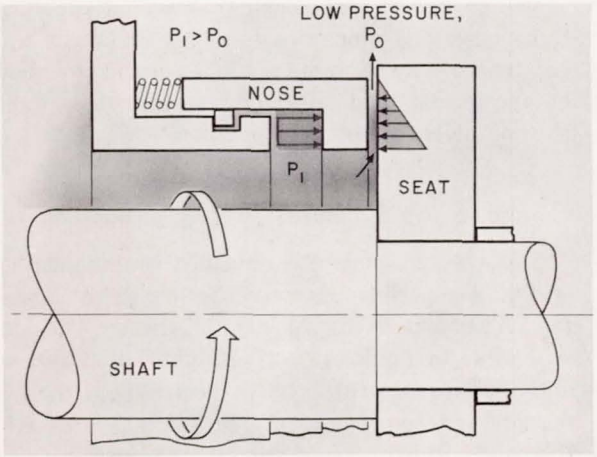

FIGURE VII–31.—Pressure balanced contact seal.

Vibration Effects

Nosepiece vibration also causes sealing gap variations. The gap changes can be very rapid and nonuniform around the circumference. Studies have shown that the predominate motion was a "rocking" of the seal nosepiece and that the forces due to rocking were very high. As an example, figure VII–33 shows the wear pattern of a seal nosepiece which was run in liquid nitrogen for 38 minutes at 10 000 rpm. The nosepiece profile before and after test is shown with the horizontal scale enlarged. Wear of 0.004 inch has occurred in the 38 minutes of operation. Of interest here is the cone-shaped wear at the outer edge, which is due to the rocking-type vibration. While most of the wear is on the outer edge, the vibration impacts have caused some chipping from the inner edge also. This wear is intolerable. This damaging vibration can be eliminated through the use of dampers in contact with the nosepiece outer diameter and through the use of improved nosepiece friction materials which do not excite the vibrations when rubbing occurs with the seal seat.

Liquid Fluorine Seals

Special problems arise when the fluid to be sealed is very corrosive. Recently, a shaft seal

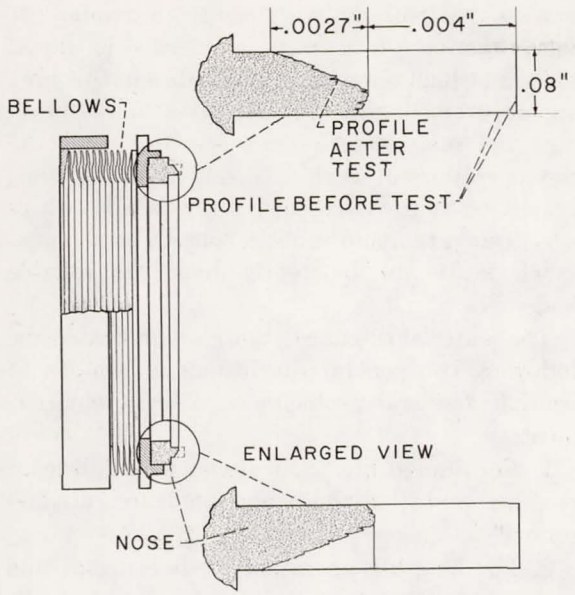

FIGURE VII–33.—Nose-piece wear due to seal vibration.

for a liquid fluorine centrifugal pump was required. Fluorine is one of the most corrosive of known chemicals. Early seals for fluorine pumps used carbon nosepieces, which had been used successfully in liquid oxygen. Attempts to run these seals resulted in pump failure and severe fires, which were traced to fluorine reaction with the nosepiece carbon of the seal.

Since fluorine was, obviously, too active chemically for the safe use of carbon materials in seals, attention was turned to selection of materials such as metal fluorides which are compatible with fluorine. Frictional qualities of these materials were checked running together in liquid fluorine. These experiments showed that nickel fluoride appeared to have promise for providing a protective layer with low friction. Accordingly, a nickel-bonded titanium carbide cermet that would form nickel fluoride reaction films was studied in friction and wear experiments in liquid fluorine. Data from those experiments in oxygen and fluorine (fig. VII–34) gives a comparison of two potentially useful material combinations. The graphitic carbon material, which was not run in fluorine, is one of the best materials for use in liquid oxygen and is given as a standard for comparison. The nickel-bonded carbide on aluminum oxide had better performance than aluminum oxide on itself. Further, the nickel-bonded carbide in fluorine had friction and wear properties comparable with the carbon in oxygen.

These friction and wear studies led to the selection of aluminum oxide for the nosepiece, and nickel-bonded titanium carbide for the seal seat. Evaluation of this combination in liquid fluorine in the subsequent seal studies confirmed the lubricating mechanism suggested from the friction experiments. This lubricating mechanism is illustrated in figure VII–35, which shows the seal schematically. The fluorine reacts with the nickel binder to form a low shear-strength nickel fluoride film illustrated in the enlarged view (fig. VII–35). This film is an impervious coating that limits the extent of fluorine reaction and provides both low friction and wear. If the film is ruptured, it is quickly repaired by fluorine reaction with the nickel. To date, the Lewis Center has completed over 20 pump tests using the aluminum oxide and nickel-bonded titanium carbide type seal materials, and a contractor has completed an additional 13 rocket engine tests using pumps with these seals. Performance has been very good, and the total time accumulated in these pump tests is over 40 000 seconds,

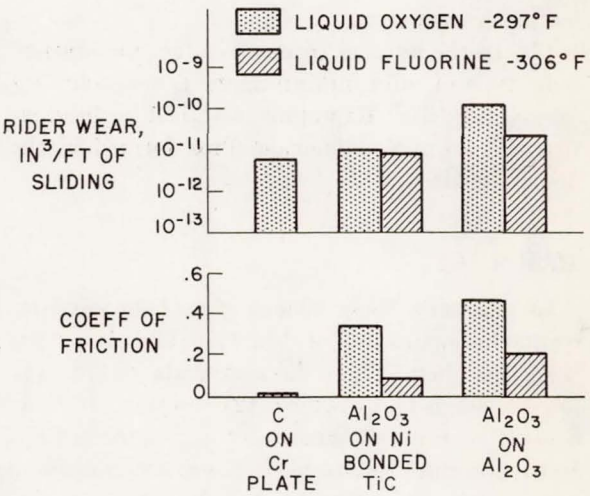

FIGURE VII–34.—Friction and wear of potential seal materials. Sliding velocity, 2300 feet per minute; load, 1000 grams.

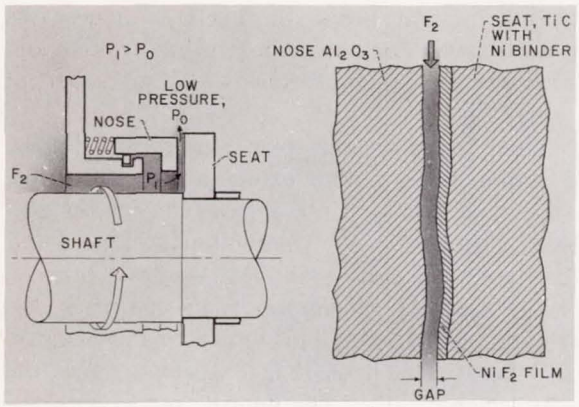

FIGURE VII–35.—Liquid fluorine seal.

which for rocket application is an appreciable amount of experience. The average running time of the NASA pumps far exceeded the normal firing time of the rocket engine.

The importance of the sealing gap geometry and lubrication in seal design has been emphasized. The points which should be noted are

(1) Positive face separation is desirable for long life applications; this is achieved by hydrostatic forces and hydrodynamic forces.

(2) Since the seal gap is very small, radical changes in seal balance can be induced by slight thermal gradients, pressure distortions, or manufacturing variations.

(3) In the absence of positive face separation, some type of solid film lubricant is necessary for satisfactory life. Examples of solid film lubrication are the nickel fluoride films formed in the fluorine seals.

SUMMARY

In summary, the influence of extreme environments on operation of bearings and seals has been described. These environments include (1) low and high temperature, (2) vacuum, and (3) contact with fluids chemically active toward the bearing and seal materials. There are additional areas and environments, which were not discussed, but which are of equal importance. Some of these are (1) the nuclear radiation effects (both neutron and gamma) on the lubrication process, particularly with solid lubricants, (2) the operation of bearings and seals in liquid sodium at high temperatures (studies in this area appear promising in that operation of the bearings and seals were quite successful), and (3) the operation of seals utilizing hydrodynamic principles (e.g., viscoseals, screw seals) where it is desired to avoid rubbing contact at all times (such seals are inherently long-life, reliable seals).

The material discussed, however, indicated the following two general conclusions as applied to bearing and seal problems in difficult environments:

1. For limited life applications, solid lubricant coatings and "built-in" lubricants are satisfactory.

2. For long-life operation, both bearings and seals require that their load-carrying surfaces be completely separated by fluid films. Such films can be generated, even by low viscosity fluids, provided loads are light, speeds are high, or hydrostatic pressures are available.

BIBLIOGRAPHY

General

BISSON, EDMOND E.; AND ANDERSON, WILLIAM J.: Advanced Bearing Technology. NASA SP–38, 1964.

BONDI, ARNOLD A.: Physical Chemistry of Lubricating Oils. Reinhold Publishing Corp., 1951.

BOWDEN, F. P.; AND TABOR, D.: The Friction and Lubrication of Solids. Clarendon Press (Oxford). Part I, 1950, Part II, 1964.

RABINOWICZ, ERNEST: Friction and Wear of Materials. John Wiley & Sons, Inc., 1965.

SHAW, MILTON C.; AND MACKS, E. FRED: Analysis and Lubrication of Bearings. McGraw-Hill Book Co., Inc., 1949.

WILCOCK, DONALD F.; AND BOOSER, E. RICHARD: Bearing Design and Application. McGraw-Hill Book Co., Inc., 1957.

Boundary and Solid-Film Lubrication

BUCKLEY, DONALD H.; AND JOHNSON, ROBERT L.: Effect of Inert, Reducing, and Oxidizing Atmospheres on Friction and Wear of Metals to 1000° F. NASA TN D–1103, 1961.

BUCKLEY, DONALD H.; JOHNSON, ROBERT L.; AND BRAINARD, WILLIAM A.: Influence of Entrained Gases and a Halogen Additive on Boundary Lubrication of Four Oils at Temperatures to 1000° F. NASA TN D-2686, 1965.

HADY, WILLIAM F.; ALLEN, GORDON, P.; AND JOHNSON, ROBERT L.: Wear and Friction of Mechanical Carbons in Liquid Oxygen as Influenced by Transfer Films. ASLE Trans., vol. 6, no. 3, July 1963, pp. 201–208.

JOHNSON, ROBERT L.; GODFREY, DOUGLAS; AND BISSON, EDMOND E.: Friction of Solid Films on Steel at High Sliding Velocities. NACA TN-1578, 1948.

JOHNSON, R. L.; SWIKERT, M. A.; AND BUCKLEY, D. H.: High Temperature Lubrication in Reactive Atmospheres. Corrosion, vol. 16, no. 8, Aug. 1960, pp. 101–104.

JOHNSON, R. L.; AND SLINEY, H. E.: Ceramic Surface Films for Lubrication at Temperatures to 2000° F. Am. Ceram. Soc. Bull. vol. 41, no. 8, Aug. 1962, pp. 504–508.

LOOMIS, WILLIAM R.: Evaluation of Five Bearing-Separator Materials and Polyphenyl Ether Lubricants for Use in Space Power Generation Systems. NASA TN D-2663, 1965.

SLINEY, H. E.: Decomposition Kinetics of Some Solid Lubricants Determined by Elevated-Temperature X-ray Diffraction Techniques. Proceedings USAF Aerospace Fluids and Lubricants Conference, P.M. Ku, ed., Southwest Research Institute, 1963, pp. 350–364.

SLINEY, HAROLD E.; STROM, THOMAS N.; AND ALLEN, GORDON P.: Fused Fluoride Coatings as Solid Lubricants in Liquid Sodium, Hydrogen, Vacuum, and Air. NASA TN D-2348, 1964.

Vacuum Lubrication

BOWDEN, F. P.; AND YOUNG, J. E.: Friction of Clean Metals and the Influence of Adsorbed Films. Proc. Roy. Soc. (London), Ser. A, vol. 208, no. 1094, Sept. 7, 1951, pp. 311–325.

BUCKLEY, DONALD H.; AND JOHNSON, ROBERT L.: Friction and Wear of Hexagonal Metals and Alloys as Related to Structure and Lattice Parameters in Vacuum to 10^{-10} Millimeter of Mercury. Paper No. 65-LC-18, ASLE, 1965.

BUCKLEY, DONALD H.; AND JOHNSON, ROBERT L.: Influence of Microstructural Inclusions on Friction and Wear of Nickel and Iron in Vacuum to 10^{-9} Millimeter of Mercury. NASA TN D-1708, 1963.

BUCKLEY, DONALD H.; AND JOHNSON, ROBERT L.: Mechanism of Lubrication for Solid Carbon Materials in Vacuum to 10^{-9} Millimeter of Mercury. ASLE Trans., vol. 7, no. 1, Jan. 1964, pp. 91–100.

BUCKLEY, DONALD H.; AND JOHNSON, ROBERT L.: Friction and Wear of Nickel-Aluminum Alloys and Some Sulfur-Modified Steels in Vacuum to 10^{-9} Millimeter of Mercury. NASA TN D-2307, 1964.

BUCKLEY, DONALD H.; AND JOHNSON, ROBERT L.: Influence of Crystal Structure on Friction Characteristics of Rare-Earth and Related Metals in Vacuum to 10^{-10} Millimeter of Mercury. NASA TN D-2513, 1964.

BUCKLEY, DONALD H.: Influence of Order-Disorder Transformation on Friction Characteristics of Copper-Gold Alloys in Vacuum. NASA TN D-2985, 1965.

BUCKLEY, DONALD H.: Influence of Crystal Orientation on Friction Characteristics of Titanium Single Crystals in Vacuum. NASA TN D-2988, 1965.

MORRAL, F. R.: Cobalt Alloys as Implants in Humans. Paper presented at the ASTM/ASM Symposium on Metals as Surgical Implant Materials (Detroit, Mich.), Oct. 1965.

Rolling Element Bearings, Low Temperatures

BUTNER, M. F.; AND ROSENBERG, J. C.: Lubrication of Bearings with Rocket Propellants. Lubrication Eng., vol. 18, no. 1, Jan. 1962, pp. 17–24.

CUNNINGHAM, ROBERT E.; AND ANDERSON, WILLIAM J.: Evaluation of 40 Millimeter-Bore Ball Bearings Operating in Liquid Oxygen at *DN* Values to 1.2 Million. NASA TN D-2637, 1965.

REMPE, W. H., JR.: Research and Development of Materials for Use as Lubricants in a Liquid Hydrogen Environment. Paper No. 65LC-9, ASLE, 1965.

SCIBBE, HERBERT W.; AND ANDERSON, WILLIAM J.: Evaluation of Ball-Bearing Performance in Liquid Hydrogen at *DN* Values to 1.6 Million. ASLE Trans., vol. 5, no. 1, Apr. 1962, pp. 220–232.

WILSON, W. A.; MARTIN, K. B.; BRENNAN, J. A.; AND BIRMINGHAM, B. W.: Evaluation of Ball Bearing Separator Materials Operating Submerged in Liquid Nitrogen. ASLE Trans. vol. 4, no. 1, Apr. 1961, pp. 50–58.

Rolling Element Bearings, High Temperature

BISSON, E. E.; JOHNSON, R. L.; AND ANDERSON, W. J.: Friction and Lubrication with Solid Lubricants at Temperatures to 1000° F with Particular Reference to Graphite. Proceedings of Conference on Lubrication and Wear, Institution of Mechanical Engineers, London, Oct. 1-3, 1957, pp. 348–354.

DEVINE, M. J.; LAMSON, E. R.; AND BOWEN, J. H., JR.: The Lubrication of Ball Bearings with Solid Films. Paper No. 61-LUBS-11, ASME, 1961.

MACKS, E. F.; NEMETH, Z. N.; AND ANDERSON, W. J.: Preliminary Investigation of Molybdenum Disulfide—Air-Mist Lubrication for Roller Bearings Operating to *DN* Values of 1×10^6 and Ball Bearings Operating to Temperatures of 1000° F. NACA RM E51G31, 1951.

NEMETH, Z. N.; AND ANDERSON, W. J.: Effect of Air and Nitrogen Atmospheres on the Temperature Limitations of Liquid and Solid Lubricants in Ball Bearings. Lubrication Eng., vol. 11, no. 4, July-Aug. 1955, pp. 267–273.

NEMETH, Z. N.; AND ANDERSON, W. J.: Investigation of Temperature Limitation of Various Lubricants for High-Temperature 20-Millimeter-Bore Ball Bearings. NACA TN-3337, 1955.

NEMETH, ZOLTON N.; AND ANDERSON, WILLIAM J.: Temperature Limitations of Petroleum, Synthetic, and Other Lubricants in Rolling-Contact Bearings. SAE Trans. vol. 63, 1955, pp. 556–566.

TAYLOR, K. M.; SIBLEY, L. B.; AND LAWRENCE, J. C.: Development of a Ceramic Rolling Contact Bearing for High Temperature Use. Paper No. 61 LUB–12, ASME, 1961.

WILSON, DONALD S.: Evaluation of Unconventional Lubricants at 1200° F in High-Speed Rolling Contact Bearings. Paper No. 61–LUBS–9, ASME, 1961.

Fatigue in Rolling Element Bearings

ANDERSON, W. J.; AND CARTER, T. L.: Effect of Lubricant Viscosity and Type on Ball Fatigue Life. ASLE Trans., vol. 1, no. 2, 1958, pp. 266–272.

CARTER, THOMAS L.: A Study of Some Factors Affecting Rolling-Contact Fatigue Life. NASA TR R–60, 1960.

JACKSON, E. G.: Rolling Contact Fatigue Evaluation of Bearing Materials and Lubricants. ASLE Trans., vol. 2, no. 1, 1959, pp. 121–128.

OTTERBEIN, M. E.: The Effect of Aircraft Gas Turbine Oils on Roller Bearing Fatigue Life. ASLE Trans., vol. 1, no. 1, Apr. 1958, pp. 33–39.

ZARETSKY, ERWIN V.; AND ANDERSON, WILLIAM J.: Rolling-Contact Fatigue Studies with Four Tool Steels and a Crystallized Glass Ceramic. J. Basic Eng., vol. 83, no. 4, Dec. 1961, pp. 603–612.

ZARETSKY, E. V.; SIBLEY, L. B.; AND ANDERSON, W. J.: The Role of Elastohydrodynamic Lubrication in Rolling-Contact Fatigue. J. Basic Eng. vol. 85, no. 3, Sept. 1963, pp. 439–450.

ZARETSKY, E. V.; PARKER, R. J.; AND ANDERSON, W. J.: Component Hardness Differences and Their Effect on Bearing Fatigue. Paper No. 65–LUB–7, ASME, 1965.

ZARETSKY, ERWIN V.; PARKER, RICHARD J.; ANDERSON, WILLIAM J.; AND REICHARD, DAVID W.: Bearing Life and Failure Distribution as Affected by Actual Component Differential Hardness. NASA TN D–3101, 1965.

Gas Bearings

CASTELLI, V.; AND ELROD, H. G.: Solution of the Stability Problem for 360 Deg. Self-Acting, Gas Lubricated Bearings. J. Basic Eng., vol. 87, no. 1, March 1965, pp. 199–212.

CHENG, H. S.; AND PAN, C. H. T.: Stability Analysis of Gas-Lubricated, Self-Acting, Plain, Cylindrical, Journal Bearings of Finite Length, Using Galerkin's Method. J. Basic Eng., vol. 87, no. 1, March 1965, pp. 185–192.

LARSON, R. H.; RICHARDSON, H. H.: A Preliminary Study of Whirl Stability for Pressurized Gas Bearings. J. Basic Eng., vol. 84, no. 4, Dec. 1962, pp. 511–520.

MCCANN, R. A.: Stability of Unloaded Gas-Lubricated Bearings. J. Basic Eng., vol. 85, no. 4, Dec. 1963, pp. 513–518.

PAN, C. H. T.; AND STERNLICHT, B.: Comparison Between Theories and Experiments for the Threshold of Instability of Rigid Rotor in Self-Acting, Plain Cylindrical Journal Bearings. J. Basic Eng., vol. 86, no. 2, June 1964, pp. 321–327.

RICHARDSON, HERBERT H.: Static and Dynamic Characteristics of Compensated Gas Bearings. ASME Trans., vol. 80, Oct. 1958, pp. 1503–1509.

STERNLICHT, B.; AND WINN, L. W.: On the Load Capacity and Stability of Rotors in Self-Acting Gas Lubricated Plain Cylindrical Journal Bearings. J. Basic Eng., vol. 85, no. 4, Dec. 1963, pp. 503–512.

Face Contact Seals

ANON.: Dynamic Sealing: Theory and Practice. Koppers Company, Inc. (Baltimore, Maryland).

ANON.: Proceedings of the First International Conference on Fluid Sealing. The British Hydromechanics Research Association (Templefield, Harlow, Essex, England), 1961.

ELWELL, R. C.; AND BIALOUS, A. J.: Description of Program and Results of Evaluation of Currently Available Sealing Methods. Vol. 1; Elwell, R. C.; Bernd, L. H.; Fleming, R. B.; Lee, R. E., Jr.; Marr, J. W.; Rentzepis, G. M.; and Sneck, H. J.; Studies on Special Topics in Sealing. Vol. 2; George, R. L.; and Elwell, R. C.: Bibliography of ASTIA Literature on Seals. Vol. 3a; George, R. L.; and Elwell, R. C.: Bibliography of Open Literature on Seals. Vol. 3b. Study of Dynamic and Static Seals for Liquid Rocket Engines. Final. Rep. (Contract No. NAS 7–102), General Electric Co., Mar. 1963.

HADY, W. F; ALLEN, G. P.; SLINEY, H. E.; AND JOHNSON, R. L.: Friction, Wear, and Dynamic Seal Studies in Liquid Fluorine and Liquid Oxygen. NASA TN D–2453, 1964.

HUDELSON, J. C.: Dynamic Instability of Undamped Bellows Face Seals in Cryogenic Liquid, NASA TN D–3198, 1966.

NAU, B. S.; STEPHENS, H. S.; AND TURNBULL, D. E., eds.: Proceedings of the Second International Conference on Fluid Sealing, The British Hydromechanics Research Association (Templefield, Harlow, Essex, England), 1964.

Viscoseal (Screw Seal)

Boon, E. F.; and Tal, S. E.: Hydrodynamic Seal for Rotating Shafts. Rep. No. DEG.-Inf.-Ser.-13, United Kingdom Atomic Energy Authority, 1961: A Translation by R. Presser from Chem.-Ingr.-Tech., vol. 31, 1959, pp. 202–212.

Ludwig, Lawrence P.; Strom, Thomas N.; and Allen, Gordon P.: Experimental Study of End Effect and Pressure Patterns in Helical Groove Fluid Film Seal (Viscoseal). NASA TN D–3096, 1965.

Ludwig, Lawrence P.; Strom, Thomas N.; and Allen, Gordon P.: Gas Ingestion and Sealing Capacity of Helical Groove Fluid Film Seal (Viscoseal) Using Sodium and Water as Sealed Fluids. NASA TN D–3348, 1966.

McGrew, J. M.; and McHugh, J. D.: Analysis and Test of the Screw Seal in Laminar and Turbulent Operation. J. Basic Eng., vol. 87, no. 1, March 1965, pp. 153–162.

Muijderman, E. A.: Spiral Groove Bearings. Philips Res. Rept. Suppl., no. 2, 1964.

Page intentionally left blank

VIII Storage and Handling of Cryogenic Fluids

DONALD L. NORED, GLEN HENNINGS, DONALD H. SINCLAIR, GORDON T. SMITH, GEORGE R. SMOLAK, AND ANDREW J. STOFAN
Lewis Research Center

TECHNOLOGY PERTINENT TO THE GENERAL USE OF CRYOGENIC FLUIDS is discussed herein. Such fluids are loosely defined as those that require special handling because of their low temperature. Figure VIII–1 illustrates the temperature levels of interest and the normal liquid temperature ranges for a variety of these fluids. The temperatures shown are well below ambient, or room temperature, and extend almost to absolute zero for liquid helium.

The inert fluids liquid helium, liquid neon, and liquid nitrogen are used for a variety of purposes, including that of simply providing a low-temperature environment. For example, liquid nitrogen is now used to freeze foods.

Liquid hydrogen and liquid methane are fuels and, along with the oxidizers liquid fluorine and liquid oxygen, are of interest to NASA because of their high rocket-performance capability. Liquid oxygen and liquid methane are also of interest commercially: Liquid oxygen is used in tonnage quantities in the steel industry, and methane, a fuel gas, is used as a liquid to simplify storage and transportation.

TABLE *VIII–1.—Properties of Cryogenic Fluids at 1 Atmosphere*

Cryogenic fluid	Boiling point, ° F	Freezing point, ° F	Density, lb/cu ft	Heat of vaporization, Btu/lb
Oxygen	—297	—362	71	92
Nitrogen	—320	—346	51	86
Neon	—411	—416	75	37
Hydrogen	—423	—434	4.4	194
Helium	—452	-----	8.5	10

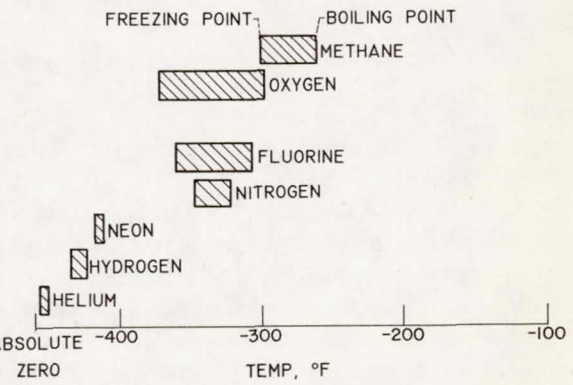

FIGURE VIII–1.—Liquid temperature range of cryogenic fluids at 1 atmosphere.

In addition to being liquids at extremely low temperatures, these fluids have other unique properties that influence their use and handling, as shown in table VIII–1. The low boiling points, well below room temperature, necessitate the use of insulation. Further, the insulation must be very efficient, because of both the large temperature difference and the low heats of vaporization. Comparing liquid helium, with a heat of vaporization of 9 Btu per pound, with water, with a heat of vaporization of 1060 Btu per pound, makes the importance of good insulation apparent.

For liquid hydrogen and liquid helium, the density is also unusual, because it is so low as to be almost that of a gas. The density of liquid hydrogen, a value only one-fifteenth that of water, requires large propellant tanks for hydrogen. This factor has created interest in improved

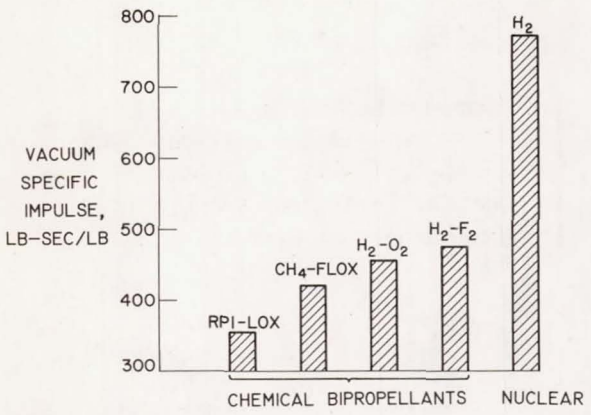

FIGURE VIII–2.—Rocket performance of cryogenic liquids.

materials and structural designs for lighter-weight tanks.

As previously mentioned, cryogenic fuels and oxidizers are of interest to NASA because of their high-energy, or rocket-performance, capability. The specific-impulse values in a vacuum, such as would be obtained in the space environment, for a number of chemical bipropellants and for the nuclear rocket are shown in figure VIII–2. Specific impulse, a measure of performance, is defined as the pounds of thrust obtained for each pound per second of propellant flow. As in miles per gallon, it is desired that this value be a maximum. In the equation for specific impulse

$$I_{sp}=K\sqrt{\frac{T}{M}}$$

where I_{sp} is the specific impulse, K is a constant of proportionality, T is the temperature of the exhaust products, and M is the molecular weight of the exhaust products, are shown two ways to increase performance: First, the exhaust temperature can be raised, for example, by use of liquid fluorine as the oxidizer, either by addition to liquid oxygen to form a mixture called FLOX or by use of pure liquid fluorine, which gives an increase in exhaust temperature of about 2000° F. Second, the molecular weight of the exhaust products can be lowered by use of a fuel that is hydrogen-rich, such as methane, or by use of pure hydrogen.

Even higher specific impulse can be achieved by use of hydrogen as the propellant with a nuclear reactor supplying the heat. The lowest molecular weight possible is thus obtained, and about a 60-percent increase in specific impulse is obtained over the chemical bipropellant specific impulse (fig. VIII–2).

The significant point in figures VIII–1 and VIII–2 and table VIII–1 is that the aerospace industry has moved from the low-temperature range of present commercial interest, which is that of liquid oxygen, to a range below −400° F. This move, coupled with the necessity of working with these newer fluids that have other unusual properties, has resulted in extensive investigations in the areas of materials, insulation, instrumentation, and handling and design techniques. In some cases, extensions to commercial practice have been all that is required. In other cases, entirely new technologies have had to be developed. The topics discussed herein concern some of the areas of technology peculiar to these cryogenic fluids. These topics should be of interest for future commercial and industrial applications.

CRYOGENIC PROPELLANT APPLICATIONS

A number of cryogenic fluids can be used as propellants (fig. VIII–2). NASA is presently using two of these fluids in large quantities, namely, liquid hydrogen and liquid oxygen. Their aerospace uses are described to convey an im-

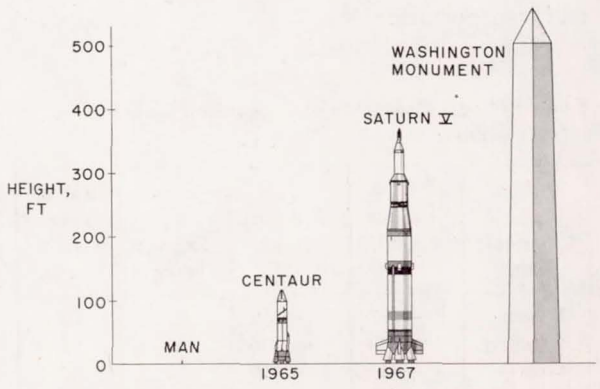

FIGURE VIII–3.—Relative size of launch vehicles that use cryogenic propellants.

pression of the present size and extent of operations using these fluids. The relative sizes of two vehicles that use liquid hydrogen and liquid oxygen as propellants are illustrated in figure VIII–3. The Atlas-Centaur vehicle is 110 feet high; the Saturn V vehicle, which will someday carry man to and from the Moon is 365 feet high. Shown for comparison are Man (approx. 6 ft high) and the Washington Monument (555 ft high). The Atlas-Centaur vehicle became operational in 1965, while the Saturn V vehicle will be flown for the first time in 1967.

The Atlas-Centaur vehicle, shown in figure VIII–4 at lift-off, is the first United States vehicle to use liquid hydrogen as a propellant. A schematic drawing of this vehicle is shown in figure VIII–5. The Atlas, or first stage, burns liquid oxygen and kerosene and uses three engines with a total of approximately 390 000 pounds of thrust. The second stage, which is the Centaur, burns liquid hydrogen and liquid oxygen as propellants and uses two 15 000-pound-thrust engines. The amount of cryogenic propellants consumed by both stages is 2.5 tons of liquid hydrogen and 102 tons of liquid oxygen.

The Saturn V vehicle is composed of three stages, as shown in figure VIII–6(a). The first stage, S-IC (fig. VIII–6(b)), burns liquid oxygen and kerosene similarly to the Atlas first stage. The five engines, with a total thrust of 7 500 000 pounds, that are used in this stage make it the Nation's most powerful booster. The second stage, S-II (fig. VIII–6(c)), uses liquid hydrogen and liquid oxygen as propellants. The liquid oxygen consumed weighs five times more than the liquid hydrogen; however, because of the low density of liquid hydrogen, the hydrogen tanks are much larger than the liquid oxygen tanks. In this stage, the hydrogen tank is insulated with a honeycomb-type insulation that is bonded to the outside of the tank wall. Five 200 000-pound-thrust engines with a total stage thrust of 1 000 000 pounds are used. The S-IVB third stage (fig. VIII–6(d)) also uses liquid hydrogen and liquid oxygen. The upper tank stores the liquid hydrogen and the lower tank, the liquid oxygen. In this stage, a foam insulation bonded to the inside of the tank wall is used to insulate the liquid-hydrogen tank, and only one 200 000-pound-thrust engine is used. The total cryogenic propellants consumed by the Saturn V vehicle are 102 tons of liquid hydrogen and 2155 tons of liquid oxygen. Meeting the

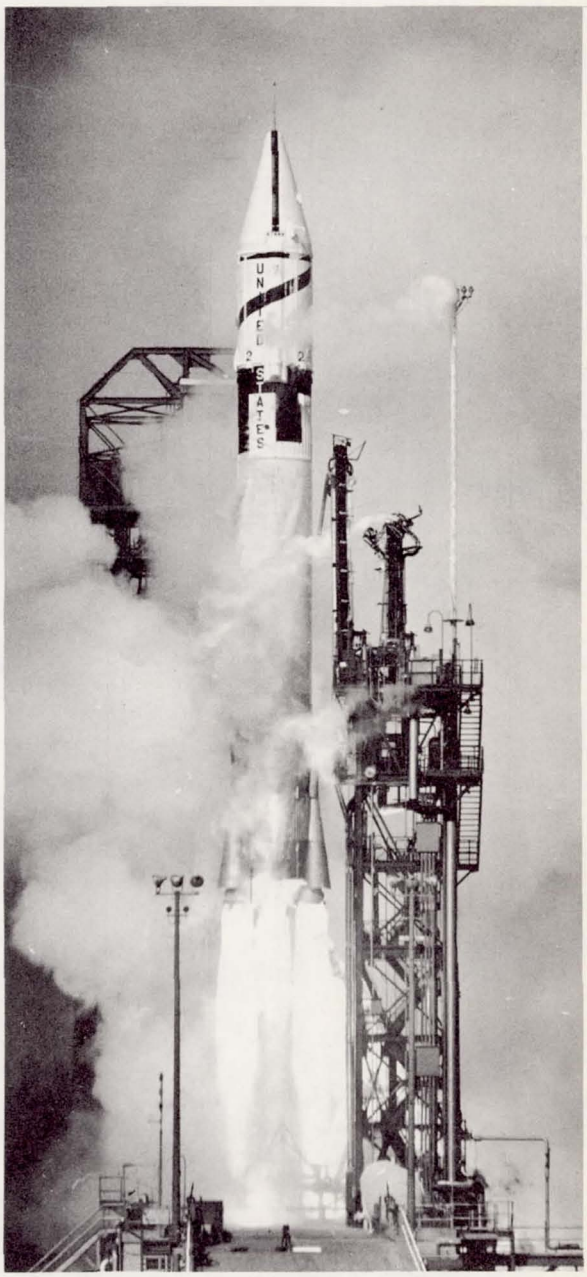

FIGURE VIII–4.—Atlas-Centaur launching.

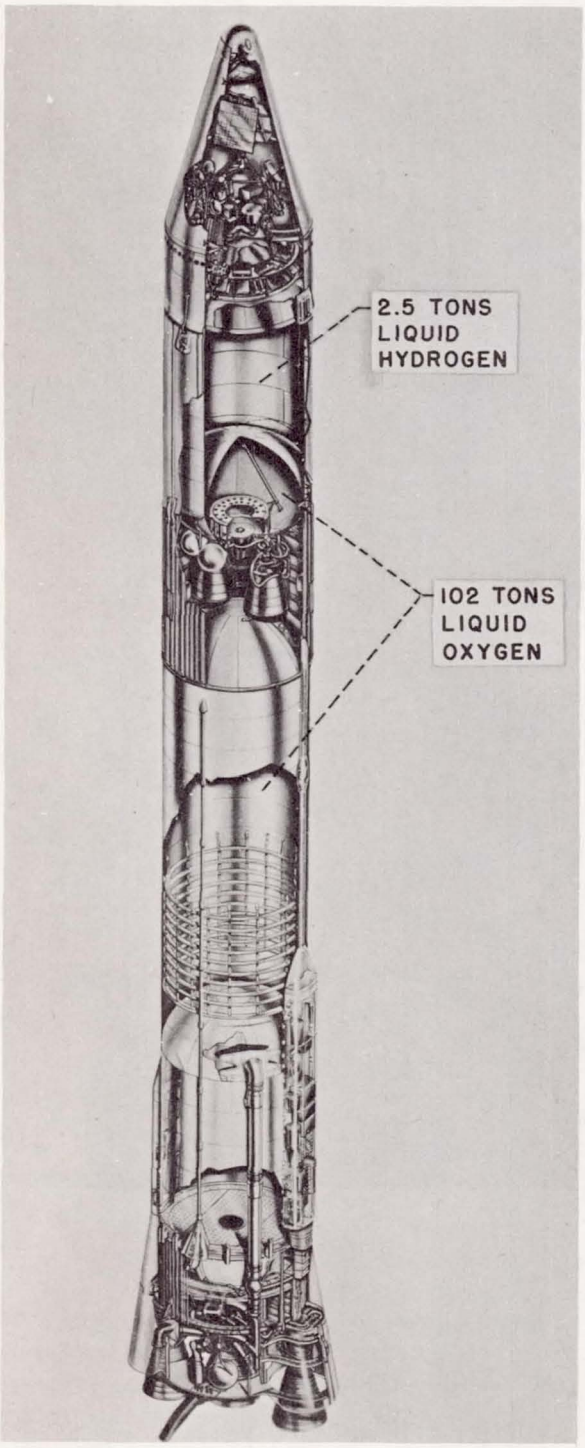

FIGURE VIII–5.—Schematic drawing of Atlas-Centaur.

daily requirements necessary to support development of this vehicle requires 22 trailer loads of liquid hydrogen, 76 trailer loads of liquid oxygen, and 26 trailer loads of liquid nitrogen.

CRYOGENIC PROPELLANT HANDLING

Even for a relatively small vehicle, such as the Atlas-Centaur, the launch pad propellant systems are extensive (fig. VIII–7). The vehicle is in the center of the figure, and the gantry is rolled back. Helium and nitrogen pressurizing gases are stored in the high-pressure tanks located at the far left at pressures in the range of 5000 pounds per square inch. Immediately to the left of the vehicle is a liquid-nitrogen Dewar. The small, white, liquid-helium Dewar located at the base of the umbilical tower holds the liquid helium required to prechill the Centaur pumps. The liquid-hydrogen Dewar for fueling the Centaur is on the right. The RP–1, or kerosene fuel, for the Atlas is supplied from the tank on the far right. The multiplicity and complexity of the systems are apparent.

In addition to launch-pad facilities, ground test facilities are also required. Launching a spacecraft commits considerable resources, national prestige, and sometimes the lives of astronauts. Reliability cannot be developed by means of repetitious flights; everything must be done right the first time. Each component and subassembly is therefore extensively tested and proved on the ground.

In the ground test facility for the Saturn S-IV stage shown in figure VIII–8, the large propellant-handling systems and a complex test structure are shown. These ground test stands are subjected to extremely severe environmental conditions. The liquid-hydrogen systems work at $-423°$ F, while the flame bucket, or exhaust deflector, experiences high-velocity exhaust gases at about 5000° F. During testing, the vibration is severe, with the vehicle held down and the test stand subjected to the full-duration firing, which may last several minutes.

Future spacecraft will require much larger rocket engines and test facilities. The largest hydrogen-oxygen engine for which hardware has

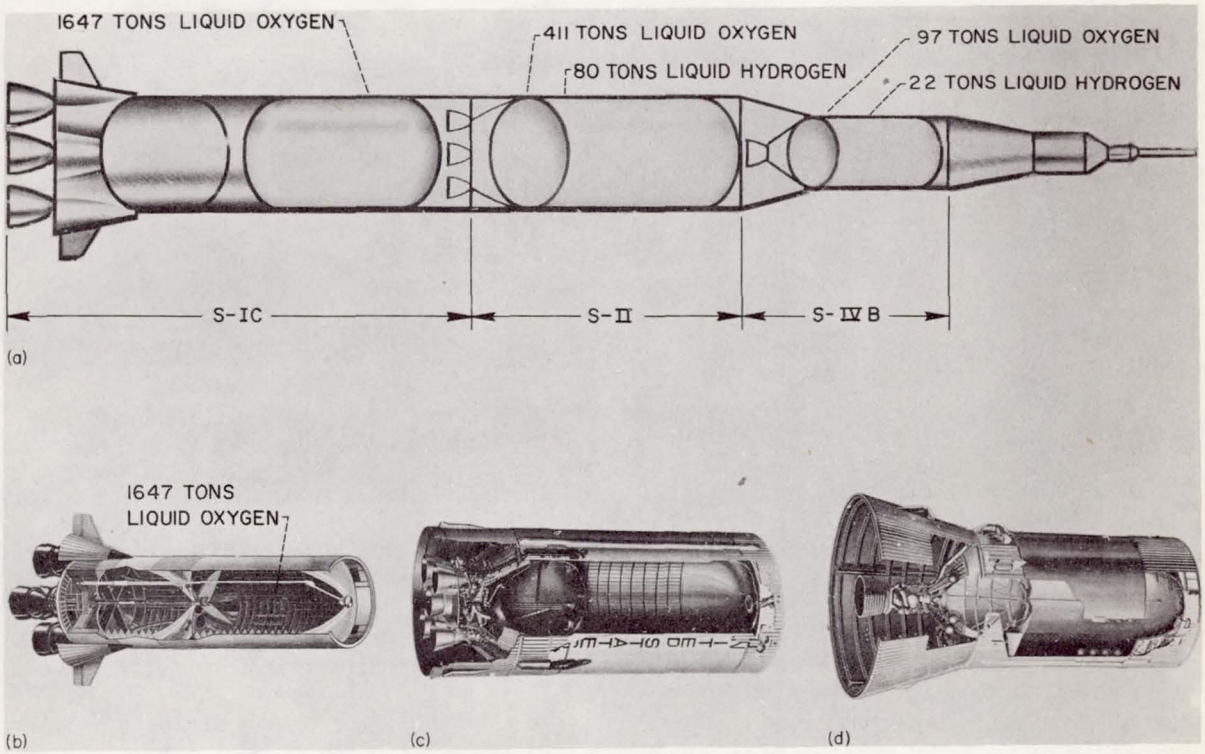

(a) Overall view.

(b) First stage, S-IC. (c) Second stage, S-II. (d) Third stage, S-IVB.

FIGURE VIII-6.—Saturn V vehicle and stages.

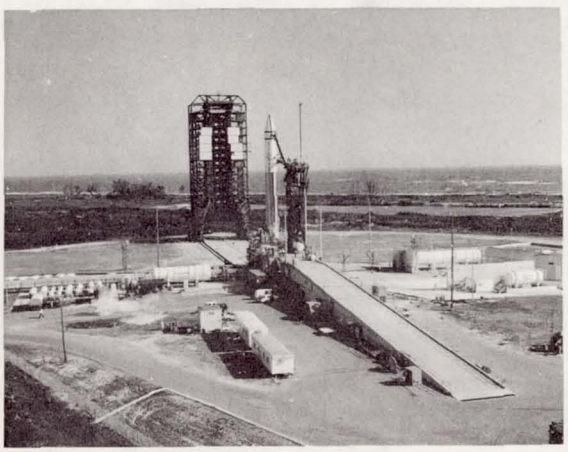

FIGURE VIII-7.—Atlas-Centaur launch pad at Cape Kennedy.

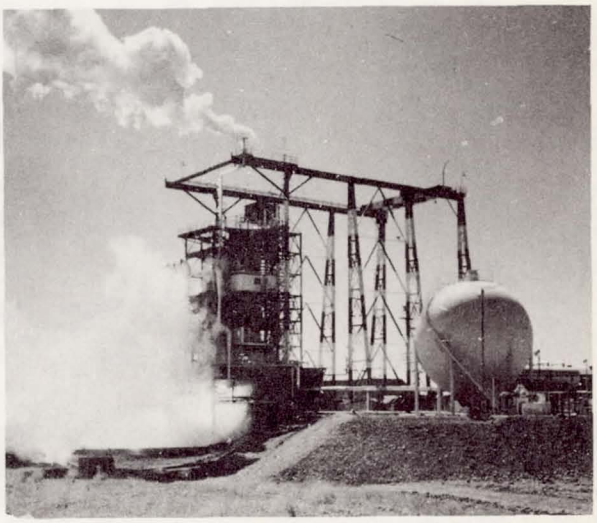

FIGURE VIII-8.—Saturn S-IV stage ground test facility.

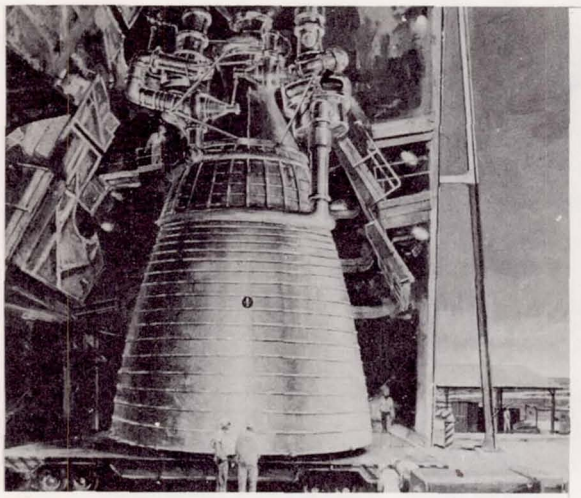

FIGURE VIII-9.—M–1 rocket engine.

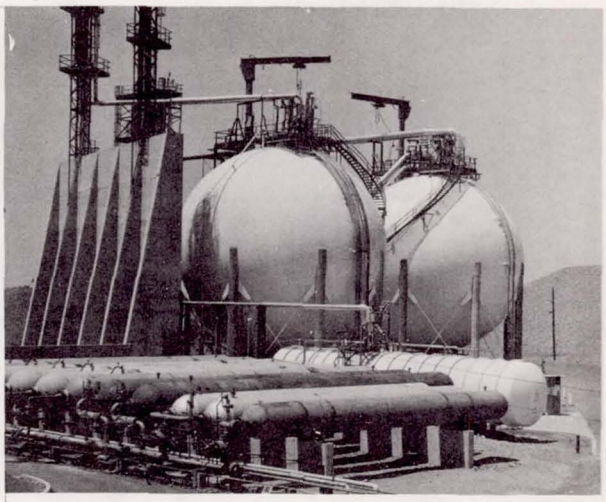

FIGURE VIII–10.—M–1 propellant storage area.

been produced is the 1 500 000-pound-thrust M–1 engine. Figure VIII–9 shows the engine as it would look on a static test stand. Note the size of the men compared with that of the engine.

One of the propellant storage areas for an M–1 ground test facility is shown in figure VIII–10. In this example, a turbine test stand, liquid hydrogen flows from a 370 000-gallon vacuum-insulated liquid-hydrogen tank through a system of pipes into the test pump and then returns to a second similar tank. The row of gas cylinders in the foreground is for the storage of gaseous helium, hydrogen, and nitrogen at about 5000 pounds per square inch. Almost hidden is a horizontal, 28 000-gallon liquid-nitrogen Dewar.

Figure VIII–11 illustrates the size of some of the components on this and similar test stands; the item is a 14-inch unjacketed liquid-hydrogen valve. It is a Y-pattern, poppet-style valve designed for liquid-hydrogen service at pressures up to about 1800 pounds per square inch. The same valve installed in a flow line but with part of the stem mechanism disassembled is shown in figure VIII–12. A pressure regulator designed to drop the inlet pressure from 5000 pounds per square inch to any selected outlet pressure from 200 to 2500 pounds per square inch is shown in figure VIII–13. This regulator can accommodate

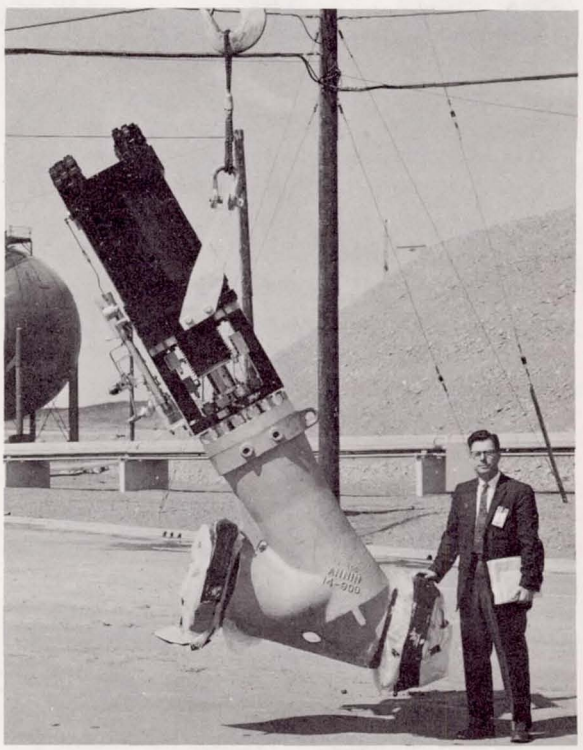

FIGURE VIII–11.—14–Inch unjacketed liquid-hydrogen valve.

hydrogen gas flow rates up to 100 pounds per second.

Not all equipment is this large, however. Fig-

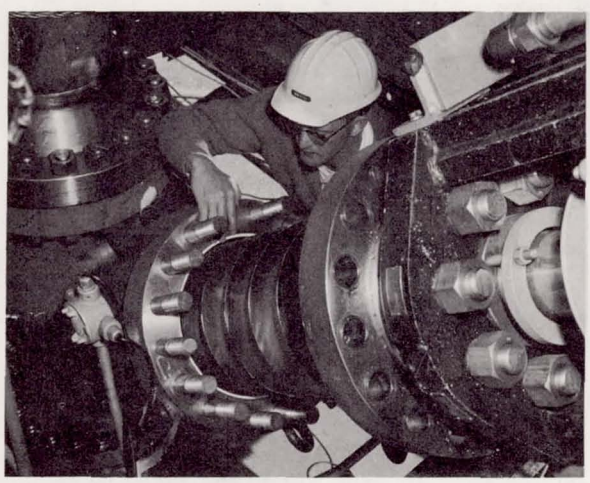

FIGURE VIII–12.—14–Inch valve installed in flow line (partly disassembled).

FIGURE VIII–13.—5000-Pound-per-square-inch gas regulator.

ure VIII–14 shows more typical components in a liquid-hydrogen transfer system; this system is entirely vacuum jacketed and has 2-inch flow lines. Conventional hand valves and vacuum-jacketed flexible hoses for attachment to trailers and rail cars are depicted.

Flexibility in piping arrangements requires joints that can be readily connected and disconnected. Such a joint is shown at the end of the flexible hose, and several others are in the main flow line. Figure VIII–15 is a schematic illustra-

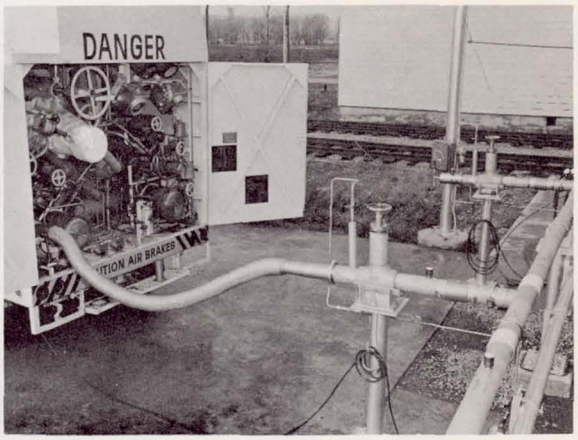

FIGURE VIII–14.—Flow line components.

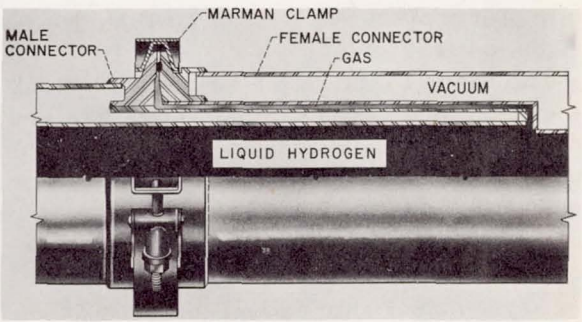

FIGURE VIII–15.—Liquid-hydrogen bayonet-type low-temperature joint.

tion of the construction of these bayonet joints. The vacuum insulation overlaps on both the male and female halves of the joint. Also, the radial clearance is kept small to allow a quiescent gas film to develop. This gas blocks the liquid and keeps it from flowing out to the warm region of the seal, where it would boil and cause a high heat leak.

Another significant design feature is that the parts are made long and thin to minimize the heat-conduction path from the warm region to the cold region. Stainless steel is used, because it is a poor thermal conductor and its thermal conductivity decreases with a decrease in temperature (fig. VIII–16), whereas the thermal conductivity of a good heat conductor, copper, increases with lower temperatures. At liquid-

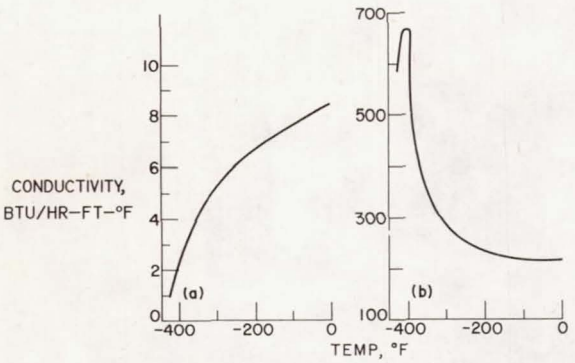

(a) Type 304 stainless steel. (b) Copper.

FIGURE VIII–16.—Thermal conductivity.

hydrogen temperatures, the thermal conductivity of copper is about 600 times as great as that of stainless steel.

The bayonet concept can be used to develop complete piping systems. Pipes, valves, tees, and elbows are made with bayonet ends. These components are manufactured in sizes from a fraction of an inch to 1 foot in diameter.

In addition to the bayonet-type joint, numerous other flange- and gasket-type joints are used for cryogenics. Figure VIII–17 illustrates an unusual application of a conventional rubber O-ring sealing element. The O-ring is compressed to 90 percent of its initial volume when the joint is made up. This procedure is different from normal O-ring sealing practice, where deformation, not a volume reduction, takes place. This type of O-ring seal can be used from room temperature to liquid-hydrogen temperature for both high-pressure and vacuum applications.

CRYOGENIC FLUID PRODUCTION

Large quantities of liquid hydrogen are required for the aerospace industry. Only a few years ago liquid hydrogen was not commercially available, and production capability had to be developed. In the past 15 years, production capacity has grown from laboratory quantities to almost 200 tons per day.

The ownership, the location, and the capacity of existing large plants are shown in table VIII–2.

TABLE *VIII–2.—Liquid-Hydrogen Production Capacity*

Owner	Location	Capacity, tons/day
Government	West Palm Beach, Fla.	[a]30
Linde	Ontario, Calif.	[a]30
Linde	Sacramento, Calif.	60
Air Products	Long Beach, Calif.	30
Air Products	New Orleans, La.	30
Air Reduction	Pedricktown, N. J.	6
		Total 186

[a] On standby after Jan. 1966.

All the plants except the first one are privately owned, and they sell their product on the open market. Plant capacity ranges from about 6 to 60 tons per day. The cost to the government depends on the location and the quantity purchased and ranges from about $0.20 to $1.00 per pound. This price is not considered excessive because of the high energy content of hydrogen.

The cost of electric power produced by a hydrogen fuel cell, such as in the Gemini spacecraft, can be compared with the cost of power produced by a gasoline-engine—generator combination, as shown in table VIII–3. Based on the raw material costs shown, a hydrogen-oxygen fuel cell running at 65-percent efficiency will

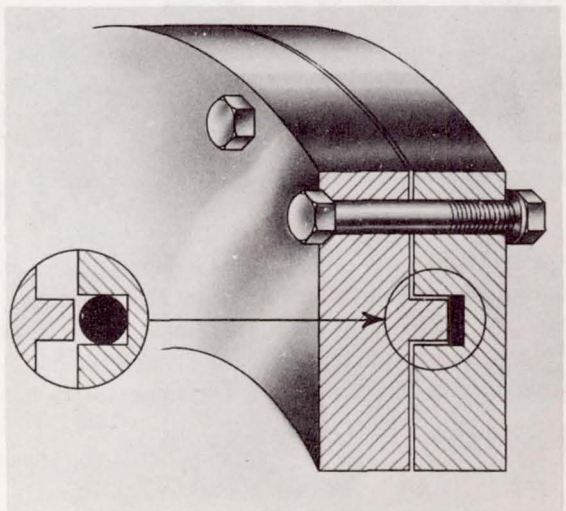

FIGURE VIII–17.—O-ring seal design for cryogenic applications.

TABLE VIII–3.—*Cost of Electric Power*

	Energy content, Btu/lb	Equivalent energy content, kW-hr/lb	Raw material cost		Delivered cost, dollars/kW-hr
			Dollars/lb	Dollars/gal	
Liquid hydrogen	52 000	15.2	0.20	.....	.....
Liquid oxygen	.....	.....	.02	.....	.....
Gasoline	18 000	5.27	[a].04	[a]0.24	.....
Hydrogen-oxygen fuel cell [b]	.....	.....	.....	.....	0.0365
Hydrogen-air fuel cell [b]	.....	.....	.....	.....	.0202
Gasoline engine [c] and generator [d]	.....	.....	.....	.....	.0228

[a] No tax.
[b] Efficiency, 65 percent.
[c] Efficiency, 35 percent.
[d] Efficiency, 95 percent.

generate 1 kilowatt-hour of electricity for about \$0.037. The hydrogen-air cell would produce electricity for about \$0.020 per kilowatt-hour. In a gasoline-engine—generator combination in which the engine efficiency is 35 percent and the generator efficiency is 95 percent, 1 kilowatt-hour of electricity will cost about \$0.023.

This cursory look at economics simply shows that the aerospace effort has brought the fuel-cell and the liquid-hydrogen technologies to a high state of development. Such things as fuel-cell-powered electric cars, for example, are not greatly beyond the technology of today.

In addition to hydrogen, the aerospace industry has also brought liquid helium to a high state of development. Liquid helium is the coldest known fluid and is used extensively as a refrigerant in the field of low-temperature physics, in electronic systems, and in space-simulation chambers.

A price history for liquid helium is shown in figure VIII–18. Cost has decreased markedly over the past 15 years. At the same time, the size of the plants has increased, as might be expected. In 1950, the largest plant produced about 1 gallon per hour. In 1965, there were plants that produced about 66 gallons per hour. Over the same period, the price decreased from about \$100 per gallon to about \$10 per gallon. In 1966, a commercial plant will go into production with a total capacity of 200 gallons per hour.

The Lewis 50-gallon-per-hour helium liquefaction plant is shown in figure VIII–19. Of interest are the large helium gas holders outside the building. Because of the high cost and relative scarcity of helium, losses had to be avoided.

The principle of operation of the gas holders is illustrated in figure VIII–20. The space between the double-wall plastic balloons is pressurized with air at a gage pressure of a few inches of water, which stabilizes the outer shell and provides pressurized helium gas for input to the liquefier. The inner bag is free to inflate or deflate against the constant air pressure.

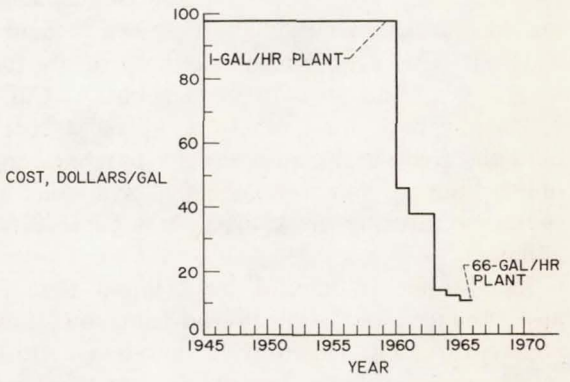

FIGURE VIII–18.—Price history of liquid helium.

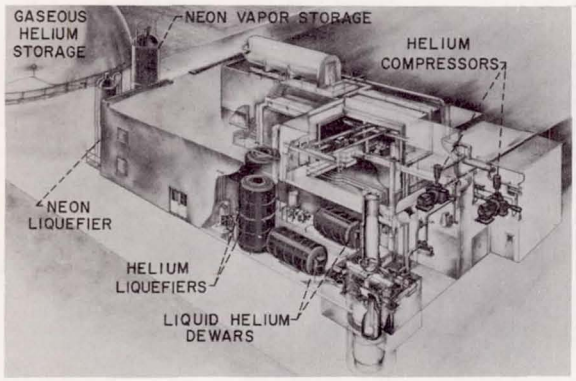

FIGURE VIII–19.—Helium liquefier.

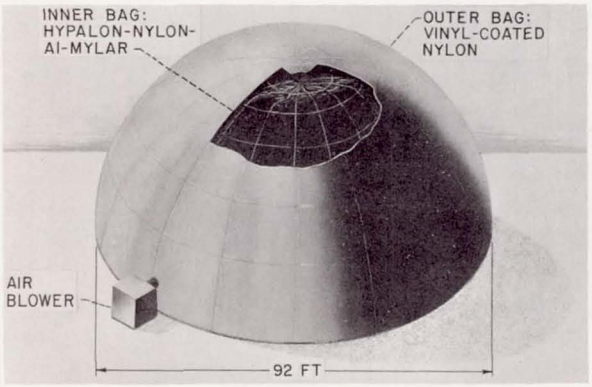

FIGURE VIII–20.—Helium gas holder. Helium capacity, 200 000 standard cubic feet.

Not only is liquid helium produced in large quantities, but it can also be readily transported by truck, rail, or air. A 5000-gallon Dewar being loaded into a transport plane is shown in figure VIII–21. This arrangement has been in use for several years to transport liquid helium to California and to Florida, where it is used to prechill the Centaur liquid-hydrogen pumps. Liquid helium is now commercially available in containers ranging in capacity from 25 to 9700 gallons.

In addition to liquid helium, liquid neon is also produced at Lewis in the same building. Neon is used in closed-cycle, low-temperature refrigeration systems, because it has excellent thermodynamic properties. Liquid neon is just becoming available in sufficient quantities for such use. The production of liquid neon is about at the point that liquid helium was 15 years ago.

STRUCTURAL MATERIALS FOR CRYOGENIC TEMPERATURES

Metals

Many material characteristics change drastically at low temperature; for example, two important changes occur when structural materials are cooled to cryogenic temperatures: they tend to become stronger and brittle.

The popular structural materials undergo various increases in yield strength at low temperature (fig. VIII–22).

The materials shown are 301 stainless steel (70 percent cold reduced), as used in the Centaur vehicle; a titanium alloy that is currently being investigated for propellant-tank application; an aluminum alloy that is used on the Saturn S-II and S-IV vehicles; and 304L annealed stainless steel, which is often used for ground storage applications. The 301 stainless steel increased about 50 percent in yield strength between room and liquid-hydrogen temperatures, the titanium alloy increased about 100 percent, and the aluminum alloy and the 304L stainless steel increased much less.

The other property change is the tendency of the material to become brittle, that is, the material cannot deform plastically. It may be strong, but it cannot accommodate stress concentrations

FIGURE VIII–21.—Air transport of liquid helium.

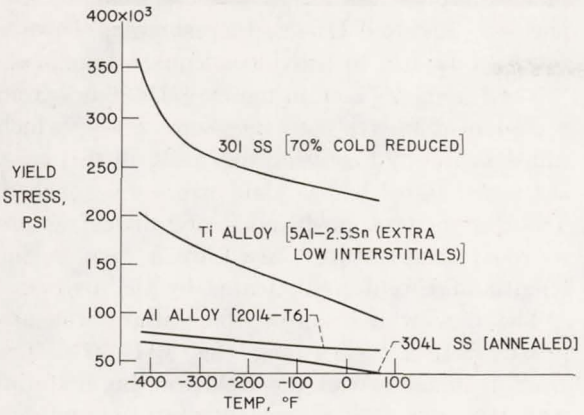

FIGURE VIII–22.—Effect of temperature on yield stress of structural alloys.

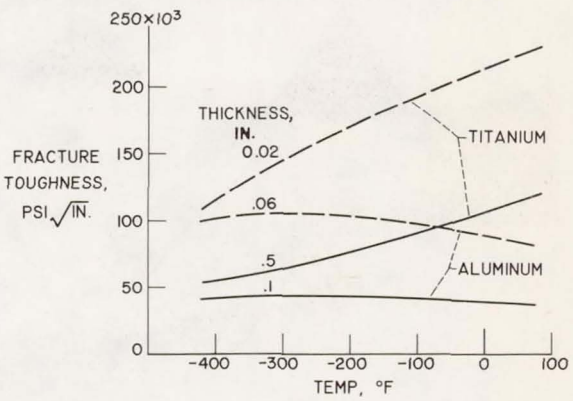

FIGURE VIII–23.—Effect of temperature and thickness on fracture toughness.

by yielding locally. Since even small flaws can cause large stress concentrations, a brittle material is sensitive to flaws, and a flaw can sometimes propagate at surprisingly low values of average stress. The fact that many of the new high-strength materials considered promising for pressure vessels are brittle at room temperature worsens the situation. Cryogenic temperatures only intensify this problem.

In applying these materials to the fabrication of cryogenic tanks, compromises must be made between strength and brittleness in order to design lightweight, reliable vessels for cryogenic operating conditions. The lack of proper design information can easily lead to a vehicle that is impractically heavy. In an attempt to design low-weight vessels with high reliability, new approaches have been investigated for the selection of materials and for the selection of their operating and proof stress levels. Currently, one approach which appears to merit consideration for future tank design makes use of fracture mechanics, or the concept of fracture toughness, which is a relatively new area of technology. Even today, for example, fracture mechanics is usually offered as a specialized graduate-level college course. Fracture toughness is a material characteristic which relates the strength of the material to the size of the flaw in the material. Toughness is proportional to the amount of energy required to extend the flaw and can be considered to be the inverse of brittleness; that is, the higher the toughness, the less brittle the material.

The effect of temperature on fracture toughness for two different thicknesses of aluminum and titanium is shown in figure VIII–23. The titanium loses fracture toughness as the temperature decreases, while the aluminum shows a slight increase in toughness with a decrease in temperature. For both aluminum and titanium, and for most other materials as well, the fracture toughness decreases with an increase in thickness. As materials become very thick, toughness reaches a minimum constant value.

Variations in thickness in actual liquid-hydrogen tank applications are shown in figures VIII–24 and VIII–25. Figure VIII–24 shows a section of an inner shell of a large, high-pressure, liquid-hydrogen tank that is used in a ground test facility. The 304 stainless-steel tank is 5½ inches

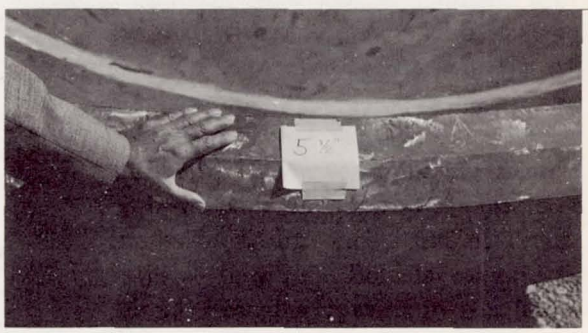

FIGURE VIII–24.—Inner-shell segment of liquid-hydrogen storage tank.

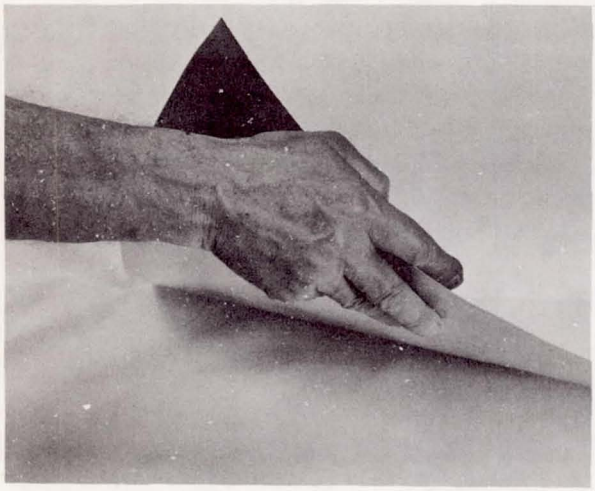

FIGURE VIII–25.—Centaur liquid-hydrogen tank material.

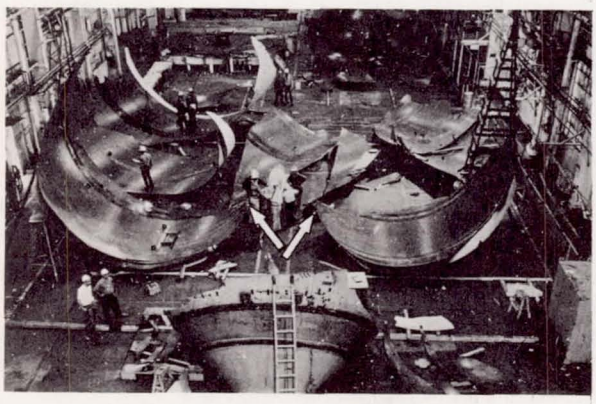

FIGURE VIII–26.—Pressure vessel failure due to weld flaw.

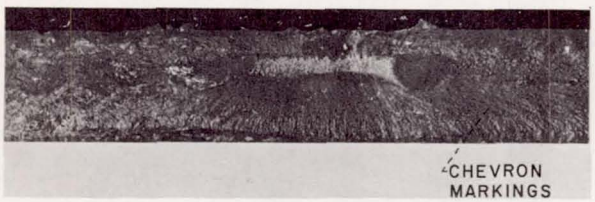

FIGURE VIII–27.—Flaw which initiated failure of pressure vessel.

thick. A piece of the Centaur liquid-hydrogen tank, made of 0.014-inch-thick 301 stainless steel, is shown in figure VIII–25. The thin material utilizes its maximum fracture toughness, but the thick material approaches its minimum value of toughness. Hence, selection of a material with sufficient toughness for its thickness can be important. Figure VIII–26, for example, shows a result of failure to provide adequate toughness.

The fragments seen in figure VIII–26 are from a 22-foot-diameter steel pressure vessel, which failed in the hydrostatic proof test; in this case, the vessel failed before yield stress was reached. This failure was an example of brittle fracture at room temperature caused by a flaw in the longitudinal weld, as indicated by the arrows.

The flaw which caused this failure was approximately 2 inches long (fig. VIII–27). The fracture toughness of the weld for this material was low, even at room temperature, and the flaw propagated in a brittle manner. The chevron markings on the right side of the material point to the fracture origin. These markings on the fracture faces were used to identify the point of failure initiation. This large flaw was undetected by both careful and repeated X-ray and ultrasonic inspections. Current nondestructive inspection techniques are not adequate to assure identification of all significant flaws.

The cause of failure of this vessel is shown graphically in figure VIII–28. The stress at fracture σ is related to the flaw size and fracture toughness by the equation

$$\sigma = \frac{K_c}{\sqrt{\pi a + \frac{1}{2}\left(\frac{K_c}{\sigma_y}\right)^2}}$$

where K_c is the fracture toughness, a is the flaw size, and σ_y is the material yield strength. At

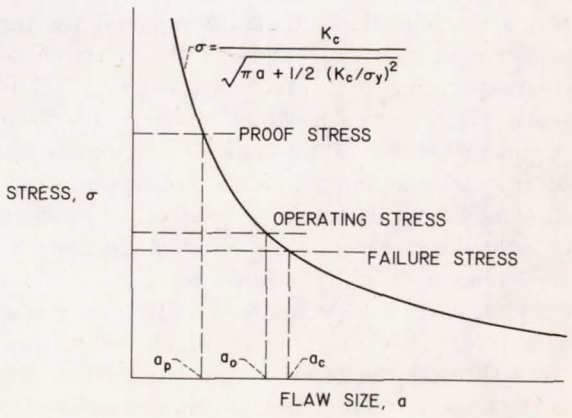

FIGURE VIII–28.—Graphical presentation of pressure vessel failure.

any time that the stress reaches or exceeds the value indicated by the curve, a catastrophic fracture results.

In the case of the 22-foot-diameter pressure vessel, a flaw a_c caused the fracture stress to be reached before the intended proof stress was reached. In fact, this flaw was sufficiently large that fracture occurred even below the intended operating stress.

This curve (fig. VIII–28) can also be used to illustrate a more general point. Usually, a proof stress level is selected at some arbitrary value above the operating stress. When the tank successfully passes the proof test, a minimum strength increment, or safety factor, is established. Making use of the concepts of fracture mechanics, however, provides additional information from the proof test. Such curves for the exact material, thickness, and temperature can be used to establish the fact that no flaw larger than that corresponding to the proof stress can be present. It can also be established that an even larger flaw a_o is required to cause fracture at operating stress. A flaw-size increment, or flaw-size safety factor, thus exists.

Even when vessels have successfully passed their proof test, however, failures may occur later in service. For maximum reliability, such failures must be prevented. In the case of launch vehicles, the fuel and the oxidant are stored with only a very thin bulkhead separating them. A failure of the bulkhead would allow direct mixing of the propellants, with catastrophic results.

The reasons for a normal service failure based upon fracture mechanics considerations are shown in figure VIII–29. The sketch shows the flaw growth that leads to a service failure. An initial flaw grows to a point at which catastrophic fracture or leakage occurs because of a crack which has grown through the thickness, as illustrated graphically by the curve. If the vessel has passed the proof test, no flaw larger than a_p is present in the vessel. As indicated by the arrows, an initial flaw a_i smaller than a_p may grow to the critical size corresponding to the operating stress level. Failure will occur when the crack reaches the critical size a_c. This growth

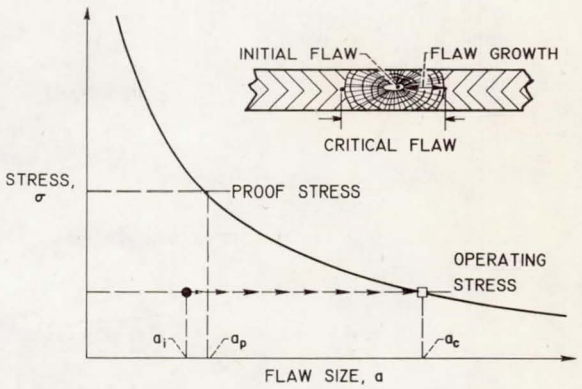

FIGURE VIII–29.—Service failure due to flaw growth.

can be caused by cyclic variations of pressure load, by hydrogen embrittlement and subsequent cracking, by stress corrosion cracking, or sometimes simply by extending the time under stress.

Two types of information necessary for a reliable design for a selected tank life are the material fracture toughness and the crack growth rate and characteristics. With knowledge of only the fracture toughness, however, the catastrophic fracture can probably be avoided if the design is for a leak-before-break condition. Establishing such a design requires only the selection of an operating stress such that crack growth will produce a stable through-the-thickness crack before the critical size is reached.

The sketch in figure VIII–29 suggests such a condition. The critical size is enough larger than the wall thickness to cause leakage to precede fracture. Without crack-growth information, the time when this leak will occur will be unknown, but the leakage may result in a tank depressurization which will thus avoid an explosive brittle fracture.

Such a leak-before-break design, however, while adequate for a container such as a helium vessel, is not acceptable for propellant tanks. In those cases, it is necessary to obtain flaw-growth data and then to utilize these data to prevent a fracture or a leak.

Figure VIII–30, with the same type curve, shows how flaw-growth data might be applied (in this case, to assure a predetermined number of cycles before fracture). Specimens containing flaws are cycled at several stress levels, and

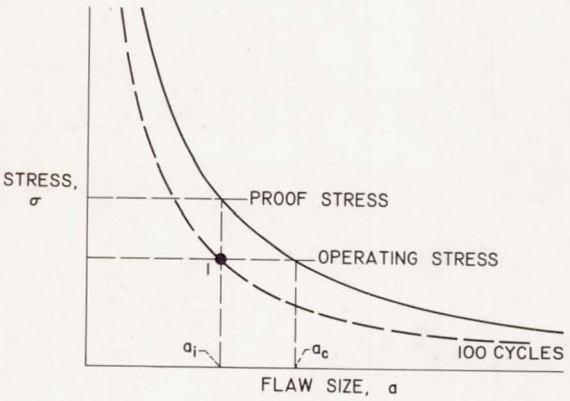

FIGURE VIII–30.—Selection of proof stress.

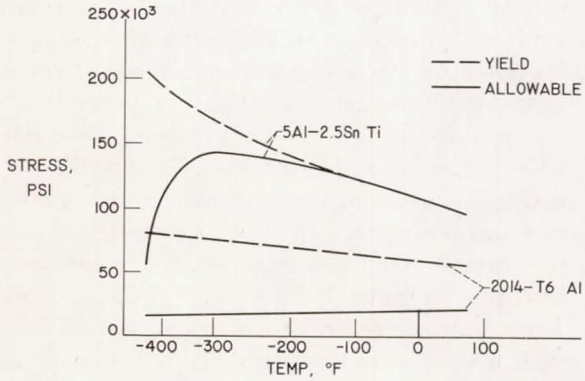

FIGURE VIII–31.—Effect of temperature on yield and allowable strength for 3000-pound-per-square-inch pressure-vessel application.

the number of cycles required to enlarge known initial flaws to critical size is determined. Such data can then be cross plotted to provide cyclic life curves, as shown in the figure for 100 cycles.

When these curves have been established, a proof stress can be identified which will guarantee a sufficient flaw-growth increment to realize the design life. The flaw size a_i, corresponding to point 1, for example, represents the flaw size which requires 100 cycles to enlarge to the critical size a_c at operating stress. The proof stress required to assure this service life can be identified as the proof stress required to proof out all flaws larger than a_i.

The 100-cycle curve is only an example; curves of 1000 cycles, 10 000 cycles, or higher could be developed if the application required it. However, when the allowable operating stresses are determined on the basis of leak-before-break or cycle-life considerations, it is not always possible to utilize the yield-strength increases that take place at cryogenic temperatures.

The allowable operating stresses established on the basis of a leak-before-break design for a 3000-pound-per-square-inch pressure-vessel application are compared in figure VIII–31. The allowable stress for the aluminum is severely compromised with respect to the yield strength over the whole temperature range. The allowable stress for the titanium follows the yield strength down to about −100° F but then diverges sharply as liquid-hydrogen temperatures are approached. This sharp divergence is due to the rapid decay in fracture toughness, which was previously illustrated.

In summary, fracture-mechanics data can be used to design lightweight, reliable metal tanks. Quite often, however, the results differ from the case in which present commercial codes are used. Sometimes, commercial codes give tanks that are too heavy or, surprisingly, not reliable enough. Moreover, the lack of a large background of empirical information is usually the case for new alloys or new environments, such as cryogenic temperatures. In these cases, the approach for the selection of materials and stress levels based on fracture-mechanics test data appears not only to be quite promising but possibly to be the only logical approach to tank design.

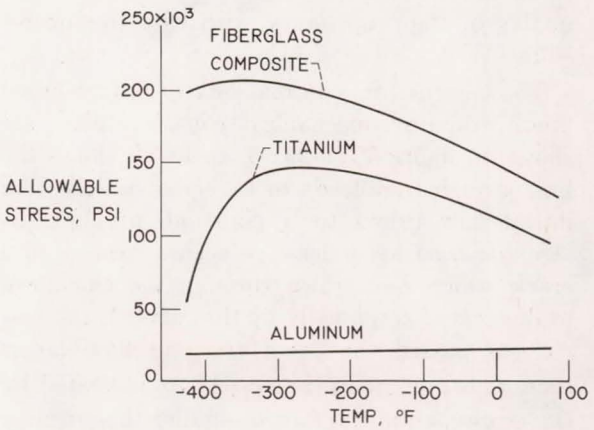

FIGURE VIII–32.—Effect of temperature on allowable strength for 3000-pound-per-square-inch pressure-vessel application.

Fiber Glass

Other promising materials for fabrication of cryogenic tanks are the fiber-glass-filament-wound composites. Figure VIII–32 shows the same allowable stress curves for titanium and aluminum as in figure VIII–31, with the addition of a curve for the fiber-glass composite. The fiber-glass composite has an increasing usable strength level with decreasing temperature, with a leveling off or slight reduction near liquid-hydrogen temperature. This increase in strength and the low density of the material make glass-fiber-filament-wound composites attractive for cryogenic pressure vessels. Not only does the material strength increase markedly with decrease in temperature, but also the fracture toughness remains high because of the nature of the construction.

The structural characteristics of a filament-wound pressure vessel are illustrated schematically (fig. VIII–33) by the wall cross section, where the hoop and the longitudinal load-carrying filaments are shown embedded in a matrix of low-modulus material, usually a resin or a plastic material. The inherent high fracture toughness of this structure arises from the fact that fracture of a single load-carrying filament is arrested by the matrix material without propagating to an adjacent filament. The matrix material in this type of structure is forced to undergo large strains in localized areas between the filaments, and, as a result, some local cracking of the resin occurs. The leakage paths indicated in the schematic diagram are developed in this way.

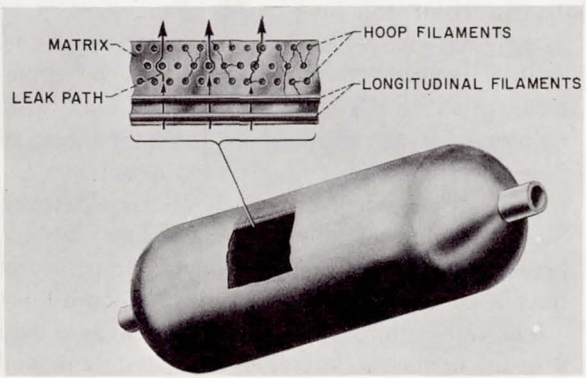

FIGURE VIII–33.—Glass-fiber-filament-wound pressure vessel.

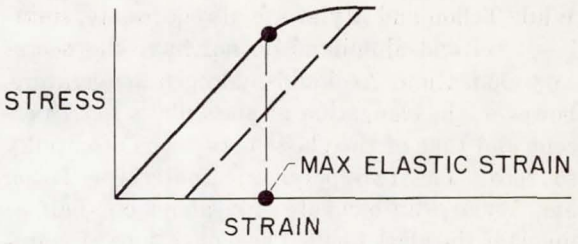

FIGURE VIII-34.—Elastic strain.

This leakage problem is present at all temperature levels and requires the use of an impermeable liner. These filament-wound vessels are light, strong, and tough, but they leak. Obtaining an effective liner is thus a prerequisite to the use of fiber glass for a pressure vessel.

The fiber glass, while strong, has a low elastic modulus, which results in a large amount of stretching of the vessel wall during pressurization. This stretching requires a flexible liner that can follow the wall. At room temperature, usually no problem is presented; a liner can be made from rubber or other elastomeric materials. At cryogenic temperatures, however, the elastomers lack the needed flexibility, and other materials must be used.

The elastic strain capabilities of several possible liner materials are compared with fiber glass in table VIII–4. The elastic strain, illustrated in figure VIII–34, is the maximum elongation a material can withstand without a permanent set due to plastic flow. At room temperature, the elastomeric materials, such as rubber, are more than adequate to satisfy the liner requirements.

TABLE *VIII–4.—Elastic Strain Capability of Liner Materials*

Material	Maximum elastic strain, percent, at —	
	75° F	—423° F
Glass fibers	2.5	2.7
Elastomers	700	~0
Teflon	3.0	1.6
Mylar	2.0	1.3
Stainless steel	.5	.6
Aluminum	.05	.5

While Teflon and Mylar are also adequate, stainless steel and aluminum do not have the necessary elongation. At liquid-hydrogen temperature, however, the elongation of glass fibers is 2.7 percent and that of the elastomers drops essentially to zero. The two polymeric materials, Teflon and Mylar, can elongate only about one-half as much as the glass fiber. The elongations of stainless steel and aluminum are only about one-fifth of that required. The inability of these materials to match the strain of the fiber glass requires design innovations if they are to be used for pressure-vessel liners.

NASA is currently investigating three different cryogenic liner concepts (fig. VIII–35). The first approach is to use a corrugated metal liner, which is essentially a two-dimensional bellows, in a fiber-glass tank (fig. VIII–36). The liner shown was made of $3\frac{1}{2}$-mil stainless steel and was manufactured over a plaster mandrel. A fiber-glass tank was then overwrapped on the liner. This particular liner underwent approximately 30 pressure cycles at liquid-nitrogen temperature before a leak developed. Without the corrugation, the leak would have developed after 1 or 2 cycles.

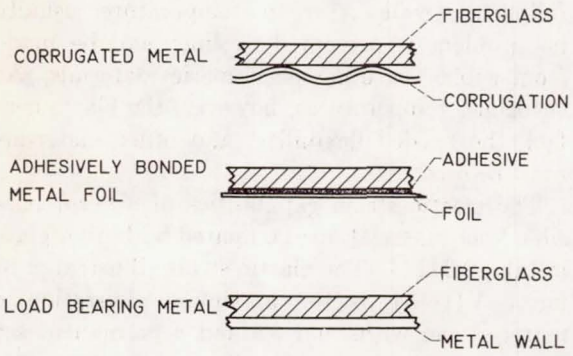

FIGURE VIII–35.—Liner concepts.

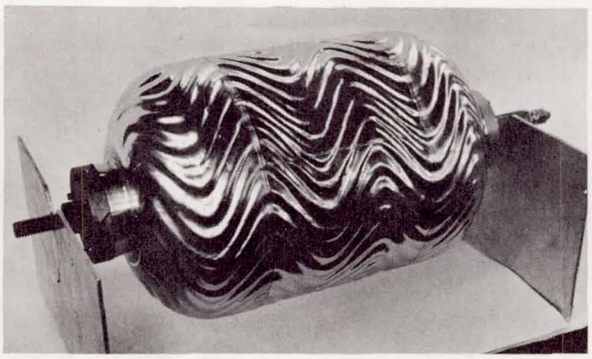

FIGURE VIII–36.—Corrugated liner.

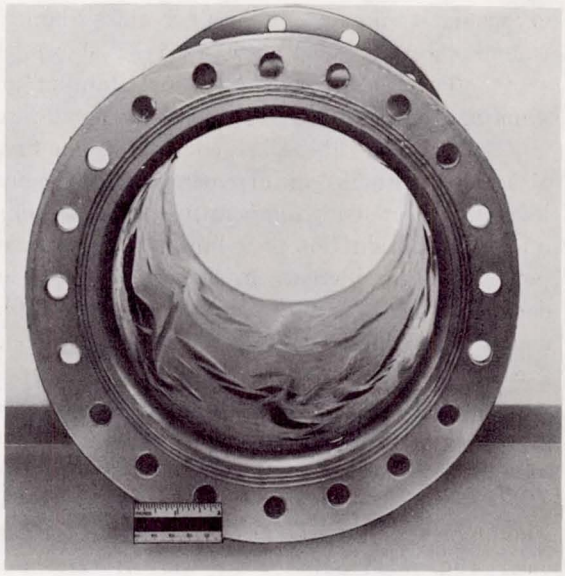

FIGURE VIII–37.—Buckling of thin-wall liner.

The second approach is to bond a thin metal foil adhesively to the inside tank walls. When the tank is pressurized, the thin foil undergoes a plastic deformation or elongation; that is, it stretches beyond its elastic limit and carries very little of the pressure load. When the tank is depressurized, the liner must be compressed to its original size without buckling out of shape. Such a compression is accomplished by adhesively bonding the thin foil to the tank wall. Otherwise, it would appear as the liner shown in figure VIII–37. This liner pulled loose from the tank wall, buckled, and then developed leaks. Since that time, however, approximately 100 pressure cycles at liquid-nitrogen temperatures have been achieved with a 3-mil aluminum liner.

The third approach is to wrap fiber glass over a metal in such a way that the metal tank and the fiber glass efficiently share the pressure load. This load-sharing technique is accomplished by having compression in the metal tank and

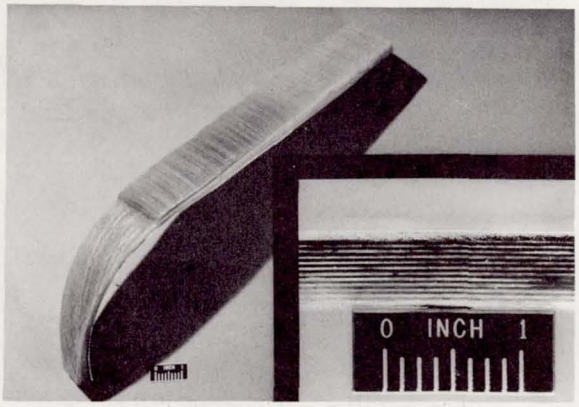

FIGURE VIII–38.—Overwrapped metal tank section. (Courtesy Aerojet General Corp.)

tension in the fiber-glass overwrap. When the tank is pressurized, the metal then shares the tension load with the fiber glass. Both the metal wall and the fiber-glass overwrap are shown in figure VIII–38. This approach is a compromise, but it still results in a fairly lightweight pressure vessel.

While all three approaches have shown promise of solving the leakage problem for a fiber-glass tank at cryogenic temperatures, problems other than leakage may exist with fiber-glass vessels. The effects of external damage to the vessel wall, repeated pressure cycles, long-term pressure loading, and resin degradation are a few of these problems. These effects will be studied, since the universal goal in both the commercial and the aerospace industry is to achieve the highest payload possible when liquids and gases are transported.

CRYOGENIC INSULATION

Storing and transporting cryogenic fluids normally require tank insulation. In special cases, this insulation is provided by a buildup of frost on a bare tank.

The lift-off of an Atlas-Centaur vehicle from the pad at Cape Kennedy is shown in figure VIII–39. The white portion of the Atlas, which is the lower stage, is frost covering the bare liquid-oxygen tank. Ice can be seen falling off the side of the tank. Such uninsulated tanks result in high heat-transfer rates through the wall because of the condensation process, as is expected. The high rate of heat transfer, in turn, results in high boiloff rates of the cryogenic propellant. In the case of the Atlas liquid-oxygen tank, storage time is short, and the boiloff gases are used to help keep the thin tank pressurized.

If liquid hydrogen at −423° F, however, is stored in the bare tank, air will condense. The condensed air contains liquid oxygen, which could create a hazard. Furthermore, the insulating effects of a frost layer are not obtained, and an undesirable high heat leak to the liquid hydrogen results. Even for short storage times, liquid hydrogen tanks thus require insulation.

Insulating a liquid hydrogen tank, however, is not always a simple problem. Before insulat-

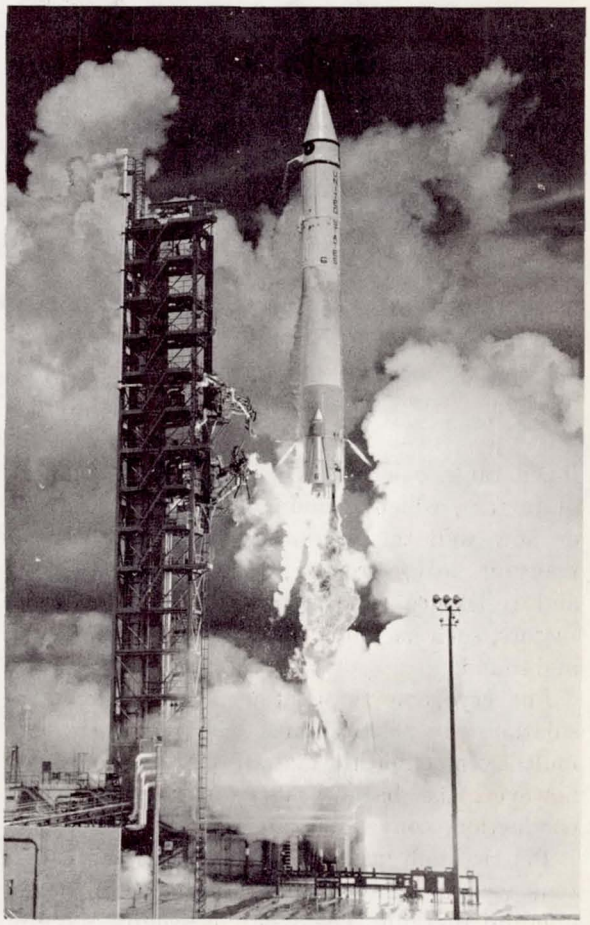

FIGURE VIII–39.—Atlas-Centaur at lift-off.

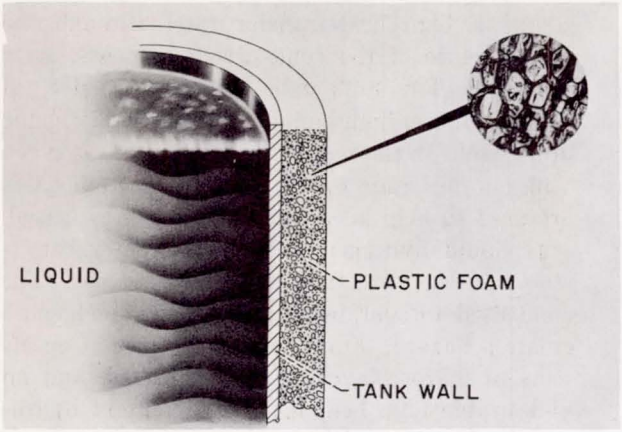

FIGURE VIII–40.—Plastic-foam insulation.

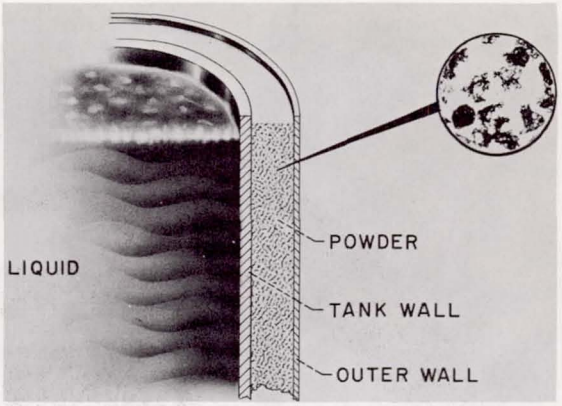

FIGURE VIII–42.—Powder insulation.

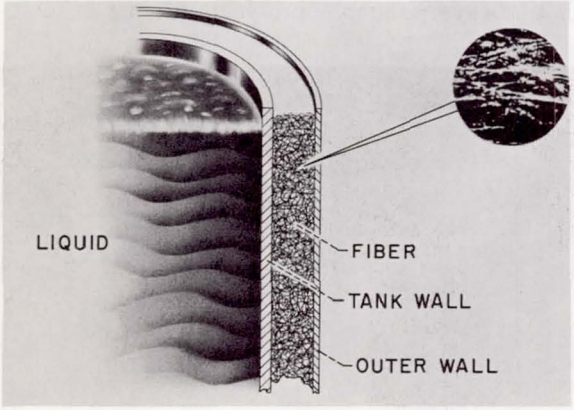

FIGURE VIII–41.—Fiber insulation.

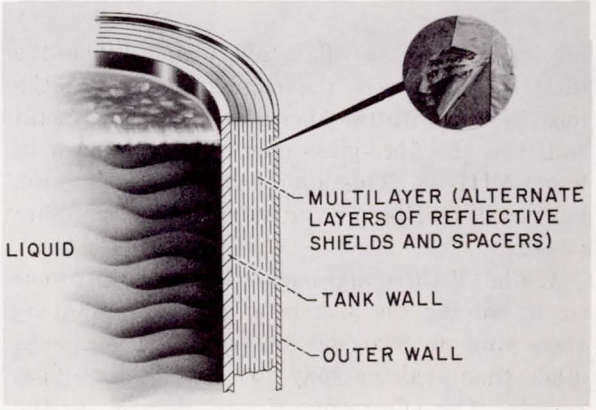

FIGURE VIII–43.—Multilayer insulation.

ing a tank, one must consider a large number of factors, which include thermal conductivity, or how well the insulation and trapped gases transmit heat; strength; weight; volume; cost; and resistance to a number of environmental factors, such as water, chemicals, fire, vibration, and sound.

For cryogenic applications, the common insulations are plastic foams, fibers, powders, and multilayer composite materials. In all of them, however, the basic heat-transfer processes of conduction, convection, and radiation occur.

Plastic foam insulation is shown attached to a tank wall in figure VIII–40 and in detail in the photomicrograph. The plastic is usually polyurethane, or polystyrene, and has a closed, cellular, rigid structure, with gas trapped in each cell. Foams are light and easily fabricated and have a high strength-to-weight ratio. They are extensively used at cryogenic test sites, because they are so easily applied.

Figure VIII–41 shows a typical fiber insulation. Glass, asbestos, rockwool, and ceramics, the most commonly used fibers, are usually made into a light-weight blanket, which is flexible and easily handled. An outer wall, or vacuum jacket, is shown. For cryogenic applications, evacuation of the gas in the insulation greatly improves the thermal performance and prevents condensation problems.

A typical powder insulation is illustrated in figure VIII–42. The vacuum jacket, first, per-

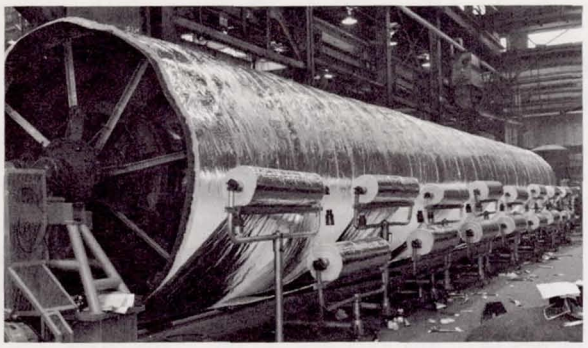

FIGURE VIII–44.—Machine winding of multilayer insulation on large tank. (Courtesy Linde Div., Union Carbide Corp.)

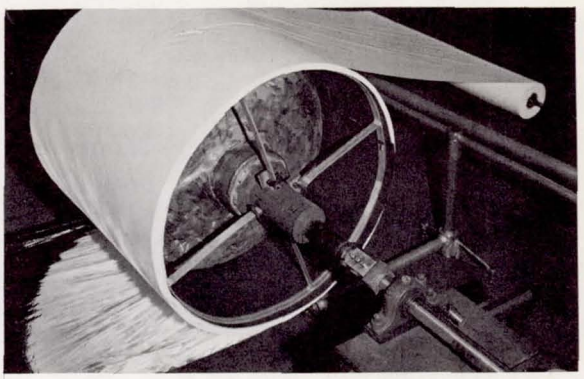

FIGURE VIII–45.—Machine winding of multilayer insulation on small tank. (Courtesy Linde Div., Union Carbide Corp.)

mits evacuation of residual gas, and second, provides a retainer for the powder particles. These powders have a low density, and, because they are extremely fine, are difficult to handle. Perlite and diatomaceous earth are two common powders. Until recently, cryogenic ground storage containers and transfer lines were insulated almost exclusively with evacuated powders.

The miltilayer insulation concept (fig. VIII–43) has revolutionized the cryogenic insulation field in the past 10 years. Multilayer insulation consists of alternate layers of highly reflective shields and low conductivity spacers. Two common shields are aluminum and aluminized Mylar. The spacers are ordinarily glass-fiber paper. In a vacuum, the reflective shields are extremely effective in minimizing radiative heat transfer. The multilayer materials have a low density but are fragile and difficult to handle unless they are made into a blanket or applied by machine, as shown in figures VIII–44 and VIII–45.

The tanks are turned in mandrels while being wrapped with alternate layers of aluminum foil and glass-fiber paper. After the wrapping has been completed, the tank and its insulation are put into a vacuum jacket or outer wall.

The advantages of a vacuum jacket with a low residual gas pressure can be illustrated with figure VIII–46. For reference, 1 atmosphere is shown at the right and 1 millionth atmosphere, common to a space chamber or vacuum tank, is shown at the left. Thermal conductivity, a

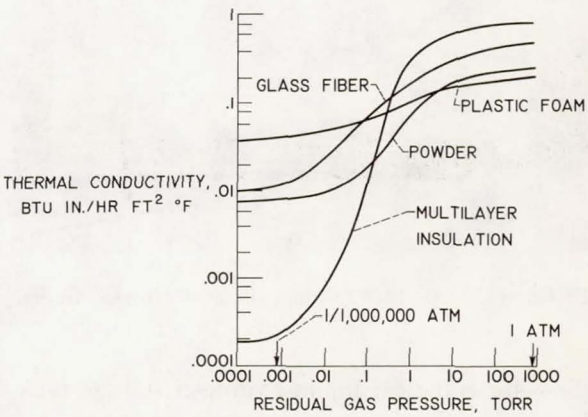

FIGURE VIII–46.—Effect of residual gas pressure.

measure of performance, is about the same for all insulators at 1 atmosphere. As the residual gas pressure is decreased, the thermal conductivities of all the insulators decrease; that is, the performance is improved. The multilayer insulation, however, is approximately 100 times better than the other types of insulation at very low pressures, where the principal modes of heat transfer are conduction and radiation. Conduction is minimized by having only point contact between the powder, the fibers, and the multilayer insulations. Since the multilayer insulation is merely a series of reflective shields, it is not surprising that it has such good thermal characteristics at very low gas pressures.

Applications of these materials are illustrated in figure VIII–47, where insulation of a 10-foot-

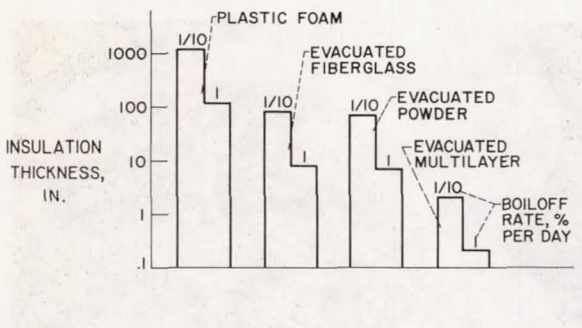

FIGURE VIII–47.—Insulation requirements for 10-foot-diameter liquid-hydrogen tank.

FIGURE VIII–48.—13 000-Gallon liquid-hydrogen trailer.

diameter spherical liquid-hydrogen storage tank is considered. Current aerospace missions require hydrogen storage for at most a few hours. Thus, a boiloff rate of 1 percent per day is quite acceptable. To provide this boiloff rate requires about 100 inches of foam, 10 inches of evacuated fiberglass or powder, and only 0.2 inch of evacuated multilayer insulation. Many future aerospace applications, however, may require the storage of liquid hydrogen for hundreds of days. For these uses, a maximum acceptable boiloff rate would be about 0.1 percent per day. This decrease in boiloff rate will require that all insulation thicknesses increase by a factor of 10, as shown.

One outstanding example of the value of multilayer insulation is its application to shipping and storage equipment. Figure VIII–48 shows a trailer with a capacity of 13 000 gallons of liquid hydrogen. Five years ago, a trailer with identical external dimensions would have held only 9300 gallons. The increased capacity was made possible by the use of multilayer insulation.

Figure VIII–49 further illustrates why multilayer insulation is so advantageous. Because the density of liquid hydrogen is low, shipping equipment is volume limited rather than weight limited. Therefore, the maximum volume is desired that will fit into the largest allowable external envelope. The maximum legal width for trucks is 8 feet, or 96 inches. In this case, 9 inches of powder are required in comparison with 3 inches of multilayer insulation. This gives 224 gallons per foot of tank length for powder as against 317 gallons per foot for multilayer insulation. Thus, the multilayer insulation has increased the available payload volume by about 40 percent, cut the evaporation loss by a factor of 4, and reduced the insulation weight from

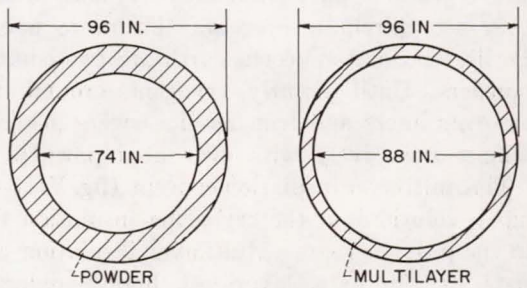

	POWDER	MULTILAYER
LIQUID VOLUME PER FOOT OF TANK LENGTH	224 GALS	317 GALS (40%)
DAILY EVAPORATION LOSS	3%	0.7%
INSULATION WEIGHT PER FOOT OF LENGTH	135 LB	10 LB

FIGURE VIII–49.—Insulation comparison for liquid-hydrogen trailer.

FIGURE VIII–50.—Liquid-hydrogen storage facility.

135 pounds to 10 pounds per foot of trailer length. The significance of reducing the insulation weight by 125 pounds per foot can best be appreciated by considering that, even for the large trailer, the product to be hauled weighs only about 200 pounds per foot of length.

Figure VIII–50 shows a 200 000-gallon liquid-hydrogen storage tank and two 34 000-gallon railroad cars insulated with multilayer insulation, This equipment is new and among the best available today. In fact, the 200 000-gallon storage vessel probably has the lowest heat leak of any large storage vessel in existence. Its design boiloff loss is about 0.05 percent per day; thus, almost 6 years would be required for the entire contents of this vessel to boil away. This represents a total heat leak of only 12 000 Btu per day.

Some typical materials currently used for multilayer reflective shields are shown in figure VIII–51. Double, or single aluminized, $\frac{1}{4}$-mil Mylar and ordinary aluminum foil (about 1 mil thick) are the most common commercial materials. These shields must have a high reflectivity. In order to satisfy future aerospace insulation requirements, materials such as silver, gold, and copper are being investigated for possible increases in reflectivity.

The effects of the number of reflective layers and the reflectivity of each layer on the rate of heat transfer through evacuated multilayer insulation are shown in figure VIII–52. About a

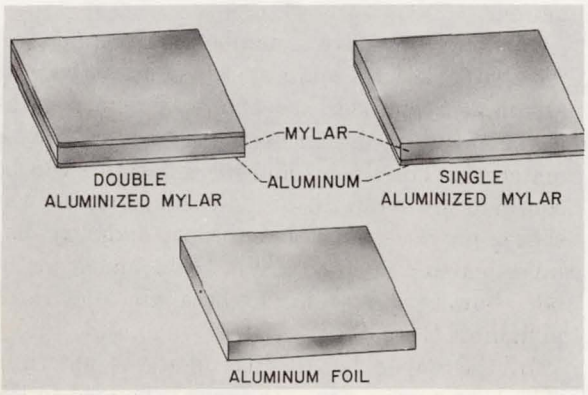

FIGURE VIII–51.—Multilayer insulation reflective shields.

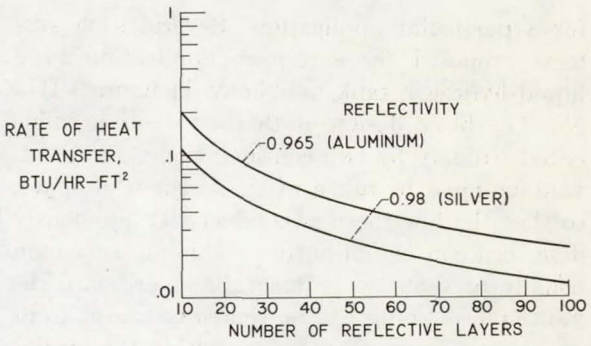

FIGURE VIII–52.—Effect of number of shields and reflectivity on heat transfer.

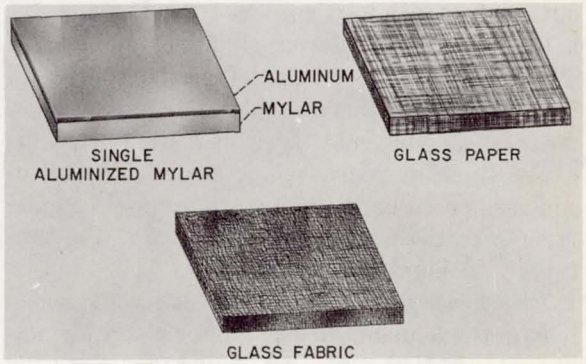

FIGURE VIII–53.—Spacer materials in current use.

40 percent reduction in the rate of heat transfer, or propellant boiloff rate, occurs when silver reflective shields (reflectivity, 0.98) are used instead of aluminum (reflectivity, 0.965).

Some of the spacer materials in current use are shown in figure VIII–53. Single aluminized Mylar ($\frac{1}{4}$ mil thick), a reflective shield, is also a spacer. Wrinkling the aluminized Mylar results in only point contacts between adjacent layers. Glass paper (about 3 mils thick) and glass fabric are also used as spacers. All these materials are used to eliminate solid conduction paths through the insulation.

Some of the newer spacers that are now being investigated (fig. VIII–54) are silk net, open cell foam (about 20 mils thick), and two combinations of net and foam.

For satisfactory use, however, shields and spacers must be integrated into a system designed

for a particular application. Several such systems proposed for aerospace application to a liquid-hydrogen tank are shown in figure VIII–55. The basic design of these systems is influenced strongly by two considerations. First, advantage must be taken of the vacuum of space, so that the low thermal conductivity previously described can be obtained. Obtaining a vacuum usually presents no problem, however, since the multilayer systems can be vented to space. Condensation of air and moisture within the insulation must be prevented during prelaunch, however, and the insulation itself must be prevented from being blown off the tank during the ascent into the vacuum of space. Second, a metal vacuum jacket, such as is used on ground equipment, is too heavy to use during prelaunch and ascent.

The two systems on the left in figure VIII–55 have a sublayer that provides a temperature at the base of the multilayer insulation which is above liquid-nitrogen temperature. Dry nitrogen gas is used on the ground to purge the multilayers. In the upper left of the figure, the sublayer is helium-purged fiberglass. The sublayer in the lower left is a passive layer of sealed polyurethane foam. In the upper right, a helium-purged multilayer blanket mounted directly on the tank wall is used. On the ground, dry nitrogen gas surrounds this insulation. Finally, in the lower right, a relatively thick layer of compressed multilayer insulation contained within a lightweight flexible barrier, or vacuum jacket, is used. This system is continuously evacuated on the ground and during the ascent into space. Dry nitrogen gas also surrounds it on the ground. Each of these systems is currently under investigation.

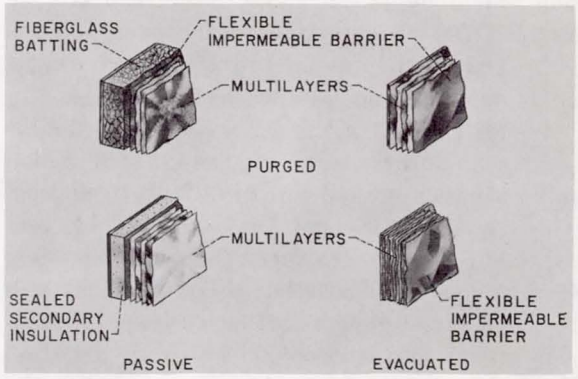

FIGURE VIII–55.—Multilayer insulation systems.

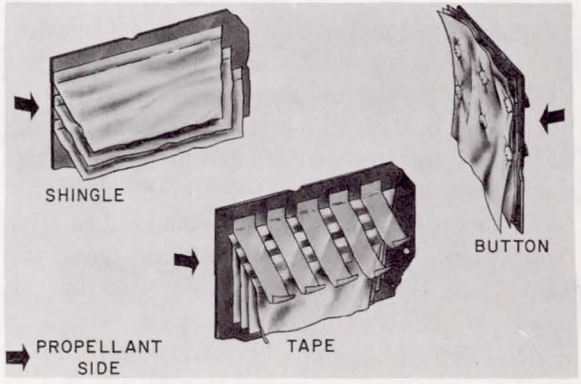

FIGURE VIII–56.—Multilayer insulation attachment methods.

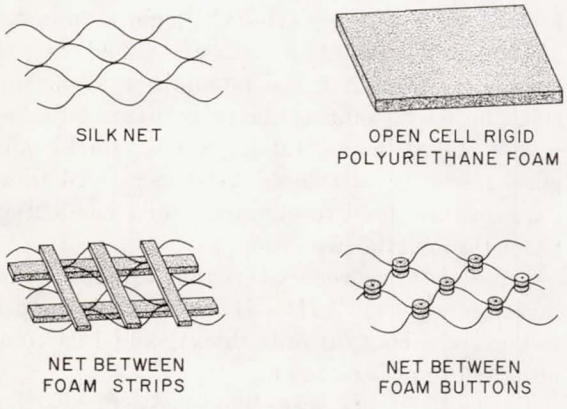

FIGURE VIII–54.—Spacer materials under investigation.

Not only are there a number of different systems possible with multilayer insulation, but the attachment methods are about as numerous as the number of designers specifying multilayer materials. The shields and the separators can be continuously wrapped around the tank, as was shown previously. The aerospace industry has investigated a number of other attachment methods, however. A few of these are illustrated in figure VIII–56.

In the upper left of the figure is shown a shingle system where each layer is bonded to the tank walls. These shingles are built up with the

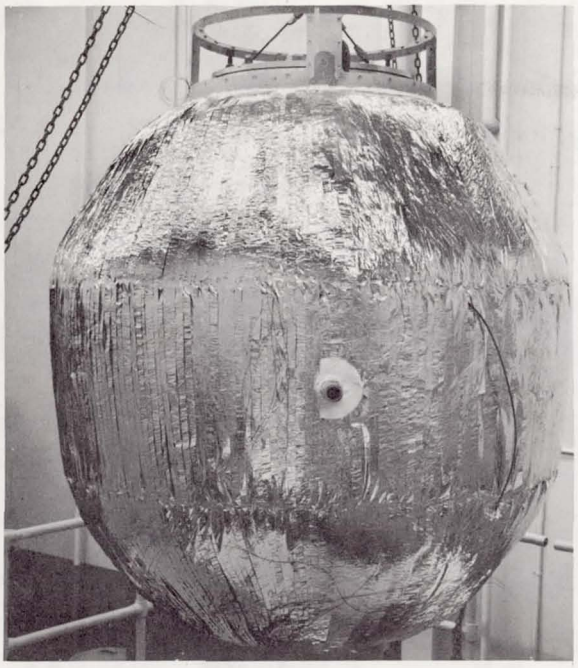

FIGURE VIII–57.—Tank with shingled multilayer insulation. (Courtesy Lockheed Missiles and Space Co.)

shingle length just sufficient to give the desired number of layers.

Figure VIII–57 shows a tank insulated in this manner. The lower center illustration in figure VIII–56 is the shingle system where each layer is attached to tape and only the upper end of the tape is attached to the tank. The tank wrapped in this manner will also appear similar to figure VIII–57. On the right in figure VIII–56 can be seen a blanket of multilayer insulation held together with nylon thread and buttons. This blanket must be attached to the tank wall in some manner. For ground facilities, installation of these blankets can become quite tedious.

Figure VIII–58 shows views of the installation of insulation blankets on the liquid-hydrogen tank at a Lewis facility. The views are into the vacuum space, which is just sufficiently wide to provide access for a man to install the $9\frac{1}{2}$-inch blanket of multilayer insulation on the loops protruding from the outer tank wall while he is standing on a suspended ladder visible on the right side.

A simpler technique for attachment is to use Velcro fasteners, as illustrated in figure VIII–59. Stiff plastic hooks are attached to nylon fabric on one side. These hooks snag when pressed into flexible nylon pile loops on the other side. In our use, one side is adhesively bonded to the tank wall and the other side is adhesively bonded to the blanket of insulation. This technique gives a readily attachable and detachable insulation system.

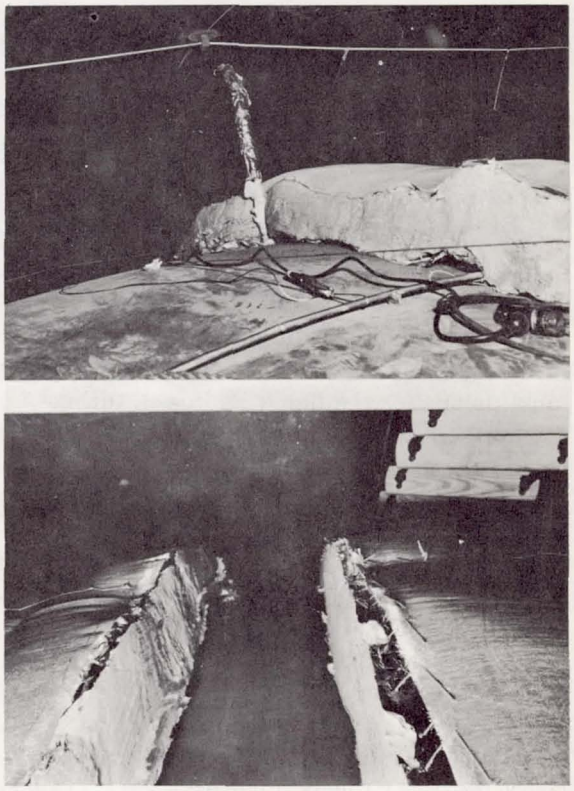

FIGURE VIII–58.—Application of multilayer insulation to ground storage tank.

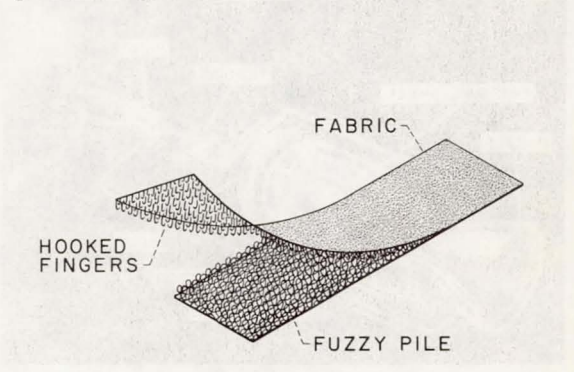

FIGURE VIII-59.—Velcro fastener.

As shown by the foregoing discussion, the field of insulation has progressed rapidly in the past few years. A number of commercial products such as the Velcro fastener have been adapted. Also, commercial applications of aerospace insulation technology have been made. One interesting example is the use of aluminized Mylar reflective shields for emergency rescue blankets. The resulting blanket is very light, folds into a small package, and is expendable. This is a recent commercial development, and certainly other good ideas will come along in the future.

CRYOGENIC INSTRUMENTATION

Common to all cryogenic systems is the need for instrumentation. Some of the components which must be controlled and monitored are seen in figure VIII–60, which shows a nuclear rocket system The liquid-hydrogen propellant tank, pumps for the liquid hydrogen, turbine for driving the pump, flow line, valves, and rocket engine all require instrumentation.

The principal cryogenic measurements are as might be expected: the common ones of temperature, pressure, flow rate, and quantity of propellants. It has generally been necessary, however, because of the low temperatures with which we are working, to extend the operating ranges of existing commercial instrumentation.

For cryogenic temperature measurements, three basic types of sensor are used. Their sensitivity characteristics strongly influence the useful range of each type. This characteristic is demonstrated by figure VIII–61. The sensitivity of the metallic resistance sensors limits their useful range to temperatures warmer than that of liquid hydrogen. The sensitivity of semiconductors limits their usefulness to temperatures colder than that of liquid nitrogen. Obviously the thermocouple is no match in sensitivity to resistance sensors.

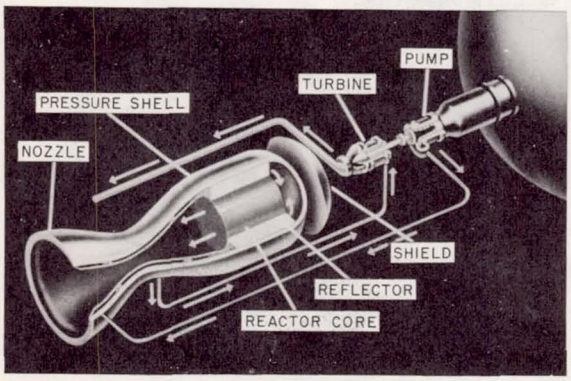

FIGURE VIII–60.—Nuclear rocket engine.

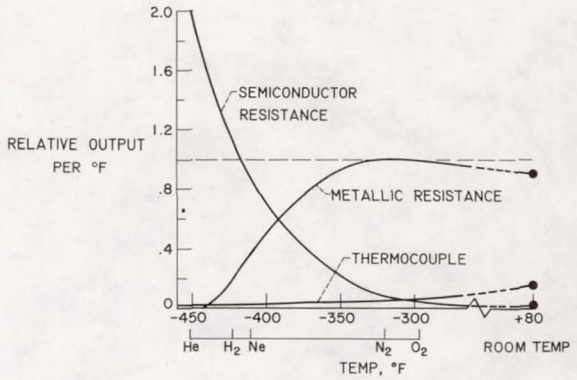

FIGURE VIII–61.—Relative sensitivity of temperature sensors.

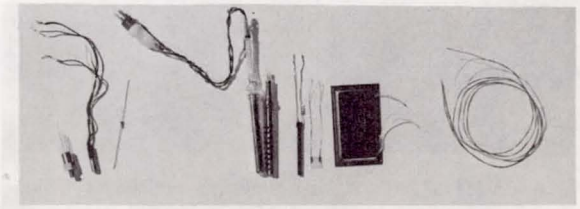

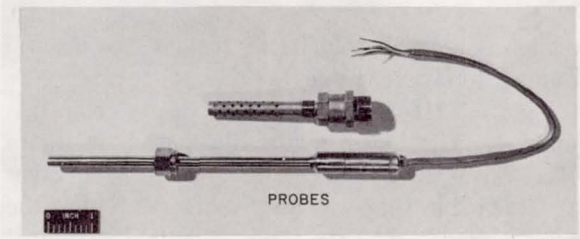

FIGURE VIII–62.—Temperature sensors.

Some commercially available cryogenic temperature sensors are shown in figure VIII–62. The semiconductor resistors are usually either germanium or carbon. The germanium sensors, of which two types—a screw-in type and an immersion type—are shown, have good repeatability, but unfortunately their present poor inter-

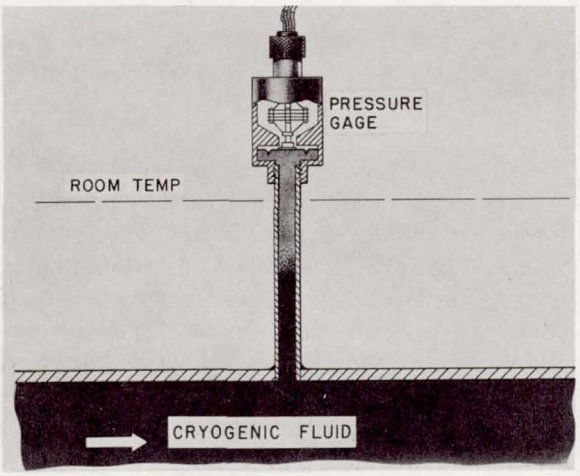

FIGURE VIII–63.— Cryogenic fluid pressure measurement. Conventional pressure-gage installation.

changeability requires that each sensor be calibrated throughout its intended temperature range.

A carbon semiconductor shown next to the germanium sensor is a composite carbon resistor like the ones used in radio and television sets. As a temperature sensor, it suffers from poor stability; that is, its calibration will change with usage.

The metal resistance temperature sensors are primarily platinum. Shown are two immersion types, a cementable-surface type and a weldable-surface type. In general, platinum sensors are preferred for cryogenic temperature measurements wherever possible because of their excellent repeatability and calibration accuracy.

At the upper right of figure VIII–62 is shown a thermocouple. In spite of its low sensitivity, it has application at cryogenic temperatures, primarily because of its small size. (The sensing element is the small junction at the very end of the wires.) Chromel-constantan is preferred to copper combinations because the thermal conductivity of copper, as previously shown, is very high at cryogenic temperatures. The high conductivity could cause a high heat input to the measuring junction and give an erroneous measurement.

Thermocouples usually have the fastest response to temperature changes because of their small mass. However, all the sensors shown tend to have a faster response at cryogenic temperature than at room temperature because the specific heat of the sensor material decreases with a decrease in temperature.

At the bottom of figure VIII–62 are shown three probes in which the sensor element is protected against vibration and high flow velocities by a tube. The lower probe is also sealed to protect the element against high pressures.

The measurement of low temperature requires several considerations. This is also true for the measurement of cryogenic fluid pressures. The principal problem is that most conventional pressure transducers either will not work in the cryogenic environment or are highly temperature sensitive. However, conventional transducers can be used to measure cryogenic fluid pressures if they are kept at essentially room temperatures.

As shown in figure VIII–63, the gage may be kept near room temperature by means of a long pressure tube. The cryogenic liquid flows into the tube and boils, thus filling the tube with warm gas, which acts as a thermal barrier between the measuring diaphragm and the cryogenic liquid. The disadvantage of such an installation is that the combination of liquid and gas in the tube causes a reduction in frequency response. This type of installation will give a response of only about 10 cycles per second. For measuring transient pressures, gages especially designed for cryogenic temperatures must be used.

Figure VIII–64 shows an application requiring such a transducer. Here, following the high-fre-

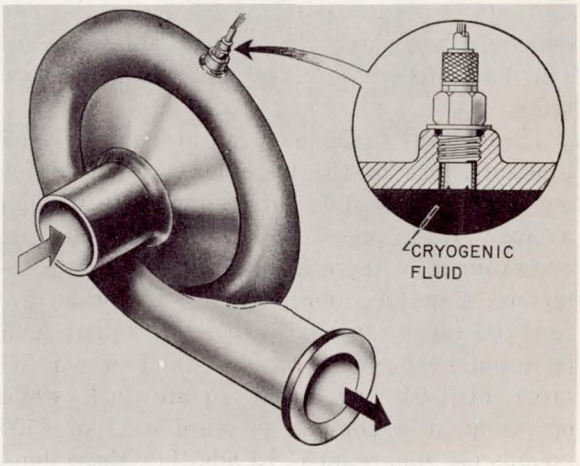

FIGURE VIII–64.—Cryogenic pressure-gage installation.

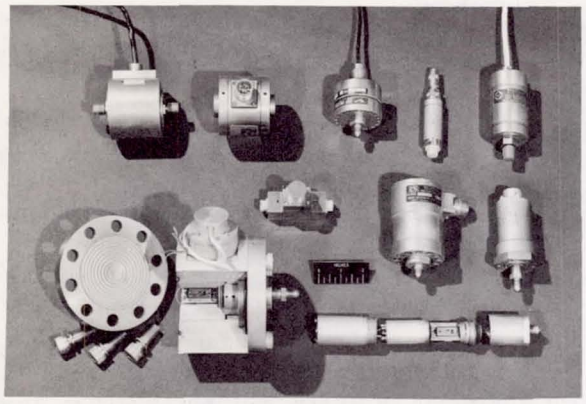

FIGURE VIII–65.—Commercially available strain-gage pressure transducers.

quency pressure fluctuations within a liquid-hydrogen pump, casing is desired. For such an application, a flush-mounted transducer is required. The cold, pulsating cryogen contacts the sensing diaphragm of this transducer directly. This type of installation can follow pressure oscillations at frequencies of several thousand cycles per second.

These cases are only two examples of how transducers can be applied to the measurement of cryogenic pressure. In actual practice, many types of pressure-measuring devices are required to meet the various vehicle and test-stand applications.

Figure VIII–65 shows some commercially available pressure transducers, here, all of the strain-gage class. These units are generally used on ground test stands. The transducers on the right are gage-type units and the one on the bottom right is a partly diassembled absolute unit. The four units on the left are differential pressure units.

The cutaway in the lower left of figure VIII–65 illustrates one of the transducers designed for measuring small differential pressures at high average system pressure. This transducer is just one example of those available on today's commercial transducer market. The full-scale differential range can be 5 pounds per square inch or less and can resolve pressure differences in the order of 0.05 pound per square inch while operating at a nominal pressure level of 3500 pounds per square inch. In addition, these units are designed for use with corrosive fluids and have been used extensively in fluorine systems. The corrugated stainless-steel separation diaphragms prevent the corrosive fluid from coming in contact with the internal measuring mechanisms.

One use of differential-type pressure gages is to measure the pressure drop across head-type flowmeters of the orifice, nozzle, and venturi designs. Figure VIII–66 shows an installation of a cryogenic head-type flowmeter attached to a differential pressure gage. These flowmeters are used successfully to measure cryogenic fluid flow rate. However, certain precautions should be taken:

(1) Since the fluids are easily vaporized, and since two-phase flow must be avoided, the meter must be well insulated and prechilled before using.

(2) The static pressure in the flow line must be above the liquid vapor pressure to prevent cavitation.

(3) The pressure-sensing lines between the orifice and the pressure gage must be symmetrical to prevent system oscillations.

(4) Pressure drop across the orifice should be as high as possible to minimize boiling at the liquid-to-gas interface in the pressure sensing lines (which appears as noise in the output of the differential pressure gage).

(5) The orifice metering area must be corrected for thermal contraction if the meter was not calibrated with the actual cryogenic fluid.

(6) The same Reynolds number range must be maintained if another fluid at room temperature is used for calibration.

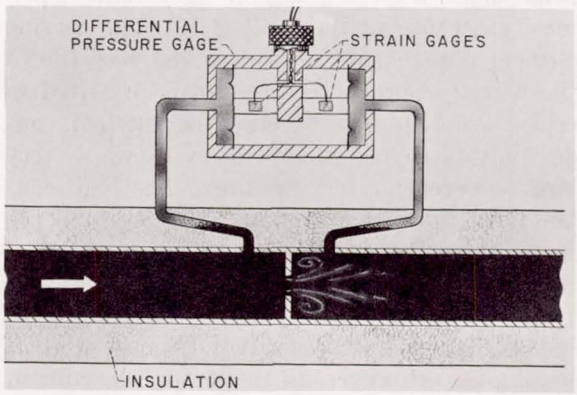

FIGURE VIII–66.—Head flowmeter installation.

There are other types of flow-measuring devices suitable for cryogenic fluids. Turbine meters, which are also volumetric types, have come into widespread use in the last few years. Figure VIII–67 shows some typical turbine meters with a cutaway view. The meter consists of a free turbine, straightening vanes, and an externally mounted electric pickup which senses turbine speed.

Figure VIII–68 shows some typical calibration results that were obtained when turbine meters were calibrated on water, liquid oxygen, and liquid hydrogen. A perfect meter is represented by the straight line passing through the origin. In the actual case, bearing friction is present so that the turbine does not start until fluid force is sufficient to overcome the friction. As the flow rate is further increased, the frictional forces are overpowered and the meter follows the ideal curve. Because of its low density, considerably higher flow rates of liquid hydrogen than liquid oxygen or water are required to overcome the frictional forces, and the meter does not approach the ideal curve until about midrange.

The useful range in water and liquid oxygen is from about 10 to 1 as compared with 2 or 3 to 1 for liquid hydrogen. Experience has shown that, for liquid oxygen applications, a water calibration will assure an accuracy of better than 2 percent over the upper nine-tenths of the range. For a hydrogen meter calibrated on water, the 2-percent accuracy will apply only to about the upper half of the meter range. If an accuracy in the order of 1 percent is required, the turbine meters must be calibrated with the actual cryogen to be measured.

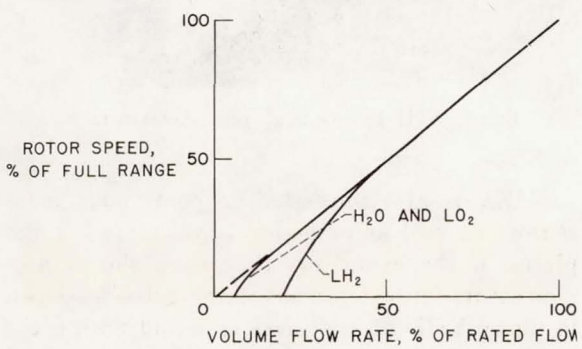

FIGURE VIII–67.—Turbine flowmeters.

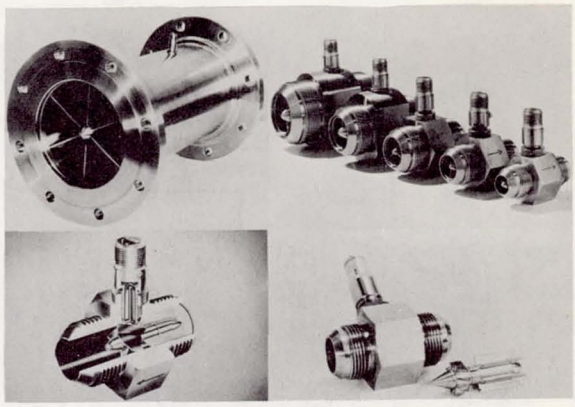

FIGURE VIII–68.—Turbine meter fluid calibration.

Turbine meters, commercially available in sizes from $\frac{1}{8}$ to 21 inches in diameter, have the advantages of small size relative to other flow-measuring devices, fast response to transient flows, and for dense fluids, the wide range of about 10 to 1. A significant disadvantage of the turbine meter is the exposure of the bearings and turbine to the flow stream where they can be easily damaged by contaminants. The parts are also vulnerable during cooldown when high gas flow can damage the bearings because of overspeeding and slugs of liquid can smash the delicate turbine mechanism.

All the meters described so far are volumetric flowmeters. In most cases, it is desired to measure mass flow rates, which requires a measurement of density in addition to volumetric flow rate.

A capacitance sensor will measure density directly. Basically, the principle of operation is shown in figure VIII–69. The amount of current flow from one capacitor plate to the other is directly related to the density of the fluid between the plates. This principle has been used commercially for a number of years. Its application has merely been extended to liquid hydrogen.

As shown in figure VIII–70, this concept has also been utilized to make point level sensors. The capacitor elements here are wires instead of plates, with the wires arranged in a horizontal plane. A difference in current flow results

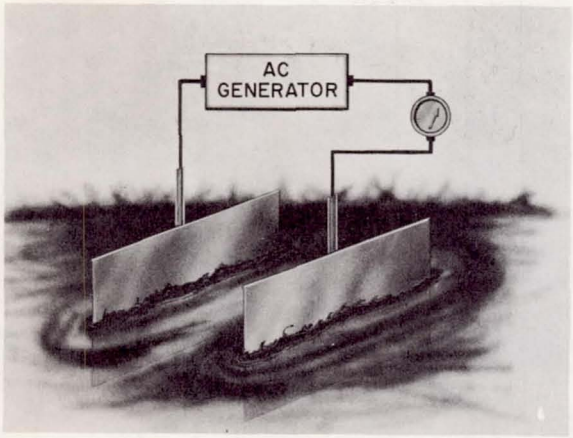

FIGURE VIII–69.—Capacitive density detection.

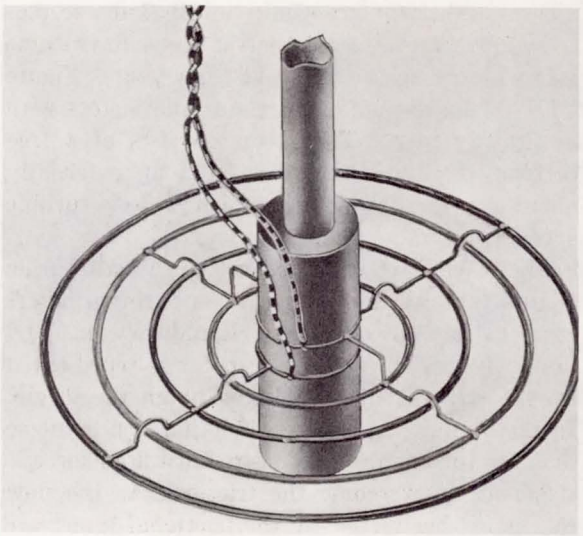

FIGURE VIII–70.—Capacitance point-level indicator.

when there is a change from gas to liquid between the elements.

Other types of point-level sensors are the vibrating-reed type, where the amplitude varies with the density of the fluid; the acoustic type, where an ultrasonic wave is bounced off the liquid-gas interface; the hot-wire type, where the difference between the cooling effect of the gas and the liquid is utilized; and the optical type, where the refraction and reflection of a light beam are utilized.

An optical-point-level sensor is shown in figure VIII–71. It consists, basically, of a transparent tube with a wedge-shaped tip, light source, and a light detector, all of which may be immersed in liquid hydrogen. The tube may be made of Lucite, but for cryogenic purposes, it is usually quartz or some other material. In a gas, light is emitted by the source, transmitted down the tube, and reflected back to the detector by the wedge-shaped tip. However, if liquid wets the tip, light is transmitted to the tip and refracted; thus no signal goes back to the detector.

All these point-level indicators are commercially available. They are only examples of how standard instrumentation has been applied to cryogenic use. In most cases, however, the aerospace requirements have been more severe than commercial requirements, and the instruments have required modifications.

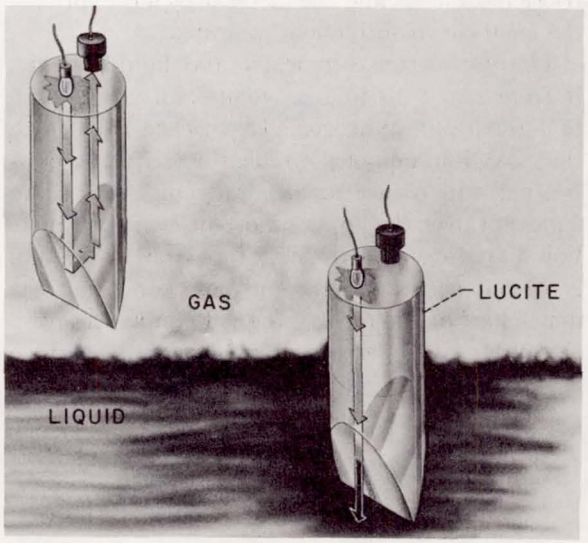

FIGURE VIII–71.—Optical point-level sensor.

NASA is also interested in continuous mass sensors as well as point-level indicators. If the plates of the capacitors that were shown previously are formed into concentric tubes as shown in figure VIII–72, the mass of liquid within the annular tube is proportional to the mass of liquid within the tank. Capacitance probes formed in

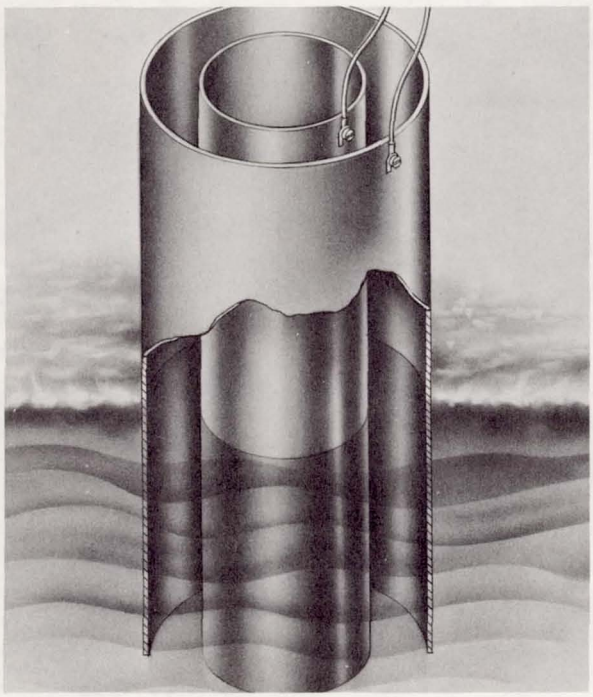

FIGURE VIII–72.—Continuous capacitance mass sensor.

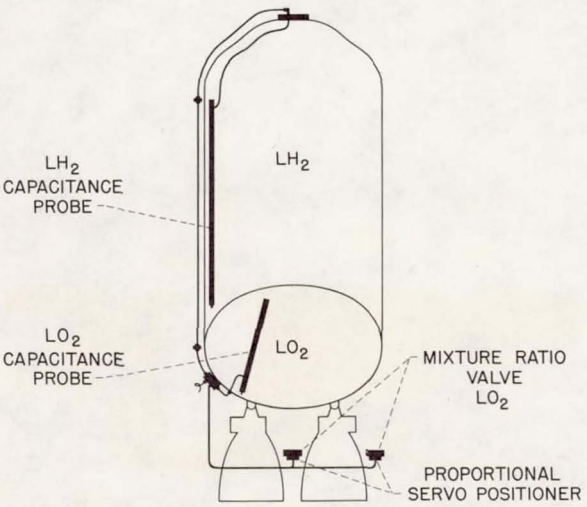

FIGURE VIII–73.—Centaur propellant-utilization system.

this way have found widespread use in the aerospace industry, both for ground storage and for flight applications. For example, as shown in figure VIII–73, the Centaur vehicle uses such capacitance probes in the propellant utilization

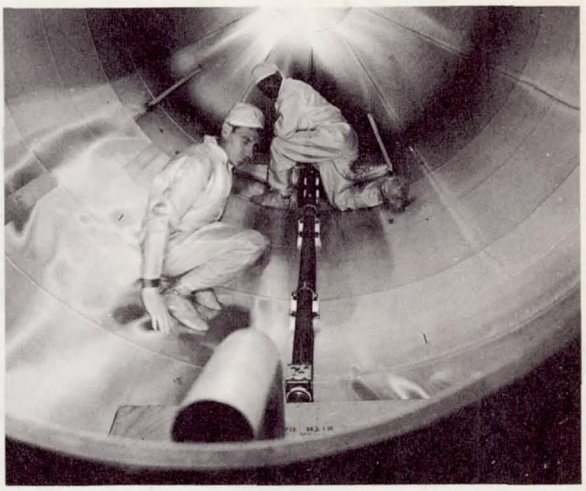

FIGURE VIII–74.—Installation of capacitance sensor.

system to sense the mass of the liquid hydrogen and liquid oxygen. The electronic package compares the mass of each propellant and adjusts the oxidant valves, shown on each engine, to provide a minimum amount of propellant on board at burnout. Installation of the probe in the Centaur liquid-hydrogen tank is shown in figure VIII–74. The probe is approximately 15 feet long and about 3 inches in diameter. This system was flown in August 1965 for the first time. The system error was less than 5 pounds out of the 30 000 pounds of propellants consumed during the flight.

CONCLUDING REMARKS

As can be seen from the discussion presented herein, NASA is deeply involved in the cryogenic field. A few typical examples of recent progress in this area have been presented. Necessarily, the examples have been drawn from the aerospace industry and the discussion has been very general. The significant point, however, is that cryogenic fluids can now be handled and used on an everyday, commonplace basis. The best illustrations of this are the launch vehicles, since they are the culmination of many NASA research and development programs. Such technology should greatly benefit future commercial applications of cryogenic fluids.

Page intentionally left blank

IX Technology Utilization

BREENE M. KERR, MELVIN S. DAY, GEORGE J. HOWICK, RICHARD L. LESHER, AND HOWARD L. TIMMS*
NASA Headquarters

THE UNITED STATES SPACE PROGRAM is a logical progression of science and technology. It does not begin and end with one specific goal. Each advancement makes other progress possible. Thus the exploration of space and related exploits are likely to become a part of our way of life and are likely also to have a profound influence on the progression of science and technology in the nonaerospace community.

To ensure an effective flow of the technical information generated by the aerospace program to the scientists and engineers who need it and to the industries and other organizations that may find it of value, NASA has created the Technology Utilization Program. Herein will be provided an overall view of its objectives and operations.

The Program is operated by the NASA Office of Technology Utilization. It has two main parts. First, the Scientific and Technical Information Division provides a brimming reservoir of readily tapped knowledge from domestic and foreign sources—presently 200 000 technical documents indexed on computer tapes. It is fed by swelling streams of reports and articles—75 000 to 100 000 per year at the current rate—from NASA's 12 research centers and field offices, from its contractors and grantees, from other branches of the Government that produce technological information, and from aerospace activities in about 40 foreign countries.

The other primary unit is the Technology Utilization Division. One of its tasks is to select from the computer-indexed storehouse those discoveries, ideas, and procedures that appear most promising for adaptation. It also provides an important means of seeking out new, and not yet recorded, useful ideas, by a corps of Technology Utilization Offices at each NASA center and field office. They continually review work under way there and in contractors' laboratories and factories for new developments of promise to nonaerospace activities. In the last 2 years, they generated more than 2000 reports of selected innovations, many of which may not have been generally accessible otherwise.

Screened and evaluated both by NASA and by industrial research institutes under contract to it, the findings of the Technology Utilization Officers are then published in a variety of formats. They range from single-sheet descriptions to extensive technology surveys that document cumulative advances in a whole field.

So begins the vital course of "transfer," which may take one or more of these several forms:

(1) Adaptation of an NASA innovation to devise new commercial products and workable new processes
(2) Employment in nonspace products of materials, devices, or circuitry developed by NASA
(3) Stimulation of scientist and engineer creativity by the infusion of new knowledge from NASA
(4) Utilization of NASA information relevant to the solution of specific design and manufacturing problems

Specifically, the transfer of technology occurs when research on air bearings for space power generators leads to use of the principle for moving heavy loads. It occurs when small biosensors developed to monitor the physical condition of astronauts permit a continuous central monitor-

* Aerospace Research Applications Center, Indiana University.

ing system for patients in a hospital cardiac ward. It occurs when a business concern can use NASA-developed procedures to shorten training time. It also occurs when a firm utilizes an NASA ultrasonic testing method to find small flaws in a welded assembly.

The task of the NASA Technology Utilization Division is not, however, simply one of finding and packaging innovations. Imagination, a special knowledge of local needs and problems, and personal contact are all necessary to increase the likelihood of successful technological transfer. This is almost impossible to provide from a central headquarters. For that reason, the Office of Technology Utilization has embarked on a program of disseminating technical information through regional centers; there are now eight of these regional dissemination centers.

The first project of this sort to use the wide-ranging computer search-and-retrieval techniques of the NASA Scientific and Technical Information Division was undertaken by Indiana University. The Aerospace Research Applications Center (ARAC), formed there in the spring of 1963, has established an effective government-university-industry partnership to assist technological transfer. ARAC had enrolled a number of fee-paying private firms, both large and small, that subscribe to its service. ARAC's operation is described as an example at the various regional dissemination centers.

SCIENTIFIC AND TECHNICAL INFORMATION

Acquiring, Abstracting, and Announcing

The NASA central collection of scientific and technical information begins with an aggressive worldwide operation to acquire new technical documents in aerospace. The information is obtained from NASA laboratories and contractors, from other government agencies and their contractors, from industrial firms working independently in space-related fields, from private and university research institutes, and from foreign governmental, industrial, and academic laboratories.

The intake from this worldwide acquisitions operation is processed by NASA evaluators who select material relevant to NASA programs and channel it into the central information system. Here the information is placed under bibliographic control; that is, it is cataloged, abstracted, and indexed in order to provide an information product suitable for a variety of users. The bibliographic data are put into a computer system.

Automation is important in our processing for two reasons. Automation makes possible the rapid handling of the data, a necessity in the fast moving aerospace field. Also, the computer can manipulate the bibliographic data in a number of different ways to produce a variety of products—printed indexes, tape indexes, continuing bibliographies, literature searches, etc. Basic among these products are two complementary abstracting-indexing journals—STAR and IAA (fig. IX–1)—in which new aerospace titles are announced. Each journal comes out twice a month on alternate weeks.

STAR (Scientific and Technical Aerospace Reports) is a comprehensive abstracting-indexing journal covering worldwide report literature on the science and technology of space and aeronautics. Each issue is arranged in two sections. In the first section are the abstracts (brief descriptions) of the reports covered, together with such cataloging information as title, author, source, etc., divided among 34 broad subject categories. The abstract section is followed by several detailed indexes: subject, corporate

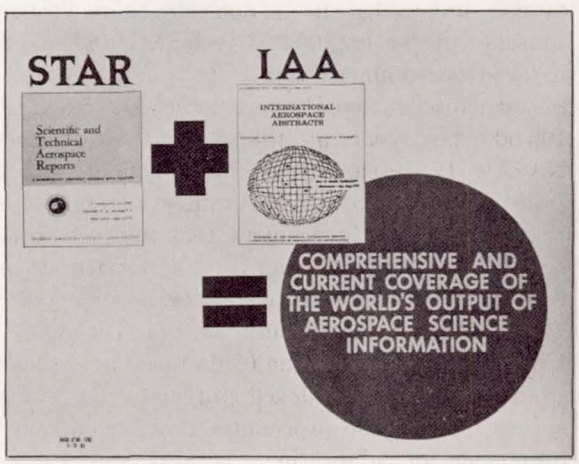

FIGURE IX–1.—STAR and IAA abstracting-indexing journals.

source, personal author, report number, accession number, and contract number. Separate cumulative index issues are published quarterly and annually. Thus, STAR and its indexes provide the user with both an announcement tool for maintaining current awareness of developments in his field and a retrospective searching tool for bringing himself up to date on a specific matter at any point in time.

By arrangement between NASA and the American Institute of Aeronautics and Astronautics, that society's publication, International Aerospace Abstracts (IAA), is issued in coordination with STAR with no overlap or duplication. IAA's worldwide coverage of scientific journals, books, and open meetings complements STAR's worldwide coverage of the report literature. The two publications thus provide comprehensive access to current literature on aerospace science and technology. More than 50 000 items a year are announced in these two journals.

The Department of Defense and its contractors are the largest single source of documents in STAR, almost a third (fig. IX–2). Documents of foreign origin (mostly Soviet) total about the same. The NASA-sponsored input, about a fifth of the total at present, is growing with the rising flow of contractor reports into our central collection.

The portion of foreign input into IAA is even greater than that of STAR, more than 40 percent, as shown in figure IX–3. This perhaps reflects the European tradition of publishing in the learned journals rather than in report literature.

Note then the large number of items of foreign origin fed into the NASA information system for use not only in our national aerospace programs but also through the regional dissemination centers for use by United States industry.

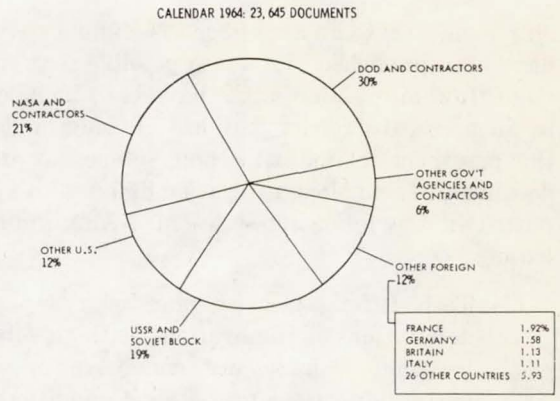

FIGURE IX–2.—Origin of items announced in STAR (Scientific and Technical Aerospace Reports).

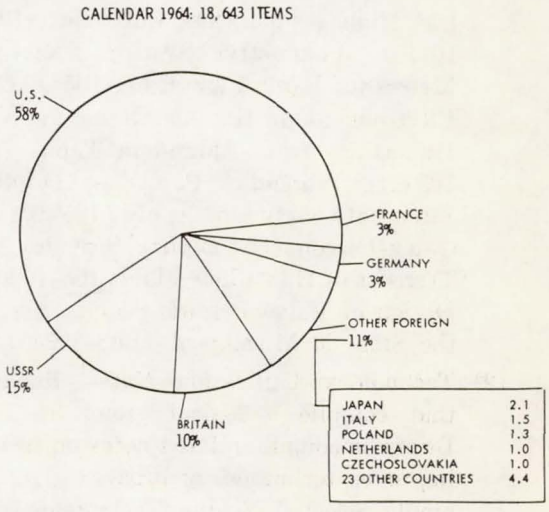

FIGURE IX–3.—Origin of items announced in IAA (International Aerospace Abstracts).

NASA Publications

NASA's own aerospace research results are reported in the following series of NASA publications:

(1) Technical Reports—Scientific and technical information that is considered important, complete, and a lasting contribution to existing knowledge

(2) Technical Notes—Information less broad in scope but nevertheless of importance as a contribution to existing knowledge

(3) Contractor Reports—Technical information generated in connection with an NASA contract or grant and released under NASA auspices

As already stated, the findings of the Technology Utilization Officers also result in a series of publications. Many of these findings are ideas, techniques, procedures, or methods that, being

only incidental to an aerospace task, might never have been published. It is also possible that the innovation in question might have been included in an aerospace report, but lost to view under the aerospace-related title and subject of the document. Technology utilization findings are reported in the following series of NASA publications:

(1) Tech Briefs—Concise one- or two-page descriptions of innovations with possible applications in science, commerce, or industry; directions for obtaining additional information are included; more than 500 have been published so far; some typical titles: Lead Oxide Ceramic Makes Excellent High Temperature Lubricant (B64–10116), Volumetric System Calibrates Meters for Large Flow Rates (65–10323), Electromagnetic Hammer Removes Weld Distortions from Aluminum Tanks (65–10342), Inorganic Paint is Durable, Fireproof, Easy to Apply (65–10156), Quick-Disconnect Coupling Provides Safe Transfer of Hazardous Fluids (65–10202), Design of Valve Permits Sealing Even if the Stem is Misaligned (B63–10341)

(2) Technology Utilization Notes—Booklets that compile a logical group of Tech Briefs or compile related notes on new or improved techniques or processes; for example, Selected Welding Techniques I and II (SP–5003 and SP–5009), Precision Tooling Techniques (SP–5013)

(3) Technology Utilization Reports—Detailed descriptions and evaluations of innovations selected for their significant industrial potential; some examples: The Retrometer—A Light Beam Communication System (SP–5005), Metal Forming Techniques (SP–5017), Micropower Logic Circuits (SP–5022), A Technique for Joining and Sealing Dissimilar Materials (SP–5016)

(4) Technology Handbooks—Collections of practices, data, etc., that should be helpful for a variety of problems; for example, Selected Shop Techniques (SP–5010), Welding for Electronic Assemblies (SP–5011), Reliable Electrical Connections (SP–5002), Space Batteries (SP–5004)

(5) Technology Surveys—Comprehensive reviews or summaries of areas of technology, with a view to combining results from many scattered references; contain bibliographies; some examples: NASA Contributions to the Technology of Inorganic Coatings (SP–5014), Plasma Jet Technology (SP–5033), Advanced Bearing Technology (SP–38), Advanced Valve Technology (SP–5019), Magnetic Tape Recording (SP–5038)

Finally, NASA publishes several other kinds of documents, including the following that are pertinent to science and engineering:

(1) Technical Translations—Information published in a foreign language considered to merit NASA distribution in English

(2) Special Publications—Information derived from or of value to NASA activities but not necessarily reporting the results of individual NASA-programed scientific efforts; publications include conference proceedings, monographs, data compilations, handbooks, sourcebooks, and special bibliographies. The most recent addition to the series is a line of continuing bibliographies; these, issued recurrently, repackage abstracts and indexing data from STAR and IAA in fast-developing areas of high interest to NASA programs. Titles issued so far include High Energy Propellants, Lunar Surface Studies, Communications Satellites, Aerospace Medicine and Biology, and Lubrication, Corrosion, and Wear.

Use of the System

All the documents—foreign and domestic—that are announced and indexed in STAR and IAA are also indexed in greater depth on magnetic tape, so that the growing mountain of technical information can be searched rapidly for answers to specific questions. The tapes, updated twice a month, are provided to NASA Centers, major research and development contractors, and

to the Technology Utilization regional dissemination centers.

Another access road into the central collection of scientific and technical information is by way of the NASA microfiche.

At the same time that incoming reports are being processed for announcement in STAR, a copy of each report is microfilmed. The images of up to 60 individual pages are then arranged in a 105- by 148-millimeter format (about 4 by 6 in.) as a flat negative called a microfiche (fig. IX–4). This microfiche is distributed free to libraries of NASA centers and major contractors and to the Technology Utilization regional dissemination centers.

The microfiche copy (unclassified), also, is available for sale through the Department of Commerce to anyone in the world.

The microfiche can be scanned and read on inexpensive equipment. It can also serve as a negative for printing out copies of selected pages or an entire document, and it is a reproducible master for producing additional copies of the microfiche itself. Microfiches are tailor-made for compact storage and fast retrieval. Microfiche copies of 1000 average-size reports can fit in a container no bigger than a shoebox. The same number of full-size documents would fill 14 linear feet of library shelf space. Thus, they represent a handy and economical means of maintaining large collections locally and reproducing the documents in limited quantities.

Finally, one rather specialized access to the NASA collection of aerospace technical literature

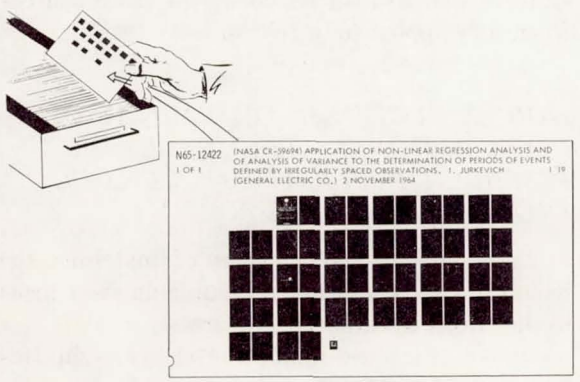

FIGURE IX–4.—NASA microfiche.

is through a Selective Dissemination of Information Program—NASA/SDI. SDI is a computer-based system for notifying individual scientists and engineers of new reports and journal articles of value in their own particular work. This system illustrates the many possibilities that arise from computer speed, capacity and flexibility in manipulating data.

SDI can be compared with a library run in reverse: a library in which people as well as acquisitions are cataloged. As new reports and articles are received, they are matched to the interests of individual users.

In SDI, the user's information needs are cataloged on magnetic tape as lists of words or phrases describing each man's particular interests; these lists are called user profiles. The documents appear on another tape as lists of indexing terms describing their contents, called document profiles; this is the same NASA tape index to new acquisitions that has already been prepared for other uses. The computer then compares user profiles with document profiles. When a predetermined degree of similarity between a man's interests and a new document is found, the man is sent a citation of the report and instructions on obtaining the full report.

SDI is currently serving 500 NASA scientists and engineers and 200 Air Force personnel. Although it is still under development and too early to make a formal evaluation, the volume of documents requested by participants in the SDI program has risen as much as 300 percent over their pre-SDI patterns. Eventually the program will be operated on a decentralized basis at the various NASA Centers, and perhaps by major contractors.

In the meantime, variations of the present program, such as standardized profiles and simplified announcement formats, are being tested which should be able to serve many more users. Numerous case histories of technology transfer can be cited to illustrate the usefulness of this system.

Other Government Information Sources

The Atomic Energy Commission has a statutory obligation similar to NASA's. It has, of

course, actively supported and aided the development of a civilian nuclear electric-power-generating industry; it has helped develop industrial and biomedical uses for radio isotopes; it has helped to create many other civilian uses for nuclear technology. Recently the Atomic Energy Commission also began to introduce commercial industry to the nonnuclear technology developed by the Atomic Energy Commission in the course of its nuclear research and development programs. The laminar flow clean room, now fairly common in the electronics and instruments industries, is an example of such secondary utilization of Atomic Energy Commission technology. Another example is the development of extremely advanced mechanical centrifuge technology, incorporating "quantum jumps" in the art of making bearings and seals. Such advances, necessary for the continued improvement of nuclear technology, obviously have many potential applications outside the nuclear industry. The focal point for obtaining such new knowledge from the Atomic Energy Commission is its Office of Industrial Cooperation at Argonne National Laboratory.

The Smithsonian Institution and the National Science Foundation also have obligations to diffuse new knowledge throughout the economy. One outgrowth is the Science Information Exchange (SIE), located within the Smithsonian Institution and supported largely by funds from the National Science Foundation. This is not a technology transfer program in the same sense as are the programs of NASA and AEC, rather SIE is a registry of current ongoing research tasks supported by Federal and non-Federal grants. SIE can tell a scientist or engineer who else is working in his field. The scientist or engineer can write to SIE and describe the specific field of interest. In return, SIE will provide him with one-page definitions of all the work in that field that has been reported to SIE. For each of these tasks, SIE can provide the name of the supporting agency, the title of the project, the names, titles, and locations of the principal investigators, the name and address of the institution conducting the research, a 200-word summary of the work under way, the starting date for the research, the planned conclusion date, the annual level of effort in dollars, and other salient information.

Since it began in 1949, SIE has accumulated about 300 000 records of research projects. SIE's coverage of current research in the life sciences is quite comprehensive. It coverage of work in the physical sciences, however, is still largely incomplete. The Physical Sciences Division was only organized in 1962; thus, it is possible that at some future date SIE might provide comprehensive coverage in the physical sciences too.

In any case, SIE offers the scientist an opportunity to find out who is doing work or has recently done work in a given field of interest. This permits him to establish research priorities in a more realistic fashion.

Further, it can lead him to people with specialized knowledge on whom he may want to call for information.

While the Department of Defense, the National Aeronautics and Space Administration, and the Atomic Energy Commission represent the great bulk of research and development conducted by the Federal Government, a dozen or so other agencies have work under way that may be potentially useful to commercial industry. Research reports on the work of those agencies, if that work is unclassified and unlimited, can generally be purchased from the Federal Clearinghouse for Scientific and Technical Information.

It is part of the job of each NASA Regional Dissemination Center to be aware of other sources of technical information within the Federal Government and to lead its clients to those sources when they appear to be relevant.

HOW A REGIONAL DISSEMINATION CENTER WORKS: AEROSPACE RESEARCH APPLICATIONS CENTER, INDIANA UNIVERSITY

The role of ARAC is that of matching the technical needs and interests of industrial firms to the NASA information resources.

Among the most important elements in this task are the ARAC scientists and engineers. These specialists, whose background and experi-

ence span a broad spectrum of science and technology, are able to understand and interpret the problems of industrial firms and to screen and identify relevant information from NASA scientific and technical information resources.

Selective Dissemination

A basic service provided to industrial firms participating in ARAC is the Selective Dissemination Service, a "current awareness effort" based on the specific technical interests of each firm. Every 2 weeks newly received NASA computer tapes containing several thousand citations of technical reports and journal articles are searched. Each member firm has several "interest profiles" which have been developed through a cooperative effort of company and ARAC engineers and scientists. These profiles reflect the company's special areas and activities.

ARAC assigns a technical staff member to each profile. This provides a continuous man-to-man contact between technical people in each company and ARAC engineers and scientists. Each profile is structured for computer search by the ARAC specialist and is machine matched against the indexed descriptions of every new report. Citations of documents that appear to match profile interests are screened and evaluated by the ARAC technical man before they are sent to scientists and engineers in each member firm.

Interest profiles serve the purpose of maintaining continuous and current awareness of participating firms in relevant areas of science and technology. Each profile is dynamic and can be easily modified as interests and needs change. ARAC is identifying and sending out over 13 000 abstracts every 2 weeks in response to matching with more than 300 profiles.

The system combines the economy and speed of computerized information retrieval with personalized processing by competent technical people working toward the needs and interests of industrial firms.

Full copies of reports of interest can be supplied by return mail in microfiche form (4- by 6-in. microfilm sheet) for those companies with reading equipment, or in 2 to 4 weeks in hard copy for those without reading equipment.

Retrospective Searches

The Retrospective Search Service is set up to focus on specific problems or areas of interest to member firms. ARAC staff specialists take a problem-solving approach to retrospective searches. These problem-oriented searches cover the entire NASA file containing more than 200 000 reports.

Search requests are studied and prepared for computer search by an ARAC technical man whose background and experience closely parallels the subject area of the problem. Typically, the company scientist or engineer is contacted by phone before the search is made to ensure that the ARAC specialist understands the problem and all relevant details.

Results of each computer printout are carefully screened and evaluated before results are sent to the company. Interpretation and assessment of results are made whenever possible. The computer is used as a time-saving device. All results pass through human hands and a technical mind before going out to the requester.

Search problems may range from that of seeking a particular material with specified characteristics to a state-of-the-art type search on an area of technology such as fluid amplifiers. On one search for the Cummins Engine Company of Columbus, Indiana, on bearing technology, a NASA report was identified which provided the basis for Cummins to completely reprogram their computer programs used in bearing design for their diesel engines.

The Selective Dissemination and Retrospective Search Services complement each other. Ongoing needs and interests are met through selective dissemination. Particular problems are handled in depth as retrospective searches. These problems can be converted to interest profiles, or incorporated in existing profiles if a company seeks to maintain a current awareness in the area in the future.

The important consideration is a clear-cut understanding of company needs and interests

by ARAC scientists and engineers. These services provide a mechanism for meeting these needs once they are identified and understood. The close operating relation between ARAC and participating firms is the all-important element in successful results.

Industrial Applications Service

NASA's Technology Utilization Division has an ongoing program designed to identify, appraise, and disseminate space program technology which offers promising commercial application potential. Additionally, ARAC scientists and engineers in the process of their day-to-day review of available information resources are alert to reports which contain industrial application ideas. These resources provide the input to ARAC's Industrial Applications Service (IAS).

The IAS consists of a weekly mailing of 10 report abstracts with indicated application potential. These go out to over 300 company mailing points. Conservative estimates hold that these abstracts are routed to as many as 3000 industry scientists and engineers each week.

All 10 abstracts are distributed to each recipient each week. No attempt is made to screen against technical interests on this service. The IAS is a shotgun approach as contrasted to the Selective Dissemination and Retrospective Search Services. The reasons behind this approach are good. First, the task of reviewing 10 short abstracts each week can be accomplished in 2 to 4 minutes. More importantly, however, the Industrial Applications Service seeks to generate new ideas, to expose company technical people to a broad cross section of technology where industrial application potential has been specifically identified by NASA and ARAC.

Member firms are extremely receptive to the Industrial Applications Service. A typical weekly mailing is

(1) Sliding electrical contact materials
(2) New microflowmeter
(3) Fluid amplification
(4) Optics used to measure torque at high rotational speeds
(5) Fine mesh screen made by simplified method
(6) Probe measures characteristics of hot gas stream (65–10133)
(7) Inert gas spraying device
(8) High temperature strain gages
(9) Thermal position sensor
(10) A precision fluid bearing

After a company man has read an abstract of interest, he may obtain the full report by return mail from ARAC. Instructions for additional followup relative to specific questions that are not covered in the report are included with it. ARAC provides supplementary information on any IAS report in response to a company's specific questions to which answers are required before proceeding with the possibility of a transfer of the technology.

Experience and Results

Since a request for supplementary information indicates a good possibility of a technology transfer, ARAC makes a maximum effort to supply the needed information through contacts with appropriate NASA regional centers, additional information retrieval at ARAC, and in some cases application advice where an ARAC staff member has background and experience closely related to the problem.

An example of a recent successful transfer involved a NASA innovation identified by the Technology Utilization Office at Marshall Space Flight Center. The idea concerned a technique for measuring blind holes of the order of 0.01 to 0.020 inch. A member firm read the abstract and asked for the report.

After review of the report the company engineer found that the technique appeared feasible for his particular measurement problem. However, his situation involved the extension of the technique to hole measurements up to 0.25-inch inside diameter. ARAC contacted Marshall Space Flight Center on this, and at Marshall's suggestion the company representative sent samples of their hole measurement problem to Marshall for testing in the 0.25-inch range. The results were favorable; the company is now using

the technique in their quality control program.

Almost 3 years of experience in ARAC shows that many of the difficulties in transferring information from NASA information resources into commercial application involve "people" problems rather than a lack of applicability of the NASA information.

For example, there is the "not invented here" complex in a few companies. Our approach to this problem has been to stress the creative effort necessary to apply the new information constructively.

Naturally, a one-to-one relevance of space technology to industrial problems does not exist. However, the breadth and depth of NASA technology can be most useful in providing increments of information for a variety of sizes and types of firm. One normally does not reach into the NASA research and development "stockpile" and pull out ready made commercial products and processes. Rather, elements and portions of the technology are used to solve industrial problems. ARAC resources are only a part of a total research and development process within a company. There must be competent technical people at the company end to take advantage of the information provided by ARAC. In a sense, ARAC offers technology "building blocks." The task of creatively using these building blocks rests with the industrial firm.

Making effective use of space technology for commercial applications is not easy. The company itself must have a positive attitude. For example, companies in the same industry have taken exactly opposite stands on the value of particular areas of NASA technology. Those with a positive but hard-headed businesslike approach have gained the most from the ARAC program. Utilization moves forward at a rapid and effective pace in companies where at least one key man is imaginative, broad thinking, and action oriented, and is also convinced that meaningful results can be achieved from the ARAC program.

While ARAC does maintain close and continuous contact with member firms, there is no substitute for a person within the firm who has been assigned a coordination role in the program. Once operations are set up, this coordination normally requires only a minimal amount of effort. Part of the coordinator's job is to establish multiple receipt points within the company; attempts to funnel all ARAC services to only one point are typically unsuccessful. To make ARAC services effective, direct contact is needed between ARAC technical people and those in the company. Thus, ARAC operating procedures have purposely been kept flexible to accommodate various internal operating plans.

ARAC activity with member firms has moved up exponentially for the past $2\frac{1}{2}$ years. Those companies that have gone into the program on a positive but realistic basis have continued to expand their use of the services, and this applies to nearly every firm. Over 90 percent of the initial member firms are with us after nearly 3 years. The oil and gas industry is represented in ARAC by Cities Service Company, Incorporated; Kerr-McGee Oil Industries, Incorporated; Socony Mobil Oil Company, Incorporated; and Texas Gas Transmission Corporation.

Here is an example of the problem-solving approach taken in ARAC. This example, as well as the other examples in this text, are cited with written approval of the companies concerned. In ARAC all personnel sign a secrecy agreement to protect the interest of all member firms. Every request is handled on a completely proprietary basis.

The Texas Gas Transmission Corporation was evaluating the use of gas-turbine-driven compressors as power sources for system expansion programs instead of conventional reciprocating gas engine units. The main component of the gas turbine compressor is a standard jet aircraft engine widely used in civil and military aviation. The company asked ARAC for information and data pertaining to the life expectancy of these gas turbines under conditions of static continuous use.

A search of NASA literature yielded no directly relevant results, so ARAC next contacted several specialized information sources. Wright-Patterson Air Force Base had been engaged in testing the type of jet engine in question for many years, and, although they had no data relating to static continuous conditions, they did

provide valuable information and an estimate of the minimum life.

The Technology Utilization Officer at Lewis Research Center was then contacted by ARAC. A meeting convened at the Lewis Center, attended by representatives of NASA, the jet engine manufacturer, Texas Gas Transmission Corporation, and ARAC, to discuss factors affecting the life of the engine and to try to arrive at a suitable life expectancy. NASA engineers thoroughly familiar with the engine were available as impartial advisors. The meeting resulted in the transfer of much valuable information relative to life expectancy. The manufacturer also volunteered to collect and provide much additional historical data.

Texas Gas Transmission Corporation was aided materially in the development of life expectancies for the economic evaluation of the equipment in question. The meeting at Lewis also generated further interest in the subject of lubrication of the new equipment.

Advances like this result from advances in information management. The ability to sit at a remote console and interact with the total NASA information storehouse on a computer time-sharing basis, is one step toward effective information handling. Through the information bank, one can find new ideas and useful pieces of information that otherwise might not have been encountered or one might find out something about causes of problems not yet defined.

It is not quite this easy yet, but information technology is a fast-moving field and NASA is continually experimenting. A contract is now being negotiated for the design and testing of a prototype remote console system for document retrieval. The use of off-the-shelf equipment will allow a man to query the information storehouse without going through a programer. It will both speed up service and give the ultimate information user a more active role in our man-machine-man system. Through computer time-sharing almost any number of points on a network could query the system simultaneously.

We envision that a scientist working on a problem will be able to query the NASA information collection from a console at his own station, interacting with the computerized central information store in virtually real time. He can thus sharpen his search strategy in the light of the running response, displayed immediately at the console, rather than waiting hours or perhaps days for the results of one approach before trying another. It is also possible, of course, that it will have the secondary benefit of stimulating his imagination with fresh insights into his problem. But, to be valuable, even such a magnificent system must be properly used. The need for the system does exist, but industry must supply the use.

ADDITIONAL INFORMATION

More information on the NASA Technology Utilization Program can be obtained from

Technology Utilization Division
Code UT
National Aeronautics and Space Administration
Washington, D. C. 20546

Patent license and waiver information may be obtained from

Assistant General Counsel for Patent Matters
Code GP
National Aeronautics and Space Administration
Washington, D. C. 20546

STAR's (Scientific and Technical Aerospace Reports) semimonthly issues and cumulative index issues are available postpaid from

Superintendent of Documents
United States Government Printing Office
Washington, D. C. 20402

(Semimonthly issue: $33/yr; $2.25/copy ($42 and $2.50, foreign). Cumulative index issue: $30/yr ($35, foreign); single copy price varies with page length.) IAA (International Aerospace Abstracts) is published semimonthly and is available from

American Institute of Aeronautics and Astronautics, Incorporated
750 Third Avenue
New York, N. Y. 10017

(Semimonthly issue: $25/yr ($33, foreign). Cumulative index volume: $25/yr ($33, foreign)).

NASA technical reports, as well as reports from many other government agencies, can be purchased from

Clearinghouse for Federal Scientific and Technical Information
Port Royal Road
Springfield, Va. 22151

A comprehensive abstracting service that provides a guide to all NASA technical reports, and the reports themselves, can also be used at Federal Regional Depository Libraries, many public libraries, at NASA-supported regional dissemination centers, at its Scientific and Technical Information Division, and at the Clearinghouse for Federal Scientific and Technical Information.

Federal Regional Depository Libraries:

Atlanta, Georgia
Georgia Institute of Technology

Berkeley, California
University of California

Boulder, Colorado
University of Colorado

Cambridge, Massachusetts
Massachusetts Institute of Technology

Chicago, Illinois
John Crerar Library

Dallas, Texas
Southern Methodist University

Kansas City, Missouri
Linda Hall Library

Los Angeles, California
University of California

New York City, New York
Columbia University

Pittsburgh, Pennsylvania
Carnegie Library of Pittsburgh

Seattle, Washington
University of Washington

Washington, D. C.
Library of Congress

You may also wish to employ the services of a regional dissemination center, or request assistance from the Technology Utilization Officer at the NASA field installation or office near you. A list of the locations follows.

NASA Field Installations and Offices:

Ames Research Center
Mountain View, California

Electronics Research Center
Cambridge, Massachusetts

Flight Research Center
Edwards, California

Goddard Space Flight Center
Greenbelt, Maryland

Jet Propulsion Laboratory
California Institute of Technology
Pasadena, California

Kennedy Space Center
Cocoa Beach, Florida

Langley Research Center
Hampton, Virginia

Lewis Research Center
Cleveland, Ohio

Manned Spacecraft Center
Houston, Texas

Marshall Space Flight Center
Huntsville, Alabama

Wallops Station
Wallops Island, Virginia

Western Operations Office
Santa Monica, California

AEC-NASA Space Nuclear Propulsion Office
Atomic Energy Commission
Washington, D. C.

Regional Dissemination Centers:

Albuquerque, New Mexico
University of New Mexico

Bloomington, Indiana
Aerospace Research Applications Center
Indiana University Foundation

College Park, Maryland
University of Maryland

Detroit, Michigan
Center for Application of Sciences and Technology
Wayne State University

Durant, Oklahoma
Technology Use Studies Center
Southeastern State College

Durham County, North Carolina
Science and Technology Research Center
Research Triangle Park

Kansas City, Missouri
Midwest Research Institute

Pittsburgh, Pennsylvania
Knowledge Availability Systems Center
University of Pittsburgh

AUTHORS

WILLIAM J. ANDERSON is Chief, Bearings Branch, at Lewis. He joined the staff of the Research Center in 1950. A native of Brooklyn, Mr. Anderson attended Massachusetts Institute of Technology where he received a B.S. degree in mechanical engineering in 1950. In 1957, Case Institute of Technology awarded him an M.S. degree in aeronautical engineering. He has specialized in bearing and lubrication problems in spacecraft and aircraft propulsion and auxiliary power systems.

FRANK E. BELLES is Head, Kinetics Section, at Lewis. He joined the Research Center in 1947. A native of Cleveland, Mr. Belles attended Western Reserve University where he received a B.S. in 1947. In 1952 he received an M.S. degree in physical chemistry from Case Institute of Technology. Mr. Belles has specialized in combustion and detonation, high-temperature chemistry, and is currently working on chemical kinetic studies by shock-tube techniques.

EDMOND E. BISSON is Assistant Chief, Fluid System Components Division, at Lewis. He joined the Langley Research Center in 1939 and transferred to Lewis in 1943. In 1955 he was appointed to his present position where he directs much of NASA's research effort in lubrication and bearings. Born in East Barre, Vermont, Mr. Bisson was graduated with honors from the University of Florida in 1938 with a B.S. degree in mechanical engineering and received his Professional Degree of Mechanical Engineer from the University of Florida in 1954.

RICHARD S. BROKAW is Chief, Physical Chemistry Branch, at Lewis. He joined the Research Center in 1952. Dr. Brokaw is responsible for research in chemical thermodynamics and equilibria in gases, chemical kinetics and transport properties in gases, and fundamentals of rocket combustion. He received his B.A. degree in 1943 at Swarthmore College and his M.A. (1949) and Ph.D (1951) from Princeton University.

EDMUND E. CALLAGHAN is Assistant Chief, Electromagnetic Propulsion Division, at Lewis. He joined the staff of the Research Center in 1944. Mr. Callaghan, a native of Brooklyn, attended Rensselaer Polytechnic Institute where he received his B.S. degree in aeronautical engineering in 1943. His research specialties include work on icing problems, heat transfer, noise, turbulence, cryogenics, and magnetics.

BRUCE J. CLARK is an Aerospace Technologist, Chemistry and Energy Conversion Division, at Lewis. He joined the Research Center in 1957. A native of Grand Rapids, Michigan, Mr. Clark attended the University of Michigan where he received B.S. and M.S. degrees in chemical engineering in 1947 and 1949 and an M.A. degree in mathematics in 1951. Mr. Clark has specialized in elementary combustion processes and is currently working on the breakup characteristics of sprays.

MELVIN S. DAY is Director of the Scientific and Technical Information Division, NASA. A native of Maine, he was graduated from Bates College in 1943, worked as a chemist, and served in the U.S. Army during World War II. In 1947 he joined the Atomic Energy Commission, later serving as Director of AEC's Technical Information Service. Mr. Day joined NASA in 1960.

ROBERT W. GRAHAM is Head, Experimental Section, Fundamental Heat Transfer Branch, at Lewis. Dr. Graham joined the Research Center in 1953. He has specialized in fluid mechanics of turbomachinery and in heat transfer research as applied to rocket engine cooling. Dr. Graham graduated with honors from Case Institute of Technology with a B.S. degree in mechanical engineering in 1948. He is also a graduate of Purdue University, receiving an M.S. degree in 1950 and a Ph.D. in 1953.

VERNON H. GRAY is Head, Liquid Metals Section, at Lewis. He joined the Research Center in 1944. A native of Nevada, Missouri, Mr. Gray attended the University of Maryland where he received a B.S. degree in mechanical engineering in 1938. Mr. Gray has specialized in aircraft icing, heat transfer, two-phase flow, and liquid metals and is currently working on heat transfer and two-phase flow problems with alkali metals in space power systems.

MELVIN J. HARTMANN is Chief, Pump and Compressor Branch, at Lewis. He joined the staff of the Research Center in 1943. Mr. Hartmann has specialized in the field of turbomachinery and has written a number of papers and articles on the subject. A native of Scribner, Nebraska, Mr. Hartmann earned a B.S. degree in mechanical engineering from the University of Nebraska in 1944.

CAVOUR H. HAUSER is Head, Pump Section, at Lewis. He joined the staff of the Research Center in 1944. A native of Minneapolis, he attended the University of Minnesota where he received a B.S. degree in mechanical engineering in 1944. In 1949 he received an M.S. degree in mechanical engineering from Case Institute of Technology. Mr. Hauser has specialized in aerodynamics

of gas turbines, hydrodynamic design, and application of pumps.

GLEN HENNINGS is Chief, Rocket Systems Division, at Lewis. He joined the staff of the Research Center in 1944 following his graduation from the University of Nebraska. Mr. Hennings has specialized in research dealing with chemical rockets and high-energy propellants. He also has wide experience in rocket safety, piston engines, and aircraft icing problems. Mr. Hennings was born in Osceola, Nebraska. He holds a B.S. degree in agricultural engineering from the University of Nebraska.

JOHN R. HOWELL is a Research Engineer, Chemical Physics Branch, at Lewis. Dr. Howell joined the Research Center in 1961. He attended Case Institute of Technology where he received a B.S. degree in chemical engineering in 1958, an M.S. degree in nuclear engineering in 1960, and a Ph.D. in engineering in 1962. He has specialized in thermal radiation heat transfer and boiling heat transfer and is currently working on heat transfer in radiative systems.

GEORGE J. HOWICK is Chief, Technology Utilization Division, NASA. He came to NASA in 1965 from Midwest Research Institute where he was involved in projects that examine and interpret the economic implications of new technology. He is a former associate editor of *Steel Magazine.*

ROBERT L. JOHNSON is Chief, Lubrication Branch, at Lewis. He joined the staff of the Research Center in 1943. A native of Glasgow, he attended Montana State College where he received a B.S. degree in mechanical engineering in 1942. His experience includes 22 years of fundamental and applied research on lubrication problems for aerospace devices.

WILLIAM L. JONES is Head, Rocket Cooling Section, at Lewis. He joined the Research Center in 1944. A native of Warren, Ohio, Mr. Jones attended Fenn College where he received a B.S. degree in mechanical engineering in 1944. He has specialized in turbojet engines, ramjets, rocket propulsion, and rocket heat transfer and is currently working on rocket nozzle heat transfer and cooling.

BREENE M. KERR is Assistant Administrator, Office of Technology Utilization, NASA. He has responsibility for disseminating to industrial and other users scientific data and technical advances from NASA research. Mr. Kerr also has operating responsibility for the Scientific and Technical Information Division. A native of Oklahoma, he received his B.S. degree from Massachusetts Institute of Technology in 1951.

ROBERT A. LAD is Chief, Chemical Physics Branch, at Lewis. Dr. Lad joined the staff of the Research Center in 1946. A native of Chicago, Illinois, he attended the University of Chicago where he received a B.S. degree in chemistry in 1939, an M.S. degree in physical chemistry in 1941, and a Ph.D. in inorganic chemistry in 1946. Dr. Lad has specialized in mass spectroscopy of hydrocarbons, solid state physics and chemistry, and surface chemistry and is currently working on chemistry and physics of the surfaces of ionic crystals.

RICHARD L. LESHER is Deputy Assistant Administrator for Technology Utilization, NASA. He is responsible for the administration and control of NASA's Regional Dissemination Program. A native of Chambersburg, Pa., Dr. Lesher was educated in business and economics, receiving a B.B.A. degree from University of Pittsburgh, M.S. from Pennsylvania State, and D.B.A. from Indiana University. Prior to joining NASA, he served on the faculties of Ohio State University and the University of Georgia.

LAWRENCE P. LUDWIG is Head, Seals Unit, Lubrication Branch, at Lewis. He joined the staff of the Research Center in 1962. A native of Racine, Wisconsin, Mr. Ludwig attended Marquette University where he received a B.S. degree in mechanical engineering in 1948. In 1957 he received an M.S. degree in mechanical engineering from Wisconsin University. Mr. Ludwig has specialized in friction, wear, and fluid dynamics and is currently working on contact and hydrodynamic seals research.

MAX J. MILLER is a Research Engineer, Fluid System Components Division, at Lewis. He joined the staff of the Research Center in 1962. A native of Griswold, Iowa, Mr. Miller attended Iowa State University where he received a B.S. degree in mechanical engineering in 1962. He has specialized in axial flow and centrifugal rocket pumps and is currently working on pump analysis computer programs.

DONALD L. NORED is Chief, Liquid Rocket Technology Branch, at Lewis. He joined the Research Center in 1958. Mr. Nored received his B.S. degree in chemical engineering from Texas Technological College in 1955. At Lewis he has worked on advanced propulsion facility design and operation, high energy rocket engines, and vehicle systems studies.

WALTER T. OLSON is Assistant Director, Public Affairs, at Lewis. Dr. Olson received his B.S. degree in chemistry from DePauw University, and Master's and Ph.D. degrees from Case Institute of Technology. He joined the Lewis staff in 1942. Research divisions directed by Dr. Olson from 1953 to 1963 were concerned with chemical rockets, high energy fuels, altitude-chamber tests of rockets, high-performance liquid propellants, electric rockets, fuel cells, and solar energy conversion.

EDWARD W. OTTO is Chief, Space Environment Branch, at Lewis. He joined the Research Center in 1944. He has specialized in propulsion systems dynamics and controls and is currently engaged in the study of the be-

havior of liquids in a zero-gravity environment. Mr. Otto, a native of Onawa, Iowa, is a graduate of Iowa State University where he received a B.S. degree in mechanical engineering in 1944.

I. IRVING PINKEL is Chief, Fluid System Components Division, at Lewis. He joined the Langley Research Center in 1940 then transferred to Lewis in 1942. Mr. Pinkel currently directs research on propellant and power generation systems for space vehicles. A native of Gloversville, New York, he was graduated with honors from the University of Pennsylvania in 1934.

ROBERT S. RUGGERI is an Aerospace Engineer, Fluid System Components Division, at Lewis. He joined the staff of the Research Center in 1944. A native of Christopher, Illinois, Mr. Ruggeri attended Tri-State College where he received a B.S. degree in aeronautical engineering in 1944. Mr. Ruggeri has specialized in aircraft deicing and aerodynamics and is currently working on cavitation research.

ROBERT SIEGEL is Head, Analytical Section, at Lewis. Dr. Siegel joined the Research Center in 1955. A native of Cleveland, he attended Case Institute of Technology where he received B.S. and M.S. degrees in mechanical engineering in 1950 and 1951. In 1953, Massachusetts Institute of Technology awarded him an Sc.D. in mechanical engineering. Dr. Siegel has specialized in fluid dynamics and heat transfer and is currently working on boiling in reduced gravity, solidification of flowing liquids, and heat transfer in rectangular channels.

DONALD H. SINCLAIR is an Aerospace Engineer, Instrument Operations Section, at Lewis. He joined the Langley Research Center in 1947 and transferred to Lewis in 1948. A native of Cleveland, Mr. Sinclair attended Yale University where he received a B.S. degree in mechanical engineering in 1945. In 1956 he received a B.S. degree in electrical engineering from Fenn College. Mr. Sinclair has specialized in instruments and is currently working on cryogenic temperature measurement.

GORDON T. SMITH is an Aerospace Engineer, Fluid Systems and Structures Section at Lewis. He joined the Research Center in 1958. A native of Lafayette, Indiana, Mr. Smith attended Purdue University where he received a B.S. degree in mechanical engineering in 1947. In 1953 he was awarded an M.S. degree in mechanical engineering from Case Institute of Technology. He has specialized in turbine cooling, strength of materials, and liquid rocket technology and is currently working on liquid rocket system technology.

GEORGE R. SMOLAK is Head, Vehicle Systems Unit, Centaur Project Office, at Lewis. He joined the staff of the Research Center in 1951. He attended the University of Michigan where he received B.S. and M.S. degrees in mechanical engineering in 1950 and 1951. Mr. Smolak has specialized in combustion, heat transfer, cryogenic storage, zero-gravity, FLOX, insulation of turbine engines, ramjets, and turbojet cycle analysis and is currently working on management of FLOX Atlas contracts.

RICHARD F. SOLTIS is an Aerospace Engineer, Fluid System Components Division, at Lewis. He joined the staff of the Research Center in 1956. A native of Cleveland, Mr. Soltis attended John Carroll University where he received a B.S. degree in physics in 1956. He has specialized in fluid mechanics, electronics, photography, and instrumentation and is currently working on pump research and high response instrumentation.

ANDREW J. STOFAN is an Aerospace Technologist, Centaur Project Office, at Lewis. He joined the staff of the Research Center in 1958. Mr. Stofan attended Hiram College where he received a B.A. degree in mathematics in 1956. In 1958 he received a B.S. degree in mechanical engineering from Carnegie Institute of Technology. Mr. Stofan has specialized in jet engine ejector nozzles and propellant sloshing and is currently working on propellant utilization systems.

HOWARD L. TIMMS is Codirector of Indiana University's Aerospace Research Applications Center and is a Professor of Management in the university's School of Business. Dr. Timms was graduated from Purdue in 1940 with a B.S. degree in mechanical engineering and holds M.B.A. and D.B.A. degrees in finance from Indiana University.

ERWIN V. ZARETSKY is Head, Unit C, Bearings Branch, at Lewis. He joined the Research Center in 1957. A native of Chicago, he was graduated from Illinois Institute of Technology in 1957 with a B.S. degree in mechanical engineering. In 1963, Mr. Zaretsky received his Juris Doctor from the Cleveland-Marshall Law School of Baldwin-Wallace College. At Lewis, Mr. Zaretsky conducts and supervises analytical and experimental research on rolling contact phenomena involving materials and lubricants.

FRANK J. ZELEZNIK is a Physicist, Thermodynamics Section, at Lewis. He joined the Research Center in 1958. A native of Cleveland, Dr. Zeleznik attended Case Institute of Technology where he received B.S., M.S., and Ph.D. degrees in chemical engineering in 1954, 1955, and 1959. He has specialized in thermodynamics and is currently working on rotational relaxation.

☆ U. S. GOVERNMENT PRINTING OFFICE: 1966—0 210-245